Secondary Metabolites from Fungi: Diversity Enhancement, Structure Elucidation and Bioactivity

Inaugural dissertation

for the attainment of the title of doctor
in the Faculty of Mathematics and Natural Sciences
at the Heinrich Heine University Düsseldorf

presented by

Hao Wang
from Shandong, P. R. China

Düsseldorf, 12. 2017

from the institute for Pharmaceutical Biology and Biotechnology
at the Heinrich Heine University Düsseldorf

Published by permission of the
Faculty of Mathematics and Natural Sciences at
Heinrich Heine University Düsseldorf

Supervisor: Prof. Dr. Dr. h.c. Peter Proksch
Co-supervisor: Prof. Dr. Matthias Kassack

Date of the oral examination: 01. 2018

CONTENTS

Abstract……..…….....…….3

Zusammfassung…….....….....…….5

1 Introduction…….....……..….....……..8

1.1 Fungi as a rich source of pharmaceutical agents……...…….……..8

1.2 Mining various ecological fungi…….…….…….……10

1.2.1 Soil-derived fungi……...…….11

1.2.2 Endolichenic fungi……...…….……11

1.2.3 Endophytic fungi…….…..……..12

1.2.4 Marine-derived fungi……...……13

1.3 Dereplication……..……...……13

1.4 Mining silent gene clusters in fungi……...14

1.4.1 OSMAC approach……..…….……14

1.4.2 Co-cultivation…….…….15

1.4.3 Epigenetic modulation……...…..16

1.4.4 Genetic modification…….....……..16

1.5 Aims and significance of this study……...…….17

2 Publication 1: Targeted solid phase fermentation of the soil dwelling fungus *Gymnascella dankaliensis* yields new brominated tyrosine-derived alkaloids....18

3 Publication 2: Indole alkaloids produced by an endophytic fungus *Aspergillus aculeatus* using an OSMAC approach…….....……71

4 Publication 3: Secondary metabolites of the lichen-associated fungus *Apiospora montagnei*……..…….152

5 Discussion……...……175

5.1 Induction of new secondary metabolites using the OSMAC approach…..……..175

5.1.1 Inducing brominated tyrosine-derived alkaloids by halogen incorporation…..175

5.1.2 Inducing indole alkaloids from *A. aculeatus* by addition of nitrate……..178

5.1.3 Inducing new secondary metabolites from *A. montagnei* through the OSMAC approach……...……..182

5.2 OSMAC approach: an easily executed, effective and potently method to express silent gene clusters of secondary metabolites……...…..……183

References……..……185

List of abbreviations…..…….…….....……198

Research contributions…..…….…….....……...…200

Declaration of academic honesty/ Erklärung…..……...……...……201

Acknowledgements……..……...……..…...……202

Curriculum vitae……..……...……..…...……204

Abstract

Fungi are an important source of structurally diverse and pharmacologically active secondary metabolites. This dissertation describes investigations on bioactive secondary metabolites from the soil-derived fungus *Gymnascella dankaliensis*, the endophytic fungus *Aspergillus aculeatus* and the lichen-associated fungus *Apiospora montagnei*. OSMAC (One Strain MAny Compounds) approaches were applied to trigger silent secondary metabolic gene clusters to exploit chemical diversity of fungi by adding halide to solid rice medium or by modification of nitrogen sources. The structures of isolated secondary metabolites were elucidated by NMR spectra and MS data. The absolute configuration of new compounds was determined by X-ray analysis, Marfey's method and by comparison of optical rotation and NMR data with the literature. Among the isolated fungal secondary metabolites, gymnastatins I–J, T and W, secalonic acids D and F, libertellenone G, *N*-hydroxyapiosporamide, apiosporamide, acremonone G and bostrycin exhibited significant cytotoxicity against the murine lymphoma cell line L5178Y. This dissertation consists of the following three published or submitted manuscripts.

Targeted solid phase fermentation of the soil dwelling fungus Gymnascella dankaliensis yields new brominated tyrosine-derived alkaloids.

Seven new brominated tyrosine-derived alkaloids, gymnastatins T–Y (**1**–**6**) and dankastatin D (**7**), together with three known likewise brominated analogues gymnastatins I–K (**8**–**10**) were isolated from the soil fungus *Gymnascella dankaliensis* through fermentation on solid rice medium following addition of NaBr. None of these compounds were detected when the fungus was cultured on rice that either lacked NaBr or that contained NaCl instead, indicating a remarkable plasticity of the fungal secondary metabolism. All structures were elucidated on the basis of one and two dimensional NMR spectroscopic analyses and MS data. The absolute configuration of the new gymnastatin T (**1**) was determined by X-ray crystallographic data. All isolated alkaloids showed potent to moderate cytotoxicity against the L5178Y mouse lymphoma cell line with IC_{50} values ranging from 0.078 to 14.1 μM.

Indole alkaloids produced by an endophytic fungus Aspergillus aculeatus using an OSMAC approach

The endophytic fungus *Aspergillus aculeatus* isolated from leaves of the papaya plant *Carica papaya* was fermented on solid rice medium, yielding a new indole alkaloid (**1**) and thirteen known compounds (**11**, **14**–**25**). In addition, an OSMAC approach was employed by adding eight different sodium or ammonium salts to the rice medium. Addition of 3.5% $NaNO_3$ caused a significant change of the metabolite pattern of the fungus as indicated by HPLC analysis. Subsequent isolation yielded several new indole derived alkaloids (**1**–**10**) in addition to three known compounds (**11**–**13**), among which compounds **2**–**10**, **12**–**13** were not detected in the rice control culture. All structures were unambiguously elucidated by one and two dimensional NMR spectroscopy and by mass spectrometry. The absolute configuration of the indole derivatives was determined by Marfey's reaction and X-ray single crystal diffraction. Compounds **19**–**22** showed cytotoxicity against the L5178Y mouse lymphoma cell line with IC_{50} values of 3.4, 1.4, 7.3 and 23.7 μM, respectively

Secondary metabolites of the lichen-associated fungus Apiospora montagnei

The endolichenic fungus *Apiospora montagnei* isolated from the lichen *Cladonia* sp. was cultured on solid rice medium, yielding the new diterpenoid libertellenone L (**1**), the new pyridine alkaloid, 23-*O*-acetyl-*N*-hydroxyapiosporamide (**2**) and the new xanthone derivative 8-hydroxy-3-hydroxymethyl-9-oxo-9*H*-xanthene-1-carboxylic acid methyl ether (**3**) together with 19 known compounds (**4**–**22**). The structures of the new compounds were elucidated by 1D and 2D NMR spectra as well as by HRESIMS data. The absolute configuration of the new 6,7-*seco*-libertellenone derivative **1** was determined by single-crystal X-ray diffraction. Four additional known compounds **23**–**26** were isolated when NaCl or NH_4Cl were added to solid rice medium. Compounds **7**–**9**, **18** and **26** exhibited significant cytotoxicity against the L5178 murine lymphoma cell line with IC_{50} values of 2.6, 0.2, 2.1, 2.7 and 1.7 μM, respectively.

Zusammenfassung

Pilze bilden eine wichtige Quelle für phamakologisch aktive Sekundärmetaboliten aus strukturell unterschiedlichsten Stoffgruppen. Diese Dissertation beschäftigt sich mit der Untersuchung der Sekundärmetabolitmuster des Bodenpilzes *Gymnascella dankalienses*, des endophytischen Pilzes *Aspergillus aculeatus* und des Flechten-assoziierten Pilzes *Apiospora montagnei*. Um die volle chemische Diversität auszunutzen und kryptische Sekundärmetaboliten aus schlafenden Genclustern zu erschließen, wurden durch Supplementierung verschiedener Halogenidsalze oder Modifikation der verfügbaren Stickstoffquellen, OSMAC (One Strain MAny Compounds) Kultivierungsexperimente auf Reismedium durchgeführt. Die Strukturaufklärung der isolierten Sekundärmetaboliten erfolgte durch Kernspinresonanz-Spektroskopie (NMR) und Massenspektrometrie (MS). Die Bestimmung der absoluten Konfiguration erfolgte per Röntgenkristallstrukturanalyse, Marfey-Analyse und dem Vergleich von spezifischen optischen Rotationen und NMR-Daten mit Literaturquellen. Unter den isolierten Pilzsekundärmetaboliten zeigten Gymnastatin I–J, T und W, sowie Secalonsäuren D und F, Libertelleron G, *N*-Hydroxyapiosporamid, Apiosporamid, Acremonon G und Bostrycin eine signifikante Zytotoxizität gegenüber der Mauslymphomzelllinie L5178Y. Diese Dissertation setzt sich aus den folgenden Publikationen zusammen, deren Manuskripte bereits veröffentlicht oder eingereicht wurden.

Die gezielte Festphasenfermentation des Bodenpilzes Gymnascella dankaliensis führt zu neuen Brom-Tyrosinalkaloiden.

Nach der Zugabe von Natriumbromid zu einer Reisfermentation des Bodenpilzes *Gymnascella dankaliesis* konnten die sieben neuen Brom-Tyrosinalkaloide Gymnastatine T–Y (**1**–**6**) und Dankastatin D (**7**), zusammen mit den ebenfalls bromierten, bekannten Gymnastatinen I–K (**8**–**10**), isoliert werden. Keine der genannten Verbindungen konnten in Reisfermentationen, denen kein Natriumbromid zugesetzt wurde oder die stattdessen Natriumchlorid enthielten, detektiert werden, was die bemerkenswerte Anpassungsfähigkeit des pilzlichen Sekundärstoffwechsels

demonstriert. Alle Strukturen wurden durch mittels ein- und zweidimensionaler NMR-Spektroskopie, sowie Massenspektrometrie aufgeklärt. Die absolute Konfiguration von Gymnastatin T (**1**) wurde über Röntgenkristallstrukturanalyse bestimmt. Alle isolierten Verbindungen zeigten starke bis moderate Zytotoxizität gegenüber der Mauslymphomzelllinie L5178Y mit IC_{50}-Werten zwischen 0,078 und 14,1 μM.

Produktion von Indolalkaloiden durch den endophytischen Pilz Aspergillus aculeatus unter Anwendung von OSMAC-Bedingungen

Der endophytische Pilz *Aspergillus aculeatus* wurde aus den Blättern des Papayabaums *Carica papaya* isoliert und anschließend auf Reismedium kultiviert. Diese initiale Fermentation führte zur Isolation eines neuen Indolalkaloids (**1**), sowie dreizehn bekannter Verbindungen (**14**–**25**). Anschließend wurden, durch Anreicherung des Reismediums mit acht verschiedenen Natrium- oder Ammoniumsalzen, OSMAC Kultivierungsansätze durchgeführt. Die Supplementierung mit 3,5% Natriumnitrat verursachte erhebliche Veränderungen des durch HPLC analysierten Sekundärstoffmusters. Die darauffolgende Isolation förderte einige neue Indolalkaloide (**1**–**10**), zusammen mit drei bekannten Verbindungen (**11**–**13**), zutage, von denen **2**–**10** und **12**–**13** nicht in den Reiskontrollkulturen detektiert wurden. Sämtliche Strukturen wurden mittels ein- und zweidimensionaler NMR-Spektoskopie und Massenspektrometrie aufgeklärt. Die absoluten Konfigurationen der Indolderivate wurden durch Marfey- und Röntgenkristallstrukturanalyse bestimmt. Verbindungen **19**–**22** zeigten Zytotoxizität gegenüber der Mauslymphomzelllinie L5178Y mit IC_{50}-Werten von jeweils 3,4, 1,4, 7,3 und 23,7 μM

Sekundärmetaboliten des Flechten-assoziierten Pilzes Apiospora montagnei

Eine Reisfermentation des endophytischen Pilzes *Apiospora montagnei*, welcher aus einer Flechte der Gattung *Cladonia* isoliert wurde, führte neben der Isolation von 19 bekannten Verbindungen (**4**–**22**), zur Isolation des neuen Diterpenoids Libertellenon L (**1**), des neuen Pyridinalkaloids 23-*O*-acetyl-*N*-hydroxyapiosporamid (**2**) und des neuen Xanthonderivats 8-Hydroxy-3-hydroxymethyl-9-oxo-9*H*-xanthen-1-

carbonsäure methyl ester (**3**). Die Strukturen der neuen Verbindungen wurden durch den Einsatz von ein- und zweidimensionaler NMR-Spektroskopie und hochauflösender Massenspektrometrie aufgeklärt. Die absolute Konfiguration des neuen 6,7-*seco*-Libertellenonderivats **1** wurde mittels Röntgenkristallstrukturanalyse bestimmt. Das Hinzufügen von Natriumchlorid oder Ammoniumchlorid zum Reismedium führte zur Isolation von vier weiteren, bekannten Verbindungen (**23**–**26**). Die Verbindungen **7**–**8**, **18** und **26** zeigten signifikante Zytotoxizität gegenüber der Mauslymphomzelllinie L5178Y mit IC_{50}-Werten von jeweils 2,6, 0,2, 2,1, 2,7 und 1,7 μM.

1. Introduction

Natural products that are produced by living organisms including plants, animals to microbes have different biological activities and can be widely utilized as colourants, pharmaceuticals, fragrances and hormones (Colegate and Molyneux, 2007; Schaefer, 2015). Morphine, the first isolated natural product, was reported as a colorless crystal from opium (*Papaver somniferum*) by a young German pharmacist, Friedrich Wilhelm Adam Sertürner in 1806 (Huxtable and Schwarz, 2001). Nowadays, more than 2 million natural products are recorded in the Dictionary of Natural Products database and the number is increasing annually (Rodrigues *et al*., 2016). The classification of natural products includes four schemes: molecular skeleton, physiological activity, chemotaxonomy and biogenesis. In practice, natural products can be divided into five main groups including terpenoids and steroids, alkaloids, fatty acid–derived substances, nonribosomal polypeptides and enzyme cofactors (McMurry, 2014). Due to their structural diversity and biological activities, natural products as leads to potential drugs play a significant role in discovery of drugs (Newman and Cragg, 2016). Usually, there are three ways to convert a natural product into a drug: develop the natural product as a drug directly, modify the natural product or synthesize a series of analogues, and use the natural product as a key scaffold for the synthesis of a library of analogues (Avery *et al*., 2010). With the search for lead compounds, a fascinating variety of secondary metabolic pathways have been revealed by feeding experiments and engineering biosynthetic gene clusters such as polyketide pathway, shikimate pathway, mevalonate pathway, methylerythritol phosphate pathway and non-ribosomal peptide pathway (Dewick, 2002). Furthermore, with the rapidly growing number of identified biosynthetic gene clusters (BGCs) of natural products, the genome mining approach was applied to express cryptic or silent BGCs, that have great potential to produce a variety of novel bioactive natural products for drug discovery over the past decade (Li *et al*., 2017).

1.1 Fungi as a rich source of pharmaceutical agents

Fungi obtain and assimilate nutrients from living or dead organisms and also produce various kinds of natural products (Kavanagh, 2017). The era of fungal drugs started in 1929 by Alexander Fleming and his discovery of the antibacterial agent penicillin from *Penicillium notatum* (Schaefer, 2015). In 1945 its structure was determined by X-ray crystallography as penicillin G with a four-membered *β*-lactam system, which is the active center by binding penicillin-binding proteins (PBP). Today, numerous marketed *β*-lactam antibiotics are produced by fermentation of high-producing strains with the applications of genetic engineering and by semi-synthesis using chemical and enzymatic process technology (Elander, 2003).

Griseofulvin isolated from *Penicillium griseofulvum* in 1939 has been used as an antifungal drug for treatment of ringworm in skin and nail in humans and animals (Petersen *et al*., 2014). Recently, griseofulvin gained attention for causing centrosomal clustering in tumor cells (Rebacz *et al*., 2007). Its mode-of-action towards fungi and mammalian cancer cells is not clear but it is interfering with the microtubule dynamics in a different way (Rønnest *et al*., 2012; Paguigan *et al*., 2017). Many analogs of griseofulvin were synthesized for the discovery of clinically used antifungal and anticancer agents (Petersen *et al*., 2014).

Lovastatin isolated from *Aspergillus terreus* was the first approved inhibitor of 3-hydroxy-3-methyl-glutaryl-CoA (HMG-CoA) reductase to reduce plasma cholesterol levels in 1987 (Tobert, 2003). Apart from this, lovastatin may have clinical utilization for chronic diseases viz bone fracture, Alzheimer's disease, Parkinson's disease, cancers, multiple sclerosis, rheumatoid arthritis and radiation-induced rectal injury (Pahan, 2006; Goswami *et al*., 2013; Anscher *et al*., 2016). Nowadays, various modifications of media and cultivation parameters are studied to increase the production of lovastatin by *A. terreus*. (Miranda *et al*., 2013; Rahim *et al*., 2017; Tarragó-Castellanos and Barrios-González, 2017). In recent studies on griseofulvin and lovastatin, significant new bioactivities have been found, offering promising opportunities for new applications. The drug repurposing strategy has great advantages

on clinical safety aspects and on reducing the cost of preclinical and clinical development (Cavalla, 2013; Cragg, Grothaus and Newman, 2014).

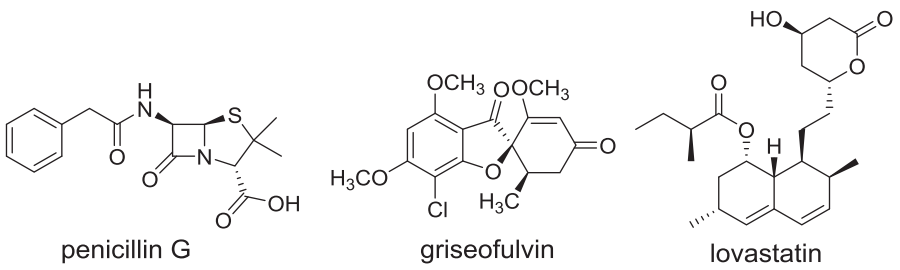

Figure 1.1 Structures of drugs from fungi.

Fungi-derived drugs have made significant contributions to the drug discovery process. Rapidly increasing number of new and bioactive secondary metabolites have been isolated from fungi in the past decades due to their wide distribution in living and non-living biota, far underexplored for cultivation, complex life cycles, suitable gene cluster for modification and investigation on fungal biosynthetic pathways (Aly, Debbab and Proksch, 2011; Wu and Yu, 2015). Fungal natural products have gained great attention to find new drugs and lead compounds for the treatment of cancers and serious infectious diseases. The approaches to increase the opportunity of searching new drugs from fungi involves dereplication of known bioactive compounds and expression of "silent" fungi and silent gene clusters (Harvey, *et al*., 2015; Gaudêncio and Pereira, 2015; Soukup and Keller, 2012).

1.2 Mining various ecological fungi

Due to the wide distribution and diversity of fungi, activities to mine various ecological fungi from soil, water, marine, plants, lichen, animals and even extreme environments have uncovered thousands of novel and bioactive natural products, including polyketides, alkaloids, terpenoids, peptides, lipids and so on (Blackwell, 2011; Hasan *et al*., 2015; Jalgaonwala, Mohite and Mahajan, 2017; Kellogg and Raja, 2017). Among the more than 5.1 million species of fungi, less than 3% of them have been investigated with regrad to bioactive secondary metabolites (Hawksworth, 2004; Blackwell, 2011). A significant number of natural products await to be uncovered from untapped fungal species.

1.2.1 Soil-derived fungi

"A handful of soil contains billions of microbial organisms," indicated a fact that soil is a mine of a great diversity of microorganisms, especially the soil near roots. More than 3,300 species of soil fungi are known and an estimated 70% of them are available in culture in 2006 (Gams, 2007). DNA metabarcoding data of soil samples revealed that soil fungal richness is correlated to environmental predictors, especially climatic factors, edaphic and spatial patterning, but is unrelated to plant diversity on global scale (Tedersoo *et al*., 2014; Tedersoo *et al*., 2016). A high fungal diversity and high cryptic diversity in tropical and subtropical areas presents an untapped soil fungal resource for discovery of drugs or lead compounds (Tedersoo *et al*. 2014). Six azaphilones and two new meroterpenes isolated from the Atlantic-forest-soil-derived fungus *Penicillium citreonigrum* caused inhibition of growth of *Staphylococcus epidermidis* (Wang *et al*., 2010). Aranorosin-2-methylether obtained from soil fungus *Gymnascella dankaliensis* showed cytotoxicity against the murine lymphoma cell line L5178Y with an IC_{50} value of 0.44 μM (Hammerschmidt *et al*. 2015).

1.2.2 Endolichenic fungi

Lichens are a self-sustaining symbiotic association between at least one photosynthetic organism and a filamentous fungus (Lutzoni and Miadlikowska, 2009). Lichen-associated fungi are potential producers of drugs or lead compounds, considering that about 20,000 lichen species are identified from about 8% of the land surface, more than 13,500 lichen-forming fungal species are adapted to live with their hosts and only 10% of them have been investigated for medicinal properties (Lutzoni and Miadlikowska, 2009; Blackwell, 2011; Singh, *et al*., 2017). A recent study indicated that crustose lichens are also a habitat of a great diversity of fungi for the exploitation of their metabolic potential (Muggia, Kopun and Grube, 2017). This result encouraged scientists to increase their efforts to study lichen-associated fungal diversity, ecological relationships with their hosts, cultivation and potential metabolites. Since the first natural product from endolichenic fungi was reported in 2007, hundreds of structurally diverse secondary metabolites have been isolated from endolichenic fungi and showed

different bioactivities, such as antibacterial, anticancer and antiviral activities (Kellogg and Raja, 2017; Singh, *et al*., 2017). Four new compounds were e.g. isolated from the endolichenic fungus *Aspergillus versicolor* obtained from the lichen *Lobaria retigera*. Among them, 8-*O*-methylversicolorin B showed cytotoxic activity against PC-3 cells and H460 cells with IC_{50} values of 12.6 and 17.3 μM, respectively (Lagarde *et al*., 2016).

1.2.3 Endophytic fungi

Endophytic fungi can be found in virtually every plant tissue especially in tropical rainforests without causing any noticeable symptoms of infection (Kusari, Pandey and Spiteller, 2013; Yan, *et al*., 2015). Endophytic fungi not only overcome host resistance but also maintain a balance with fungal and bacterial inhabitants that may produce potential antifungal and antibacterial agents to overcome drug resistance (Debbab and Proksch, 2013; Schulz *et al*., 2015). Another reason why secondary metabolites from endophytic fungi gained attention is that endophytes are capable of producing small molecules biosynthesized by their host-plants, such as the antineoplastic drug paclitaxel (Stierle *et al*., 1993) and camptothecin (Puri *et al*., 2005), anticancer lead drugs podophyllotoxin (Eyberger, Dondapati and Porter, 2006; Puri *et al*., 2006) and deoxypodophyllotoxin (Kusari, Lamshöft and Spiteller, 2009), or the antidepressant hypericin (Kusari *et al*., 2008). Endophytic fungi from traditional medicinal plants can be used for their production of biologically active compounds (Alvin, Miller and Neilan, 2014). Unluckily, the commercial production of above biopharmaceuticals by endophytic fungi in industrial scale has not been achieved due to low yield and unstable production (Kusari and Spiteller, 2011). Take paclitaxel for example, current study found that endophytic fungus *Penicillium aurantiogriseum* and plant *Taxus* have evolved paclitaxel biosynthetic pathways independently and not by horizontal gene transfer (Yang *et al*., 2014). This gave an explication for failures on previous genetic engineering of fungi by transferring paclitaxel biosynthetic genes from *Taxus* to fungi to improve paclitaxel biosynthesis (Wei *et al*., 2012). It remains important to explore the potential of endophytic fungi for lead drugs, particularly from uninvestigated tropical rainforests in developing countries.

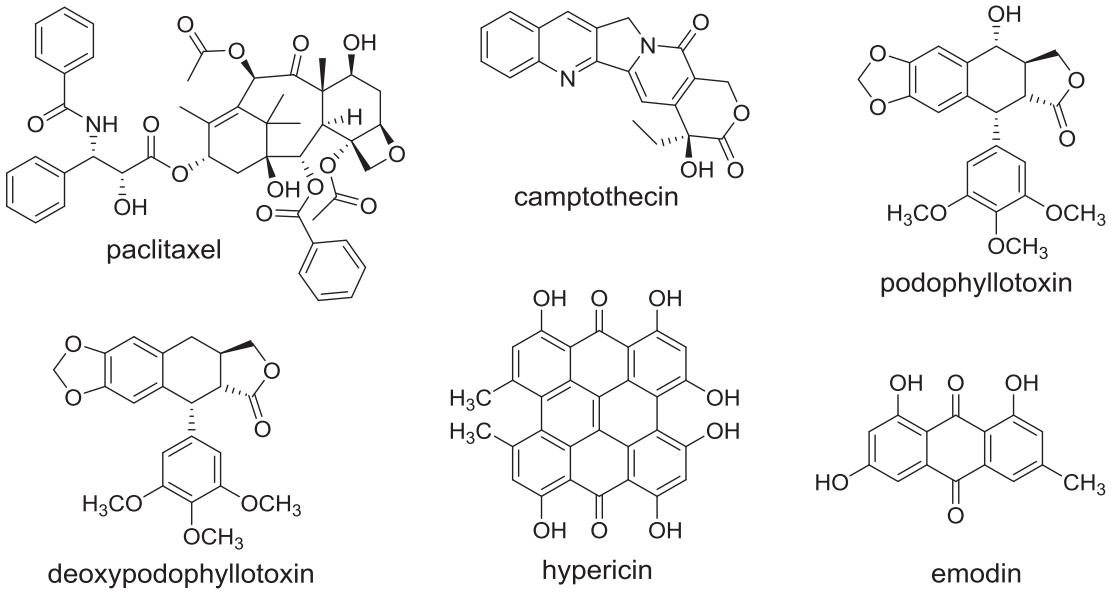

Figure 1.2.3 Structures of compounds produced by endophytic fungi.

1.2.4 Marine-derived fungi

Marine-derived fungi live in an environment with high salinity, high hydrostatic pressure, low water potential and different nutrient conditions from those of terrestrial habitats, which are an excellent source of bioactive natural products for lead structures (Raghukumar, 2008; Imhoff, 2016). Marine fungi are widely distributed from the surface of seawater to the deep sea, from the coast line to polar ice covers, from plants to animals in marine ecosystems (Hyde *et al*., 1998). Over the last two decades, a great number of secondary metabolites have been isolated from marine fungi derived from algae, sponges, mangroves and sediments, which possess antifungal, antibacterial, cytotoxic, and antiviral activities (Hasan *et al*., 2015; Xu *et al*., 2015; Imhoff, 2016; Daletos *et al*., 2017). Considering the fact that only about 1.5% of fungi from nearly 80,000 species have been described so far, the large potential of various bioactive secondary metabolites from the untapped diversity of marine fungi is still to be discovered (Imhoff, 2016; Raghukumar, 2017).

1.3 Dereplication

To improve chemical screening for novel secondary metabolites, dereplication was performed by combination of high performance liquid chromatography (HPLC) as

separation technique and mass spectrometry (MS) and/or nuclear magnetic resonance spectrometry (NMR) used as detection methods to identify known compounds or to follow the trail of target compounds in extracts or fractions (Kingston, 2011; Gaudêncio and Pereira, 2015). In-house libraries of secondary metabolites based on UV or MS, various databases (Antibase, Marinlit, Dictionary of Natural Products and Chemspider) and differential expression analysis softwares (MZmine, MZmatch and XCMZ for MS data and PCA or OPLS-DA for LC-NMR data) were used for identification (Harvey, *et al*., 2015; Gaudêncio and Pereira, 2015). Bioactivity screens together with dereplication based methods revealed numerous novel compounds from fungi (Nielsen and Larsen, 2015). The approach was applied during investigation of the endophyte fungus *Setophoma* sp., leading to the isolation of seven depsides that showed antibacterial activity (de Medeiros *et al*., 2015).

1.4 Mining silent gene clusters in fungi

Even though there are wide distribution and diversity of species of fungi on earth, only a fraction of fungi are obtained due to problems related to cultivation and re-isolation from different habitats, which led to the rediscovery of secondary metabolites (Appendino, Fontana and Pollastro, 2010). Furthermore, sequencing data of the fungal genomes indicated that a large part of secondary metabolic gene clusters are silent under standard laboratory culture conditions (Galagan *et al*., 2003; Debbab, Aly and Proksch, 2012; Rutledge and Challis, 2015). Several strategies for triggering silent gene cluster were applied, including the OSMAC (One Strain MAny Compounds) approach, co-cultivation, chemical epigenetic modulation and genetic modification (Wiemann and Keller, 2014).

1.4.1 OSMAC approach

OSMAC is an approach that may result in a steep accumulation of target compounds or enhanced diverse secondary metabolites from fungi by modification of cultivation parameters such as media type and composition, temperature, shape of culturing flask, and aeration (Daletos *et al*., 2017). For instance, the endophytic fungus

Paraphaeosphaeria quadriseptata produced several new compounds when cultivated in PDB medium prepared with distilled water rather than with tap water (Paranagama, Wijeratne and Gunatilaka, 2007). In addition, the marine-derived fungus *Trichoderma* sp. TPU199 produced two epidithiodiketopiperazines gliovirin and pretrichodermamide A when cultured in bacto-malt extract broth medium (Seephonkai *et al*., 2006). A further study found that this fungus utilizes halide ions from sodium halide in the medium and produced DC1149B, DC1149R and iododithiobrevamide (Yamazaki *et al*., 2015). Fermentation of the soil-derived fungus *Aspergillus* sp. under deuterium-enrichment conditions led to the isolation of six isotope-labeled metabolites with challenges for structure determination due to ion cluster in MS and signal overlap in NMR (Wang *et al*., 2015).

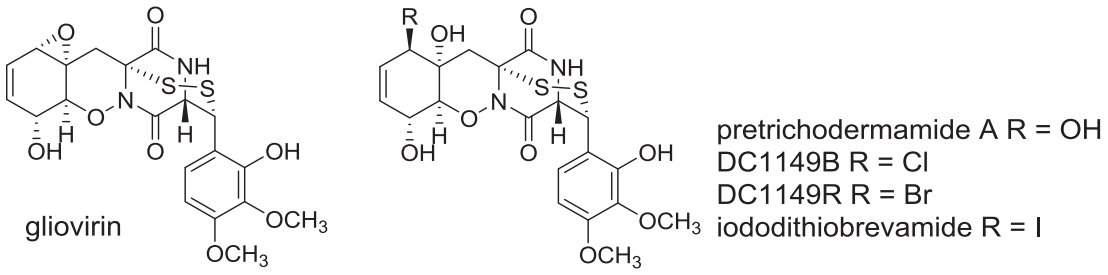

Figure 1.4.1 Structures of compounds produced by fungus *Trichoderma* sp. TPU199.

1.4.2 Co-cultivation

Fungi rarely occur in axenic form in their ecological habitats (Blackwell, 2011). To mimic the natural ecological situation, co-culture methods between fungi and bacteria, or between fungi and fungi were developed (Kusari, Pandey and Spiteller, 2013). Direct interaction among these microbes may activate silent gene clusters to trigger the production of new secondary metabolites (Marmann *et al*., 2014; Daletos *et al*., 2017). For example, co-cultivation of the fungal endophyte *Fusarium tricinctum* and *Bacillus subtilis* on solid rice medium yielded three new compounds macrocarpon C, 2-(carboxymethylamino)-benzoic acid and (–)-citreoisocoumarinol, which were not detected in axenic cultures of the fungus or the bacterium. Furthermore this co-cultivation led to an up to 78-fold enhanced production of the fungal secondary metabolite lateropyrone, which exhibited antibacterial activity against *B. subtilis* as

well as against the human pathogens *S. aureus*, *S. pneumoniae* and *E. faecalis* with MIC values ranging from 2 to 8 μg/mL (Ola *et al*., 2013). Co-cultivation of the endophytic fungi *Alternaria tenuissima* and *Nigrospora sphaerica* derived from the stems of *Smallanthus sonchifolius* increased the production of stemphyperylenol from *A. tenuissima*, which showed cytotoxic activity against *N. sphaerica* but no phytotoxicity to their host plant (Chagas, Dias and Pupo, 2013).

1.4.3 Epigenetic modulation

Epigenetic modulation can be used to increase the expression of secondary metabolic genes without alteration of the encoding sequence (Zheng *et al*., 2008). Two classes of inhibitors are commonly used including histone deacetylase (HDAC) inhibitors such as trichostatin A (TSA) and suberoylanilide hydroxamic acid (SAHA), and DNA methyltransferase (DNMT) inhibitors such as 5-azacytidine (5-AC) and 5-aza-2′-deoxcytidine (decitabine) (Cole, 2008; Xu *et al*., 2008). For instance, nygerone A with a 1-phenylpyridin-4(1*H*)-one core was isolated from the fungus *Aspergillus niger* ATCC 1015 upon treatment of the culture with the HDAC inhibitor SAHA (Henrikson *et al*., 2009).

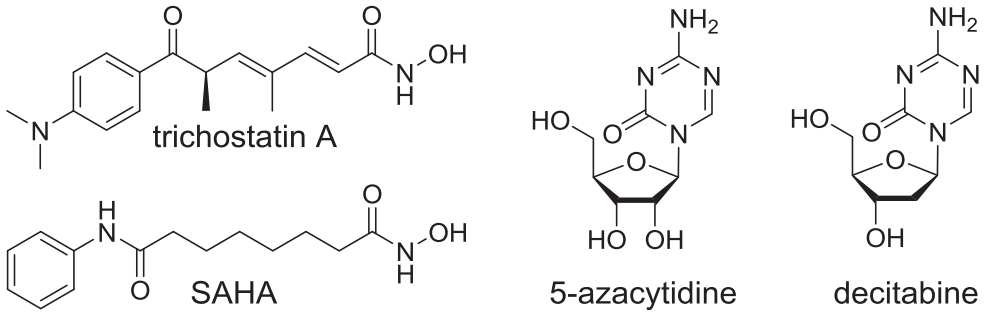

Figure 1.4.3 Structures of chemical epigenetics.

1.4.4 Genetic modification

Recently, in order to express the accumulation of cryptic biosynthetic gene clusters in fungi, a series of strategies have been applied for the discovery of natural products including genome mining, cloning, editing, amplification and deletion (Scharf and Brakhage, 2013; Li, Jiang and Lu, 2017). For example, by deletion of genes *PfCclA* and

*PfHdaA*in, the endophytic fungus *Pestalotiopsis fici* yielded fifteen new polyketides (Wu *et al*., 2016).

1.5 Aims and significance of this study

As mentioned above, fungi are potentially rich sources of structurally novel and bioactive natural products. The aim of this study was to investigate new bioactive natural products for anticancer and antibacterial properties from promising fungal strains, including the soil-dwelling fungus *Gymanscella dankaliensis*, the endolichenic fungus *Apiospora montagnei* and the endophytic fungus *Aspergillus aculeatus*. These three fungi were chosen based on cytotoxic and antibacterial activity screening of fungal crude extracts and dereplication by HPLC analysis with an in-house library of secondary metabolites based on UV and LC-MS analysis together with search in Antibase and Marinlit databases. OSMAC approaches and co-cultivation with bacteria were applied to enhance the diversity of secondary metabolites of fungi.

The soil-derived fungus *G. dankaliensis* produced seven new brominated tyrosine-derived alkaloids through cultivation on rice medium containing sodium bromide. In addition, it was found that addition of sodium chloride or ammonium chloride to the rice medium led to the isolation of two additional secondary metabolites from the endolichenic fungus *A. montagnei*. Furthermore, fermentation of the endophytic fungus *A. aculeatus* on rice medium containing sodium nitrate resulted in the accumulation of nine new indole alkaloids. In summary, several types of secondary metabolites were isolated from the fermentation of these fungi including brominated tyrosine-derived alkaloids, diterpenoids, pyridine alkaloids, xanthone derivatives, secalonic acids and indole alkaloids. X-ray crystallographic analysis and Marfey's method were applied to determine the absolute configuration of the respective compounds.

The isolated natural products were subjected to cytotoxicity assays against the mouse lymphoma cell line L5178Y and the human ovarian cancer cell line A2780, as well as to antibacterial activities against *Streptomyces lividans*, *Bacillus subtilis*, *Bacillus cereus* and *Mycobacterium tuberculosis*.

Publication 1

Targeted solid phase fermentation of the soil dwelling fungus *Gymnascella dankaliensis* yields new brominated tyrosine-derived alkaloids

Published in "*Royal Society of Chemistry Advances*".

RSC Advances

PAPER

View Article Online
View Journal | View Issue

CrossMark click for updates

Cite this: *RSC Adv.*, 2016, **6**, 81685

Targeted solid phase fermentation of the soil dwelling fungus *Gymnascella dankaliensis* yields new brominated tyrosine-derived alkaloids†

Hao Wang,[a] Haofu Dai,[b] Christian Heering,[c] Christoph Janiak,[c] Wenhan Lin,[d] Raha S. Orfali,[e] Werner E. G. Müller,[f] Zhen Liu*[a] and Peter Proksch*[a]

Received 5th June 2016
Accepted 19th August 2016

DOI: 10.1039/c6ra14554j

www.rsc.org/advances

Seven new brominated tyrosine-derived alkaloids, gymnastatins T–Y (**1–6**) and dankastatin D (**7**), together with three known likewise brominated analogues gymnastatins I–K (**8–10**) were isolated from the soil fungus *Gymnascella dankaliensis* through fermentation on solid rice medium following addition of NaBr. None of these compounds were detected when the fungus was cultured on rice that either lacked NaBr or that contained NaCl instead, indicating a remarkable plasticity of the fungal secondary metabolism. All structures were elucidated on the basis of one and two dimensional NMR spectroscopic analyses and MS data. The absolute configuration of the new gymnastatin T (**1**) was determined by X-ray crystallographic data. All isolated alkaloids showed potent to moderate cytotoxicity against the L5178Y mouse lymphoma cell line with IC_{50} values ranging from 0.078 to 14.1 μM.

Introduction

More than 5000 halogenated natural products have been reported so far with many of them exhibiting a variety of biological activities including antibacterial, antifungal, antiviral, antitumor, anti-inflammatory, and antioxidant activity.[1–3] Fungi are known as rich sources of numerous bioactive metabolites and receive increasing attention in the quest for new drug candidates[4] as exemplified by plinabulin[5] which is currently in clinical trials as a new anticancer drug or by the antifungal echinocandins.[6] Numerous fungal metabolites are chlorinated, however, only few brominated fungal metabolites have been isolated so far.[7] Two classes of halogenating enzymes including halogenases and haloperoxidases have been discovered from a broad range of organisms and the mechanisms of enzymatic halogenation were described as well.[8] In recent years several halogenated natural products have been obtained by culturing fungi in media containing halogen salts.[9–11] The plasticity of halogenating enzymes with regard to accepting different halogens can be applied for a targeted fermentation since adding different halogens (*e.g.* NaCl or NaBr) to the medium will direct the fungal metabolism in producing mainly chlorinated[12] or alternatively brominated metabolites as shown in this study.

The soil dwelling fungus *Gymnascella dankaliensis* that was isolated from desert sand close to the pyramids of Giza provides an excellent example for the application of this experimental approach. This fungus which has also been reported from a marine *Halichondria* sponge is known to produce a variety of mainly chlorinated tyrosine derived alkaloids.[13–17] In a previous study[12] we could show that addition of KBr to rice medium resulted in bromination of fungal metabolites as indicated by the typical isotope peaks during LC-MS analysis of the respective extracts. The nature of the brominated compounds could, however, not be elucidated. We have now obtained seven new brominated tyrosine-derived alkaloids, gymnastatins T–Y (**1–6**) and dankastatin D (**7**), as well as three likewise brominated known analogues following fermentation of *G. dankaliensis* on solid rice medium containing NaBr as halogen source. All isolated alkaloids were tested against the L5178Y mouse lymphoma cells and showed significant to moderate activity (Fig. 1).

[a]*Institute of Pharmaceutical Biology and Biotechnology, Heinrich-Heine-Universität Düsseldorf, Universitätsstrasse 1, 40225 Düsseldorf, Germany. E-mail: zhenfeizi0@sina.com; proksch@uni-duesseldorf.de*

[b]*Key Laboratory of Biology and Genetic Resources of Tropical Crops, Ministry of Agriculture, Institute of Tropical Bioscience and Biotechnology, Chinese Academy of Tropical Agricultural Sciences, Haikou 571101, China*

[c]*Institute of Inorganic and Structural Chemistry, Heinrich-Heine-University Düsseldorf, Universitätsstrasse 1, 40225 Düsseldorf, Germany*

[d]*State Key Laboratory of Natural and Biomimetic Drugs, Peking University, Beijing 100191, China*

[e]*Department of Pharmacognosy, Faculty of Pharmacy, King Saud University, Riyadh, Saudi Arabia*

[f]*Institut für Physiologische Chemie, Universitätsmedizin der Johannes Gutenberg-Universität Mainz, Duesbergweg 6, 55128 Mainz, Germany*

† Electronic supplementary information (ESI) available: MS, 1D and 2D NMR spectra of compounds **1–7**, as well as X-ray crystallographic parameters of **1**. CCDC 1481781. For ESI and crystallographic data in CIF or other electronic format see DOI: 10.1039/c6ra14554j

Publication 1

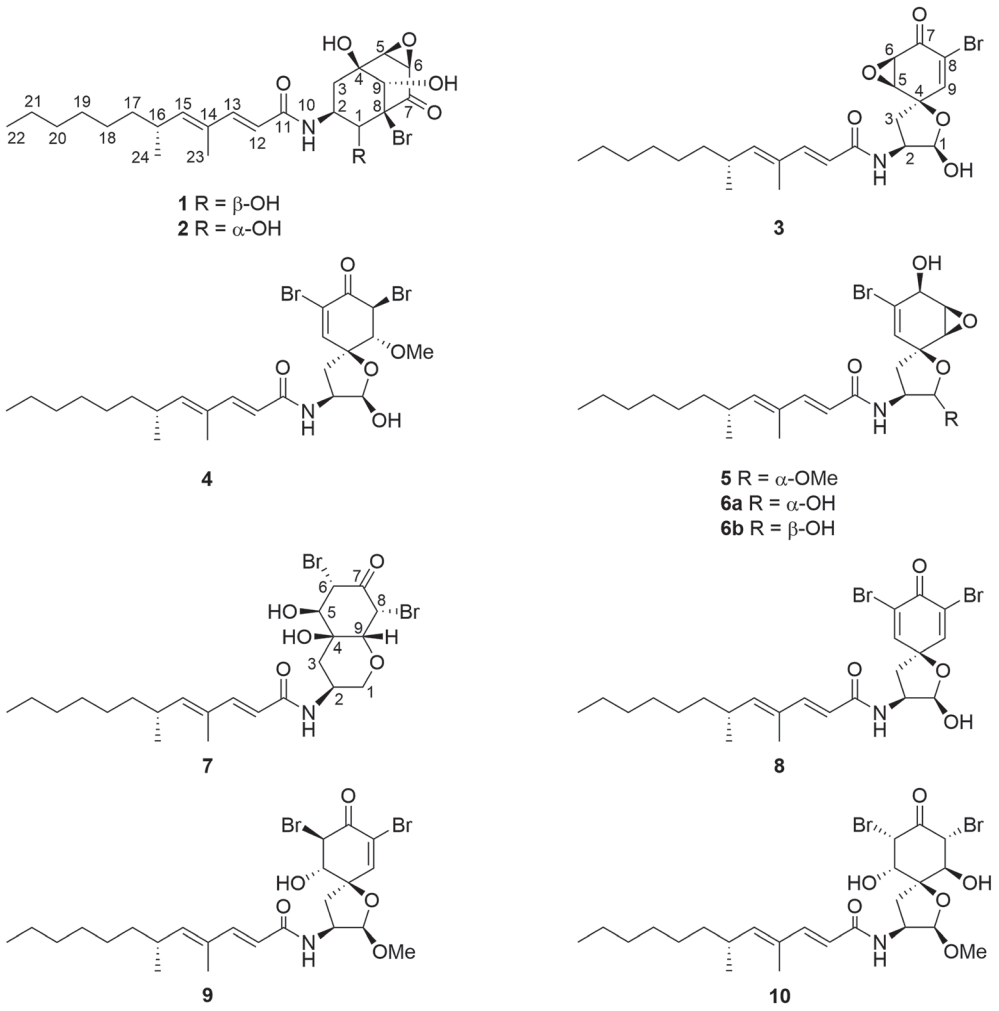

Fig. 1 Structures of compounds isolated from *G. dankaliensis*.

Results and discussion

Gymnastatin T (**1**) possessed the molecular formula $C_{23}H_{34}BrNO_6$ as evident from its HRESIMS. Comparison of its ^{1}H and ^{13}C NMR data (Table 1) with those of the known brominated gymnastatins I–K (**8–10**)[16] indicated the presence of a branched aliphatic chain from C-11 to C-22. This was further confirmed by the COSY correlations between H-12/H-13, H-15/H-16, H-16/H_{ab}-17, H-16/H_3-24, and H_2-21/H_3-22, in addition to the HMBC correlations from H-10 and H-12 to C-11, from H_3-23 to C-13, C-14, and C-15, from H_3-24 to C-15, C-16, and C-17, from H-17a (δ_H 1.32) to C-18 and C-19, and from H_3-22 to C-20 and C-21 (Fig. 2). The remaining ^{1}H and ^{13}C signals of **1** were comparable to those of gymnastatin G.[14] The nature of the bicyclo[3.3.1]nonane ring was established by the COSY correlations between 1-OH/H-1, H-1/H-2, H-2/H-3α, H-2/H-3β, H-2/NH-10, H-5/H-6, and 9-OH/H-9, as well as by key HMBC correlations from 1-OH to C-1, C-2, and C-8, from H-3α and H-3β to C-4, C-5, and C-9, from 4-OH to C-3, C-4, C-5, and C-9, from H-6 and H-9 to C-7, and from 9-OH to C-4, C-8, and C-9. Assignments of the remaining oxygen atom linked to C-5 and C-6, and of the bromine atom at C-8 were indicated by the chemical shifts of the respective carbons [δ_C 59.1 (C-5), 53.7 (C-6), and 78.7 (C-8)]. The HMBC correlation from NH-10 to C-11 indicated the linkage between the aliphatic chain and the bicyclononane ring *via* an amide bond. Thus, the planar structure of **1** was elucidated as shown. The coupling constants ($^3J_{1,2}$ = 2.8 Hz, $^3J_{2,3\alpha}$ = 5.5 Hz, and $^3J_{2,3\beta}$ = 12.8 Hz) together with the NOE correlations between H-1/H-2, H-2/H-3α, H-3α/H-5, H-5/H-6, and between 1-OH/NH-10, NH-10/H-3β, H-3β/H-9, H-9/1-OH suggested a chair conformation of the cyclohexane ring (C-1 to C-4, C-9, C-8) with H-1, H-2, H-3α, H-5 and H-6 being on the same face of the ring while 1-OH, NH-10, H-3β, and H-9 were oriented to the opposite face (Fig. 3). The large coupling constants ($^3J_{12,13}$ = 15.5 Hz) and the NOE correlations between H-12/H_3-23, and H-13/H-15 indicated 12*E*, 14*E* configuration. The absolute configuration of **1** was determined as 1*S*, 2*S*, 4*R*, 5*S*, 6*R*, 8*S*, 9*S*, and 16*R* by X-ray single crystal analyses (Fig. 4).

The molecular formula of gymnastatin U (**2**) was identical to that of **1** as indicated by HRESIMS. Detailed analysis of the ^{1}H, ^{13}C NMR and of the 2D NMR data indicated that both compounds shared the same gross structure. The $^3J_{1,2}$ value of **2**

Publication 1

Table 1 ^{1}H and ^{13}C NMR data of compounds **1** and **2**

	1[a]		**1**[b]		**2**[b]	
No.	δ_C	δ_H (J in Hz)	δ_C	δ_H (J in Hz)	δ_C	δ_H (J in Hz)
1	74.6, CH	3.67, dd (5.9, 2.8)	76.8, CH	3.83, d (2.8)	80.2, CH	3.92, d (10.7)
2	46.3, CH	3.84, dddd (12.8, 7.7, 5.5, 2.8)	47.8, CH	4.09, ddd (11.0, 7.1, 2.8)	50.9, CH	4.12, ddd (12.7, 10.7, 5.5)
3α	35.6, CH_2	1.88, dd (12.8, 5.5)	36.5, CH_2	2.09, dd (13.0, 7.1)	39.0, CH_2	2.34, dd (13.4, 5.5)
3β		1.92, dd (12.8, 12.8)		2.07, dd (13.0, 11.0)		1.74, dd (13.4, 12.7)
4	69.4, C		71.0, C		70.9, C	
5	59.1, CH	3.60, dd (3.8, 2.2)	60.9, CH	3.66, dd (3.8, 2.3)	60.8, CH	3.63, dd (3.7, 2.0)
6	53.7, CH	3.79, d (3.8)	55.9, CH	3.80, d (3.8)	54.3, CH	3.68, d (3.7)
7	199.8, C		199.7, C		195.1, C	
8	78.7, C		77.9, C		80.3, C	
9	73.5, CH	3.97, dd (8.6, 2.2)	75.8, CH	4.15, d (2.3)	79.8, CH	3.85, d (2.0)
10		8.02, d (7.7)				
11	164.7, C		168.5, C		169.3, C	
12	119.5, CH	5.99, d (15.5)	118.8, CH	5.99, d (15.4)	119.0, CH	5.91, d (15.4)
13	144.0, CH	6.97, d (15.5)	147.6, CH	7.16, d (15.4)	147.5, CH	7.18, d (15.4)
14	130.9, C		132.7, C		132.6, C	
15	145.6, CH	5.59, d (9.8)	148.5, CH	5.62, d (9.8)	148.5, CH	5.64, d (9.7)
16	32.4, CH	2.49, m	34.3, CH	2.56, m	34.3, CH	2.56, m
17	36.7, CH_2	1.32, m; 1.21, m	38.4, CH_2	1.38, m; 1.27, m	38.4, CH_2	1.39, m; 1.27, m
18	26.9, CH_2	1.19, m	28.6, CH_2	1.26, m	28.6, CH_2	1.26, m
19	28.7, CH_2	1.22, m	30.5, CH_2	1.27, m	30.5, CH_2	1.28, m
20	31.2, CH_2	1.22, m	33.0, CH_2	1.27, m	33.0, CH_2	1.27, m
21	22.0, CH_2	1.24, m	23.7, CH_2	1.28, m	23.7, CH_2	1.30, m
22	13.9, CH_3	0.84, t (7.0)	14.4, CH_3	0.89, t (7.0)	14.4, CH_3	0.89, t (7.1)
23	12.4, CH_3	1.70, s	12.7, CH_3	1.79, s	12.7, CH_3	1.80, s
24	20.5, CH_3	0.93, d (6.6)	20.9, CH_3	0.98, d (6.7)	20.9, CH_3	0.99, d (6.7)
1-OH		6.49, d (5.9)				
4-OH		5.94, s				
9-OH		4.62, d (8.6)				

[a] Measured in DMSO-d_6. [b] Measured in methanol-d_4.

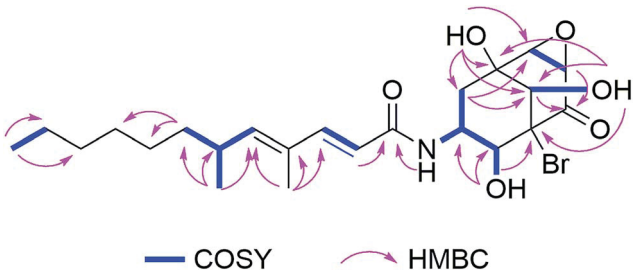

Fig. 2 Key COSY and HMBC correlations for **1**.

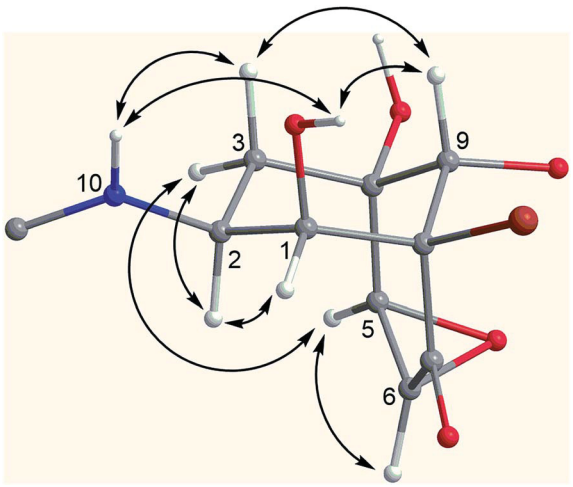

Fig. 3 Key NOE correlations and computer-generated model using MM2 force field calculations for **1**.

(10.7 Hz), however, was much larger than that of **1** (2.8 Hz), suggesting **2** to be the 1-epimer of **1**. In the ROESY spectrum of **2**, the observed correlations between H-2/H-3α, H-3α/H-5, and between H-1/H-3β, H-3β/H-9, H-9/H-1 confirmed this assumption. Based on the close biogenetic similarity of **1** and **2** as well as the X-ray structure of **1**, the absolute configuration of **2** can be assumed to be 1*R*, 2*S*, 4*R*, 5*S*, 6*R*, 8*S*, 9*S*, and 16*R*.

Gymnastatin V (**3**) had the molecular formula $C_{23}H_{32}BrNO_5$ as established by HRESIMS, indicating the loss of one Br atom and addition of one further oxygen and one proton compared to the known gymnastatin I (**8**).[16] The ^{1}H and ^{13}C NMR data of **3** (Table 2) were very similar to those of **8**, except for the replacement of the C-5/C-6 double bond of **8** by an epoxy ring as indicated by the characteristic resonances at δ_C 58.2 (C-5), 52.4 (C-6), and δ_H 3.80 (H-5), 3.63 (H-6), respectively. The HMBC correlations from H-5 to C-4 (δ_C 81.2) and C-9 (δ_C 147.4), from H-6 to C-7 (δ_C 186.3) and C-8 (δ_C 119.0), as well as from H-3α (δ_H

Publication 1

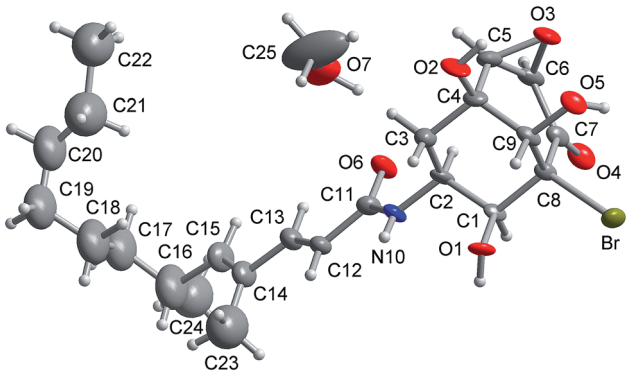

Fig. 4 Molecular structure of **1** (with a methanol molecule) from single-crystal X-ray diffractometry.

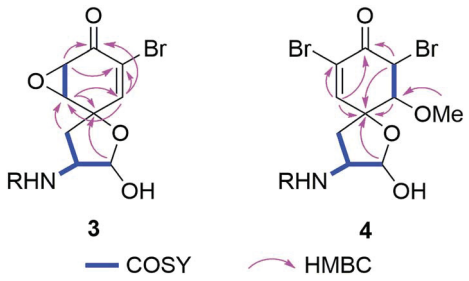

Fig. 5 Key COSY and HMBC correlations for **3** and **4**.

2.55), H-3β (δ_H 2.16) and H-9 (δ_H 6.94) to C-5 confirmed the location of this epoxy group at the C-5/C-6 position (Fig. 5). The remaining structure of **3** was identical to that of **8** as indicated by 2D NMR. The NOE relationships between H-1/H-2, H-1/H-9, H-2/H-3α, H-2/H-9, and H-3α/H-9 of **3** indicated that these protons were oriented on the same face, whereas the NOE correlations between NH-10/H-3β, H-3β/H-5, and H-5/H-6 suggested that these latter protons were oriented towards the opposite side (Fig. 6). The geometries of the double bonds in the aliphatic side chain were determined as 12*E* and 14*E*, respectively based on their coupling constants and NOE correlations as described for **1**. Thus, the structure of **3** was elucidated as shown.

Gymnastatin W (**4**) shared the same molecular formula as gymnastatin J (**9**).[16] Both compounds differed only by the positions of their methoxy and hydroxy groups as indicated by detailed analysis of their 2D NMR spectra. The assignment for the methoxy group at C-9 in **4** was evident from the COSY correlation between H-8 (δ_H 4.57) and H-9 (δ_H 3.68) in addition to the HMBC correlations from 9-OMe (δ_H 3.67) to C-9 (δ_C 85.9) and from H-8 to C-7 (δ_C 183.1). Analysis of the COSY and HMBC spectra led to the planar structure of **4** (Fig. 5). The large

Table 2 ^{1}H and ^{13}C NMR data of compounds **3**–**5**

	3[a]		**4**[a]		**5**[b]	
No.	δ_C	δ_H (J in Hz)	δ_C	δ_H (J in Hz)	δ_C	δ_H (J in Hz)
1	96.4, CH	5.56, d (4.4)	96.4, CH	5.55, d (4.4)	110.0, CH	4.96, s
2	51.9, CH	4.78, m	52.6, CH	4.76, m	57.5, CH	4.40, dd (7.3, 2.2)
3α	38.8, CH_2	2.55, dd (13.0, 8.5)	33.6, CH_2	2.83, dd (12.4, 8.6)	40.6, CH_2	2.56, dd (14.1, 7.3)
3β		2.16, dd (13.0, 10.8)		1.80, dd (12.4, 10.6)		1.87, dd (14.1, 2.2)
4	81.2, C		86.4, C		84.4, C	
5	58.2, CH	3.80, dd (3.8, 2.6)	153.9, CH	7.46, s	133.2, CH	6.09, dd (2.4, 1.7)
6	52.4, CH	3.63, d (3.8)	119.9, C		125.0, C	
7	186.3, C		183.1, C		67.6, CH	4.35, dd (2.8, 1.7)
8	119.0, C		54.7, CH	4.57, d (11.5)	55.7, CH	3.54, dd (4.1, 2.8)
9	147.4, CH	6.94, d (2.6)	85.9, CH	3.68, d (11.5)	59.3, CH	3.40, dd (4.1, 2.4)
10		6.12, d (8.1)		5.95, d (8.4)		
11	166.8, C		166.6, C		169.2, C	
12	116.7, CH	5.76, d (15.3)	117.0, CH	5.75, d (15.3)	118.6, CH	6.01, d (15.4)
13	147.7, CH	7.26, d (15.3)	147.3, CH	7.24, d (15.3)	147.7, CH	7.19, d (15.4)
14	130.7, C		130.8, C		132.7, C	
15	148.8, CH	5.68, d (9.8)	148.4, CH	5.66, d (9.7)	148.4, CH	5.65, d (9.8)
16	33.2, CH	2.50, m	33.2, CH	2.50, m	34.3, CH	2.57, m
17	37.2, CH_2	1.35, m; 1.25, m	37.2, CH_2	1.35, m; 1.26, m	38.4, CH_2	1.40, m; 1.27, m
18	27.4, CH_2	1.21, m	27.5, CH_2	1.21, m	28.3, CH_2	1.28, m
19	29.4, CH_2	1.23, m	29.4, CH_2	1.24, m	30.4, CH_2	1.28, m
20	31.8, CH_2	1.22, m	31.8, CH_2	1.23, m	33.0, CH_2	1.27, m
21	22.6, CH_2	1.26, m	22.6, CH_2	1.27, m	23.3, CH_2	1.30, m
22	14.1, CH_3	0.86, t (7.1)	14.1, CH_3	0.87, t (7.0)	14.4, CH_3	0.89, t (7.0)
23	12.5, CH_3	1.76, s	12.5, CH_3	1.76, s	12.5, CH_3	1.81, s
24	20.5, CH_3	0.97, d (6.6)	20.5, CH_3	0.97, d (6.6)	20.8, CH_3	1.00, d (6.7)
1-OMe					54.9, CH_3	3.41, s
9-OMe			62.6, CH_3	3.67, s		

[a] Measured in $CDCl_3$. [b] Measured in methanol-d_4.

Publication 1

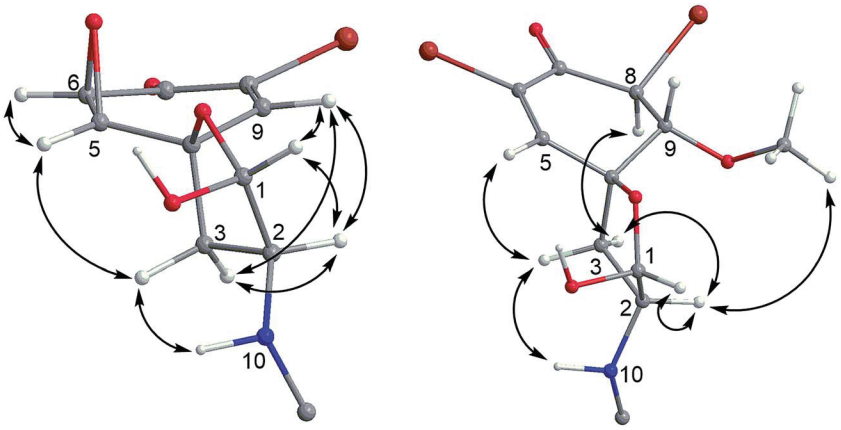

Fig. 6 Key NOE correlations and computer-generated models using MM2 force field calculations for **3** (left) and **4** (right).

coupling constant between H-8 and H-9 (11.5 Hz) along with the NOE correlations between H-1/H-2, H-2/H-3α, H-2/9-OMe, H-3α/H-8, and between NH-10/H-3β, H-3β/H-5 revealed that H-1, H-2, H-8, and 9-OMe were oriented at the same face of the ring as H-3α whereas H-5 and NH-10 were oriented to the opposite face as found also for H-3β. The above evidence led to assignment of the relative configuration of **4** as shown in Fig. 6.

The molecular formula of gymnastatin X (**5**) was established as $C_{24}H_{36}BrNO_5$ as indicated by HRESIMS. The 1 : 1 isotopic peaks at *m*/*z* 498 and 500 indicated the presence of one bromine atom in the structure. Its NMR data closely resembled those of the known chlorinated compound gymnastatin D.[13] Inspection of 2D NMR spectra of **5** indicated the replacement of chlorine by bromine at C-6 and the appearance of an additional methoxy group (δ_C 54.9 and δ_H 3.41) at C-1, which was evident from the HMBC correlation from the methoxy protons to C-1 (δ_C 110.0) and in turn from H-1 (δ_H 4.96) to the methoxy carbon (Fig. 7). When comparing the NMR data of **5** with those of the reported C-1 isomers of gymnastatin D, the coupling constants $^3J_{1,2}$ (close to zero), $^3J_{2,3\alpha}$ (7.3 Hz), $^3J_{2,3\beta}$= (2.2 Hz), $^4J_{5,7}$ (1.7 Hz), $^4J_{5,9}$= (2.4 Hz), $^3J_{7,8}$ (2.8 Hz), $^3J_{8,9}$= (4.1 Hz) and the correlations between H-2/H-3α, H-3α/H-9, H-1/H-3β and H-3β/H-5 detected in the ROESY spectrum of **5** indicated its relative configuration as shown (Fig. 8).

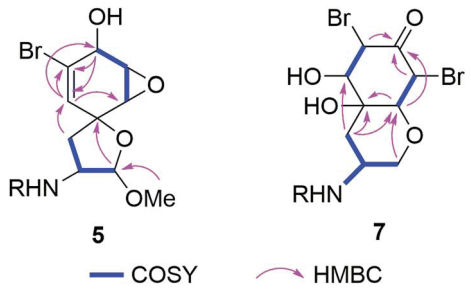

Fig. 7 Key COSY and HMBC correlations for **5** and **7**.

Gymnastatin Y (**6**) had the molecular formula $C_{23}H_{34}BrNO_5$ as determined by HRESIMS, lacking a methyl group compared to **5**, which was confirmed by the disappearance of the methoxy group signal in the NMR spectra of **6**. HPLC analysis and NMR spectra (Table 3) of **6** suggested that it existed as a 3 : 1 mixture of two stereoisomers (**6a** and **6b**) as previously also reported for gymnastatin D.[13] The ^{1}H NMR data of **6a** were very similar to those of **5**, except for the absence of the methoxy group at C-1. Interpretation of 2D NMR indicated that **6a** and **6b** were stereoisomers of 1-demethoxy gymnastatin X (**5**). Compound **6a**

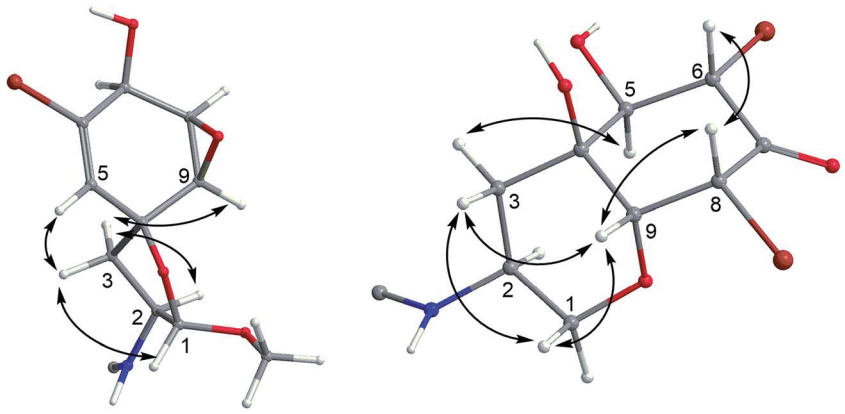

Fig. 8 Key NOE correlations and computer-generated model using MM2 force field calculations for **5** (left) and **7** (right).

Publication 1

Table 3 ^{1}H and ^{13}C NMR data of compounds **6** and **7**

	6a[a]		**6b**[a]		**7**[b]	
No.	δ_C	δ_H (J in Hz)	δ_C	δ_H (J in Hz)	δ_C	δ_H (J in Hz)
1α			97.0, CH	5.37, d (4.3)	71.2, CH_2	4.18, m
1β	103.3, CH	5.38, s				3.15, t (11.0)
2	58.2, CH	4.33, m	53.3, CH	4.55, ddd (11.6, 8.1, 4.3)	43.4, CH	4.27, m
3α	40.8, CH_2	2.59, m	37.5, CH_2	2.37, dd (12.7, 8.1)	39.7, CH_2	2.72, ddd (12.4, 4.7, 1.5)
3β		1.90, m		2.04, dd (12.7, 11.6)		1.49, dd (12.4, 12.4)
4	83.6, C		81.6, C		72.6, C	
5	134.9, CH	6.06, m	134.9, CH	6.06, m	73.8, CH	4.19, m
6	124.4, C		124.4, C		58.8, CH	4.89, d (9.9)
7	67.7, CH	4.34, m	67.7, CH	4.34, m	188.1, C	
8	55.4, CH	3.53, m	55.4, CH	3.53, m	52.2, CH	5.29, dd (3.3, 1.0)
9	59.6, CH	3.52, m	58.1, CH	3.40, m	83.5, CH	3.90, d (3.3)
10						5.22, d (8.3)
11	169.3, C		169.3, C		166.2, C	
12	119.0, CH	6.04, d (15.4)	119.0, CH	6.04, d (15.4)	116.2, CH	5.67, d (15.2)
13	147.5, CH	7.19, d (15.4)	147.5, CH	7.19, d (15.4)	147.8, CH	7.24, d (15.2)
14	132.8, C		132.8, C		130.7, C	
15	148.4, CH	5.64, d (9.5)	148.4, CH	5.64, d (9.5)	148.6, CH	5.67, d (9.8)
16	34.3, CH	2.56, m	34.3, CH	2.56, m	33.1, CH	2.50, m
17	38.4, CH_2	1.39, m; 1.27, m	38.4, CH_2	1.39, m; 1.27, m	37.0, CH_2	1.35, m; 1.25, m
18	28.6, CH_2	1.26, m	28.6, CH_2	1.26, m	27.1, CH_2	1.21, m
19	30.5, CH_2	1.27, m	30.5, CH_2	1.27, m	29.4, CH_2	1.25, m
20	33.0, CH_2	1.27, m	33.0, CH_2	1.27, m	31.6, CH_2	1.23, m
21	23.7, CH_2	1.29, m	23.7, CH_2	1.29, m	22.4, CH_2	1.27, m
22	14.4, CH_3	0.89, t (7.0)	14.4, CH_3	0.89, t (7.0)	13.9, CH_3	0.87, t (7.0)
23	12.7, CH_3	1.81, s	12.7, CH_3	1.81, s	12.3, CH_3	1.75, s
24	20.9, CH_3	0.99, d (6.7)	20.9, CH_3	0.99, d (6.7)	20.3, CH_3	0.97, d (6.7)

[a] Measured in methanol-d_4. [b] Measured in $CDCl_3$.

possessed similar $^{3}J_{1,2}$ value (almost zero) and NOE correlations as **5**, suggesting that both shared the same relative configuration, whereas the larger coupling constant between H-1 and H-2 (4.3 Hz) and NOE correlations between H-1 and H-2 observed for **6b** suggested an opposite configuration at C-1.

Compound **7** had the molecular formula $C_{23}H_{35}Br_2NO_5$ as indicated by HRESIMS. Comparison of its NMR spectroscopic data (Table 3) with those of gymnastatins T–Y (**1–6**) suggested that it featured a different bicyclic ring system but shared the same aliphatic side chain. Further analysis of 2D NMR spectra of **7** suggested the presence of the same ring system as reported earlier for dankastatins A–C.[15,17] This was confirmed by the COSY correlations between H-1α/H-2, H-1β/H-2, H-2/H-3α, H-2/H-3β, H-5/H-6, and H-8/H-9 as well as by the HMBC correlations from H-1β and H-3α to C-9, from H-3β to C-4 and C-5, and from H-6 and H-9 to C-7 (Fig. 7). The location of the two bromine atoms was deduced by comparing the carbon signals with those of dankastatins A–C. The coupling constants between H-1β and H-2 ($J_{1\beta,2}$ = 11.0 Hz), between H-2 and H-3β ($J_{2,3\beta}$ = 12.4 Hz), and between H-5 and H-6 ($J_{5,6}$ = 9.9 Hz) indicated *trans*-axial arrangement of these protons. Combined with the NOE correlations between H-1β/H-3β, H-1β/H-9, H-3β/H-9, H-9/H-8, H-8/H-6, and between H-5/H-3α, the relative configuration of the ring system was determined as shown in Fig. 8. The stereochemistry of the side chain was assigned as 12*E* and 14*E* due to the large coupling constants ($^{3}J_{12,13}$ = 15.2 Hz) and the NOE correlations between H-12/H_3-23, and H-13/H-15. Therefore, the structure of **7** was elucidated and the compound was named dankastatin D.

The three known analogues were identified as gymnastatins I–K (**8–10**) by comparison of their NMR and mass spectroscopic data with the literature.[16]

Cytotoxicity of all isolated alkaloids (**1–10**) was evaluated against the mouse lymphoma cell line (L5178Y) (Table 4). Among them, compounds **1**, **4**, **8** and **9** exhibited significant activity with IC_{50} values of 1.3, 0.99, 0.55 and 0.078 μM, respectively, even stronger than that of positive control kahalalide F. Comparison of the cytotoxicity of **4** *vs.* **6** and **9** *vs.* **10** suggested the conjugated ketone system to be important for the activity of those compounds. Gymnastatin I (**8**) showed similar activity compared to its chlorinated analogue gymnastatin A, whereas gymnastatin J (**9**) exhibited much stronger activity than its chlorinated analogue gymnastatin B.

When comparing the structures of the brominated alkaloids isolated in our study with those of chlorinated analogues reported previously,[12–17] it became evident that addition of NaBr to the medium caused an increase in the structural diversity of the fungal metabolites. Gymnastatins T (**1**), V (**3**), Y (**6**), I (**8**), J (**9**), and K (**10**) can be considered to be derivatives of gymnastatins G,[14] aranochlor A,[18] gymnastatin D, A, B, and C,[13] that are formed by a mere replacement of chlorine atoms *vs.* bromine atoms, whereas the structures of gymnastatins U (**2**), V (**4**), Y (**5**),

Table 4 Cytotoxicity of isolated brominated alkaloids

Compound	IC_{50} (μM)
1	1.3
2	3.0
3	3.6
4	0.99
5	14.1
6	6.2
7	3.0
8	0.55
9	0.078
10	9.6
Gymnastatin A	0.64[b]
Gymnastatin B	5.8[b]
Kahalalide F[a]	4.3

[a] Positive control. [b] Data from ref. 12.

and K (**7**) differ also with regard to other substituents and/or their stereochemistry, compared to their chlorinated analogues.

The brominated tyrosine-derived alkaloids isolated in this study (**1–10**) can be divided into three different subtypes including bicyclo[3.3.1]nonane derivatives (**1** and **2**), 1-oxa-spiro [4.5]decane derivatives (**3–6** and **8–10**), and 2-oxa-bicyclo[4.4.0] decane derivative (**7**). A plausible biosynthetic pathway modified after Hammerschmidt *et al.*[12] and Amagata *et al.*[14] is proposed. Gymnastatin N is suggested to be an important intermediate, which is corroborated by the co-isolation of its oxidative product 12′-hydroxygymnastatin N (**11**) and aldehyde product (**12**) originating from reduction of the carboxyl group of gymnastatin N (Fig. 9). The present study provides further evidence regarding the biosynthetic relationships of *Gymnascella* derived alkaloids, and proved the plasticity of the fungal secondary metabolism, which can be useful for biosynthetic research and the quest for new bioactive compounds.

Experimental section

General procedures

Optical rotations were measured with a Jasco P-2000 polarimeter. NMR spectra were recorded on a Bruker ARX 600 NMR spectrometer. Chemical shifts were referenced to the solvent residual peaks. Mass spectra (ESI) were recorded with a LC-MS HP1100 Agilent Finnigan LCQ Deca XP Thermoquest and HRESIMS were recorded with a UHR-QTOF maXis 4G (Bruker Daltonics) mass spectrometer. HPLC analysis was performed with a Dionex UltiMate-3400SD system coupled with an LPG-3400SD pump and a photodiode array detector (DAD 300RS). The analytical column (125 × 4 mm) was prefilled with Eurosphere-10 C_{18} (Knauer, Germany), and the following gradient was used (MeOH, 0.1% formic acid in H_2O): 0 min (10% MeOH); 5 min (10% MeOH); 35 min (100% MeOH); 45 min (100% MeOH). Semi-preparative HPLC was performed using a Merck Hitachi HPLC System (UV detector L-7400; pump L-7100; Eurosphere-100 C_{18}, 300 × 8 mm, Knauer, Germany), with mixtures of MeOH–H_2O as mobile phase. Column chromatography included Merck MN silica gel 60 M (0.04–0.063 mm). TLC plates precoated with silica gel F_{254} (Merck) were used to monitor and collect fractions; detection was under 254 and 366 nm or by spraying the plates with anisaldehyde reagent. Distilled and spectral grade solvents were used for column chromatography and spectroscopic measurements, respectively.

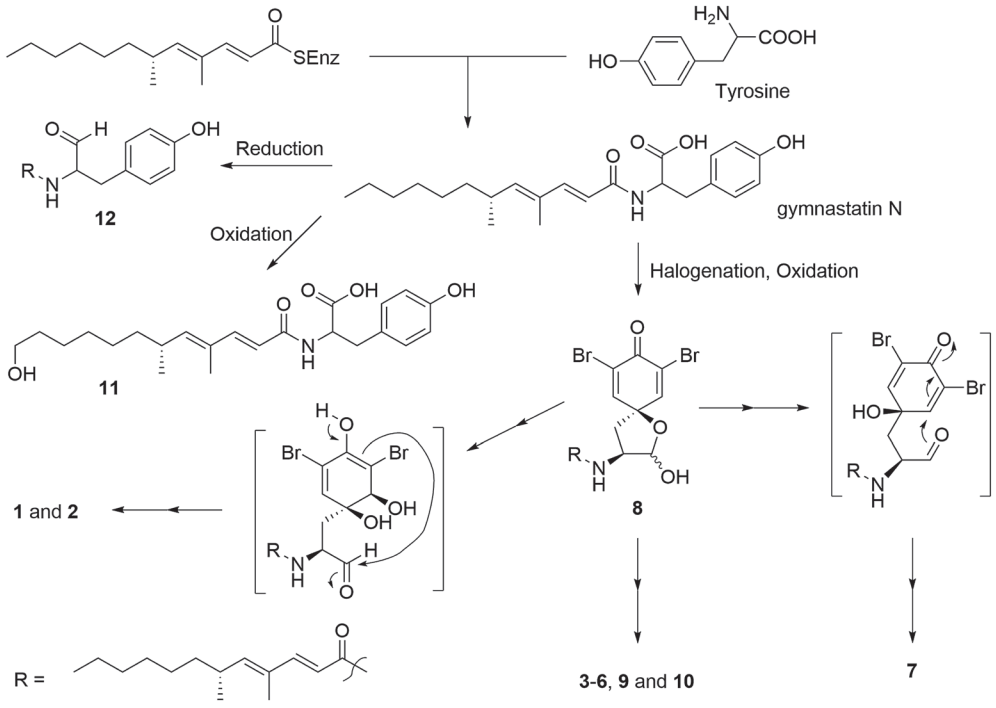

Fig. 9 Plausible biosynthesis of brominated alkaloids from *G. dankaliensis*.

Publication 1

Fungal material and cultivation

The fungus was isolated from a soil sample close to the Giza pyramids, Egypt, and identified by DNA amplification, sequencing of the ITS region and comparison with GenBank data (GenBank accession No. HM991265.1) as *G. dankaliensis* as previously described.[19] The fungal strain was grown on solid rice medium containing 3.5% NaBr (3.50 g NaBr, 100 mL distilled water was added to 100 g commercially available rice and then autoclaved) in two Erlenmeyer flasks (1 L each) at 27 °C under static conditions for 28 days.[20]

Extraction and isolation

Fungal culture was extracted twice with 500 mL ethyl acetate. The crude extract (9.35 g) was chromatographed on a silica column using *n*-hexane, *n*-hexane–ethyl acetate (60 : 1), CH_2Cl_2–MeOH gradient to give five fractions [A (1.87 g), B (1.32 g), C (2.13 g), D (3.15 g), E (0.87 g)]. Fraction B was further separated on a silica gel column with a CH_2Cl_2–MeOH gradient (100 : 0 to 150 : 1), affording twelve subfractions (B1–12). Fraction B9 (43.1 mg) was purified by semi-preparative HPLC using MeOH–H_2O (78 : 22) to yield **8** (4.1 mg) and **9** (4.7 mg), while fraction B10 (21.2 mg) was purified by semi-preparative HPLC using MeOH–H_2O (76 : 24) to give **7** (1.6 mg). Fraction C was fractionated by silica gel column chromatography with a gradient of CH_2Cl_2–MeOH (500 : 1 to 25 : 1) as solvent system, to give eight subfractions (C1–8). Fraction C2 (185.2 mg) was further purified by semi-preparative HPLC using MeOH–H_2O (from 77 : 23 to 80 : 20 in 25 minutes) to afford **3** (14.2 mg), **4** (7.5 mg), and **10** (17.9 mg). Fraction D was separated by silica gel column chromatography eluting with CH_2Cl_2–MeOH (200 : 1 to 15 : 1), to give eight subfractions (FrD1–8). **1** (7.2 mg) and **2** (3.5 mg) were obtained from FrD3 (285.1 mg) and FrD4 (252.3 mg) by semi-preparative HPLC using MeOH–H_2O (72 : 28), respectively. FrD5 (301.4 mg) was further purified by semi-preparative HPLC using MeOH–H_2O (70 : 30) to give **5** (1.7 mg) and **6** (2.1 mg).

Gymnastatin T (1). Colorless needle crystal; $[\alpha]_D^{20}$ −47.3 (*c* 0.50, MeOH); UV (MeOH): λ_{max} 271.2 (4.02) nm; HRESIMS *m*/*z* 500.1644 $[M + H]^+$ (calcd 500.1622 for $C_{23}H_{35}BrNO_6$); ^1H and ^{13}C NMR data, Table 1.

Gymnastatin U (2). White powder; $[\alpha]_D^{20}$ −37.5 (*c* 0.65, MeOH); UV (MeOH): λ_{max} 271.2 (3.83) nm; HRESIMS *m*/*z* 500.1641 $[M + H]^+$ (calcd 500.1622 for $C_{23}H_{35}BrNO_6$); ^1H and ^{13}C NMR data, Table 1.

Gymnastatin V (3). Colorless oil; $[\alpha]_D^{20}$ −1.8 (*c* 0.56, MeOH); UV (MeOH): λ_{max} 271.2 (3.73) nm; HRESIMS *m*/*z* 482.1534 $[M + H]^+$ (calcd 482.1537 for $C_{23}H_{33}BrNO_5$); ^1H and ^{13}C NMR data, Table 2.

Gymnastatin W (4). White powder; $[\alpha]_D^{20}$ −27.0 (*c* 0.88, MeOH); UV (MeOH): λ_{max}271.9 (3.98) nm; HRESIMS *m*/*z* 576.0952 $[M + H]^+$ (calcd 576.0955 for $C_{24}H_{36}Br_2NO_5$); ^1H and ^{13}C NMR data, Table 2.

Gymnastatin X (5). Colorless oil; $[\alpha]_D^{20}$ −10.2 (*c* 0.22, MeOH); UV (MeOH): λ_{max} 270.4 (3.94) nm; HRESIMS *m*/*z* 498.1845 $[M + H]^+$ (calcd 498.1850 for $C_{24}H_{37}BrNO_5$); ^1H and ^{13}C NMR data, Table 2.

Gymnastatin Y (6). White powder; $[\alpha]_D^{20}$ −3.9 (*c* 1.04, MeOH); UV (MeOH): λ_{max} 271.9 (3.94) nm; HRESIMS *m*/*z* 484.1689 $[M + H]^+$ (calcd 484.1693 for $C_{23}H_{35}BrNO_5$); ^1H and ^{13}C NMR data, Table 3.

Dankastatin D (7). Colorless oil; $[\alpha]_D^{20}$ −29.4 (*c* 0.25, MeOH); UV (MeOH): λ_{max} 270.4 (3.73) nm; HRESIMS *m*/*z* 564.0959 $[M + H]^+$ (calcd 564.0955 for $C_{23}H_{36}Br_2NO_5$); ^1H and ^{13}C NMR data, Table 3.

X-ray crystallographic analysis of gymnastatin T (1)

Crystallization conditions. X-ray quality crystal of **1** was obtained by slow evaporation from MeOH solution. A suitable single crystal was carefully selected under a polarizing microscope.

Data collection. Bruker Kappa APEX2 CCD diffractometer, Mo-Kα radiation (λ = 0.71073 Å), multilayer mirror, ω- and ϕ-scan; data collection with APEX2, cell refinement and data reduction with SAINT,[21] experimental absorption correction with SADABS.[22]

Structure analysis and refinement. The structure was solved by direct methods using SHELXS-97; refinement was done by full-matrix least squares on F^2 using the SHELXL-97 program suite.[23] All non-hydrogen positions were refined with anisotropic displacement parameters. Hydrogen atoms were positioned geometrically and refined using riding models. Graphics were drawn with DIAMOND,[24] analyses of the inter- and intramolecular hydrogen bonding interactions were done with PLATON for *Windows*.[25]

Crystal data of 1. $C_{23}H_{34}BrNO_6 \cdot CH_4O$, M = 532.46, orthorhombic system, space group $P2_12_12_1$, a = 7.0251(3) Å, b = 11.3852(5) Å, c = 32.3080(15) Å, V = 2584.1(2) Å^3, Z = 4, D_{calc} = 1.369 g cm^{-3}, crystal size 0.40 × 0.05 × 0.01 mm^3, μ(Mo-Kα) = 1.633 mm^{-1}, 2.5° < θ < 25.3°, N_t = 39 194, N = 6086 (R_{int} = 0.0445), R_1 = 0.03626, wR_2 = 0.1637, S = 1.092, Flack parameter[26] 0.043(4).

Cytotoxicity assay

Cytotoxicity against the mouse lymphoma cell line L5178Y (European Collection of Authenticated Cell Cultures; Catalogue No. 87111908) was tested using the MTT method with kahalalide F as positive control and media with 0.1% DMSO as negative control as described previously.[27] The cells were grown in RPMI medium and 10% FCS (fetal calf serum) (Biochrom/Merck). Thiazolyl blue tetrazolium bromide (MTT; # M2128 Sigma) was used as an indicator for cell viability. The viability assay reaction is based upon the oxidation of the yellowish MTT solution to solid formazan *via* the mitochondrial dehydrogenases in living cells.[28] The crystals formed were solubilized with acidified isopropanol and the intensity was determined colorimetrically at 570 nm.[29]

Acknowledgements

H. W. wishes to thank the China Scholarship Council, the Ministry of Education of China, for a doctoral scholarship. P. P. wants to thank BMBF (project BALIPEND) for support.

Publication 1

Furthermore we are indebted to Prof. Mohammed Abdel-Aziz (Microbial Chemistry Department, Genetic Engineering and Biotechnology Division, National Research Center, Egypt) for his help during fungal collection.

Notes and references

1 G. W. Gribble, *Acc. Chem. Res.*, 1998, **31**, 141–152.
2 G. W. Gribble, *Heterocycles*, 2012, **84**, 157–207.
3 G. W. Gribble, *Mar. Drugs*, 2015, **13**, 4044–4136.
4 A. Schueffler and T. Anke, *Nat. Prod. Rep.*, 2014, **31**, 1425–1448.
5 A. M. Mayer, K. B. Glaser, C. Cuevas, R. S. Jacobs, W. Kem, R. D. Little, J. M. McIntosh, D. J. Newman, B. C. Potts and D. E. Shuster, *Trends Pharmacol. Sci.*, 2010, **31**, 255–265.
6 T. Emri, L. Majoros, V. Toth and I. Pocsi, *Appl. Microbiol. Biotechnol.*, 2013, **97**, 3267–3284.
7 G. W. Gribble, *J. Chem. Educ.*, 2004, **81**, 1441–1449.
8 G. W. Gribble, *Prog. Chem. Org. Nat. Prod.*, 2010, **91**, 349–365.
9 H. Yamazaki, H. Rotinsulu, R. Narita, R. Takahashi and M. Namikoshi, *J. Nat. Prod.*, 2015, **78**, 2319–2321.
10 L. S. de Medeiros, J. V. da Silva, L. M. Abreu, L. H. Pfenning, C. L. Silva, S. S. Thomasi, T. Venâncio, K.-H. van Pée, K. F. Nielsen and E. Rodrigues-Filho, *Molecules*, 2015, **20**, 17627–17644.
11 S. Sureram, C. Kesornpun, C. Mahidol, S. Ruchirawat and P. Kittakoop, *RSC Adv.*, 2013, **3**, 1781–1788.
12 L. Hammerschmidt, A. H. Aly, M. Abdel-Aziz, W. E. Müller, W. Lin, G. Daletos and P. Proksch, *Bioorg. Med. Chem.*, 2015, **23**, 712–719.
13 T. Amagata, M. Doi, T. Ohta, K. Minoura and A. Numata, *J. Chem. Soc., Perkin Trans. 1*, 1998, 3585–3600.
14 T. Amagata, K. Minoura and A. Numata, *J. Nat. Prod.*, 2006, **69**, 1384–1388.
15 T. Amagata, M. Tanaka, T. Yamada, K. Minoura and A. Numata, *J. Nat. Prod.*, 2008, **71**, 340–345.
16 T. Amagata, K. Takigawa, K. Minoura and A. Numata, *Heterocycles*, 2010, **81**, 897–907.
17 T. Amagata, M. Tanaka, T. Yamada, Y. P. Chen, K. Minoura and A. Numata, *Tetrahedron Lett.*, 2013, **54**, 5960–5962.
18 T. Mukhopadhyay, R. G. Bhat, K. Roy, E. K. S. Vijayakumar and B. N. Ganguli, *J. Antibiot.*, 1998, **51**, 439–441.
19 J. Kjer, A. Debbab, A. H. Aly and P. Proksch, *Nat. Protoc.*, 2010, **5**, 479–490.
20 Two different concentrations of NaBr (3.5%, which is the same as the concentration of salt in seawater and a higher one, 10%) in the media were used for fungal fermentation. The obtained crude extracts showed almost identical peaks as detected by LC-MS analysis. However, the amount of crude extract (4.7 g per flask) obtained from the medium with 3.5% NaBr was much bigger than that from the medium with 10% NaBr (1.5 g per flask). HPLC analysis of fungal extract from NaBr-added medium showed several new peaks, which were identified as brominated metabolites by LC-MS based on their characteristic isotope patterns ($M^+ : [M + 2]^+ : [M + 4]^+ = 1 : 2 : 1$ for compounds containing two Br atoms and $M^+ : [M + 2]^+ = 1 : 1$ for compounds containing one Br atom, respectively).
21 Apex2, *Data Collection Program for the CCD Area-Detector System; SAINT, Data Reduction and Frame Integration Program for the CCD Area-Detector System*, Bruker Analytical X-ray Systems, Madison, Wisconsin, USA, 1997–2006.
22 G. M. Sheldrick, *Program SADABS: area-detector absorption correction*, University of Göttingen, Germany, 1996.
23 G. M. Sheldrick, *Acta Crystallogr., Sect. A: Found. Crystallogr.*, 2008, **64**, 112–122.
24 K. Brandenburg, *Diamond (Version 3.2), Crystal and Molecular Structure Visualization, Crystal Impact – K. Brandenburg & H. Putz Gbr*, Bonn, Germany, 2009.
25 (*a*) A. L. Spek, *Acta Crystallogr., Sect. D: Biol. Crystallogr.*, 2009, **65**, 148–155; (*b*) A. L. Spek, *J. Appl. Crystallogr.*, 2003, **36**, 7–13; (*c*) A. L. Spek, *PLATON – A Multipurpose Crystallographic Tool*, Utrecht University, Utrecht, The Netherlands, 2008; (*d*) L. J. Farrugia, *Windows implementation, Version 40608*, University of Glasgow, Scotland, 2008.
26 (*a*) H. D. Flack, M. Sadki, A. L. Thompson and D. J. Watkin, *Acta Crystallogr., Sect. A: Found. Crystallogr.*, 2011, **67**, 21–34; (*b*) H. D. Flack and G. Bernardinelli, *Chirality*, 2008, **20**, 681–690; (*c*) H. D. Flack and G. Bernardinelli, *Acta Crystallogr., Sect. A: Found. Crystallogr.*, 1999, **55**, 908–915; (*d*) H. D. Flack, *Acta Crystallogr., Sect. A: Found. Crystallogr.*, 1983, **39**, 876–881.
27 M. Ashour, R. Edrada, R. Ebel, V. Wray, W. Wätjen, K. Padmakumar, W. E. G. Müller, W. H. Lin and P. Proksch, *J. Nat. Prod.*, 2006, **69**, 1547–1553.
28 B. Chuenjitkuntaworn, T. Osathanon, N. Nowwarote, P. Supaphol and P. Pavasant, *J. Biomed. Mater. Res., Part A*, 2016, **104**, 264–271.
29 W. E. G. Müller, M. Geisert, R. K. Zahn, A. Maidhof, M. Bachmann and H. Umezawa, *Eur. J. Cancer Clin. Oncol.*, 1983, **19**, 665–670.

Supplementary information

Targeted solid phase fermentation of the soil dwelling fungus *Gymnascella dankaliensis* yields new brominated tyrosine-derived alkaloids

Hao Wang,[a] Haofu Dai,[b] Christian Heering,[c] Christoph Janiak,[c] Wenhan Lin,[d] Raha S. Orfali,[e] Werner E.G. Müller,[f] Zhen Liu*[a] and Peter Proksch*[a]

Contents

Figure S1. HRESIMS of compound **1**……..……...……30

Figure S2. ^{1}H NMR (600MHz, DMSO-d_6) spectrum of compound **1**……..…...30

Figure S3. ^{13}C NMR (150MHz, DMSO-d_6) spectrum of compound **1**……..…..31

Figure S4. ^{1}H-^{1}H COSY (600MHz, DMSO-d_6) spectrum of compound **1**…….....…31

Figure S5. HSQC (600MHz, 150MHz, DMSO-d_6) spectrum of compound **1**……32

Figure S6. HMBC (600MHz, 150MHz, DMSO-d_6) spectrum of compound **1**…...…32

Figure S7. ROESY (600MHz, DMSO-d_6) spectrum of compound **1**……..33

Figure S8. ^{1}H NMR (600MHz, methanol-d_4) spectrum of compound **1**……..……33

Figure S9. ^{13}C NMR (150MHz, methanol-d_4) spectrum of compound **1**……..…34

Figure S10. ^{1}H-^{1}H COSY (600MHz, methanol-d_4) spectrum of compound **1**…….34

Figure S11. HSQC (600MHz, 150MHz, methanol-d_4) spectrum of compound **1**...…35

Figure S12. HMBC (600MHz, 150MHz, methanol-d_4) spectrum of compound **1**…..35

Figure S13. ROESY (600MHz, methanol-d_4) spectrum of compound **1**…….36

Figure S14. HRESIMS of compound **2**…….....……36

Figure S15. ^{1}H NMR (600MHz, methanol-d_4) spectrum of compound **2**……37

Figure S16. ^{13}C NMR (150MHz, methanol-d_4) spectrum of compound **2**……...……37

Figure S17. ^{1}H-^{1}H COSY (600MHz, methanol-d_4) spectrum of compound **2**…….…38

Figure S18. HSQC (600MHz, 150MHz, methanol-d_4) spectrum of compound **2**…...38

Figure S19. HMBC (600MHz, 150MHz, methanol-d_4) spectrum of compound **2..**…39

Figure S20. ROESY (600MHz, methanol-d_4) spectrum of compound **2**……..…39

Figure S21. HRESIMS of compound **3**…….....……40

Figure S22. ^{1}H NMR (600MHz, $CDCl_3$) spectrum of compound **3**……40

Figure S23. ^{13}C NMR (150MHz, $CDCl_3$) spectrum of compound **3**……...…41

Figure S24. ^{1}H-^{1}H COSY (600MHz, $CDCl_3$) spectrum of compound **3**……..41

Figure S25. HSQC (600MHz, 150MHz, $CDCl_3$) spectrum of compound **3**……..….42

Figure S26. HMBC (600MHz, 150MHz, $CDCl_3$) spectrum of compound **3**……..….42

Figure S27. ROESY (600MHz, $CDCl_3$) spectrum of compound **3**……..43

Figure S28. HRESIMS of compound **4**……..……..….43

Figure S29. ^{1}H NMR (600MHz, $CDCl_3$) spectrum of compound **4**……44

Figure S30. ^{13}C NMR (150MHz, $CDCl_3$) spectrum of compound **4**……...44

Figure S31. ^{1}H-^{1}H COSY (600MHz, $CDCl_3$) spectrum of compound **4**…….….45

Figure S32. HSQC (600MHz, 150MHz, $CDCl_3$) spectrum of compound **4**……..…..45

Figure S33. HMBC (600MHz, 150MHz, $CDCl_3$) spectrum of compound **4**……..….46

Figure S34. ROESY (600MHz, $CDCl_3$) spectrum of compound **4**……..46

Figure S35. HRESIMS of compound **5**……...…..….47

Figure S36. ^{1}H NMR (600MHz, methanol-d_4) spectrum of compound **5**……47

Figure S37. ^{1}H-^{1}H COSY (300MHz, methanol-d_4) spectrum of compound **5**…….48

Figure S38. HSQC (600MHz, 150MHz, methanol-d_4) spectrum of compound **5**…...48

Figure S39. HMBC (600MHz, 150MHz, methanol-d_4) spectrum of compound **5**…..49

Figure S40. ROESY (600MHz, methanol-d_4) spectrum of compound **5**…….49

Figure S41. HRESIMS of compound **6**……...…….50

Figure S42. ^{1}H NMR (600MHz, methanol-d_4) spectrum of compound **6**……50

Figure S43. ^{1}H-^{1}H COSY (600MHz, methanol-d_4) spectrum of compound **6**…….51

Figure S44. HSQC (600MHz, 150MHz, methanol-d_4) spectrum of compound **6**…...51

Figure S45. HMBC (600MHz, 150MHz, methanol-d_4) spectrum of compound **6**…..52

Figure S46. ROESY (600MHz, methanol-d_4) spectrum of compound **6**…….52

Figure S47. HRESIMS of compound **7**……..…..53

Figure S48. ^{1}H NMR (600MHz, $CDCl_3$) spectrum of compound **7**……..…..53

Figure S49. ^{1}H-^{1}H COSY (600MHz, $CDCl_3$) spectrum of compound **7**…….....54

Figure S50. HSQC (600MHz, 150MHz, $CDCl_3$) spectrum of compound **7**……54

Figure S51. HMBC (600MHz, 150MHz, $CDCl_3$) spectrum of compound **7**……...55

Figure S52. ROESY (600MHz, $CDCl_3$) spectrum of compound **7**……...…...55

X-ray crystallographic parameters of compound **1** (CCDC 1481781)…….....56

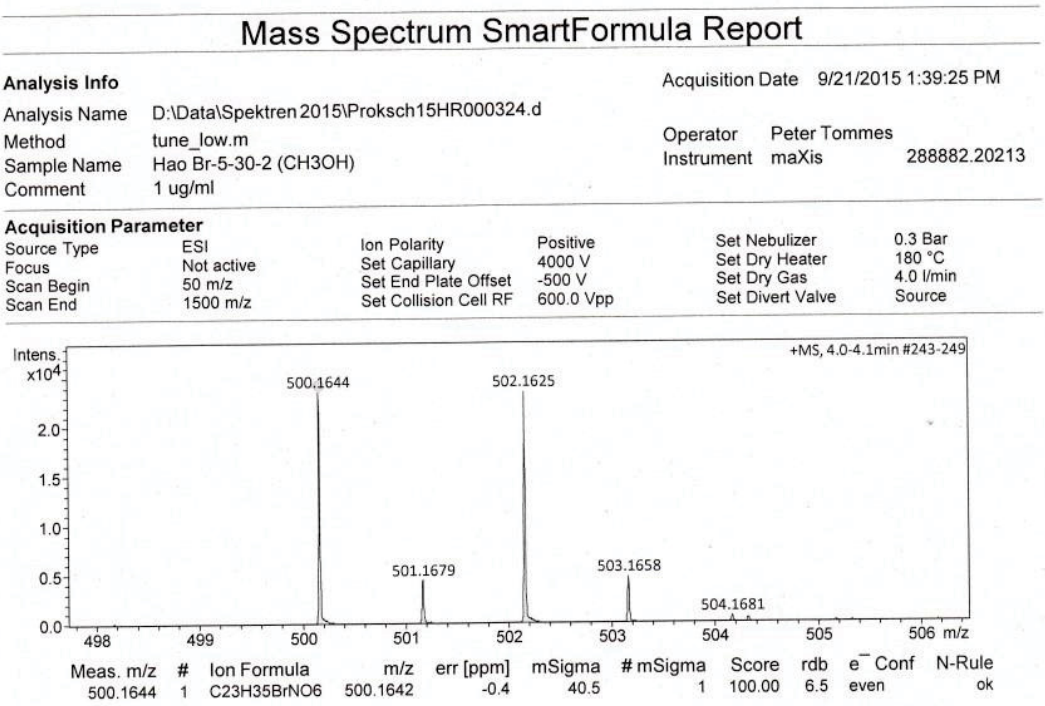

Figure S1. HRESIMS of compound **1**.

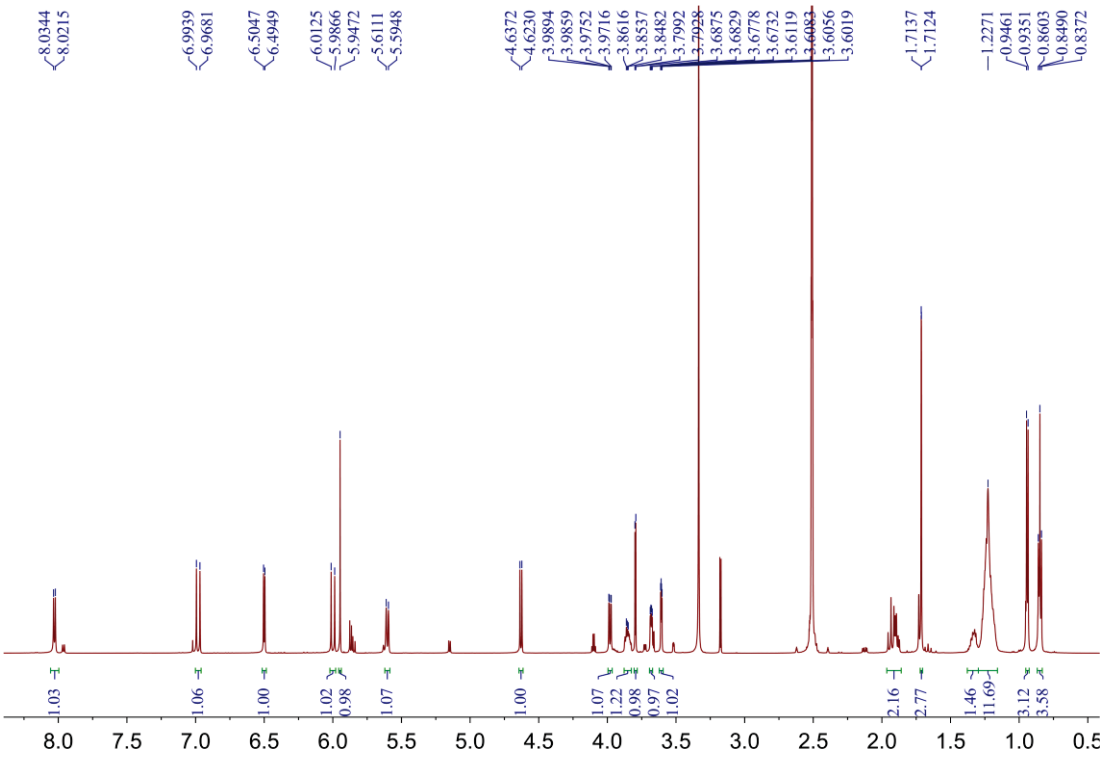

Figure S2. ^{1}H NMR (600MHz, DMSO-d_6) spectrum of compound **1**.

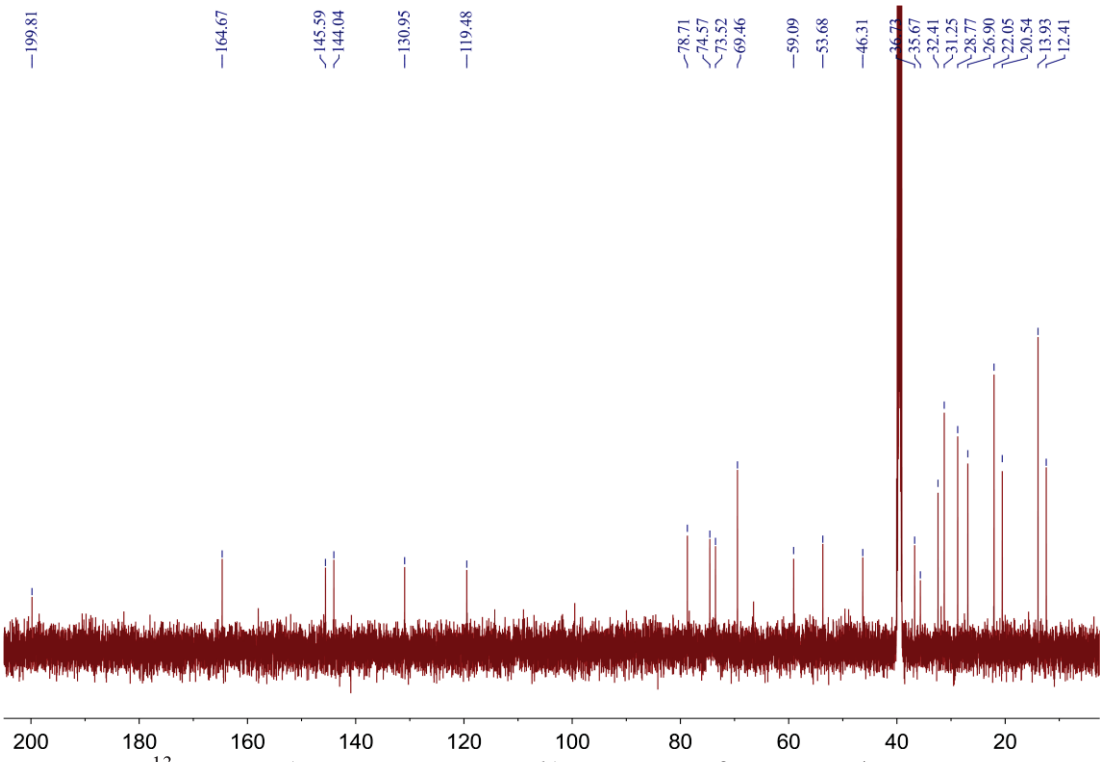

Figure S3. ^{13}C NMR (150MHz, DMSO-d_6) spectrum of compound **1**.

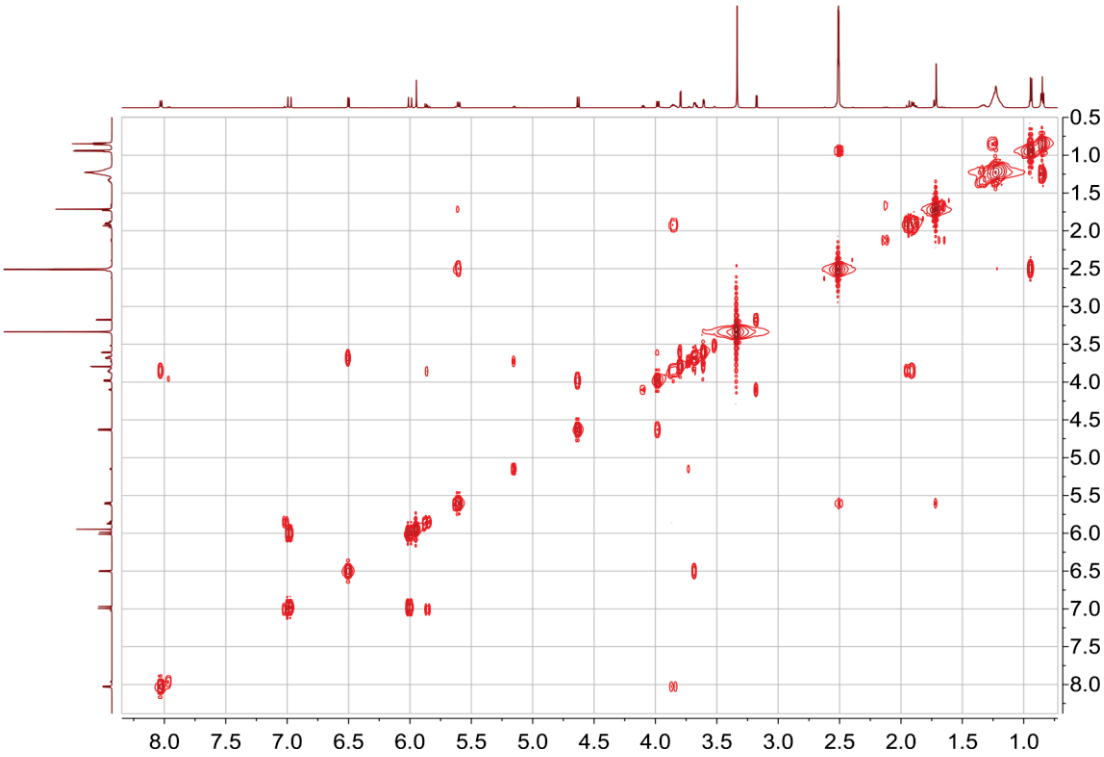

Figure S4. ^{1}H-^{1}H COSY (600MHz, DMSO-d_6)spectrum of compound **1**.

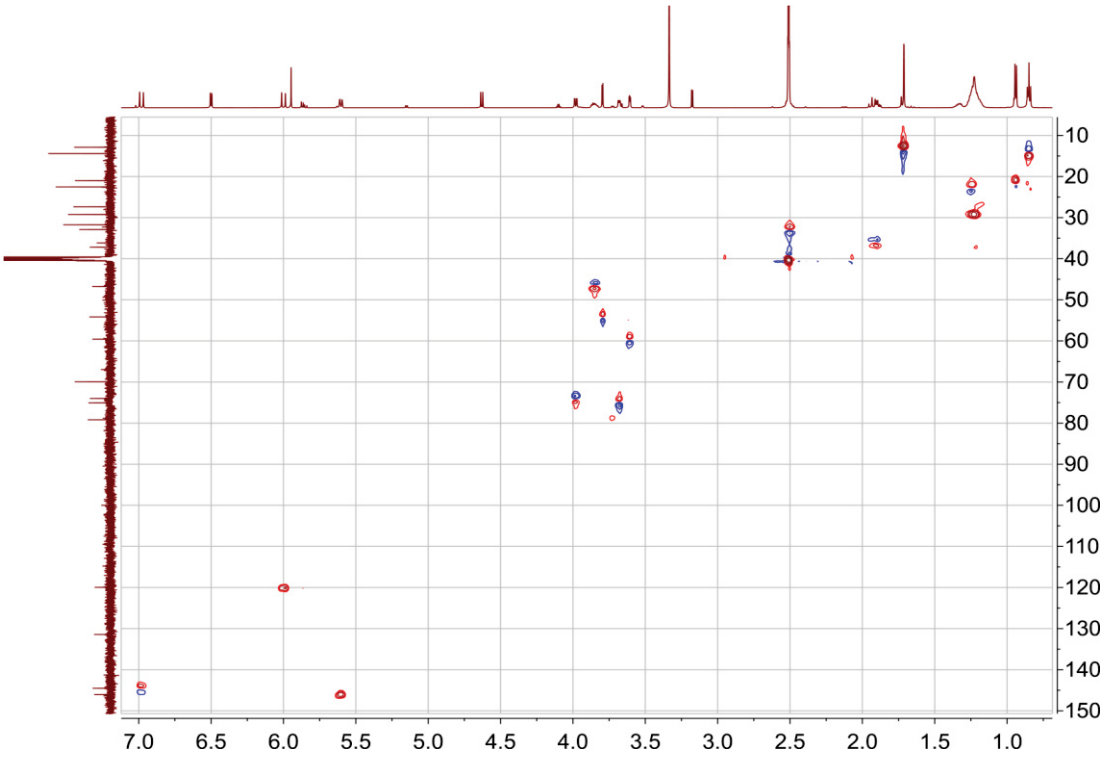

Figure S5. HSQC (600MHz, 150MHz, DMSO-d_6) spectrum of compound **1**.

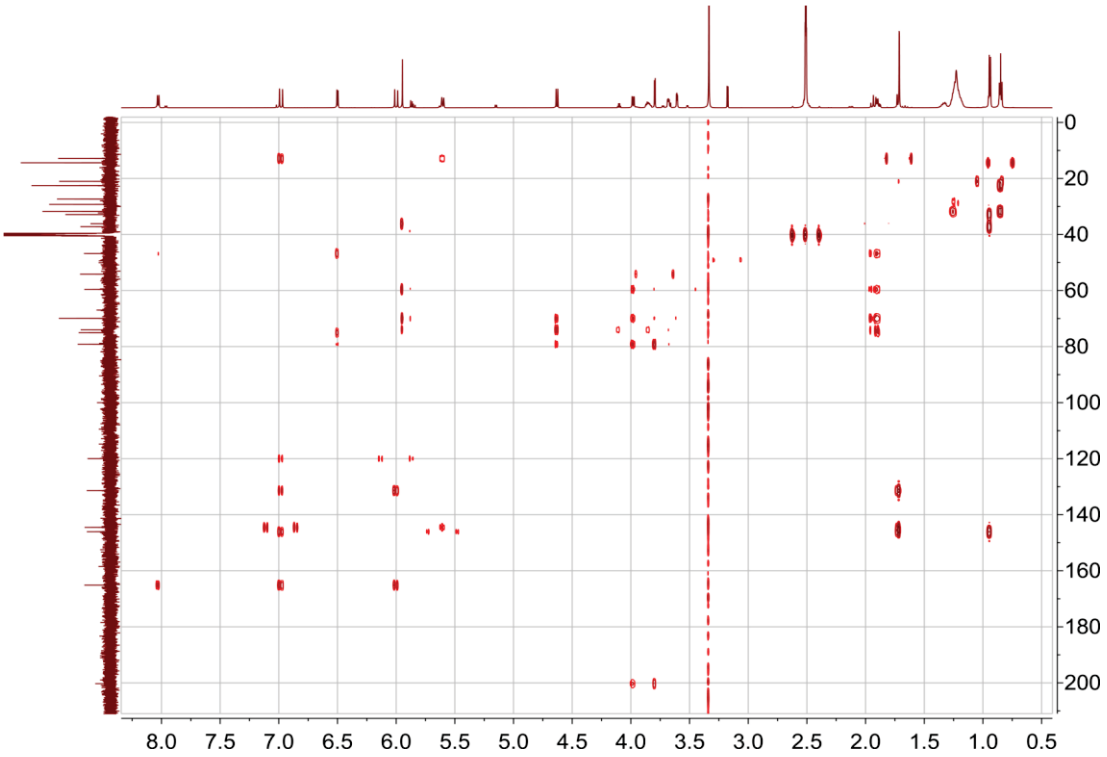

Figure S6. HMBC (600MHz, 150MHz, DMSO-d_6) spectrum of compound **1**.

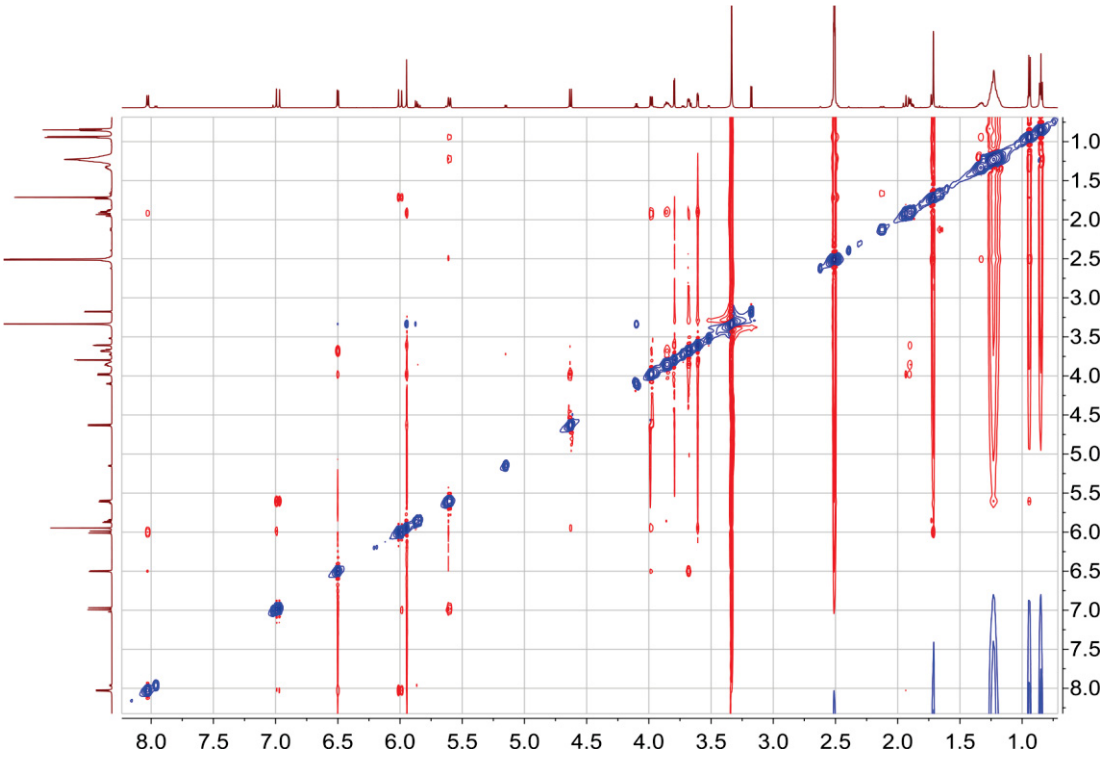

Figure S7. ROESY (600MHz, DMSO-d_6) spectrum of compound **1**.

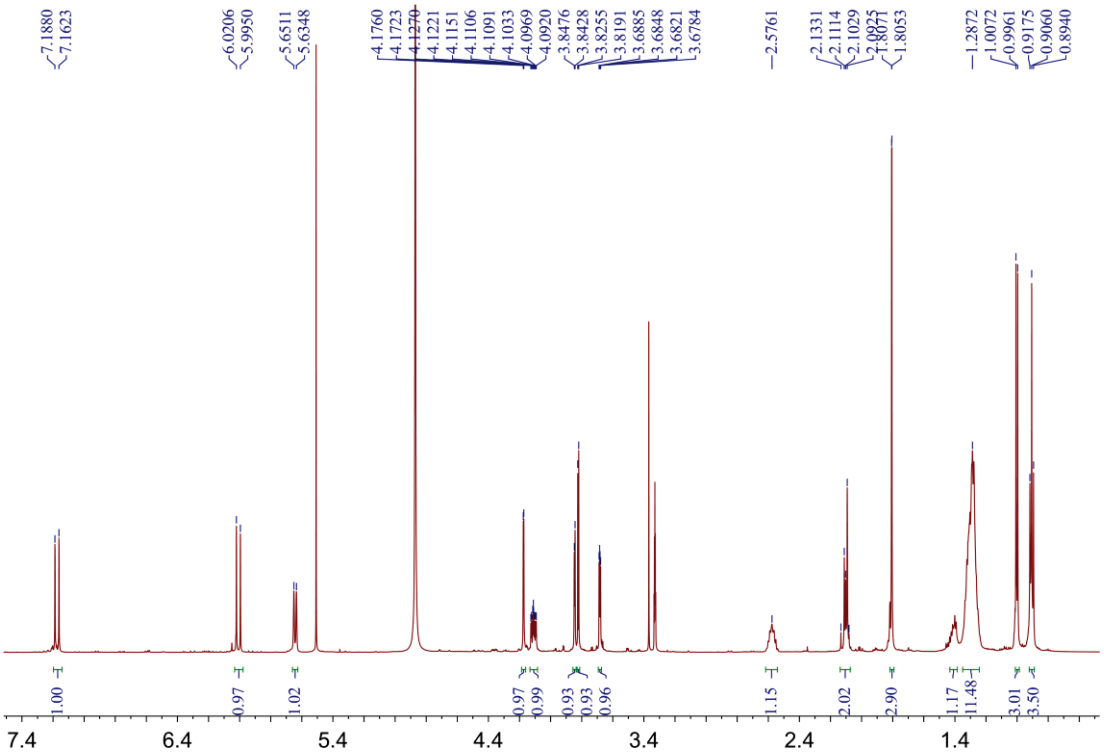

Figure S8. ^{1}H NMR (600MHz, methanol-d_4) spectrum of compound **1**.

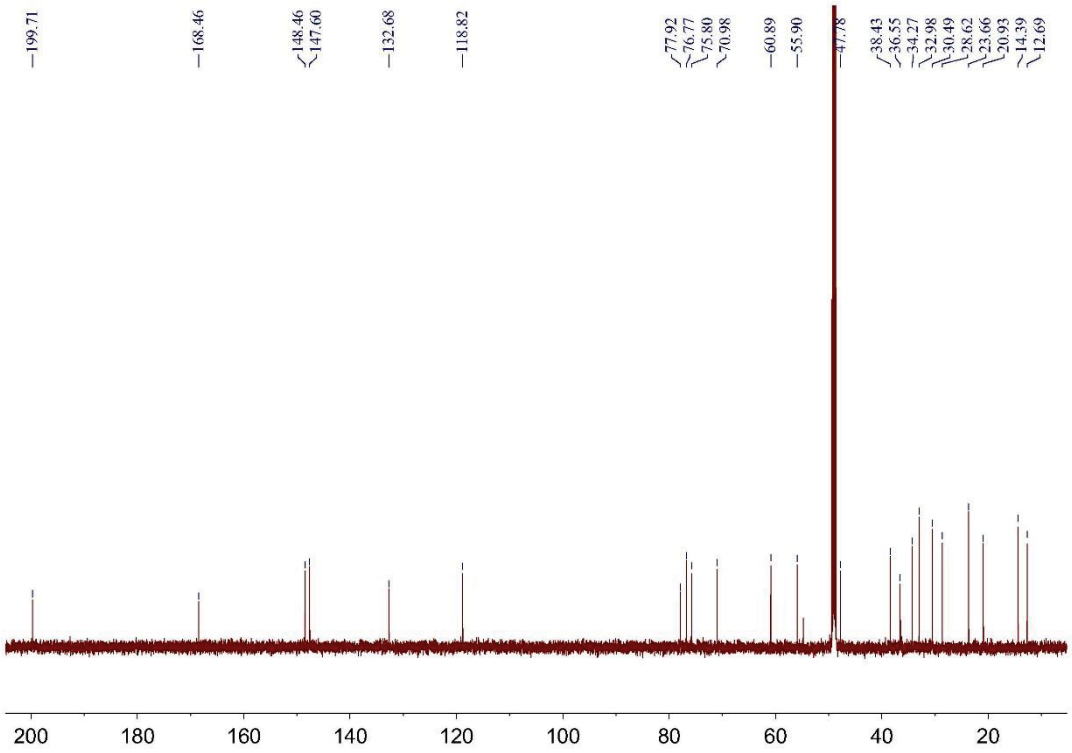

Figure S9. ^{13}C NMR (150MHz, methanol-d_4) spectrum of compound **1**.

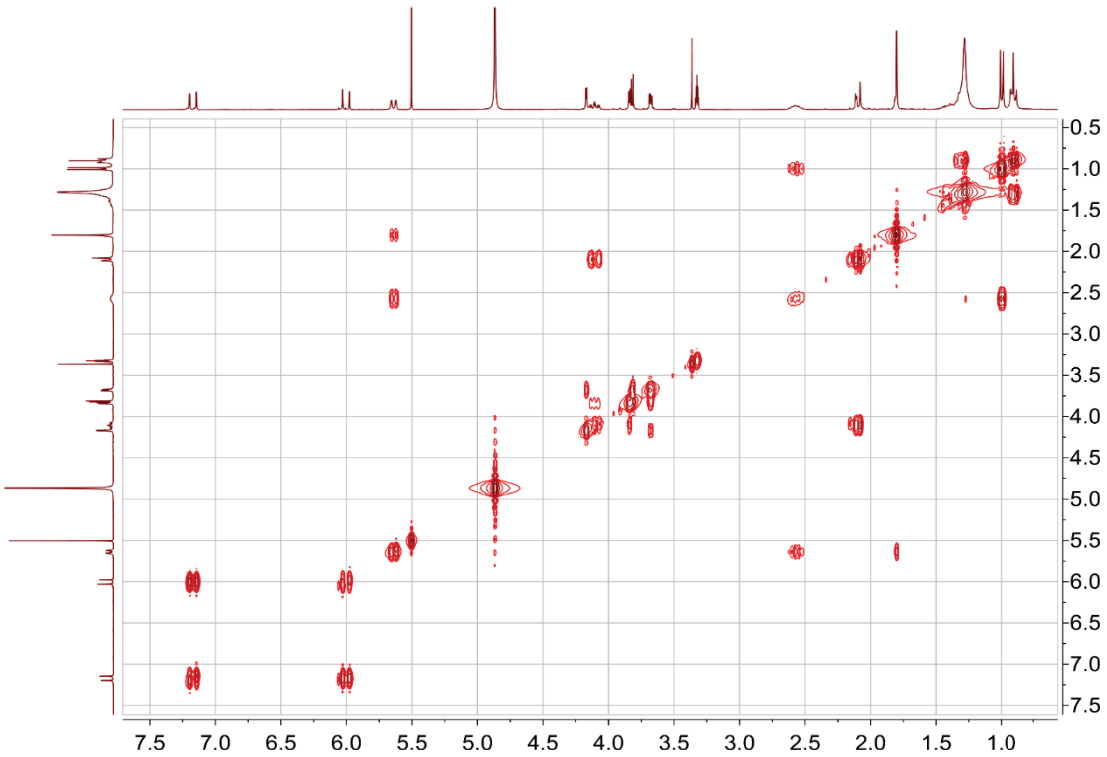

Figure S10. ^{1}H-^{1}H COSY (600MHz, methanol-d_4) spectrum of compound **1**.

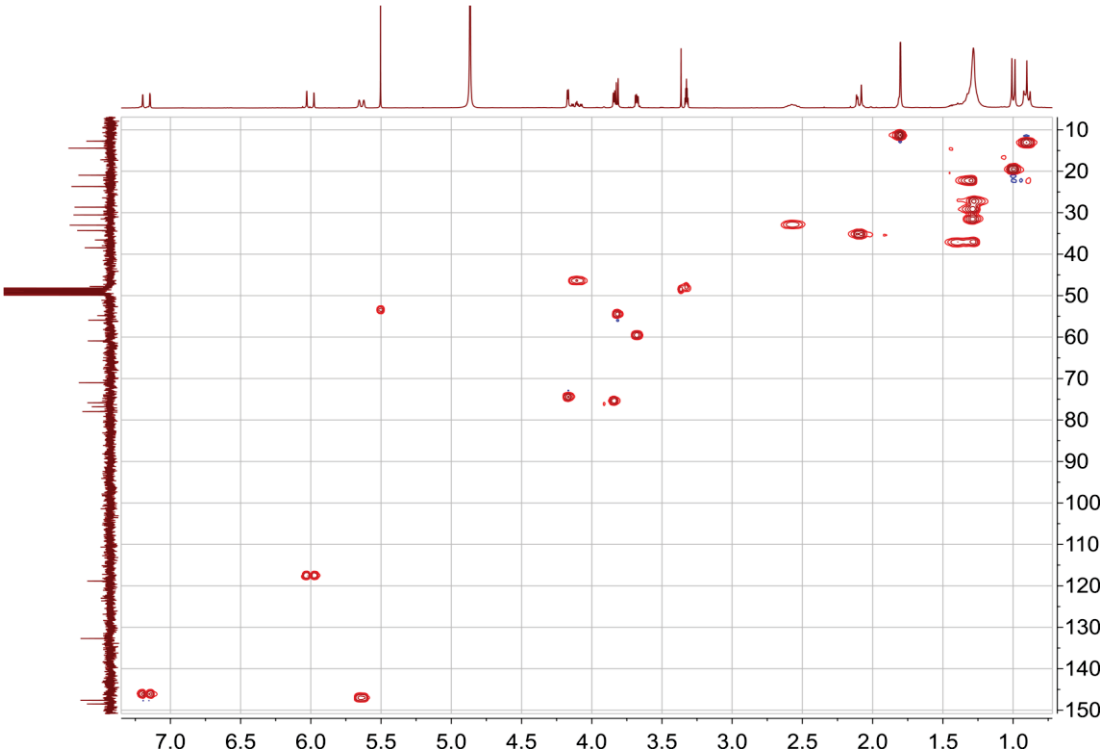

Figure S11. HSQC (600 MHz, 150 MHz, methanol-d_4) spectrum of compound **1**.

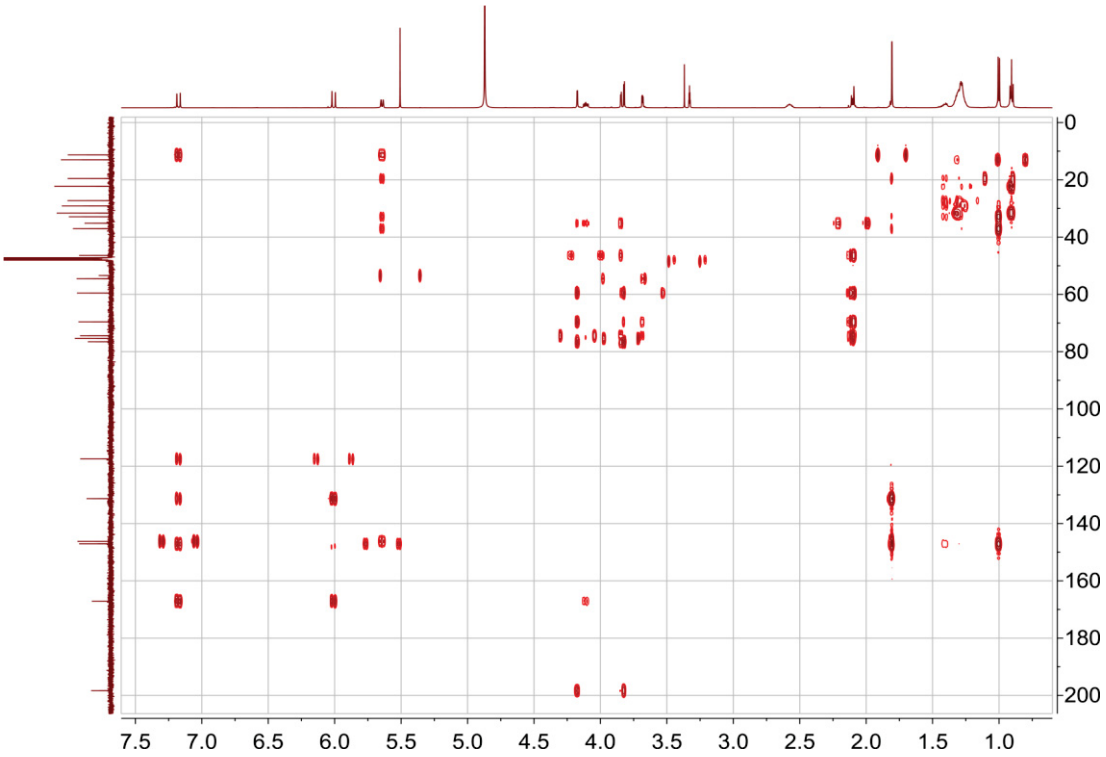

Figure S12. HMBC (600MHz, 150MHz, methanol-d_4)spectrum of compound **1**.

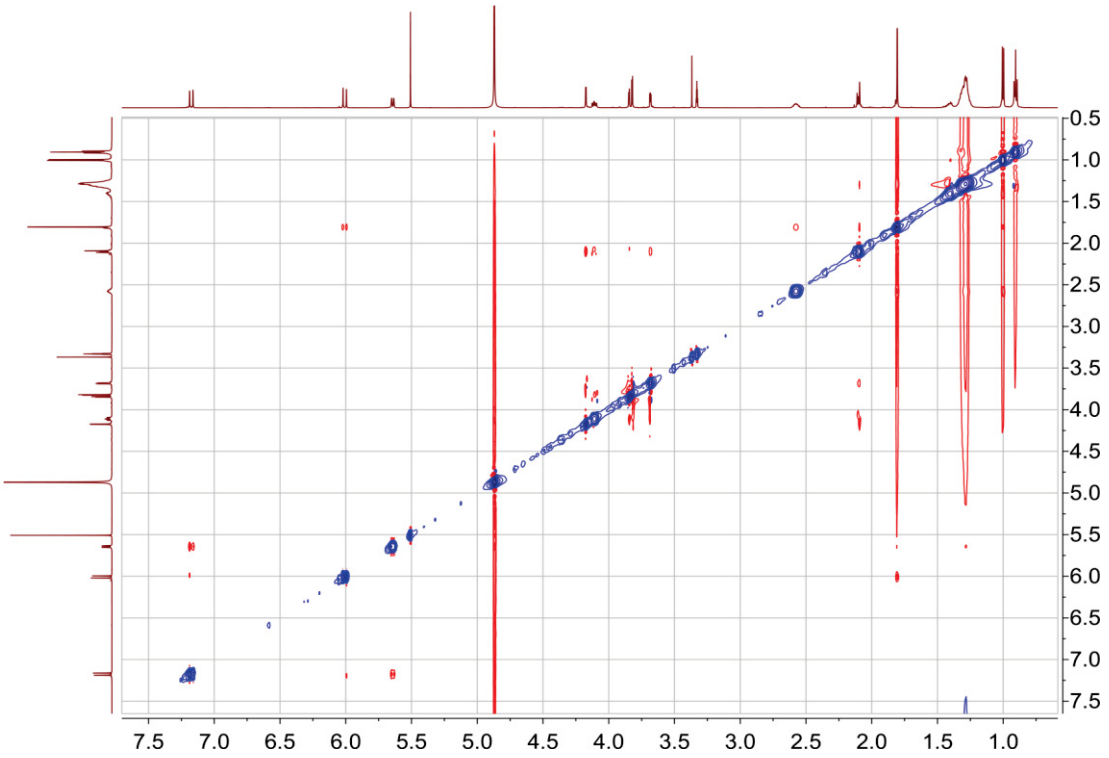

Figure S13. ROESY (600MHz, methanol-d_4)spectrum of compound **1**.

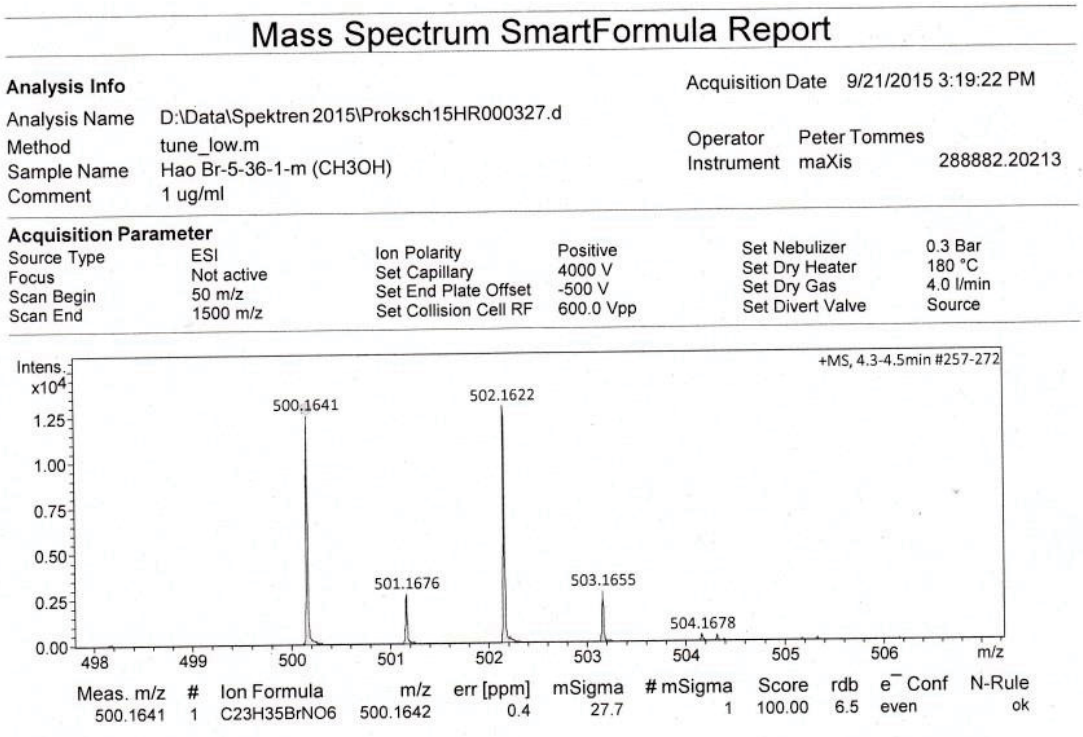

Figure S14. HRESIMS of compound **2**.

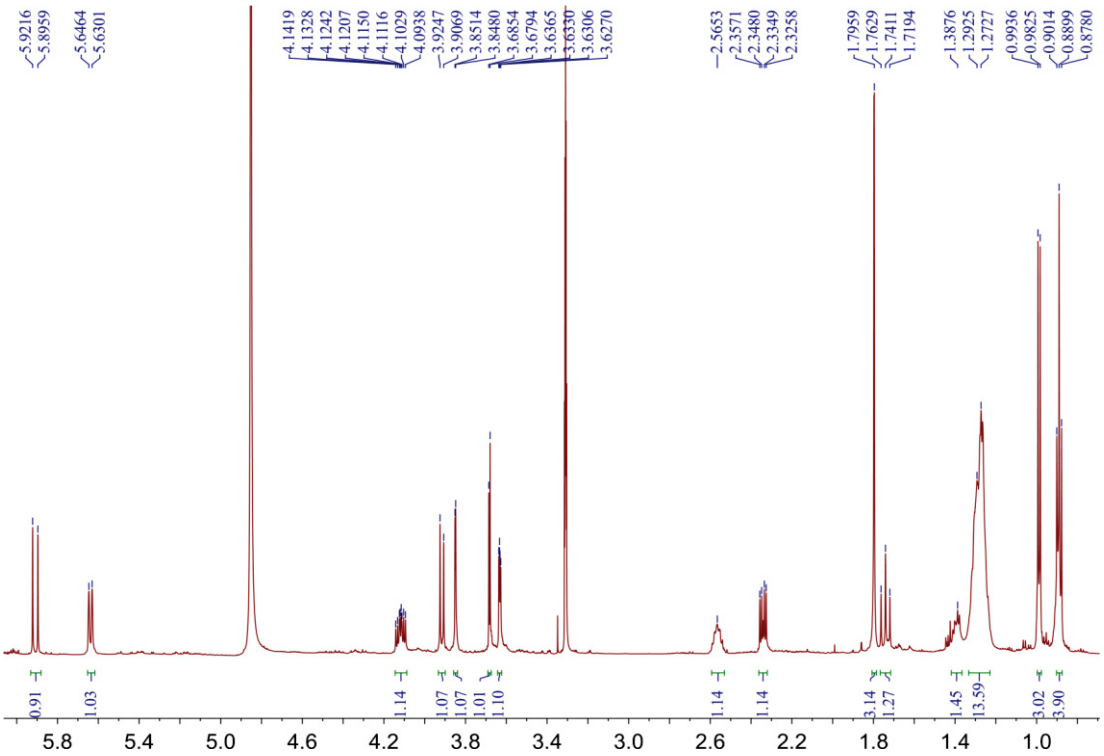

Figure S15. ^{1}H NMR (600MHz, methanol-d_4) spectrum of compound **2**.

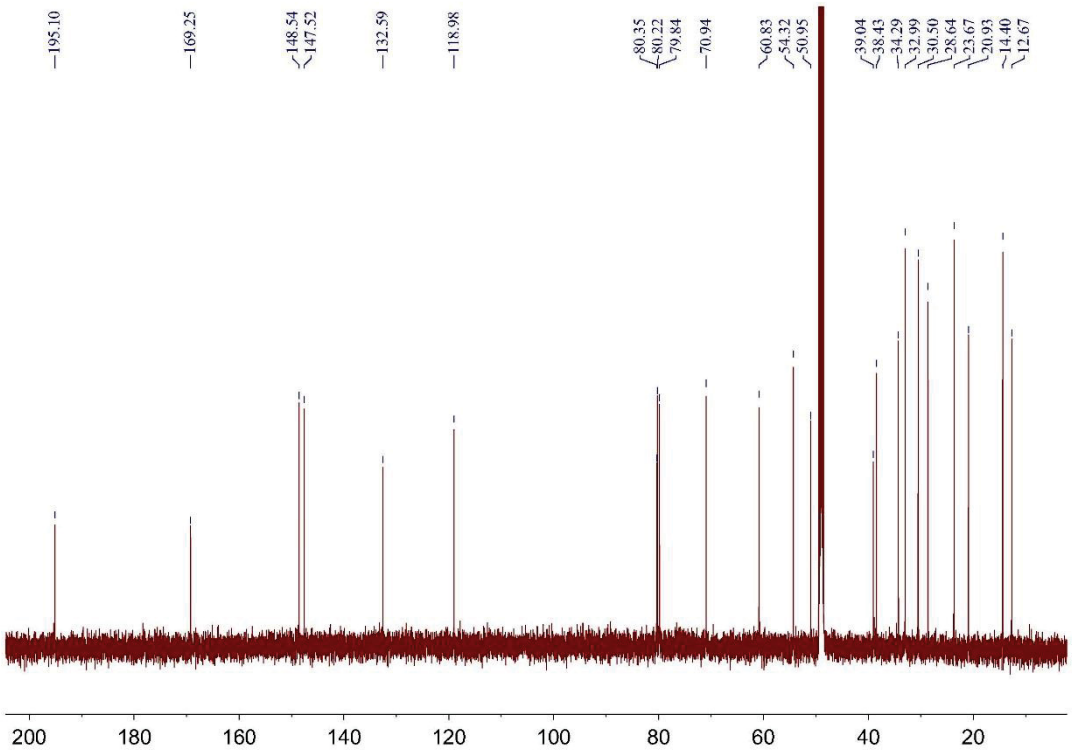

Figure S16. ^{13}C NMR (150MHz, methanol-d_4) spectrum of compound **2**.

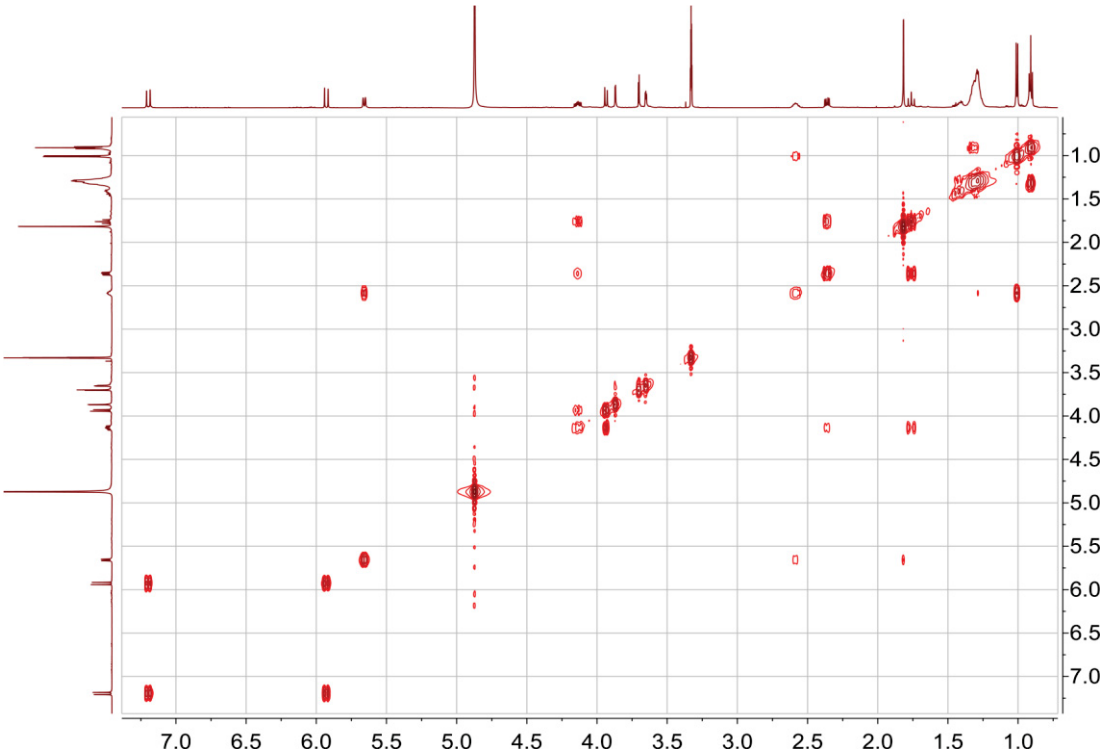

Figure S17. ^{1}H-^{1}H COSY (600MHz, methanol-d_4) spectrum of compound **2**.

Figure S18. HSQC (600MHz, 150MHz, methanol-d_4) spectrum of compound **2**.

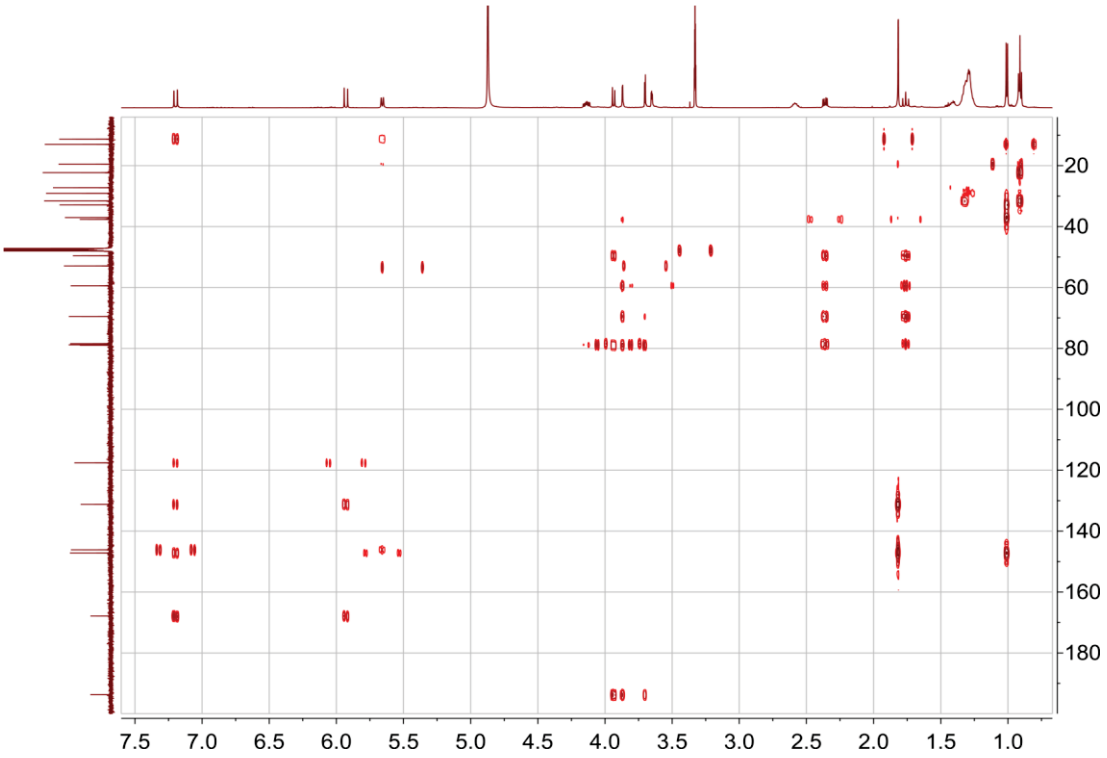

Figure S19. HMBC (600MHz, 150MHz, methanol-d_4) spectrum of compound **2**.

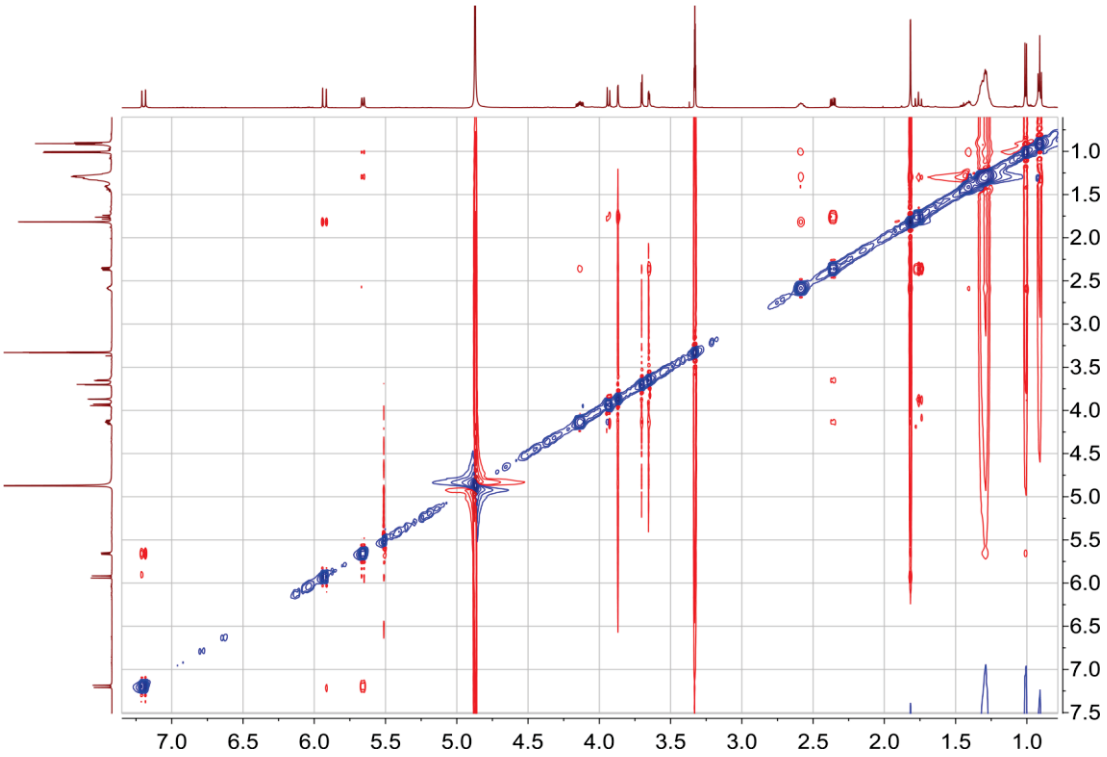

Figure S20. ROESY (600MHz, methanol-d_4) spectrum of compound **2**.

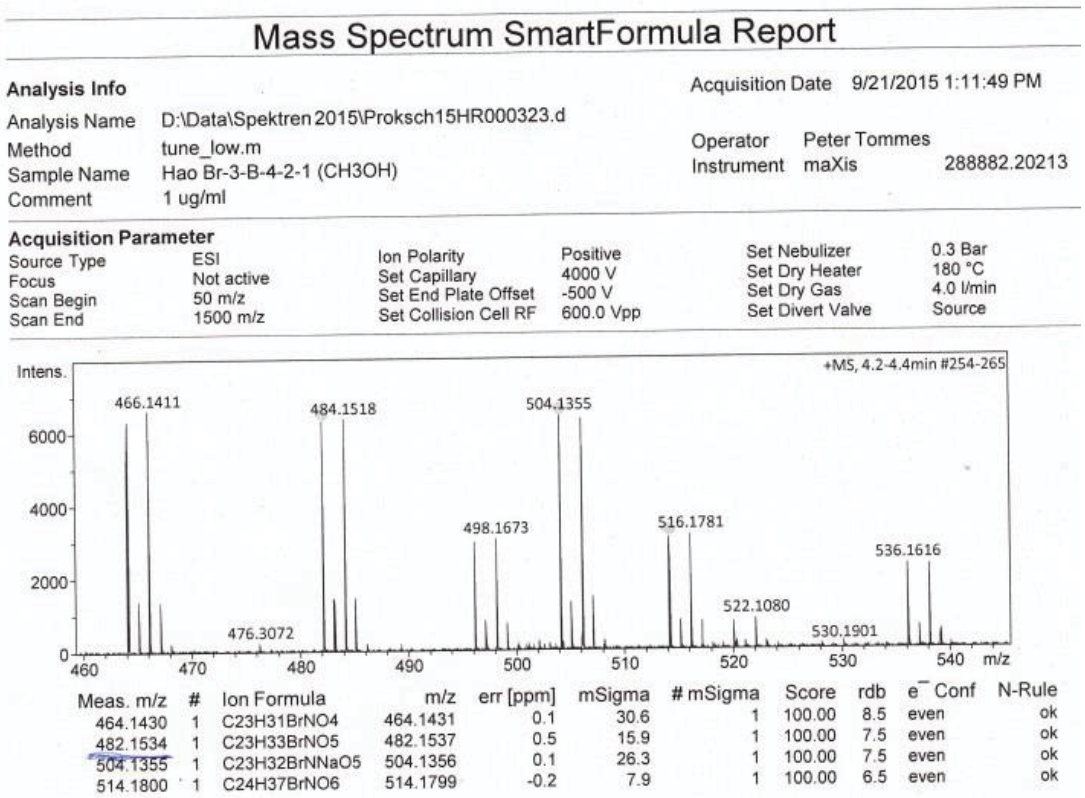

Mass Spectrum SmartFormula Report

Analysis Info

Analysis Name	D:\Data\Spektren 2015\Proksch15HR000323.d	Acquisition Date	9/21/2015 1:11:49 PM
Method	tune_low.m	Operator	Peter Tommes
Sample Name	Hao Br-3-B-4-2-1 (CH3OH)	Instrument	maXis 288882.20213
Comment	1 ug/ml		

Acquisition Parameter

Source Type	ESI	Ion Polarity	Positive	Set Nebulizer	0.3 Bar
Focus	Not active	Set Capillary	4000 V	Set Dry Heater	180 °C
Scan Begin	50 m/z	Set End Plate Offset	-500 V	Set Dry Gas	4.0 l/min
Scan End	1500 m/z	Set Collision Cell RF	600.0 Vpp	Set Divert Valve	Source

Meas. m/z	#	Ion Formula	m/z	err [ppm]	mSigma	# mSigma	Score	rdb	e⁻ Conf	N-Rule
464.1430	1	C23H31BrNO4	464.1431	0.1	30.6	1	100.00	8.5	even	ok
482.1534	1	C23H33BrNO5	482.1537	0.5	15.9	1	100.00	7.5	even	ok
504.1355	1	C23H32BrNNaO5	504.1356	0.1	26.3	1	100.00	7.5	even	ok
514.1800	1	C24H37BrNO6	514.1799	-0.2	7.9	1	100.00	6.5	even	ok

Figure S21. HRESIMS of compound **3**.

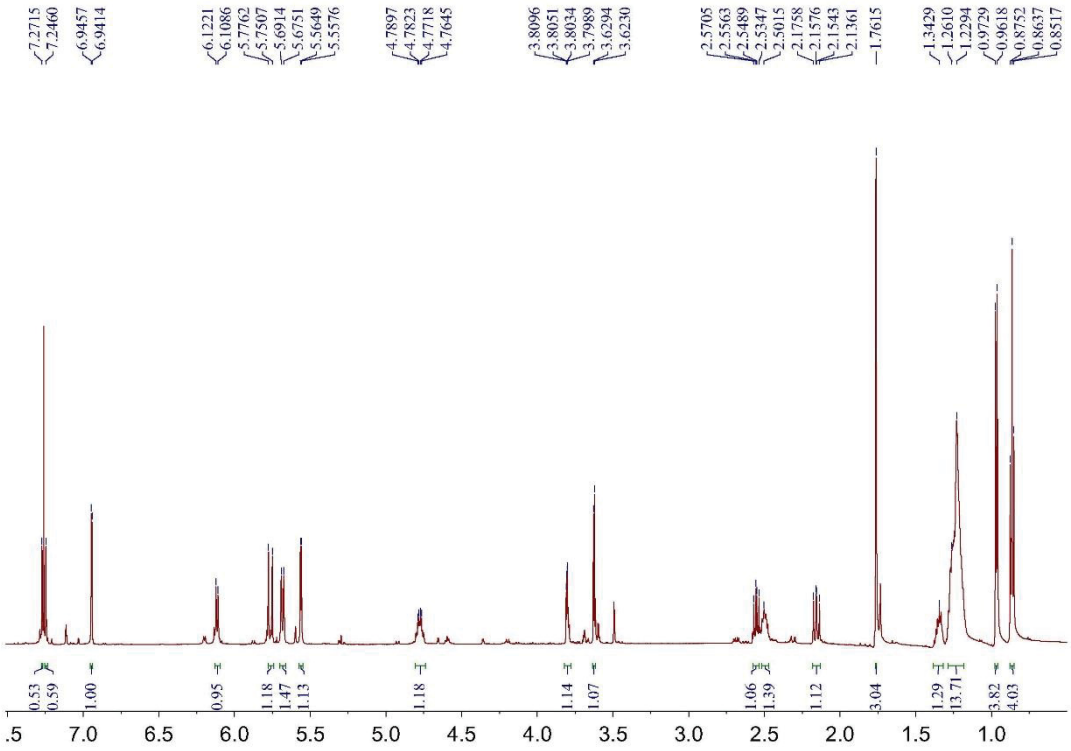

Figure S22. ^{1}H NMR (600MHz, $CDCl_3$) spectrum of compound **3**.

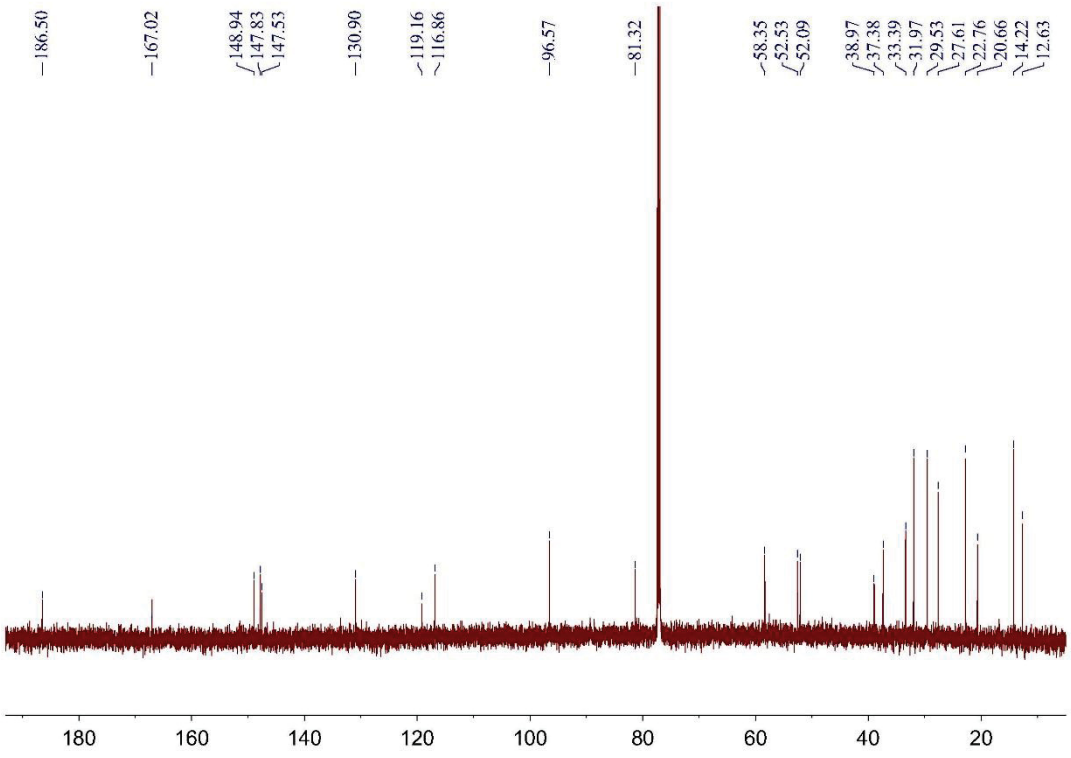

Figure S23. ^{13}C NMR (150MHz, $CDCl_3$) spectrum of compound **3**.

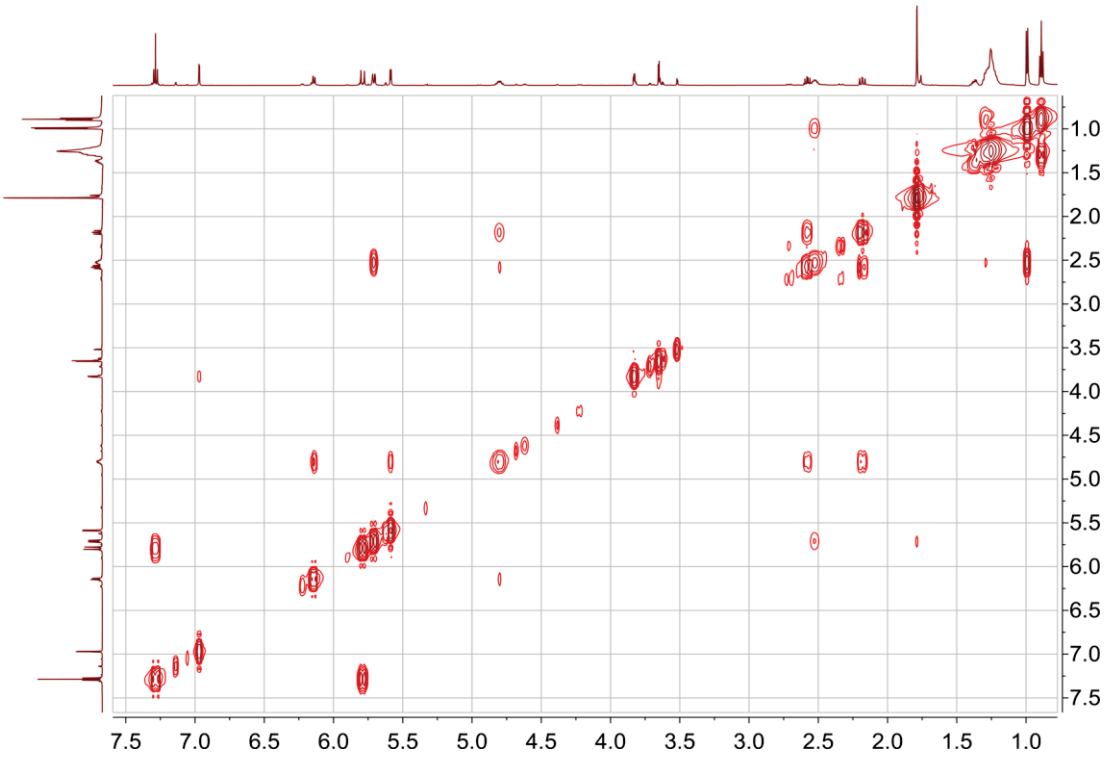

Figure S24. ^{1}H-^{1}H COSY (600MHz, $CDCl_3$) spectrum of compound **3**.

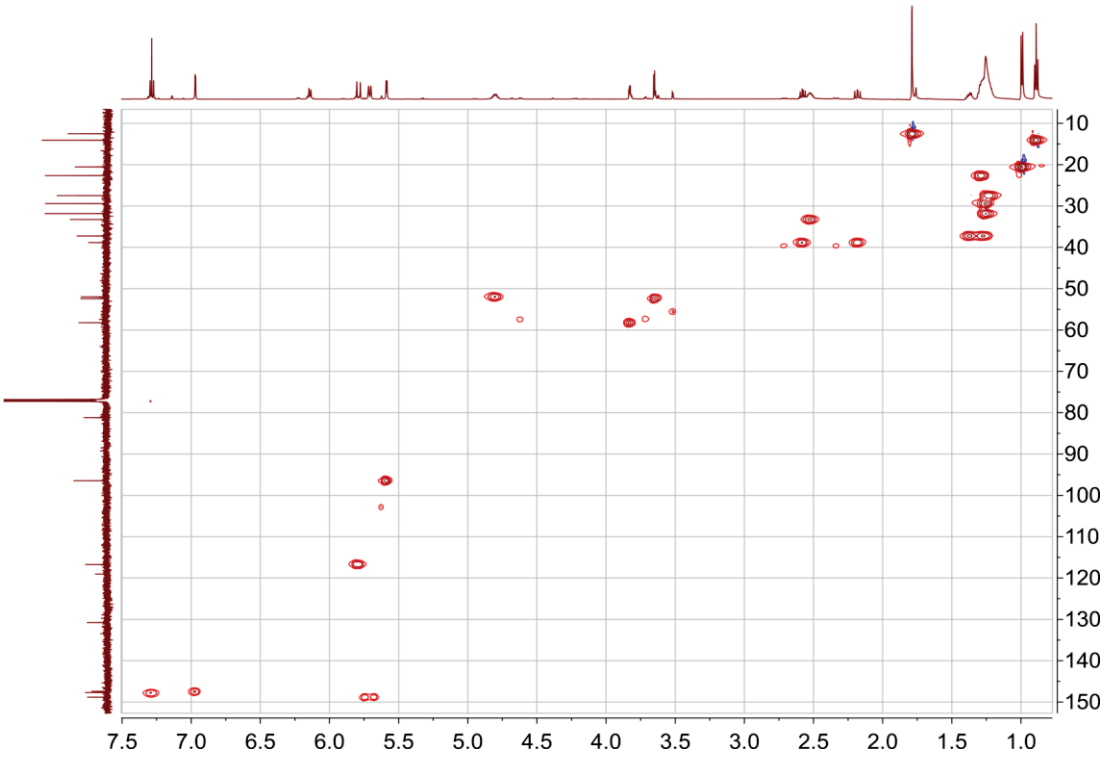

Figure S25. HSQC (600MHz, 150MHz, $CDCl_3$) spectrum of compound **3**.

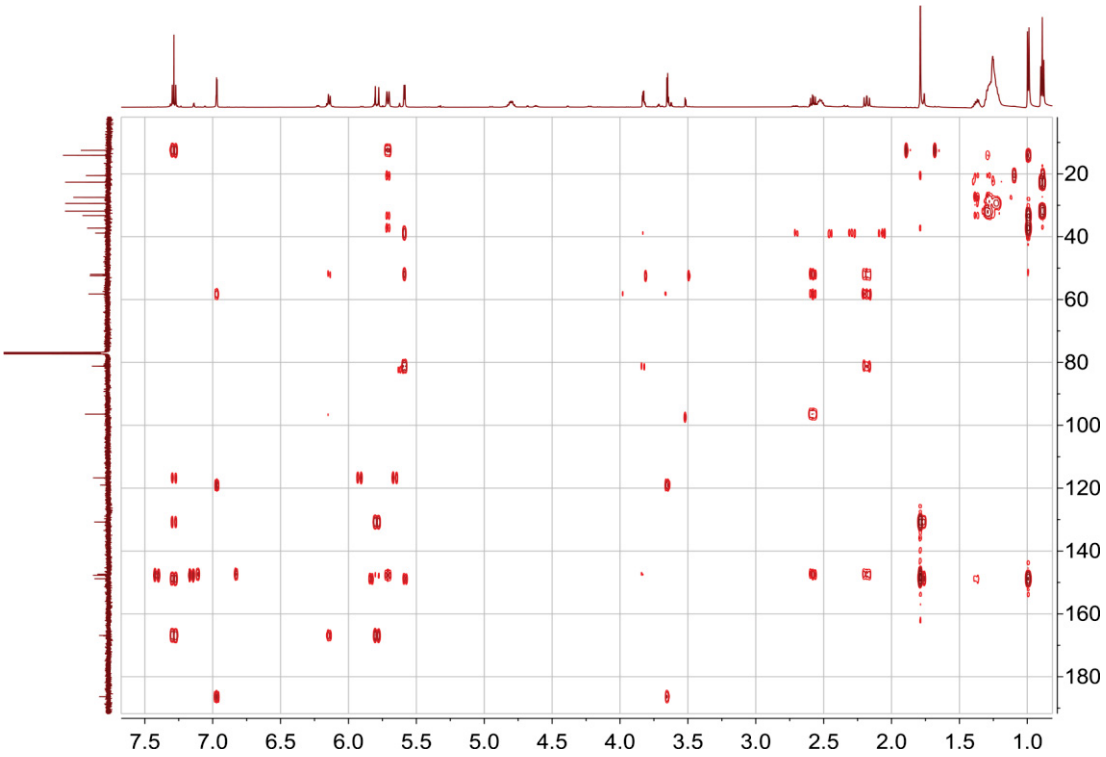

Figure S26. HMBC (600MHz, 150MHz, $CDCl_3$) spectrum of compound **3**.

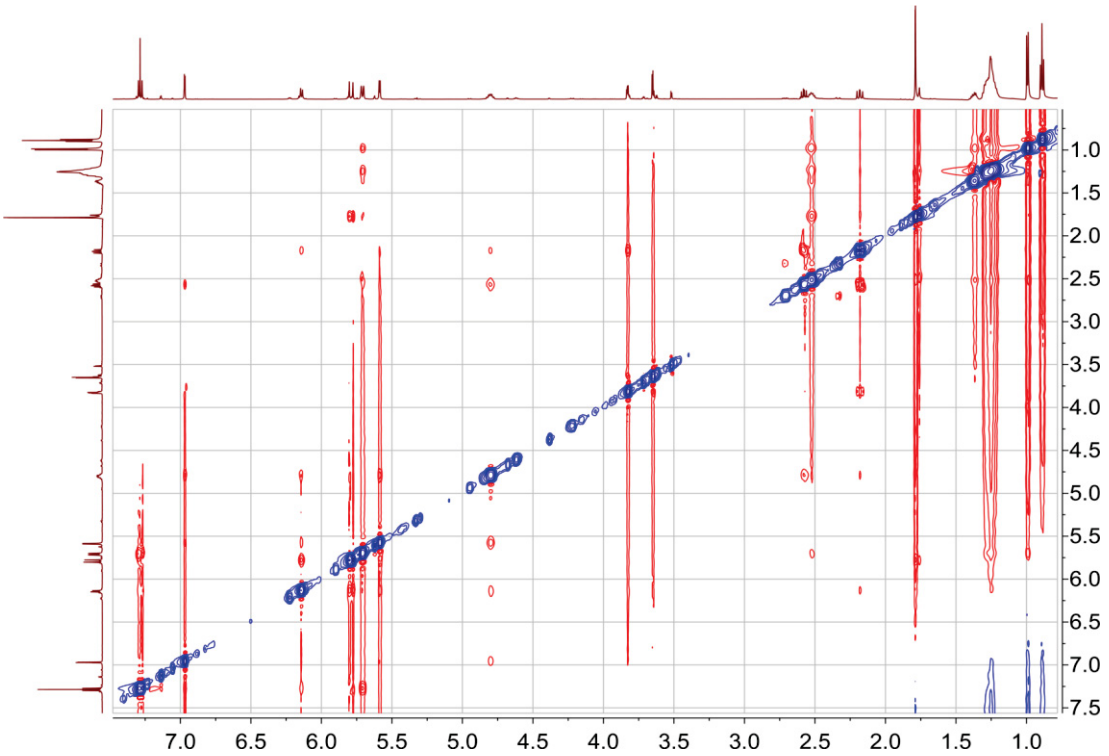

Figure S27. ROESY (600MHz, $CDCl_3$) spectrum of compound **3**.

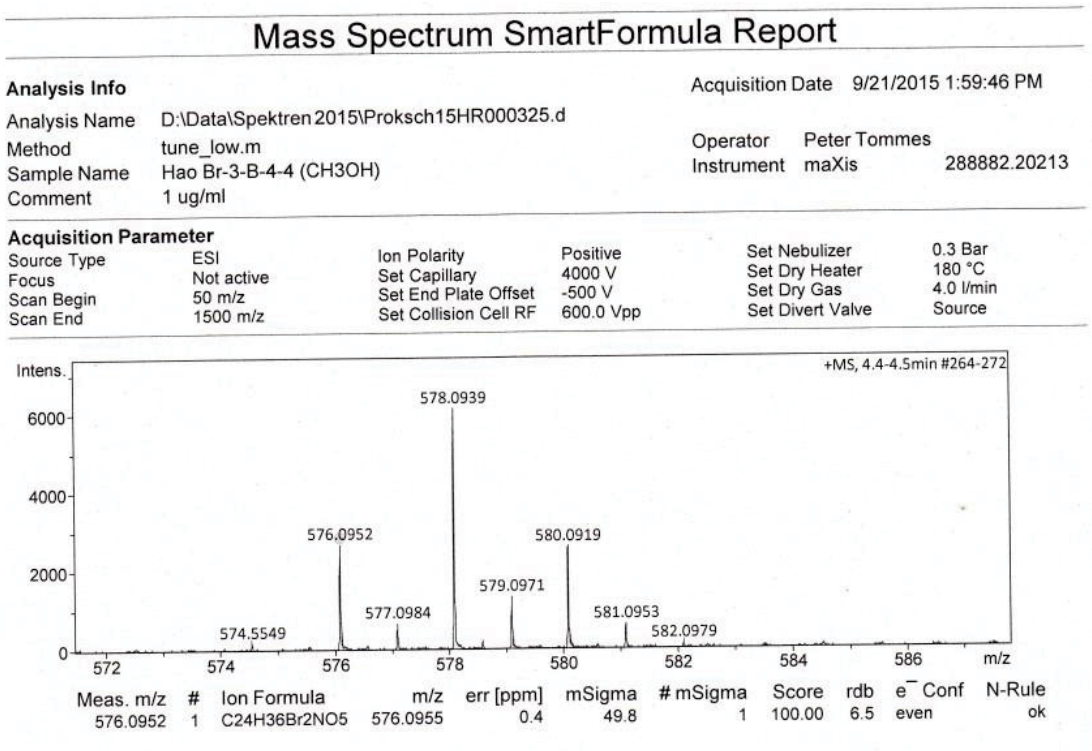

Figure S28. HRESIMS of compound **4**.

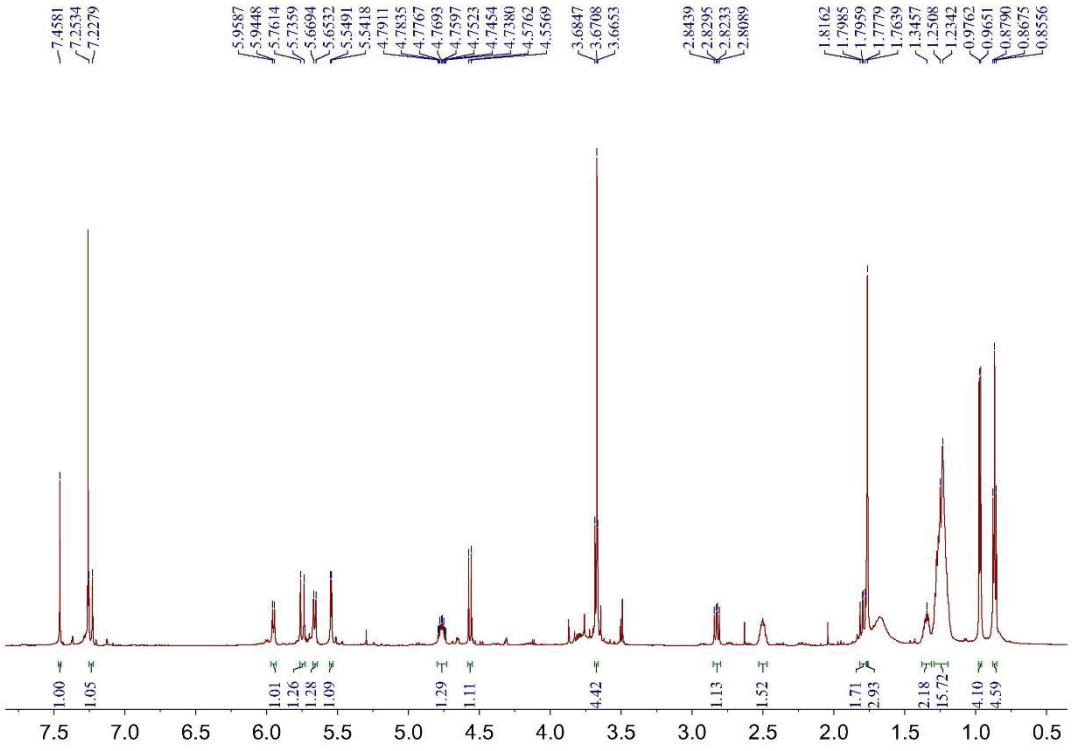

Figure S29. ^{1}H NMR (600MHz, $CDCl_3$) spectrum of compound **4**.

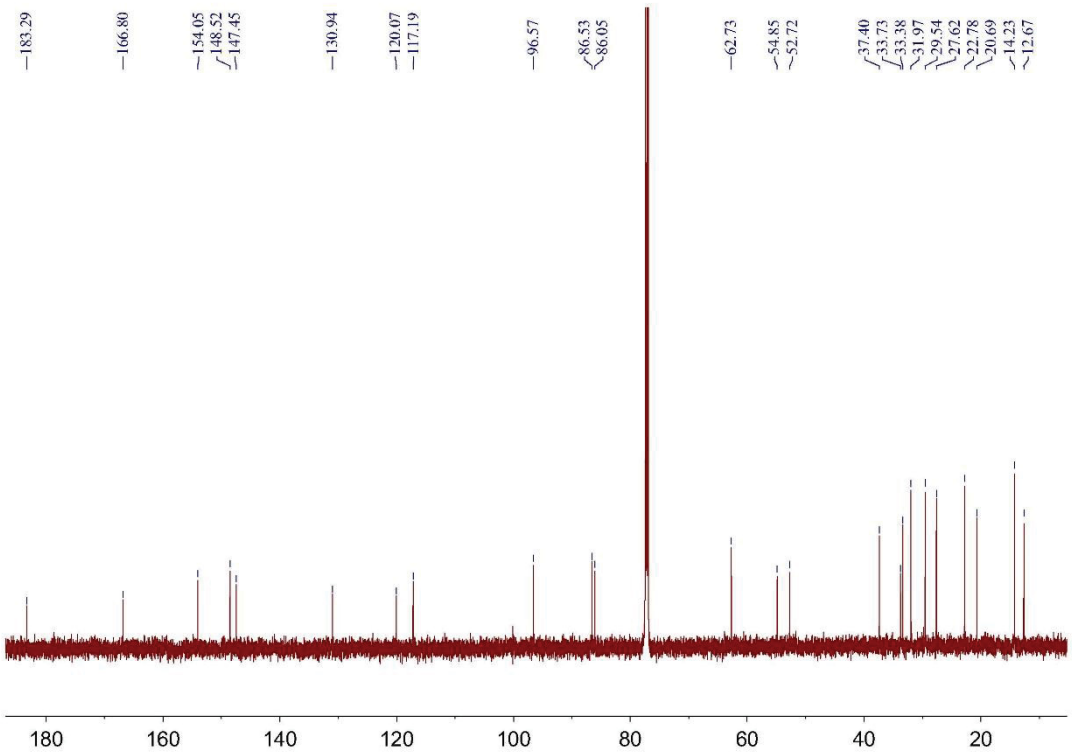

Figure S30. ^{13}C NMR (150MHz, $CDCl_3$) spectrum of compound **4**.

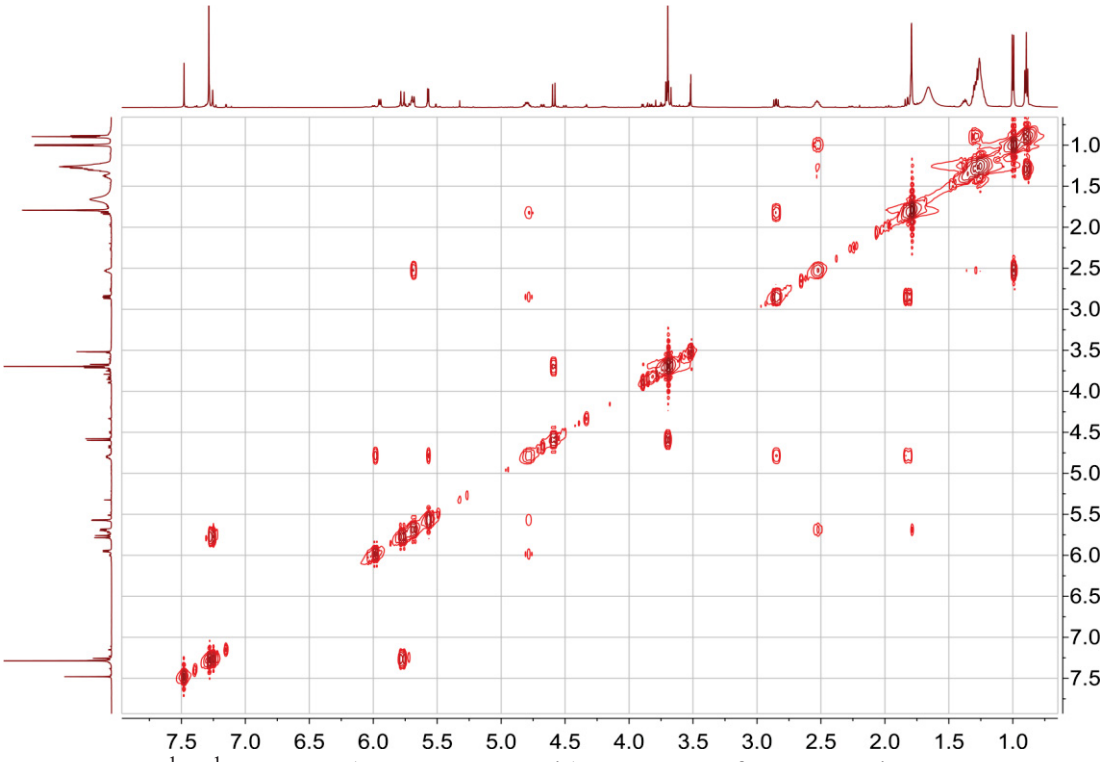

Figure S31. ^{1}H-^{1}H COSY (600MHz, $CDCl_3$) spectrum of compound **4**.

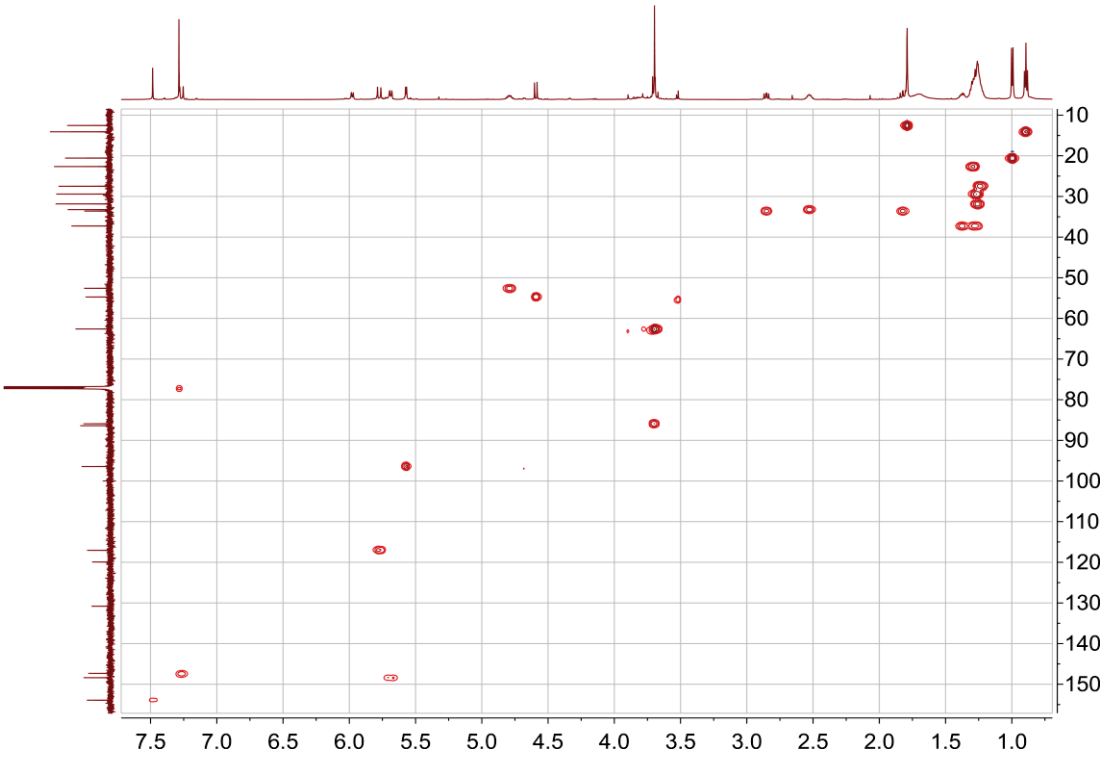

Figure S32. HSQC (600MHz, 150MHz, $CDCl_3$) spectrum of compound **4**.

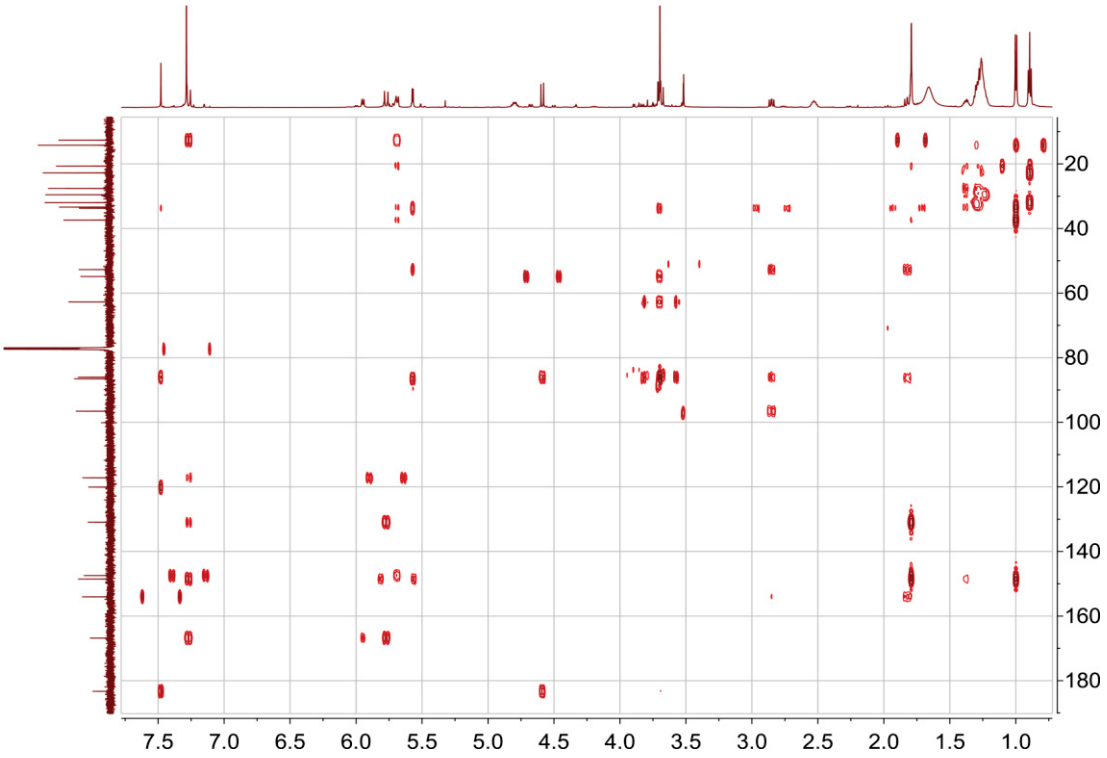

Figure S33. HMBC (600MHz, 150MHz, $CDCl_3$) spectrum of compound **4**.

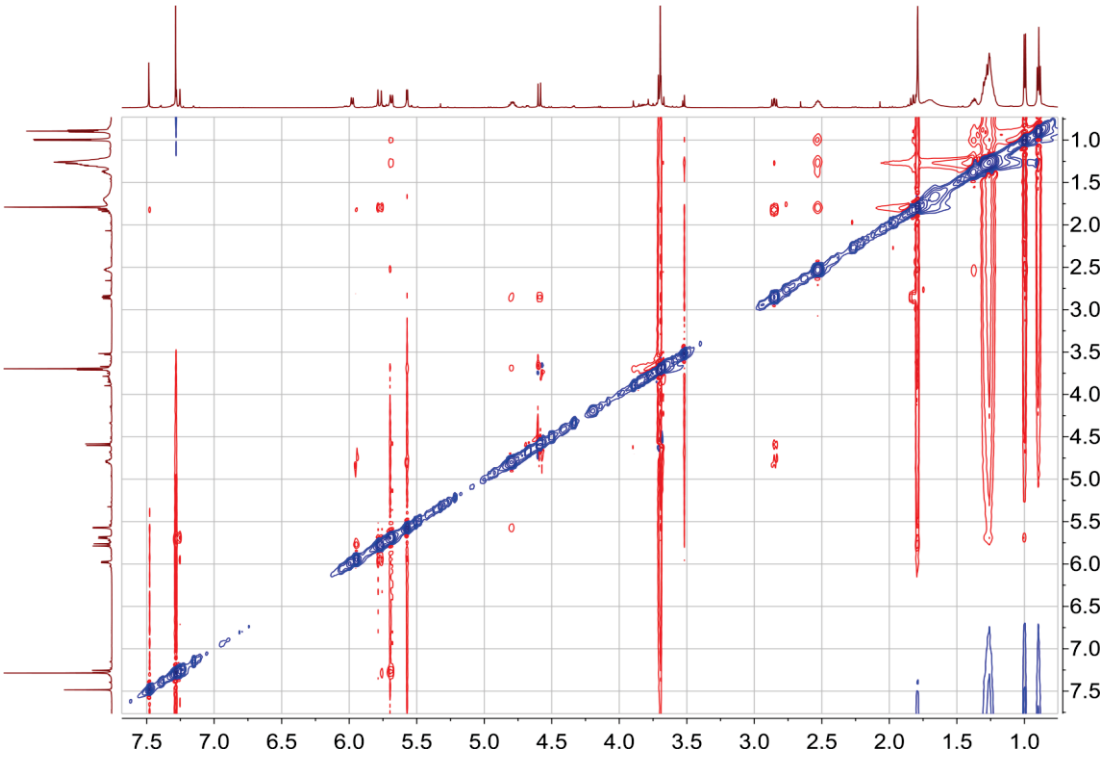

Figure S34. ROESY (600MHz, $CDCl_3$) spectrum of compound **4**.

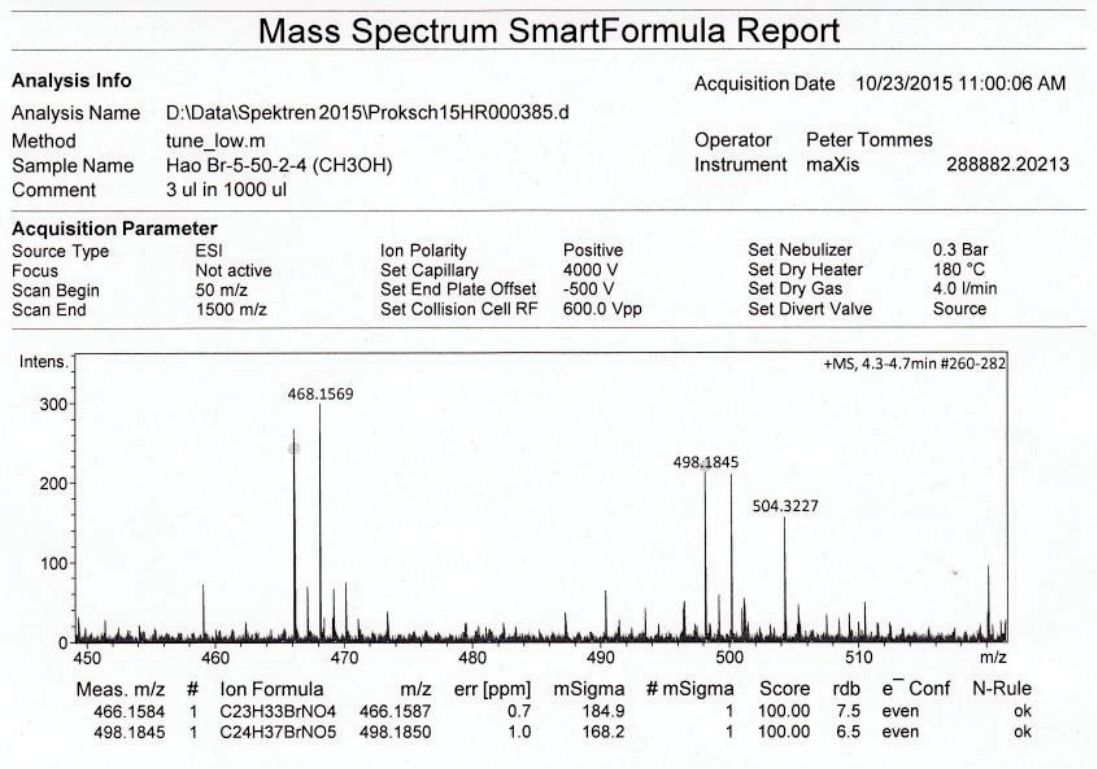

Figure S35. HRESIMS of compound **5**.

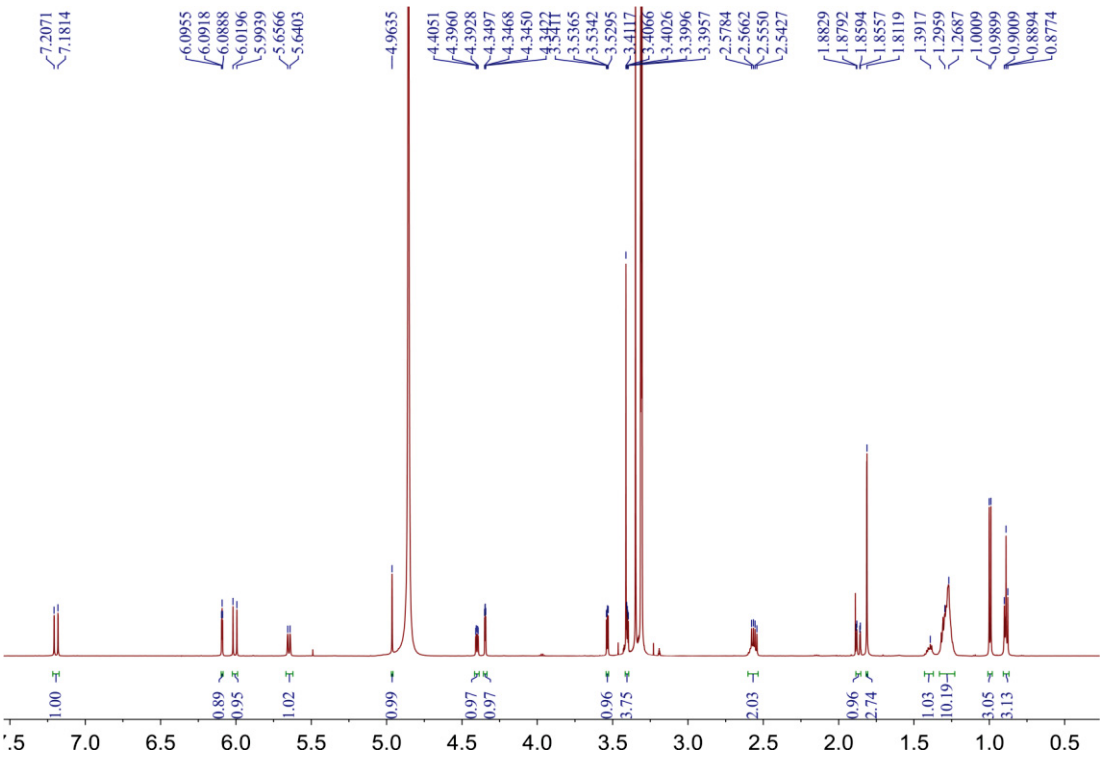

Figure S36. ^{1}H NMR (600MHz, methanol-d_4) spectrum of compound **5**.

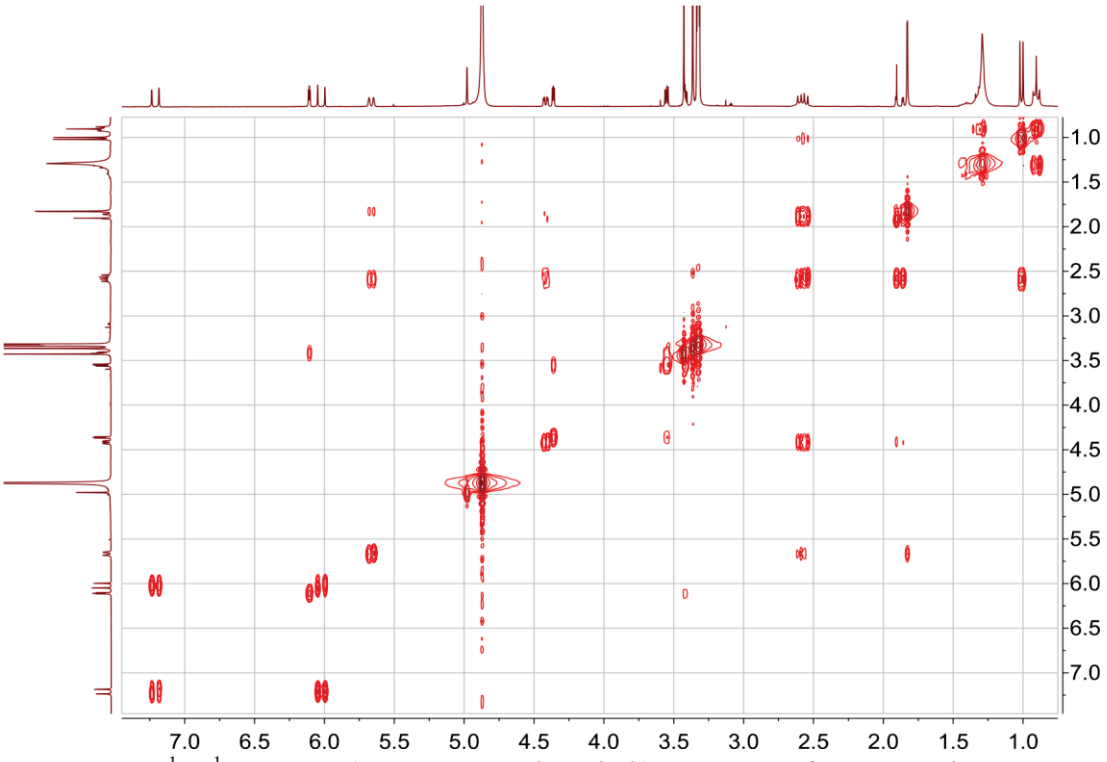

Figure S37. ^{1}H-^{1}H COSY (300MHz, methanol-d_4) spectrum of compound **5**.

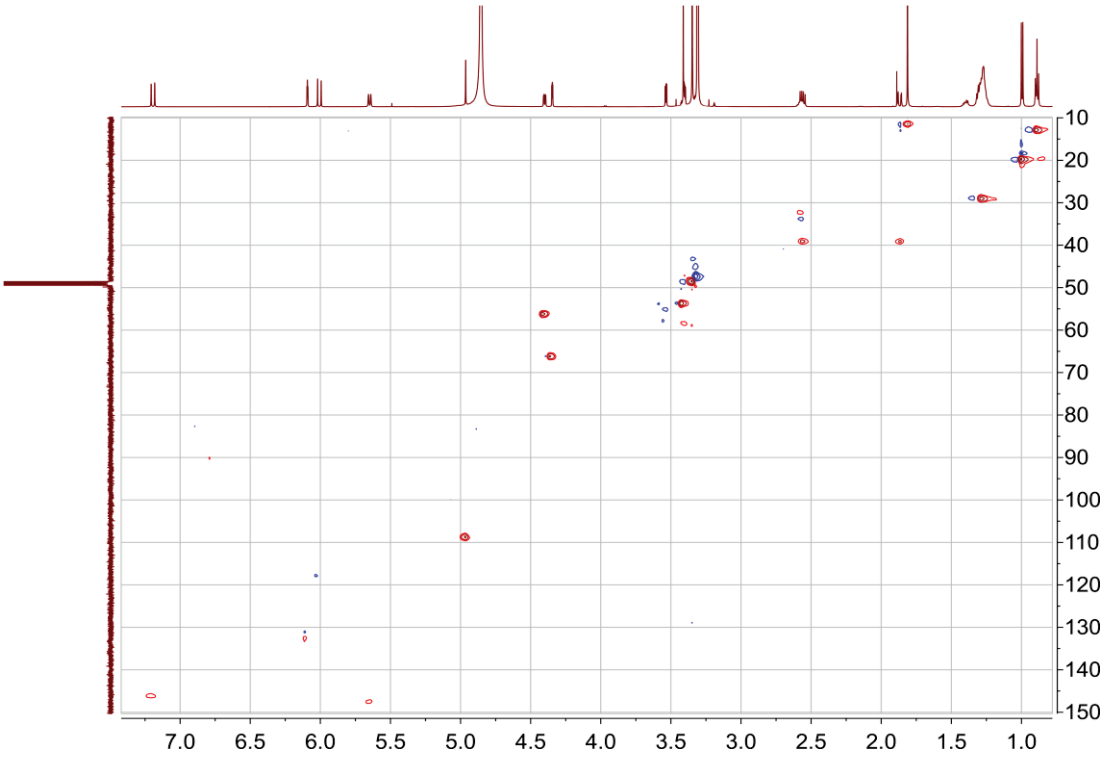

Figure S38. HSQC (600MHz, 150MHz, methanol-d_4) spectrum of compound **5**.

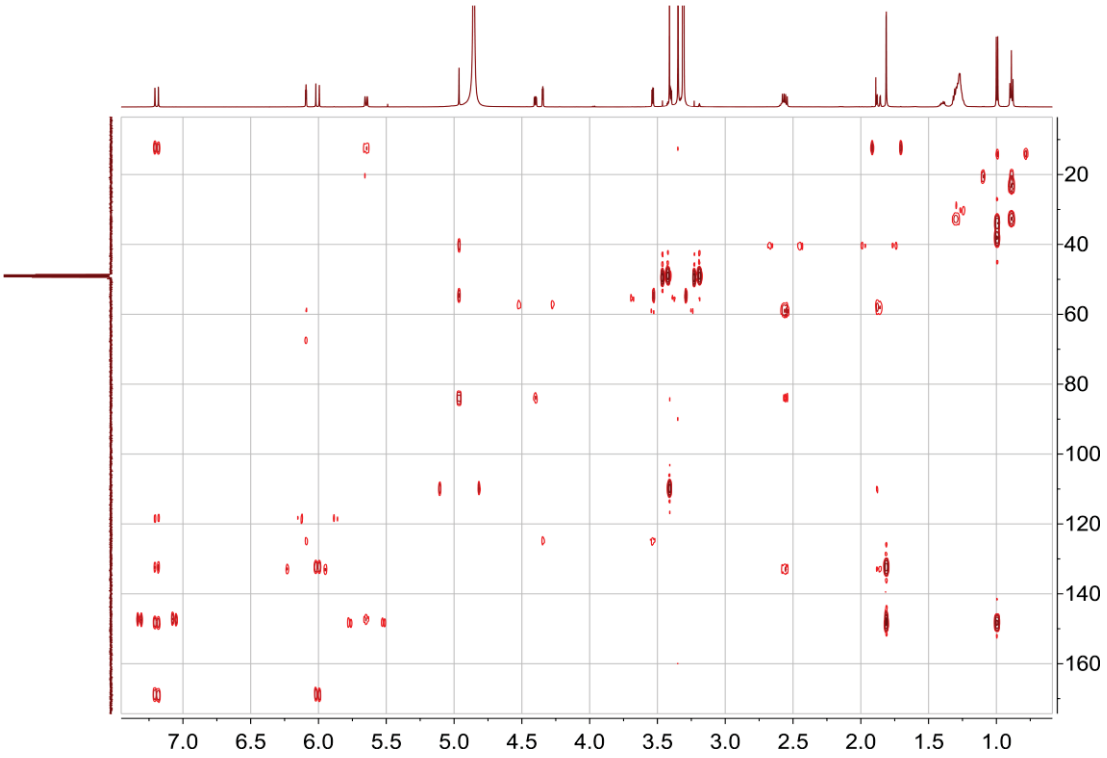

Figure S39. HMBC (600MHz, 150MHz, methanol-d_4) spectrum of compound **5**.

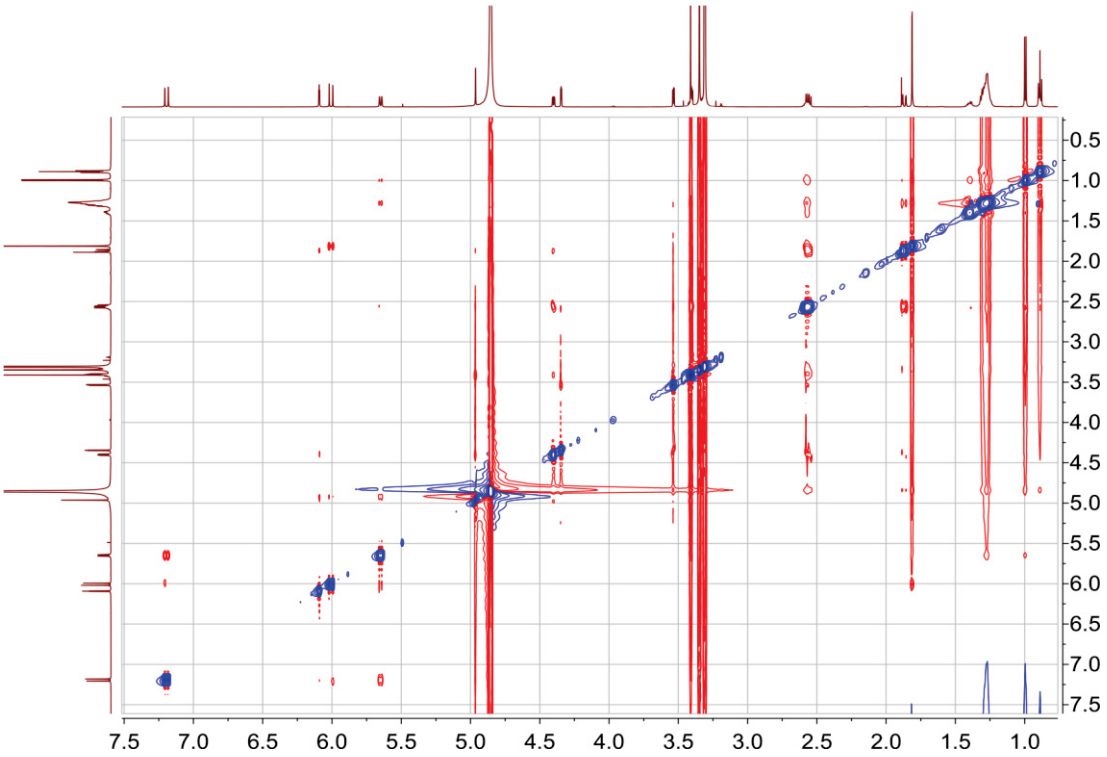

Figure S40. ROESY (600MHz, methanol-d_4) spectrum of compound **5**.

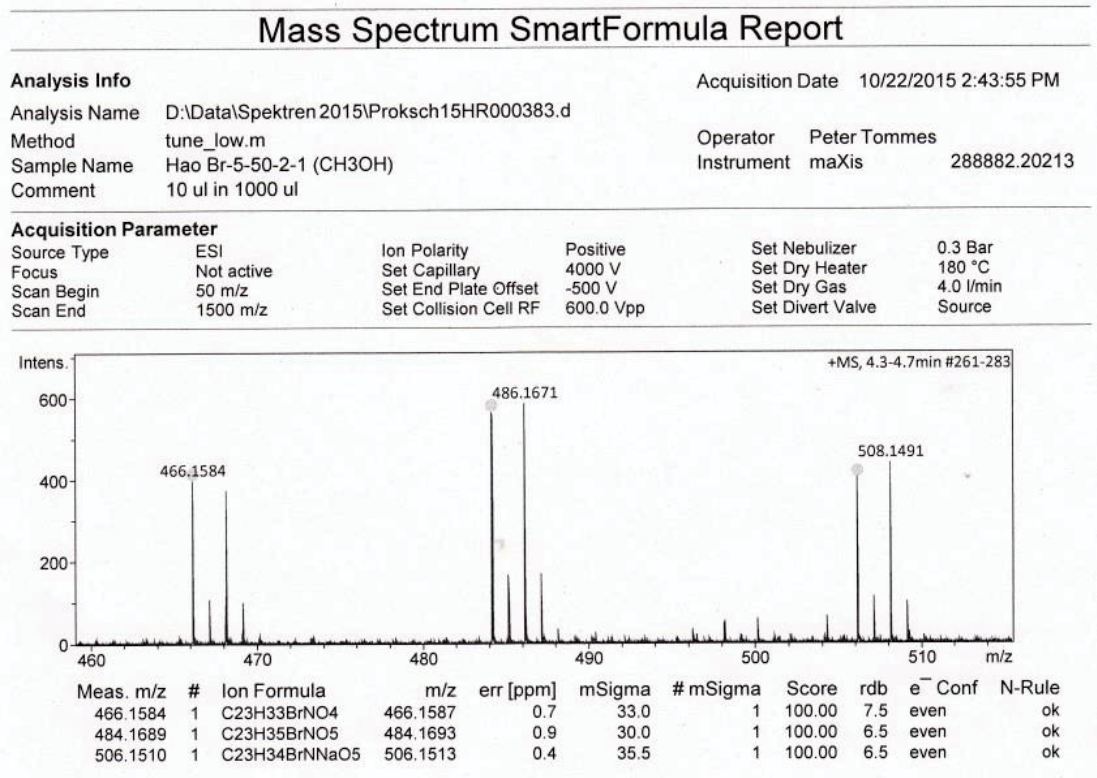

Mass Spectrum SmartFormula Report

Analysis Info

Analysis Name	D:\Data\Spektren 2015\Proksch15HR000383.d	Acquisition Date	10/22/2015 2:43:55 PM
Method	tune_low.m	Operator	Peter Tommes
Sample Name	Hao Br-5-50-2-1 (CH3OH)	Instrument	maXis 288882.20213
Comment	10 ul in 1000 ul		

Acquisition Parameter

Source Type	ESI	Ion Polarity	Positive	Set Nebulizer	0.3 Bar
Focus	Not active	Set Capillary	4000 V	Set Dry Heater	180 °C
Scan Begin	50 m/z	Set End Plate Offset	-500 V	Set Dry Gas	4.0 l/min
Scan End	1500 m/z	Set Collision Cell RF	600.0 Vpp	Set Divert Valve	Source

Meas. m/z	#	Ion Formula	m/z	err [ppm]	mSigma	# mSigma	Score	rdb	e⁻ Conf	N-Rule
466.1584	1	C23H33BrNO4	466.1587	0.7	33.0	1	100.00	7.5	even	ok
484.1689	1	C23H35BrNO5	484.1693	0.9	30.0	1	100.00	6.5	even	ok
506.1510	1	C23H34BrNNaO5	506.1513	0.4	35.5	1	100.00	6.5	even	ok

Figure S41. HRESIMS of compound **6**.

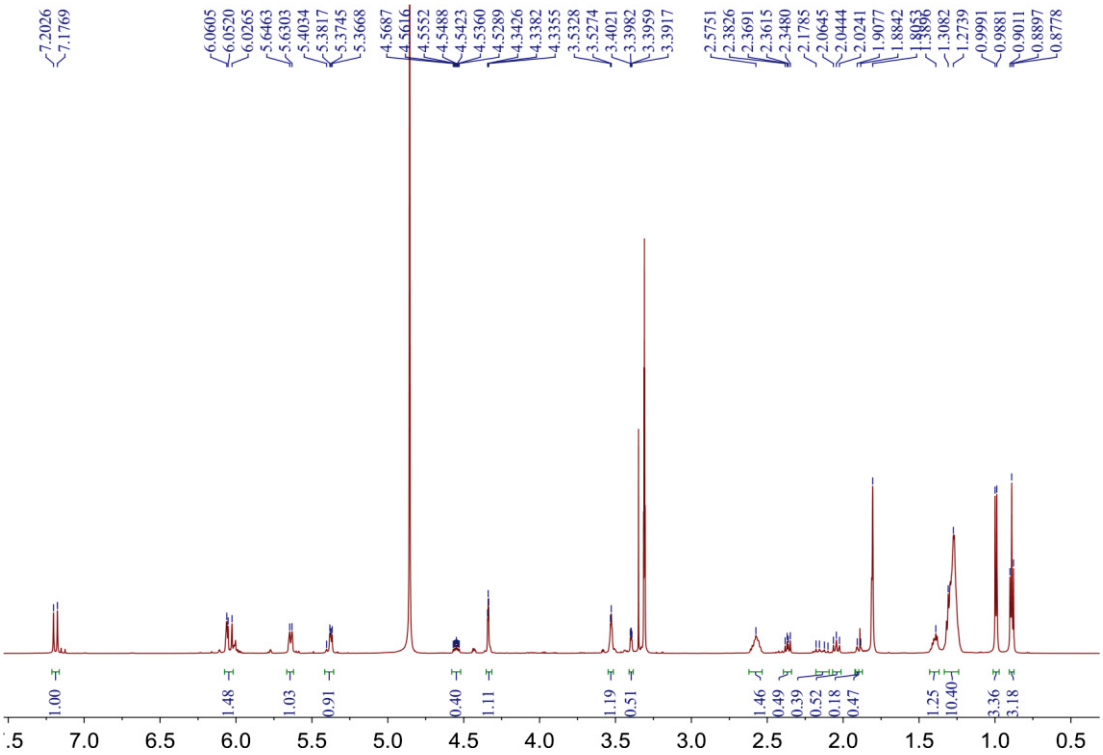

Figure S42. ^{1}H NMR (600MHz, methanol-d_4) spectrum of compound **6**.

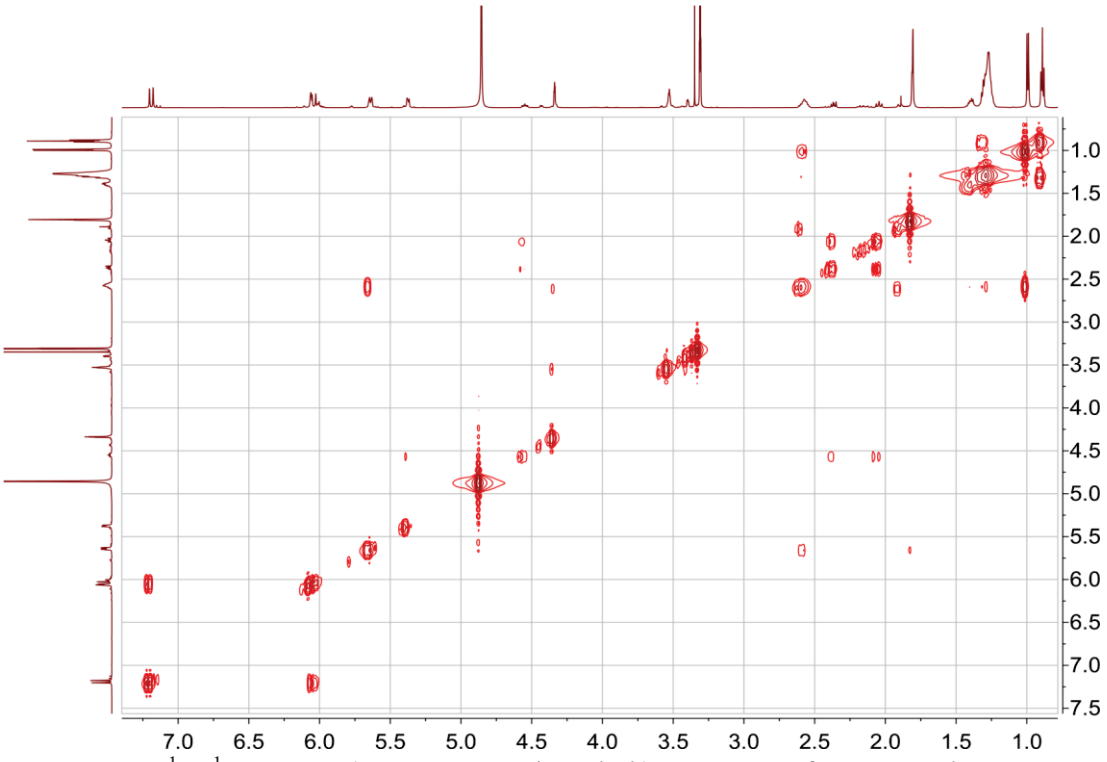

Figure S43. ^{1}H-^{1}H COSY (600MHz, methanol-d_4) spectrum of compound **6**.

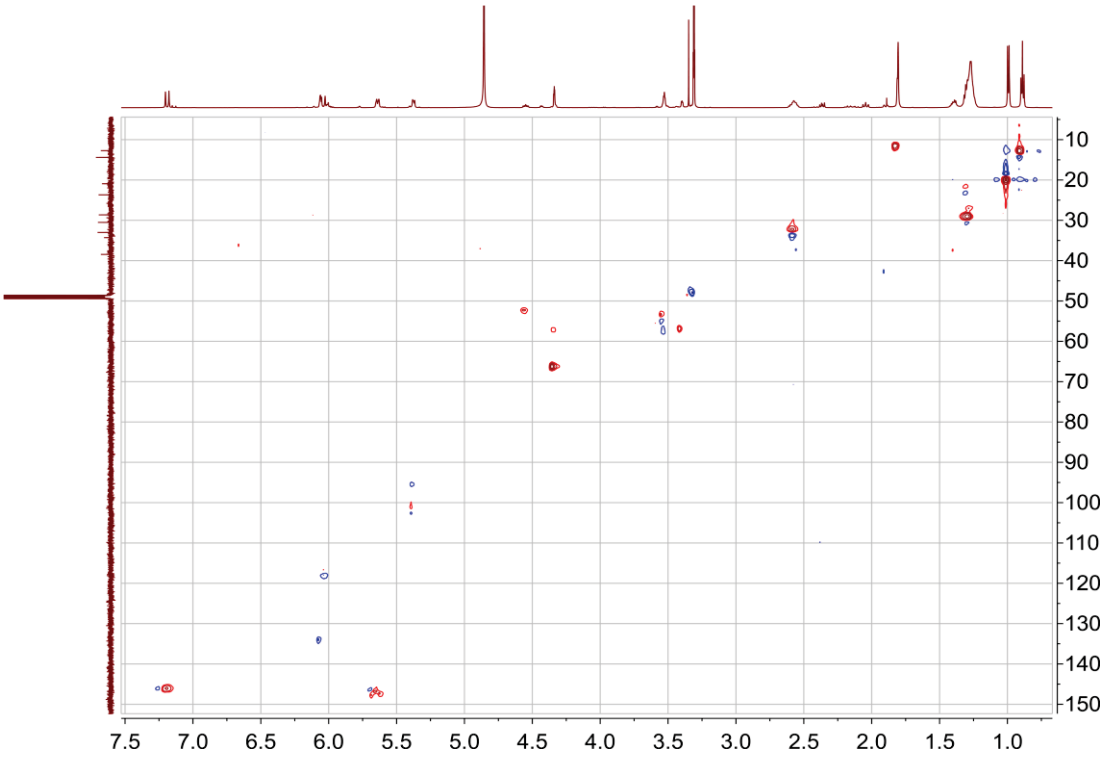

Figure S44. HSQC (600MHz, 150MHz, methanol-d_4) spectrum of compound **6**.

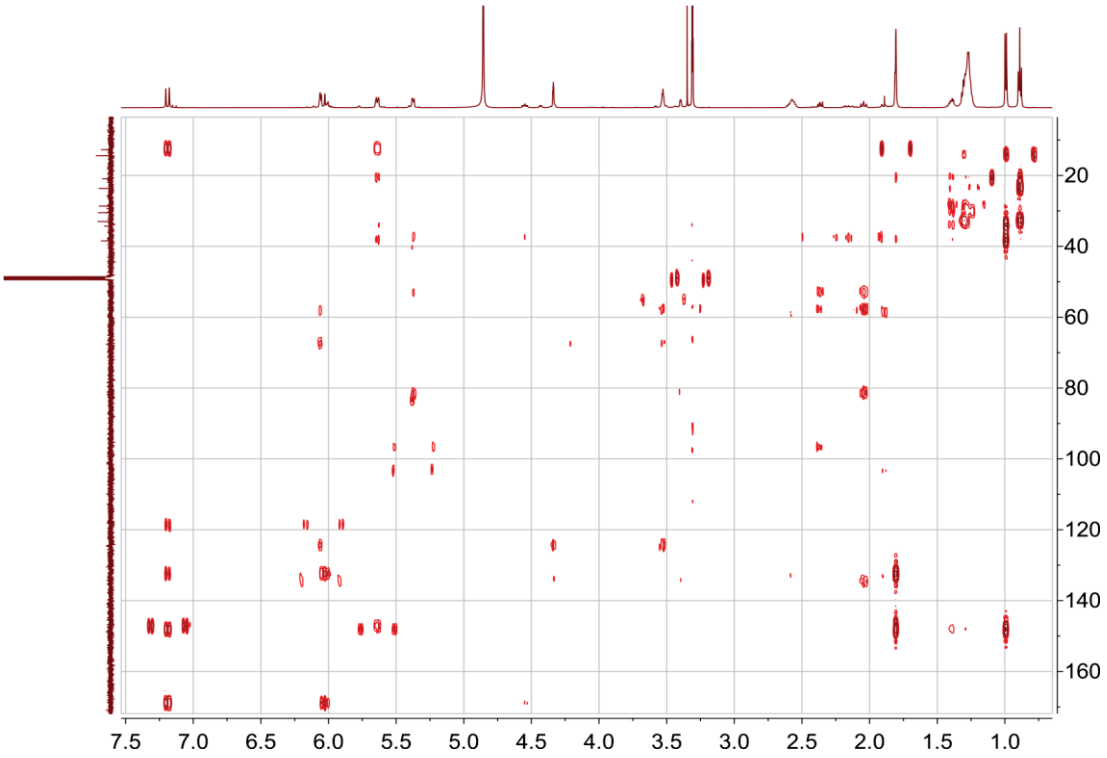

Figure S45. HMBC (600MHz, 150MHz, methanol-d_4) spectrum of compound **6**.

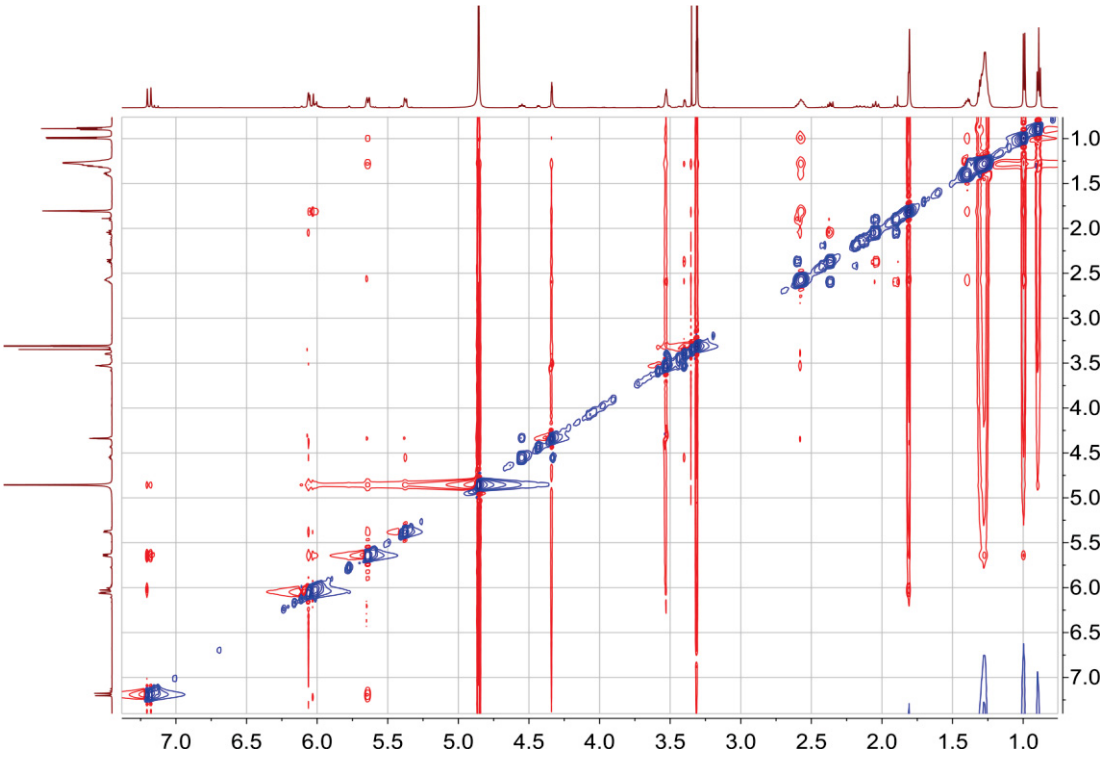

Figure S46. ROESY (600MHz, methanol-d_4) spectrum of compound **6**.

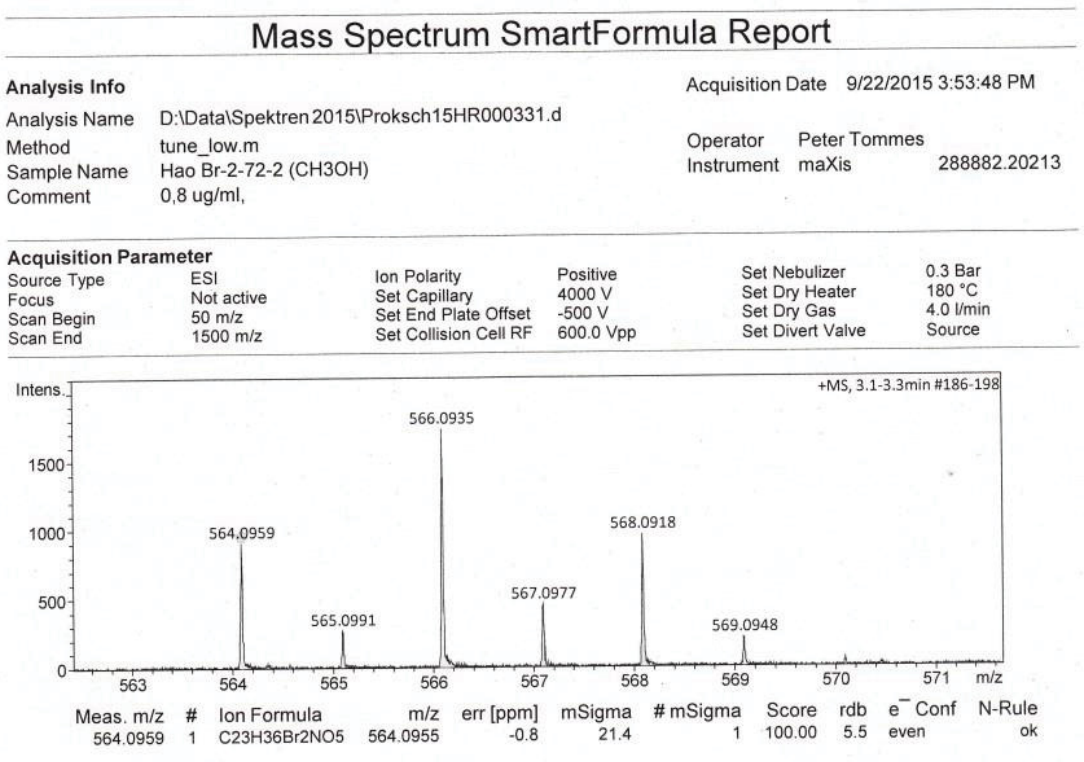

Figure S47. HRESIMS of compound **7**.

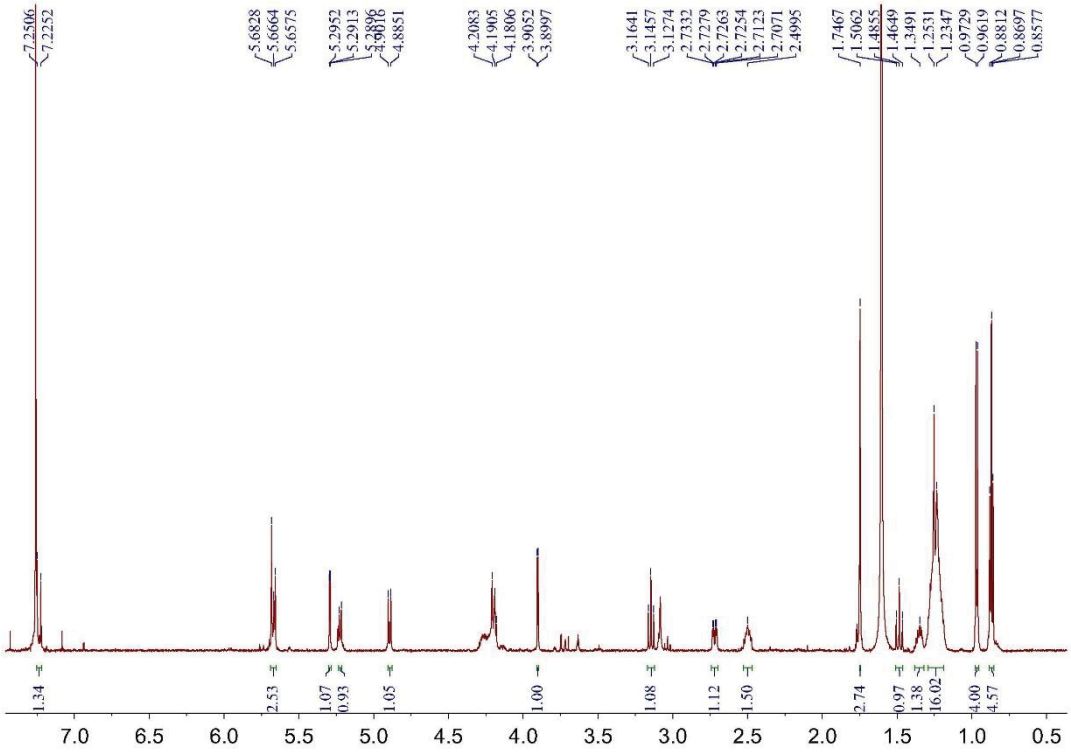

Figure S48. ^{1}H NMR (600MHz, $CDCl_3$) spectrum of compound **7**.

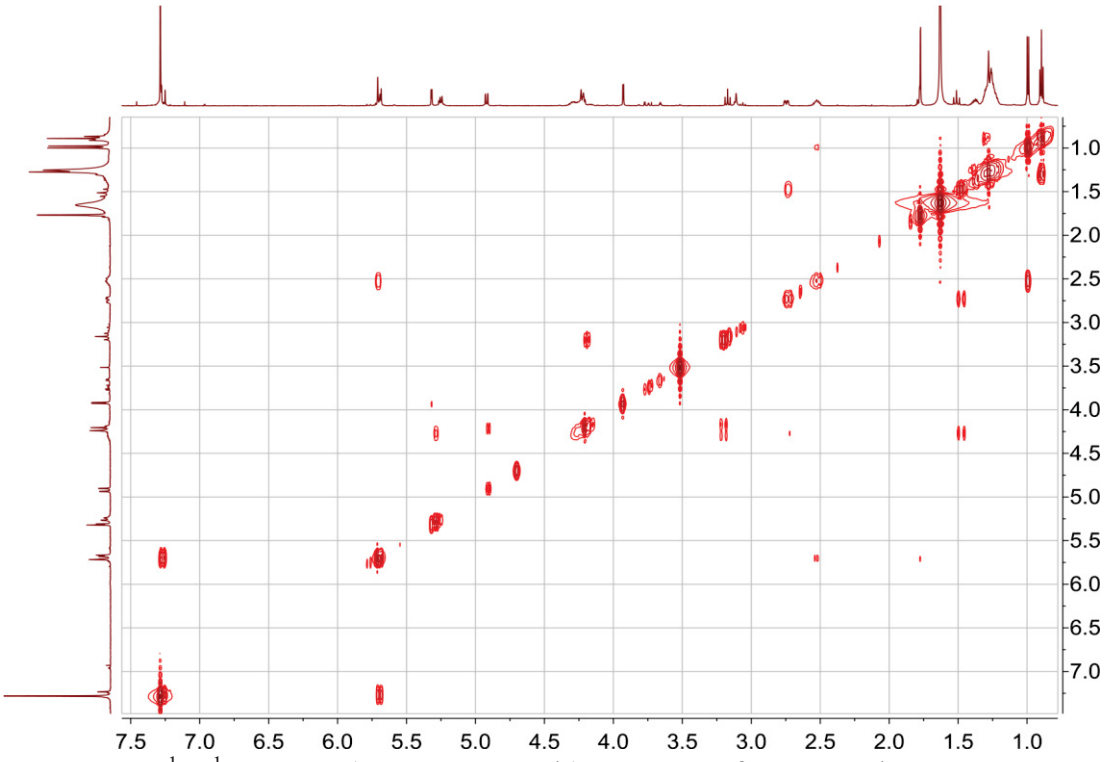

Figure S49. ^{1}H-^{1}H COSY (600MHz, $CDCl_3$) spectrum of compound **7**.

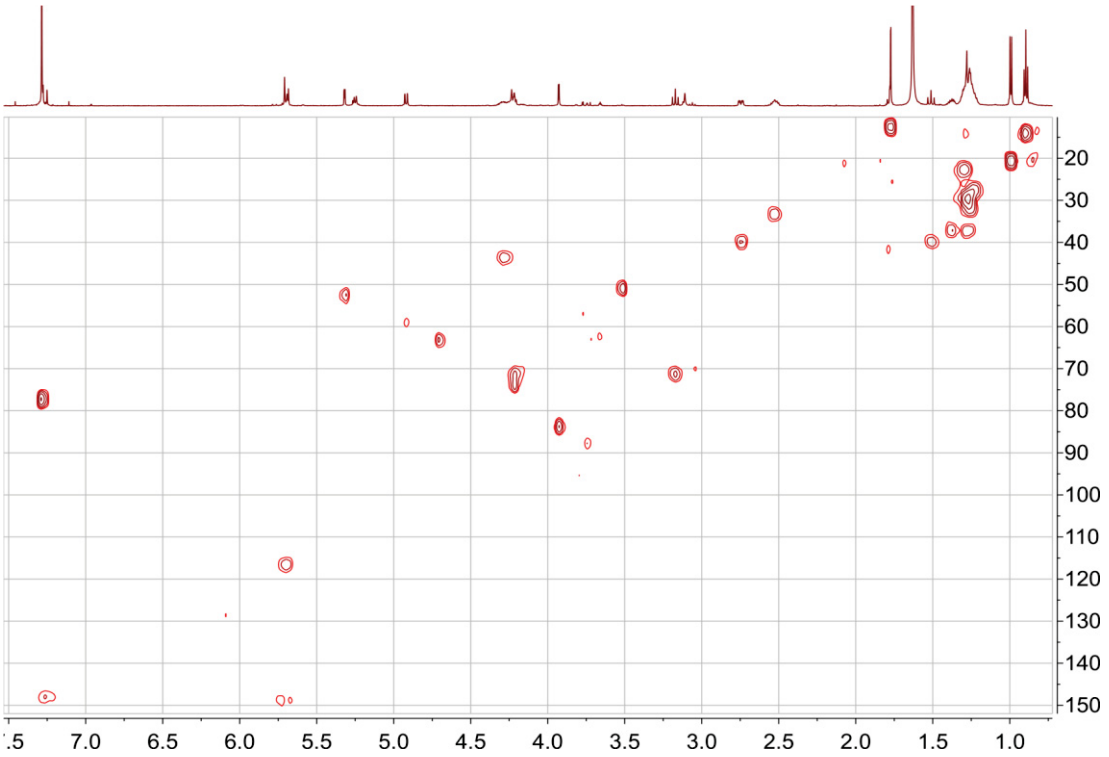

Figure S50. HSQC (600MHz, 150MHz, $CDCl_3$) spectrum of compound **7**.

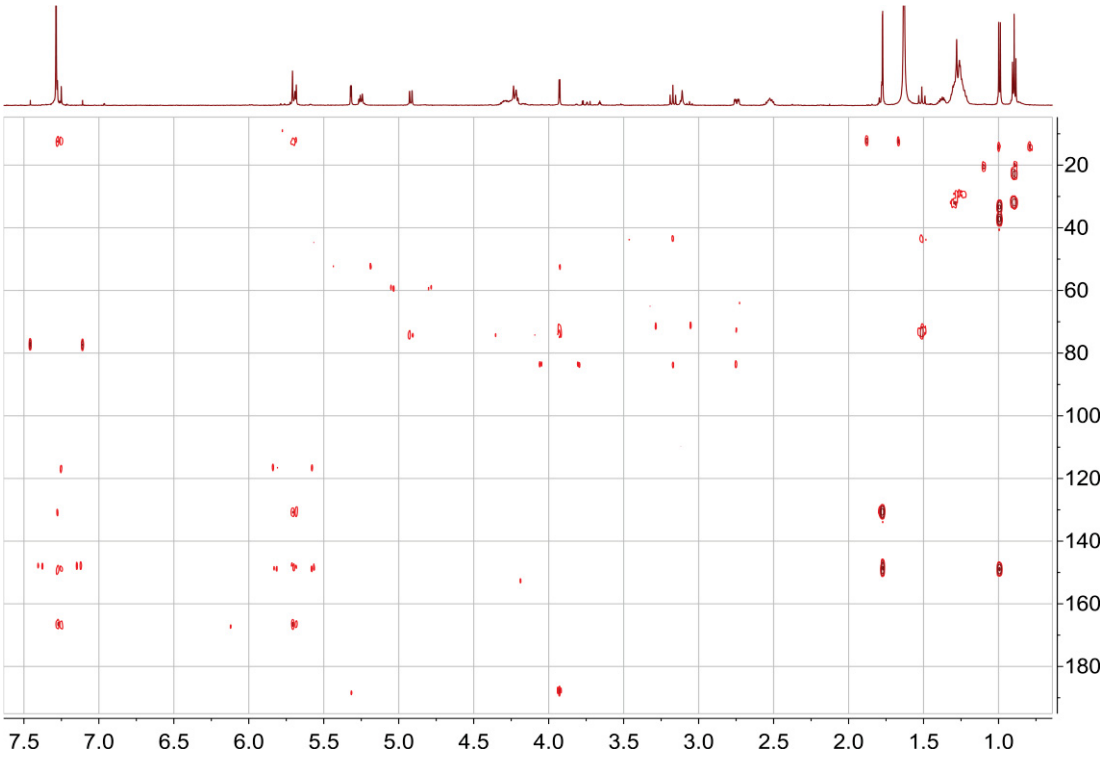

Figure S51. HMBC (600MHz, 150MHz, $CDCl_3$) spectrum of compound **7**.

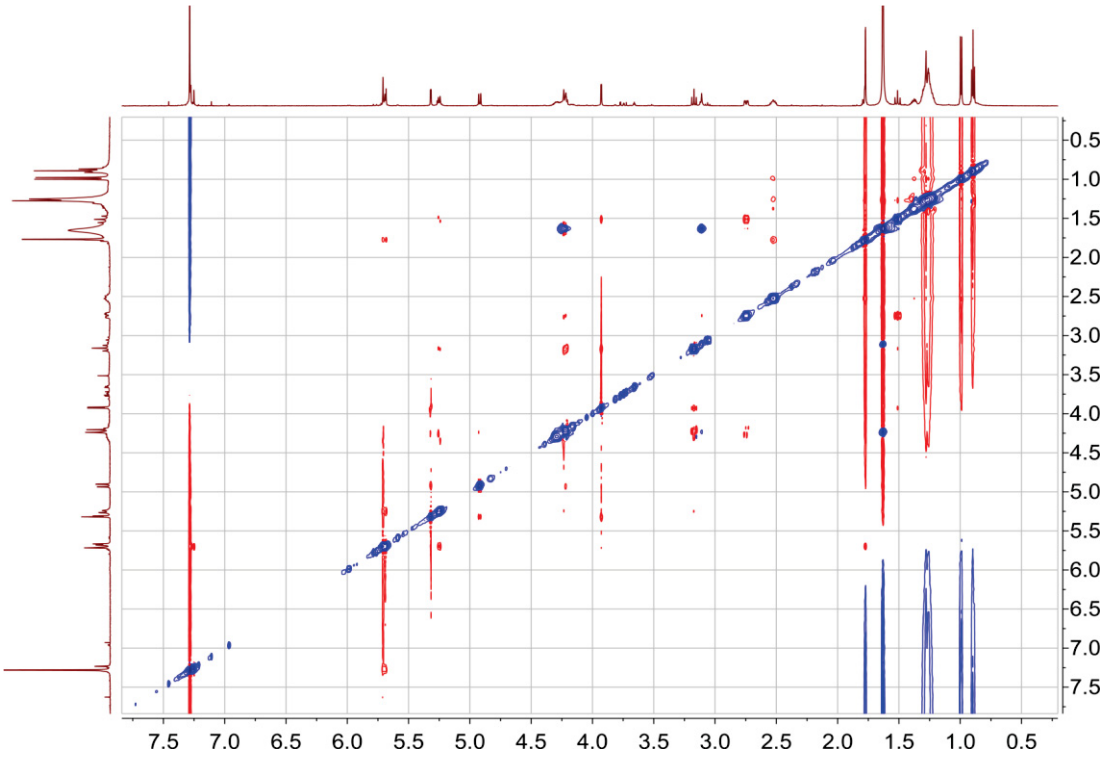

Figure S52. ROESY (600MHz, $CDCl_3$) spectrum of compound **7**.

X-ray crystallographic parameters of compound 1 (CCDC 1481781)

Crystallization conditions: X-ray quality crystal of **1** was obtained by slow evaporation from MeOH solution. A suitable single crystal was carefully selected under a polarizing microscope. *Data collection*: Bruker Kappa APEX2 CCD diffractometer (with microfocus tube), Mo-Kα radiation (λ = 0.71073 Å), multilayer mirror, ω- and -scan; data collection with APEX2, cell refinement and data reduction with SAINT,[1] experimental absorption correction with SADABS.[2] *Structure Analysis and Refinement*: The structure was solved by direct methods using SHELXS-97; refinement was done by full-matrix least squares on F^2 using the SHELXL-97 program suite.[3] All non-hydrogen positions were refined with anisotropic displacement parameters. Hydrogen atoms were positioned geometrically (with C-H = 0.95 Å for aromatic/olefinic CH, 1.00 Å for tertiary CH, 0.99 Å for CH_2 and 0.98 Å for CH_3) and refined using riding models (AFIX 43, 13, 23 and 133 or 137, respectively), with U_{iso}(H) = -1.2U_{eq}(CH, CH_2) and -1.5U_{eq}(CH_3). The hydrogen atoms on the hydroxyl groups with O1 and O7 (methanol solvent molecule) were found and refined with U_{iso}(H) = 1.5U_{eq}(O). The N-H hydrogen atom has been found and refined with U_{iso}(H) = 1.5U_{eq}(N). The H atoms on O2 and O5 had to be calculated and refined with AFIX 83 to avoid their wrong intramolecular positioning (O2-H towards O5 and O5-H towards O3) which would lead to C-O-H angles < 92°. The apparent disorder due higher thermal motion and less constrained crystal packing of the bent alkyl chain and the methyl group of the methanol solvent molecules leads to short intermolecular H···H contacts and short C-C bonds as artefacts which are noted as Alert level A and B in the Checkcif file.

The gymnastatin T molecule (**1**) crystallizes in the non-centrosymmetric orthorhombic space group $P\,2_12_12_1$. A methanol solvent molecule of crystallization is embedded in the crystal lattice per formula unit (**Figure S53**). The O-H and N-H group are part of a hydrogen-bonding network (**Figure S54**, **Table S5**). The larger thermal ellipsoids of the carbon atoms of the bent alkyl chain indicate their higher thermal motion and less constrained crystal packing compared to the more rigid hydrogen-bonded part, the OH-functionalized bicyclo[3.3.1]nonane ring of the molecule. The unit cell packing can be seen as a separation of the hydrophilic hydrogen-bonding part, the OH-substituted bicyclo[3.3.1]nonane ring of the molecule (in layers parallel to the *ab* plane) and the hydrophobic branched alkyl chain (sandwiched between the hydrophilic layers) (**Figure S55**).[4] The bent alkyl chains from adjacent molecules interdigitate (interlock) along the *c* direction.[5]

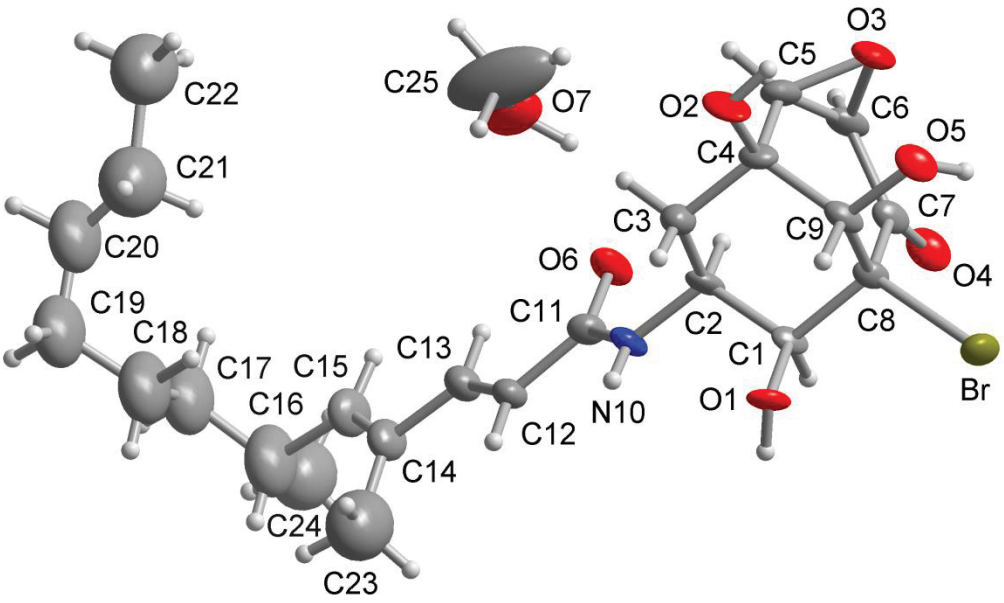

Figure S53. Molecular structure of **1** from single-crystal X-ray diffractometry (50% thermal ellipsoids, 20% for C25, H atoms of arbitrary radii).

Table S1. Crystal data and structure refinement for **1**

Compound	**1**
Data set	Br_5_30_2
CCDC number	1481781
Empirical formula	$C_{23}H_{34}BrNO_6 \cdot CH_3OH$
M/g mol^{-1}	532.46
Crystal size/mm^3	0.40 × 0.05 × 0.01
Temperature/K	150
θ range/° (completeness)	2.5–25.3° (0.99)
h; k; l range	-8/9, 14/14, -41/42
Crystal system	Orthorhombic
Space group	$P2_12_12_1$
a/Å	7.0251(3)
b/Å	11.3852(5)
c/Å	32.3080(15)
α/°	90
β/°	90
γ/°	90
V/Å^3	2584.1(2)
Z	4
D_{calc}/g cm^{-3}	1.369
μ (Mo Kα)/mm^{-1}	1.63
F(000)	1120
Max./min. transmission	0.674, 0.746
Reflections collected	39194
Independent reflect. (R_{int})	6086 (0.0445)
Data/restraints/parameters	6088/5/275
Max./min. Δρ/e Å^{-3} [a]	1.469/-0.977
R_1/wR_2 [I>2σ(I)] [b]	0.0626/0.1579
R_1/wR_2 (all data) [b]	0.0747/0.1637
Goodness-of-fit on F^2 [c]	1.092
Flack parameter [d]	0.043(4)

[a] Largest difference peak and hole; [b] $R_1 = [\sum(||F_o| - |F_c||)/\sum|F_o|]$; $wR_2 = [\sum[w(F_o^2 - F_c^2)^2]/\sum[w(F_o^2)^2]]^{1/2}$; [c] Goodness-of-fit $= [\sum[w(F_o^2 - F_c^2)^2]/(n - p)]^{1/2}$; [d] Absolute structure parameter.[6]

Table S2. Fractional atomic coordinates and isotropic or equivalent isotropic displacement parameters (Å^2) for **1**.

	x	*y*	*z*	U_{iso}*/U_{eq}
Br	0.94426 (9)	1.08655 (6)	0.19418 (2)	0.0331 (2)
C1	0.8297 (8)	0.9768 (5)	0.2698 (2)	0.0202 (12)
H1A	0.8167	0.9026	0.2535	0.024*
O1	1.0197 (6)	0.9889 (4)	0.28372 (16)	0.0254 (10)
H1	1.064 (12)	0.922 (5)	0.279 (2)	0.038*
C2	0.6985 (8)	0.9727 (5)	0.3068 (2)	0.0254 (13)
H2A	0.5659	0.9626	0.2961	0.030*
C3	0.7037 (10)	1.0866 (6)	0.3311 (2)	0.0302 (13)
H3A	0.8320	1.0969	0.3432	0.036*
H3B	0.6109	1.0822	0.3541	0.036*
C4	0.6570 (9)	1.1935 (5)	0.3039 (2)	0.0275 (13)
O2	0.6805 (9)	1.2931 (4)	0.32925 (18)	0.0448 (15)
H2	0.6520	1.3538	0.3158	0.067*
C5	0.4558 (11)	1.1811 (6)	0.2891 (2)	0.0343 (16)
H5A	0.3559	1.1797	0.3111	0.041*
O3	0.4054 (7)	1.2410 (4)	0.25144 (16)	0.0322 (11)
O5	0.7751 (6)	1.3017 (4)	0.24330 (16)	0.0283 (10)
H5	0.7530	1.2839	0.2185	0.042*
C6	0.4112 (9)	1.1138 (6)	0.2507 (2)	0.0306 (15)
H6A	0.2859	1.0722	0.2499	0.037*
C7	0.5720 (9)	1.0579 (5)	0.2273 (2)	0.0249 (13)
O4	0.5394 (8)	0.9852 (4)	0.20181 (16)	0.0357 (11)
C8	0.7758 (7)	1.0839 (6)	0.24217 (19)	0.0213 (11)
C9	0.7976 (9)	1.1982 (5)	0.2668 (2)	0.0252 (14)
H9	0.9294	1.1992	0.2785	0.030*
N10	0.7407 (8)	0.8721 (5)	0.33274 (19)	0.0263 (12)
H10	0.864 (9)	0.879 (7)	0.343 (2)	0.039*
C11	0.6062 (8)	0.7934 (6)	0.3423 (2)	0.0258 (14)

O6	0.4378 (7)	0.8024 (4)	0.32919 (16)	0.0358 (11)
C12	0.6652 (10)	0.6938 (6)	0.3689 (2)	0.0275 (14)
H12	0.7938	0.6869	0.3776	0.033*
C13	0.5372 (11)	0.6140 (6)	0.3806 (2)	0.0331 (15)
H13	0.4106	0.6271	0.3714	0.040*
C15	0.4129 (13)	0.4462 (7)	0.4146 (3)	0.047 (2)
H15	0.2948	0.4750	0.4045	0.056*
C16	0.407 (3)	0.3322 (11)	0.4394 (4)	0.094 (2)
H16	0.5385	0.3039	0.4457	0.113*
C17	0.296 (3)	0.3515 (12)	0.4784 (4)	0.094 (2)
H17A	0.2717	0.2749	0.4919	0.113*
H17B	0.1712	0.3870	0.4715	0.113*
C14	0.5664 (13)	0.5091 (6)	0.4058 (2)	0.0389 (16)
C18	0.400 (3)	0.4306 (11)	0.5081 (4)	0.094 (2)
H18A	0.5280	0.3969	0.5131	0.113*
H18B	0.4183	0.5078	0.4946	0.113*
C19	0.307 (3)	0.4500 (12)	0.5485 (4)	0.094 (2)
H19A	0.2852	0.3732	0.5620	0.113*
H19B	0.3936	0.4962	0.5664	0.113*
C20	0.130 (2)	0.5107 (12)	0.5447 (4)	0.094 (2)
H20A	0.0428	0.4550	0.5306	0.113*
H20B	0.0811	0.5194	0.5732	0.113*
C21	0.102 (3)	0.6087 (14)	0.5274 (6)	0.116 (3)
H21A	0.1329	0.5957	0.4979	0.139*
H21B	0.2038	0.6605	0.5383	0.139*
C22	-0.091 (3)	0.6901 (14)	0.5273 (5)	0.116 (3)
H22A	-0.0559	0.7726	0.5233	0.173*
H22B	-0.1576	0.6812	0.5538	0.173*
H22C	-0.1748	0.6649	0.5047	0.173*
C23	0.771 (3)	0.4818 (15)	0.4187 (6)	0.116 (3)
H23A	0.8468	0.4636	0.3942	0.173*
H23B	0.7712	0.4142	0.4375	0.173*

H23C	0.8251	0.5501	0.4329	0.173*
C24	0.297 (3)	0.2407 (15)	0.4134 (5)	0.116 (3)
H24A	0.1806	0.2764	0.4025	0.173*
H24B	0.2640	0.1734	0.4309	0.173*
H24C	0.3772	0.2142	0.3904	0.173*
C25	0.173 (4)	0.944 (4)	0.3908 (14)	0.34 (3)
H25A	0.0883	0.9704	0.4131	0.503*
H25B	0.1786	1.0047	0.3692	0.503*
H25C	0.3012	0.9314	0.4020	0.503*
O7	0.1023 (9)	0.8365 (8)	0.3735 (2)	0.066 (2)
H7	0.148 (19)	0.826 (13)	0.347 (2)	0.099*

Table S3. Atomic displacement parameters (Å^2) for **1**.

	U^{11}	U^{22}	U^{33}	U^{12}	U^{13}	U^{23}
Br	0.0232 (3)	0.0367 (3)	0.0396 (3)	0.0050 (3)	0.0103 (3)	0.0075 (3)
C1	0.016 (3)	0.009 (3)	0.036 (4)	-0.003 (2)	-0.001 (2)	0.007 (2)
O1	0.0088 (19)	0.019 (2)	0.048 (3)	0.0035 (15)	0.0011 (17)	0.002 (2)
C2	0.012 (2)	0.021 (3)	0.043 (4)	0.004 (2)	-0.001 (3)	0.010 (3)
C3	0.031 (3)	0.026 (3)	0.033 (3)	0.007 (3)	0.004 (3)	0.005 (3)
C4	0.029 (3)	0.019 (3)	0.035 (4)	0.009 (2)	0.001 (3)	-0.004 (3)
O2	0.065 (4)	0.023 (2)	0.047 (3)	0.027 (3)	-0.012 (3)	-0.011 (2)
C5	0.025 (3)	0.032 (4)	0.046 (4)	0.012 (3)	0.011 (3)	0.008 (3)
O3	0.025 (3)	0.022 (2)	0.049 (3)	0.0080 (19)	-0.003 (2)	0.007 (2)
O5	0.025 (2)	0.015 (2)	0.044 (3)	-0.0085 (18)	-0.008 (2)	0.004 (2)
C6	0.014 (3)	0.026 (3)	0.052 (4)	0.001 (2)	0.001 (3)	0.013 (3)
C7	0.019 (3)	0.018 (3)	0.038 (3)	-0.005 (2)	-0.001 (3)	0.010 (2)
O4	0.035 (3)	0.024 (2)	0.048 (3)	-0.009 (2)	-0.011 (2)	0.004 (2)
C8	0.014 (2)	0.016 (3)	0.034 (3)	-0.003 (2)	0.000 (2)	0.005 (3)
C9	0.018 (3)	0.016 (3)	0.041 (4)	-0.003 (2)	-0.006 (3)	0.009 (3)

N10	0.018 (2)	0.023 (3)	0.038 (3)	0.004 (2)	-0.004 (2)	0.011 (2)
C11	0.016 (3)	0.024 (3)	0.038 (4)	-0.002 (2)	0.001 (2)	0.003 (3)
O6	0.016 (2)	0.040 (3)	0.051 (3)	-0.002 (2)	-0.002 (2)	0.019 (2)
C12	0.025 (3)	0.026 (3)	0.032 (4)	0.006 (3)	0.001 (3)	0.006 (3)
C13	0.033 (3)	0.030 (4)	0.037 (4)	0.004 (3)	0.001 (3)	0.009 (3)
C15	0.051 (5)	0.034 (4)	0.054 (5)	-0.009 (4)	0.010 (4)	0.016 (3)
C16	0.134 (6)	0.069 (4)	0.078 (4)	-0.011 (4)	0.014 (4)	0.023 (3)
C17	0.134 (6)	0.069 (4)	0.078 (4)	-0.011 (4)	0.014 (4)	0.023 (3)
C14	0.046 (4)	0.027 (3)	0.044 (4)	-0.001 (4)	0.007 (4)	0.012 (3)
C18	0.134 (6)	0.069 (4)	0.078 (4)	-0.011 (4)	0.014 (4)	0.023 (3)
C19	0.134 (6)	0.069 (4)	0.078 (4)	-0.011 (4)	0.014 (4)	0.023 (3)
C20	0.134 (6)	0.069 (4)	0.078 (4)	-0.011 (4)	0.014 (4)	0.023 (3)
C21	0.139 (8)	0.090 (6)	0.118 (6)	0.003 (5)	0.024 (6)	0.016 (5)
C22	0.139 (8)	0.090 (6)	0.118 (6)	0.003 (5)	0.024 (6)	0.016 (5)
C23	0.139 (8)	0.090 (6)	0.118 (6)	0.003 (5)	0.024 (6)	0.016 (5)
C24	0.139 (8)	0.090 (6)	0.118 (6)	0.003 (5)	0.024 (6)	0.016 (5)
C25	0.13 (2)	0.41 (6)	0.47 (7)	-0.01 (3)	-0.03 (3)	-0.28 (6)
O7	0.036 (3)	0.096 (6)	0.066 (4)	0.012 (3)	0.000 (3)	-0.013 (4)

Table S4. Geometric parameters (Å, º) for **1**.

Br—C8	1.951 (6)	C15—C14	1.326 (12)
C1—O1	1.415 (7)	C15—C16	1.525 (14)
C1—C2	1.509 (10)	C15—H15	0.9500
C1—C8	1.559 (8)	C16—C17	1.500 (19)
C1—H1A	1.0000	C16—C24	1.54 (2)
O1—H1	0.84 (5)	C16—H16	1.0000
C2—N10	1.450 (8)	C17—C18	1.51 (2)
C2—C3	1.516 (10)	C17—H17A	0.9900
C2—H2A	1.0000	C17—H17B	0.9900
C3—C4	1.536 (9)	C14—C23	1.53 (2)
C3—H3A	0.9900	C18—C19	1.476 (19)

C3—H3B	0.9900	C18—H18A	0.9900
C4—O2	1.410 (8)	C18—H18B	0.9900
C4—C5	1.499 (10)	C19—C20	1.43 (2)
C4—C9	1.553 (10)	C19—H19A	0.9900
O2—H2	0.8400	C19—H19B	0.9900
C5—O3	1.438 (8)	C20—C21	1.262 (18)
C5—C6	1.491 (11)	C20—H20A	0.9900
C5—H5A	1.0000	C20—H20B	0.9900
O3—C6	1.449 (8)	C21—C22	1.64 (2)
O5—C9	1.410 (8)	C21—H21A	0.9900
O5—H5	0.8400	C21—H21B	0.9900
C6—C7	1.500 (9)	C22—H22A	0.9800
C6—H6A	1.0000	C22—H22B	0.9800
C7—O4	1.190 (8)	C22—H22C	0.9800
C7—C8	1.539 (8)	C23—H23A	0.9800
C8—C9	1.534 (9)	C23—H23B	0.9800
C9—H9	1.0000	C23—H23C	0.9800
N10—C11	1.338 (8)	C24—H24A	0.9800
N10—H10	0.93 (6)	C24—H24B	0.9800
C11—O6	1.261 (8)	C24—H24C	0.9800
C11—C12	1.482 (9)	C25—O7	1.44 (3)
C12—C13	1.333 (10)	C25—H25A	0.9800
C12—H12	0.9500	C25—H25B	0.9800
C13—C14	1.459 (9)	C25—H25C	0.9800
C13—H13	0.9500	O7—H7	0.91 (6)
O1—C1—C2	109.2 (5)	C14—C15—C16	126.5 (10)
O1—C1—C8	109.5 (5)	C14—C15—H15	116.7
C2—C1—C8	109.2 (5)	C16—C15—H15	116.7
O1—C1—H1A	109.6	C17—C16—C15	109.3 (11)
C2—C1—H1A	109.6	C17—C16—C24	107.2 (14)
C8—C1—H1A	109.6	C15—C16—C24	107.6 (11)

C1—O1—H1	102 (6)	C17—C16—H16	110.9
N10—C2—C1	110.9 (5)	C15—C16—H16	110.9
N10—C2—C3	111.9 (6)	C24—C16—H16	110.9
C1—C2—C3	111.6 (5)	C16—C17—C18	111.7 (13)
N10—C2—H2A	107.4	C16—C17—H17A	109.3
C1—C2—H2A	107.4	C18—C17—H17A	109.3
C3—C2—H2A	107.4	C16—C17—H17B	109.3
C2—C3—C4	112.1 (5)	C18—C17—H17B	109.3
C2—C3—H3A	109.2	H17A—C17—H17B	107.9
C4—C3—H3A	109.2	C15—C14—C13	116.6 (8)
C2—C3—H3B	109.2	C15—C14—C23	126.5 (9)
C4—C3—H3B	109.2	C13—C14—C23	116.8 (9)
H3A—C3—H3B	107.9	C19—C18—C17	115.9 (14)
O2—C4—C5	111.8 (5)	C19—C18—H18A	108.3
O2—C4—C3	106.2 (6)	C17—C18—H18A	108.3
C5—C4—C3	108.1 (6)	C19—C18—H18B	108.3
O2—C4—C9	110.2 (6)	C17—C18—H18B	108.3
C5—C4—C9	111.0 (6)	H18A—C18—H18B	107.4
C3—C4—C9	109.4 (5)	C20—C19—C18	112.4 (13)
C4—O2—H2	109.5	C20—C19—H19A	109.1
O3—C5—C6	59.3 (4)	C18—C19—H19A	109.1
O3—C5—C4	117.2 (6)	C20—C19—H19B	109.1
C6—C5—C4	120.7 (6)	C18—C19—H19B	109.1
O3—C5—H5A	115.9	H19A—C19—H19B	107.9
C6—C5—H5A	115.9	C21—C20—C19	126.8 (16)
C4—C5—H5A	115.9	C21—C20—H20A	105.6
C5—O3—C6	62.2 (5)	C19—C20—H20A	105.6
C9—O5—H5	109.5	C21—C20—H20B	105.6
O3—C6—C5	58.6 (4)	C19—C20—H20B	105.6
O3—C6—C7	117.0 (5)	H20A—C20—H20B	106.1
C5—C6—C7	118.6 (6)	C20—C21—C22	128.8 (16)
O3—C6—H6A	116.7	C20—C21—H21A	105.1

C5—C6—H6A	116.7	C22—C21—H21A	105.1
C7—C6—H6A	116.7	C20—C21—H21B	105.1
O4—C7—C6	119.9 (6)	C22—C21—H21B	105.1
O4—C7—C8	121.9 (6)	H21A—C21—H21B	105.9
C6—C7—C8	117.5 (6)	C21—C22—H22A	109.5
C9—C8—C7	114.7 (5)	C21—C22—H22B	109.5
C9—C8—C1	110.0 (5)	H22A—C22—H22B	109.5
C7—C8—C1	104.8 (5)	C21—C22—H22C	109.5
C9—C8—Br	109.8 (4)	H22A—C22—H22C	109.5
C7—C8—Br	108.6 (4)	H22B—C22—H22C	109.5
C1—C8—Br	108.7 (4)	C14—C23—H23A	109.5
O5—C9—C8	114.7 (6)	C14—C23—H23B	109.5
O5—C9—C4	111.9 (5)	H23A—C23—H23B	109.5
C8—C9—C4	107.9 (5)	C14—C23—H23C	109.5
O5—C9—H9	107.4	H23A—C23—H23C	109.5
C8—C9—H9	107.4	H23B—C23—H23C	109.5
C4—C9—H9	107.4	C16—C24—H24A	109.5
C11—N10—C2	121.2 (5)	C16—C24—H24B	109.5
C11—N10—H10	130 (5)	H24A—C24—H24B	109.5
C2—N10—H10	109 (5)	C16—C24—H24C	109.5
O6—C11—N10	122.1 (6)	H24A—C24—H24C	109.5
O6—C11—C12	121.3 (6)	H24B—C24—H24C	109.5
N10—C11—C12	116.7 (5)	O7—C25—H25A	109.5
C13—C12—C11	119.8 (6)	O7—C25—H25B	109.5
C13—C12—H12	120.1	H25A—C25—H25B	109.5
C11—C12—H12	120.1	O7—C25—H25C	109.5
C12—C13—C14	128.4 (7)	H25A—C25—H25C	109.5
C12—C13—H13	115.8	H25B—C25—H25C	109.5
C14—C13—H13	115.8	C25—O7—H7	110 (10)
O1—C1—C2—N10	-61.9 (7)	O1—C1—C8—Br	61.3 (6)

C8—C1—C2—N10	178.3 (5)	C2—C1—C8—Br	-179.2 (4)
O1—C1—C2—C3	63.6 (6)	C7—C8—C9—O5	-69.6 (7)
C8—C1—C2—C3	-56.2 (7)	C1—C8—C9—O5	172.6 (5)
N10—C2—C3—C4	-179.4 (5)	Br—C8—C9—O5	53.0 (6)
C1—C2—C3—C4	55.7 (7)	C7—C8—C9—C4	55.8 (7)
C2—C3—C4—O2	-175.8 (6)	C1—C8—C9—C4	-62.0 (6)
C2—C3—C4—C5	64.1 (7)	Br—C8—C9—C4	178.4 (4)
C2—C3—C4—C9	-56.8 (7)	O2—C4—C9—O5	-57.0 (7)
O2—C4—C5—O3	87.9 (7)	C5—C4—C9—O5	67.4 (7)
C3—C4—C5—O3	-155.6 (6)	C3—C4—C9—O5	-173.5 (5)
C9—C4—C5—O3	-35.6 (8)	O2—C4—C9—C8	176.0 (5)
O2—C4—C5—C6	156.6 (6)	C5—C4—C9—C8	-59.6 (7)
C3—C4—C5—C6	-86.9 (8)	C3—C4—C9—C8	59.5 (7)
C9—C4—C5—C6	33.1 (8)	C1—C2—N10—C11	-124.2 (7)
C4—C5—O3—C6	111.3 (7)	C3—C2—N10—C11	110.5 (7)
C5—O3—C6—C7	-108.6 (7)	C2—N10—C11—O6	0.4 (11)
C4—C5—C6—O3	-105.4 (7)	C2—N10—C11—C12	179.9 (6)
O3—C5—C6—C7	105.8 (6)	O6—C11—C12—C13	-2.4 (11)
C4—C5—C6—C7	0.4 (9)	N10—C11—C12—C13	178.1 (7)
O3—C6—C7—O4	-128.0 (6)	C11—C12—C13—C14	178.6 (7)
C5—C6—C7—O4	164.9 (6)	C14—C15—C16—C17	115.7 (14)
O3—C6—C7—C8	61.2 (8)	C14—C15—C16—C24	-128.2 (13)
C5—C6—C7—C8	-5.9 (8)	C15—C16—C17—C18	-69.2 (16)

O4—C7—C8—C9	166.0 (6)	C24—C16—C17—C18	174.4 (12)
C6—C7—C8—C9	-23.4 (7)	C16—C15—C14—C13	178.5 (9)
O4—C7—C8—C1	-73.3 (7)	C16—C15—C14—C23	-0.6 (17)
C6—C7—C8—C1	97.3 (6)	C12—C13—C14—C15	177.1 (8)
O4—C7—C8—Br	42.7 (7)	C12—C13—C14—C23	-3.7 (14)
C6—C7—C8—Br	-146.7 (4)	C16—C17—C18—C19	-176.8 (13)
O1—C1—C8—C9	-59.0 (6)	C17—C18—C19—C20	-64.6 (17)
C2—C1—C8—C9	60.5 (6)	C18—C19—C20—C21	-56 (2)
O1—C1—C8—C7	177.2 (5)	C19—C20—C21—C22	-171.3 (17)
C2—C1—C8—C7	-63.2 (6)		

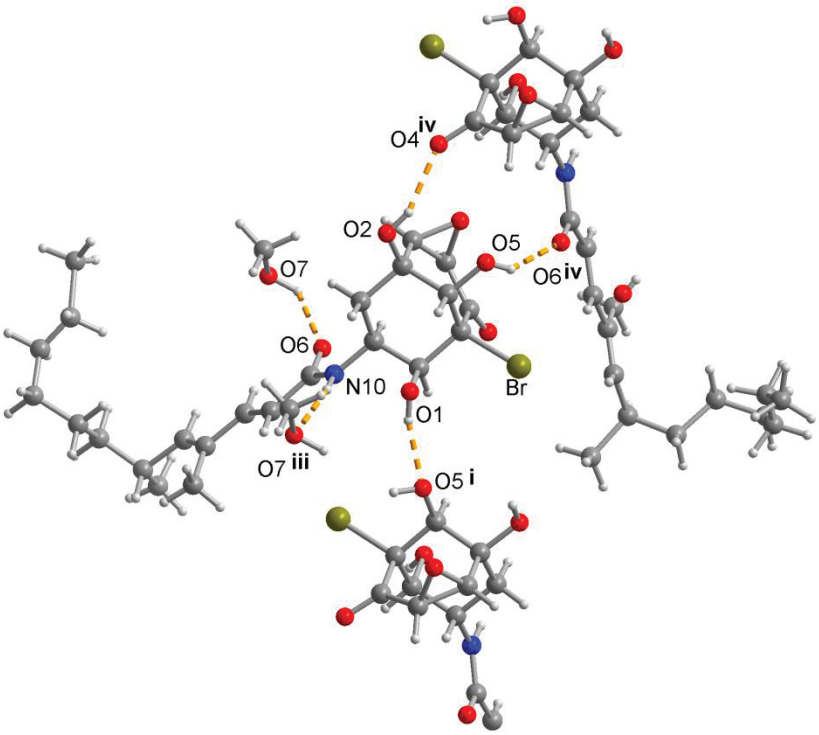

Figure S54. Hydrogen-bonding network in **1** indicated as dashed orange lines. See

Table X for details. Symmetry codes: (i) -*x*+2, *y*-1/2, -*z*+1/2; (iii) *x*+1, *y*, *z*; (iv) -*x*+1, *y*+1/2, -*z*+1/2.

Table S5. Hydrogen-bond geometry (Å, º) for **1**.[a]

D—H···A	D—H (Å)	H···A (Å)	D···A (Å)	D—H···A (°)
O1—H1···O5^{i}	0.84(5)	1.91(6)	2.717(6)	160(8)
C1—H1*A*···O3^{ii}	1.00	2.42	3.225(7)	137
N10—H10···O7^{iii}	0.93(6)	2.00(6)	2.889(9)	158(7)
O2—H2···O4^{iv}	0.84	2.09	2.859(7)	152
O5—H5···O6^{iv}	0.84	2.05	2.779(7)	144
C6—H6*A*···Br^{v}	1.00	3.00	3.767(7)	134
C6—H6*A*···O1^{v}	1.00	2.36	3.276(7)	151
O7—H7···O6	0.91(6)	2.14(12)	2.784(8)	128(12)

[a] Standard deviations for refined atom contacts are given in parentheses. Symmetry codes: (i) -*x*+2, *y*-1/2, -*z*+1/2; (ii) -*x*+1, *y*-1/2, -*z*+1/2; (iii) *x*+1, *y*, *z*; (iv) -*x*+1, *y*+1/2, -*z*+1/2; (v) *x*-1, *y*, *z*.

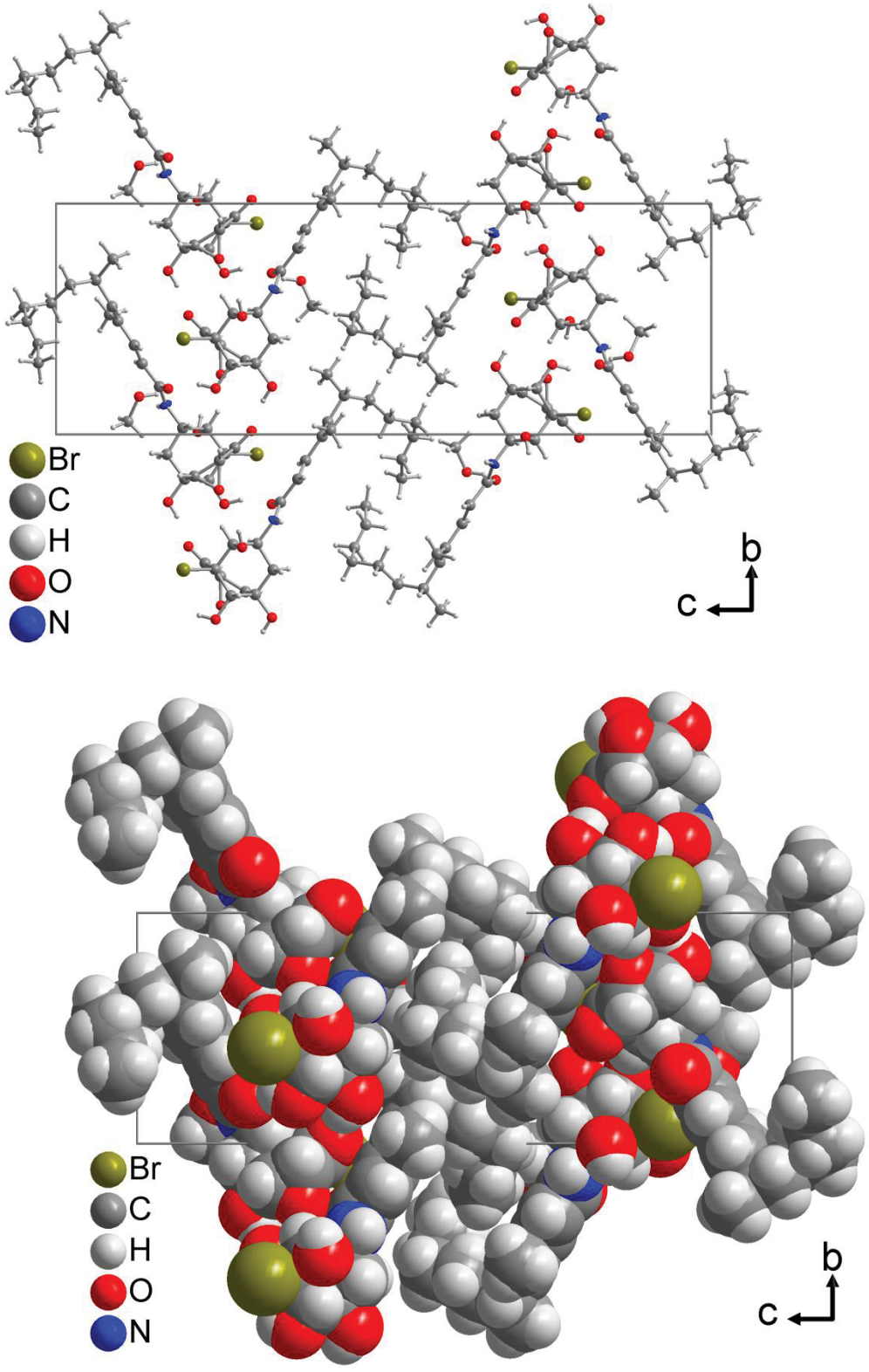

Figure S55. Unit cell packing diagram of **1** projected onto the *bc* plane – in ball-and-stick and in space-filling mode – showing the separation of the hydrophilic hydrogen-bonding part of the molecule (in layers parallel to the *ab* plane) and the interdigitated (interlocking) hydrophobic branched alkyl chain (sandwiched between the hydrophilic

layers).

Notes and references

1. Apex2, Data Collection Program for the CCD Area-Detector System; SAINT, Data Reduction and Frame Integration Program for the CCD Area-Detector System. Bruker Analytical X-ray Systems, Madison, Wisconsin, USA, 1997-2006.
2. G. M. Sheldrick, Program SADABS: Area-detector absorption correction, University of Göttingen, Germany, 1996.
3. G. M. Sheldrick, *Acta Crystallogr. Sect. A*, 2008, **64**, 112-122.
4. (a) J. K. Maclaren, J. Sanchiz, P. Gili and C. Janiak, *New J. Chem.*, 2012, **36**, 1596-1609; (b) J. K. Maclaren and C. Janiak, *Inorg. Chim. Acta*, 2012, **389**, 183-190; (c) T. Dorn, A. C. Chamayou and C. Janiak, *New. J. Chem.*, 2006, **30**, 156-167.
5. M. Enamullah, V. Vasylyeva and C. Janiak, *Inorg. Chim. Acta*, 2013, **408**, 109-119.
6. (a) H. D. Flack, M. Sadki, A. L. Thompson and D. J. Watkin, *Acta Crystallogr. Sect. A: Fundam. Crystallogr.*, 2011, **67**, 21–34; (b) H. D. Flack and G. Bernardinelli, *Chirality*, 2008, **20**, 681–690; (c) H. D. Flack and G. Bernardinelli, *Acta Crystallogr. Sect. A: Fundam. Crystallogr.*, 1999, **55**, 908–915; (d) H. D. Flack, *Acta Crystallogr. Sect. A: Fundam. Crystallogr.*, 1983, **39**, 876–881.

Publication 2

Submitted to "*Tetrahedron*".

Indole Alkaloids Produced by an Endophytic Fungus *Aspergillus aculeatus* using an OSMAC Approach

Hao Wang [a], Peter M. Eze [b], Simon-Patrick Höfert [c], Christoph Janiak [c], Rudolf Hartmann [d], Festus B.C. Okoye [e], Charles O. Esimone [b], Raha S. Orfali [f], Haofu Dai [g], Zhen Liu [a,*], Peter Proksch [a,*]

[a]*Institute of Pharmaceutical Biology and Biotechnology, Heinrich-Heine-University Düsseldorf, Universitätsstrasse 1, 40225 Düsseldorf, Germany*

[b]*Department of Pharmaceutical Microbiology and Biotechnology, Faculty of Pharmaceutical Sciences, Nnamdi Azikiwe University, Awka, Nigeria*

[c]*Institute of Inorganic and Structural Chemistry, Heinrich-Heine-University Düsseldorf, Universitätsstrasse 1, 40225 Düsseldorf, Germany*

[d]*Institute of Complex Systems: Structural Biochemistry, Forschungszentrum Juelich, Wilhelm-Johnen-Straße, 52428 Juelich, Germany*

[e]*Department of Pharmaceutical and Medicinal Chemistry, Faculty of Pharmaceutical Sciences, Nnamdi Azikiwe University, Awka, Nigeria*

[f]*Department of Pharmacognosy, Faculty of Pharmacy, King Saud University, Riyadh, Saudi Arabia*

[g]*Key Laboratory of Biology and Genetic Resources of Tropical Crops, Ministry of Agriculture, Institute of Tropical Bioscience and Biotechnology, Chinese Academy of Tropical Agricultural Sciences, Haikou 571101, China*

Abstract

The endophytic fungus *Aspergillus aculeatus* isolated from leaves of the papaya plant *Carica papaya* was fermented on solid rice medium, yielding a new indole alkaloid (**1**) and thirteen known compounds (**11**, **14**–**25**). In addition, an OSMAC approach was employed by adding eight different sodium or ammonium salts to the rice medium. Addition of 3.5% $NaNO_3$ caused a significant change of the metabolite pattern of the fungus as indicated by HPLC analysis. Subsequent isolation yielded several new indole derived alkaloids (**1**–**10**) in addition to three known compounds (**11**–**13**), among which compounds **2**–**10**, **12**–**13** were not detected in the rice control culture. All structures were unambiguously elucidated by one and two dimensional NMR spectroscopy and by mass spectrometry. The absolute configuration of the indole derivatives was determined by Marfey's reaction and X-ray single crystal diffraction. Compounds **19**–**22** showed cytotoxicity against the L5178Y mouse lymphoma cell line with IC_{50} values of 3.4, 1.4, 7.3 and 23.7 μM, respectively.

Keywords: *Aspergillus aculeatus*; OSMAC; X-ray diffraction; indole alkaloid.

Introduction

Endophytic fungi thrive widely in different healthy tissues of living plants, and have significant influence on the growth of their hosts.[1-2] Endophytes also comprise a large reservoir of structurally diverse secondary metabolites including alkaloids, steroids, terpenoids, xanthones, peptides and quinones, which exhibit a variety of biological activities including anticancer, antibacterial, antifungal, anti-inflammatory and antidepressant activity.[2-3] For example, 14-membered macrolides isolated from the endophytic fungus *Pestalotiopsis microspora* showed significant cytotoxicity against the murine lymphoma cell line L5178Y while fusaric acid derivatives produced by the fungal endophyte *Fusarium oxysporum* showed significant phytotoxicity to leaves of barley.[4-5] However, the high rediscovery rate of known compounds from fungi is a severe obstacle for the search for new drug leads.[6] One of the approaches to increase the diversity of metabolites from fungi involves the application of the OSMAC (One Strain MAny Compounds) method which is based on systematic variations of the cultivation parameters (media type and composition, pH value, temperature etc.).[7] For instance, the fermentation of the fungus *Gymnascella dankaliensis* on solid rice medium following addition of 3.5% NaBr led to the isolation of ten brominated tyrosine-derived alkaloids, which showed cytotoxicity against the L5178Y mouse lymphoma cell line.[8-9] In addition, cultivation of *Fusarium tricinctum* on fruit and vegetable juice-supplemented solid rice media that led to the production of the new fusarielins K and L.[10]

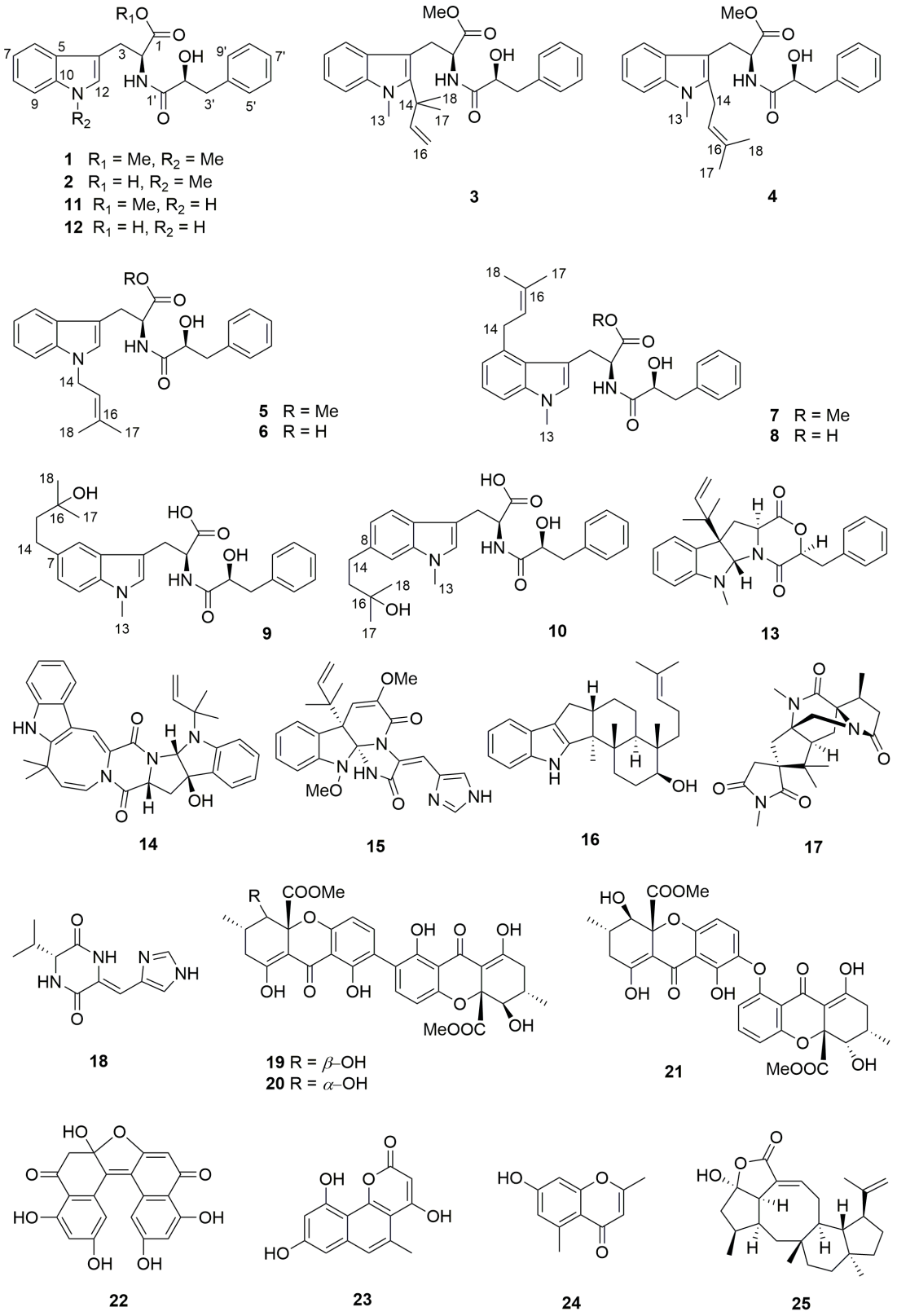

Figure 1. Structures of compounds **1**–**25** isolated from *A. aculeatus*.

The fungus *Aspergillus aculeatus* has been reported to produce several bioactive secondary metabolites, such as secalonic acids D and F, aculeatusquinone B and D,

aculeacins A–G and aspergillusol A.[11-15] In this study, *A. aculeatus* was isolated from leaves of *Carica papaya* collected in Awka in Nigeria. The fungus was fermented on solid rice medium, yielding a new indole alkaloid (**1**) together with thirteen known compounds including *N*-[(2*S*)-2-hydroxy-1-oxo-3-phenylpropyl]-L-tryptophan methyl ester (**11**),[16] okaramine A (**14**),[17] oxaline (**15**),[18] emindole SB (**16**),[19] 16-keto-aspergillimide (**17**),[20] JBIR 75 (**18**),[21] secalonic acids D and F (**19** and **20**),[11] asperdichrome (**21**),[22] RF 3192C (**22**),[23] pannorin (**23**),[24] altechromone A (**24**),[25] and variecolactone (**25**).[26] Due to the pronounced chemical diversity of this fungus we decided to subject *A. aculeatus* to an OSMAC approach by adding either 3.5% NaCl, 3.5% NaBr, 3.5% NaI, 1% NaF, 3.5% $NaNO_3$, 3.5% NH_4Cl, 3.5% $(NH_4)_2SO_4$ or 3.5% CH_3COONH_4 to the rice medium. The selection of these salts for the OSMAC study was based on previous experiments with other fungi that had indicated the usefulness of these chemical stimuli for the accumulation of cryptic metabolites.[8,9,27] The fungus did not grow on rice medium containing 1% NaF or 3.5% CH_3COONH_4. Addition of 3.5% $NaNO_3$, however, caused a significant change of the metabolite pattern as indicated by HPLC analysis. Addition of the remaining salts had no influence. Subsequent workup of the extract resulting from addition of 3.5% $NaNO_3$ yielded several new indole alkaloids (**1**–**10**) in addition to three known indole analogues *N*-[(2*S*)-2-hydroxy-1-oxo-3-phenylpropyl]-L-tryptophan methyl ester (**11**), *N*-[(2*S*)-2-hydroxy-1-oxo-3-phenylpropyl]-L-tryptophan (**12**) and acu- dioxomorpholine (**13**).[16] Compounds **2**–**10**, **12**–**13** were not detected in the rice control culture. On the other hand, from all compounds isolated from the rice control culture, only oxaline (**15**), JBIR

75 (**18**), secalonic acid F (**20**) and RF 3192C (**22**) could be detected in the fungal culture after addition of 3.5% $NaNO_3$. In this study we report the structure elucidation and the biological activities of the isolated compounds.

Results and Discussion

Compound **1** had the molecular formula $C_{22}H_{24}O_4N_2$ as established by HRESIMS exhibiting 12 degrees of unsaturation. The ^{13}C NMR spectrum of **1** (Table 1) included 22 signals, corresponding to two methyls, two methylenes, two alphatic methines and ten aromatic methines as well as six quaternary carbons. The ^{1}H NMR spectrum of **1** (Table 2) showed the presence of a monosubstituted benzene ring and an indole moiety as indicated by signals between δ_H 6 and 8, two -CH_2-CH- units and two methyl groups (δ_H 3.70 and 3.62). These data were similar to those of the co-isolated known alkaloid *N*-[(2*S*)-2-hydroxy-1-oxo-3-phenylpropyl]-L-tryptophan methyl ester (**11**).[16] However, the detection of an additional methyl substituent at δ_C 32.7 and δ_H 3.70 and the HMBC correlation from the protons of this methyl group to C-10 (δ_C 138.5) and C-12 (δ_C 129.0) indicated its attachment to N-11. Detailed analysis of the 2D NMR spectra of **1** (Figure 2) revealed that its remaining substructure was identical to that of **11**. The absolute configuration of **1** was determined by X-ray single crystal analysis as 2*S*, 2′*S* (Figure 3), being identical to that of **11**. Thus, the structure of **1**, for which the trial name aculeatine A is proposed, was elucidated as shown in Figure 1.

Compound **2** possessed the molecular formula $C_{21}H_{22}O_4N_2$ as determined by HRESIMS, which indicated the loss of a methyl group compared to **1**. This was confirmed by the absence of the ^{1}H and ^{13}C signals of the methoxy group attached to

C-1 in the NMR spectra of **2** (Tables 1 and 2). The structure of **2** was confirmed by detailed analysis of the 2D NMR spectra. Its absolute configuration was determined as 2*S*, 2′*S* by X-ray single crystal analysis (Figure 3).

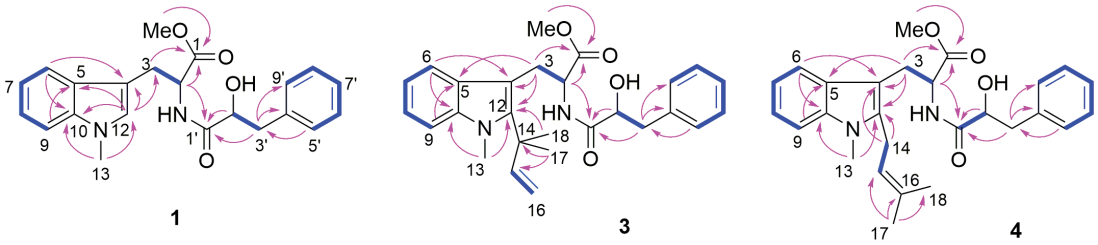

Figure 2. COSY and key HMBC correlations of compounds **1**, **3** and **4**.

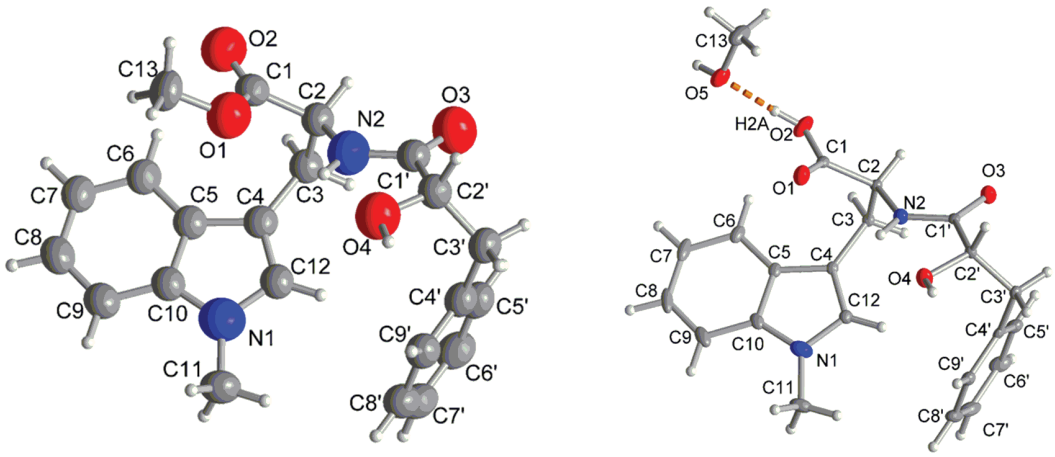

Figure 3. Molecular structure of **1** and **2** from single-crystal X-ray diffractometry.

The molecular formula of compound **3** was determined as $C_{27}H_{32}O_4N_2$ by HRESIMS. The ^{13}C NMR spectrum of **3** exhibited five additional carbons compared to **1**. The ^{1}H NMR spectrum of **3** was similar to that of compound **1** except for the observation of two singlet methyls at δ_H 1.66 (Me-17 and 18) and signals of a terminal double bond at δ_H 6.23 (H-15), 5.11 and 4.98 (H_2-16) as well as the absence of the singlet aromatic proton at C-12. The COSY correlations between H-15 and H_2-16 together with the HMBC correlations from Me-17 and Me-18 to C-12 (δ_C 142.2), C-14 (δ_C 41.9) and C-15 (δ_C 149.1) and from Me-13 (δ_H 3.72) to C-12 and C-10 (δ_C 139.0) indicated the attachment of a 1,1-dimethylprop-2-en-1-yl side chain at C-12. Detailed

analysis of the 2D NMR spectra of **3** (Figure 2) revealed that its remaining substructure was identical to that of **1**.

Compound **4** had the same molecular formula as **3**. The ^{1}H and ^{13}C NMR data were also similar to those of **3**. The appearance of a broad triplet proton (δ_H 5.11, H-15) and one methylene group (δ_H 3.48 and 3.44, H_2-14) together with two olefinic methyl groups (δ_H 1.74 and 1.82, Me-17 and 18) in the ^{1}H NMR spectrum of **4** suggested the existence of a 3-methyl-but-2-en-1-yl group at C-12, which was confirmed by the COSY correlations between H-15 and H_2-14 together with the HMBC correlations from Me-17 and 18 to C-15 (δ_C 122.4) and C-16 (δ_C 133.9), and from H_2-14 to C-4 (δ_C 106.0) and C-12 (δ_C 138.8) (Figure 2).

Compound **5** was isolated as white powder. Its molecular formula was established as $C_{26}H_{30}O_4N_2$ by HRESIMS. The ^{1}H and ^{13}C NMR spectra of **5** were similar to those of **4** except for the appearance of a singlet methine at δ_H 6.70 (H-12) and the absence of the methyl group attached to N-11. The COSY correlations between H-15 (δ_H 5.32) and H_2-14 (δ_H 4.66) along with the HMBC correlations from H-14 to C-10 (δ_C 137.8) and C-12 (δ_C 127.6), and from both Me-17 (δ_H 1.74) and Me-18 (δ_H 1.83) to C-15 (δ_C 121.5) and C-16 (δ_C 137.1) indicated the presence of a 3-methyl-but-2-en-1-yl residue and its attachment to N-11 of compound **5** (Figure 4).

The molecular formula of **6** was determined as $C_{25}H_{28}O_4N_2$, indicating the lack of a methyl group compared to **5**, which was confirmed by the absence of signals of the methoxy group at C-1 compared to **5** (Tables 3 and 4). The remaining substructure of **6** was unambiguously elucidated to be identical to that of **5** by detailed analysis of 2D

NMR spectra.

Table 1. ^{13}C NMR data of compounds **1–5** (CD_3OD, 150 MHz).

No.	**1**	**2**	**3**	**4**	**5**
1	173.4, C	174.8, C	173.9, C	173.8, C	173.5, C
2	53.7, CH	53.7, CH	55.3, CH	54.3, CH	53.6, CH
3	28.4, CH_2	28.4, CH_2	29.2, CH_2	28.0, CH_2	28.5, CH_2
4	109.2, C	109.5, C	107.5, C	106.0, C	109.4, C
5	129.1, C	129.4, C	130.3, C	129.1, C	129.4, C
6	119.6 CH	119.8 CH	119.2 CH	119.0 CH	119.6 CH
7	119.9, CH	119.9, CH	120.1, CH	120.0, CH	120.0, CH
8	122.6, CH	122.5, CH	122.7, CH	122.0, CH	122.5, CH
9	110.2, CH	110.1, CH	109.7, CH	109.7, CH	110.6, CH
10	138.5, C	138.5, C	139.0, C	138.4, C	137.8, C
12	129.0, CH	129.0, CH	142.2, C	138.8, C	127.6, CH
13	32.7, CH_3	32.7, CH_3	33.8, CH_3	30.0, CH_3	
14			41.9, C	24.8, CH_2	44.8, CH_2
15			149.1, CH	122.4, CH	121.5, CH
16			112.8, CH_2	133.9, C	137.1, C
17			30.0, CH_3	25.8, CH_3	25.8, CH_3
18			29.9, CH_3	18.1, CH_3	18.1, CH_3
1′	175.8, C	175.8, C	176.0, C	176.1, C	175.9, C
2′	73.4, CH	73.6, CH	73.7, CH	73.7, CH	73.5, CH
3′	41.4, CH_2	41.5, CH_2	41.2, CH_2	41.4, CH_2	41.6, CH_2
4′	138.8, C	139.0, C	139.1, C	138.9, C	138.9, C
5′, 9′	130.9 CH	130.9 CH	130.6 CH	130.6 CH	130.9 CH
6′, 8′	129.1, CH	129.1, CH	129.0, CH	129.0, CH	129.1, CH
7′	127.5, CH	127.5, CH	127.3, CH	127.4, CH	127.5, CH
OMe	52.8, CH_3		52.6, CH_3	52.8, CH_3	52.8, CH_3

Table 2. ^{1}H NMR data of compounds **1–5** (CD_3OD, 600 MHz).

No.	1	2	3	4	5
2	4.74, dd (6.2, 5.4)	4.71, dd (6.2, 5.2)	4.69, dd (8.5, 7.3)	4.65, dd (7.2, 6.6)	4.74, dd (6.1, 5.4)
3	3.21, dd (14.6, 6.2)	3.24, dd (14.7, 6.2)	3.45, dd (14.9, 7.3)	3.15, dd (14.7, 6.6)	3.22, dd (14.7, 6.1)
	3.07, dd (14.6, 5.4)	3.14, dd (14.7, 5.2)	3.26, dd (14.9, 8.5)	3.10, dd (14.7, 7.2)	3.05, dd (14.7, 5.4)
6	7.41, d (7.9)	7.49, d (7.9)	7.50, d (7.8)	7.40, d (7.8)	7.40, d (7.9)
7	7.03, dd (7.9, 7.2)	7.02, dd (7.9, 7.2)	7.07, dd (7.8, 7.2)	7.02, dd (7.8, 7.1)	7.02, dd (7.9, 7.1)
8	7.15, dd (8.2, 7.2)	7.14, dd (8.2, 7.2)	7.14, dd (8.1, 7.2)	7.10, dd (8.2, 7.1)	7.13, dd (8.2, 7.1)
9	7.29, d (8.2)	7.29, d (8.2)	7.25, d (8.1)	7.26, d (8.2)	7.29, d (8.2)
12	6.61, s	6.66, s			6.71, s
13	3.70, s	3.70, s	3.72, s	3.60, s	
14				3.48, dd (16.6, 6.6)	4.66, d (6.9)
				3.44, dd (16.6, 6.6)	
15			6.23, dd (17.5, 10.6)	5.11, br t (6.6)	5.32, br t (6.9)
16			5.11, d (10.6)		
			4.98, d (17.5)		
17			1.66, s	1.74, s	1.74, s
18			1.66, s	1.82, s	1.83, s
2′	4.24, dd (7.1, 4.0)	4.22, dd (7.4, 3.8)	4.10, dd (8.1, 3.7)	4.17, dd (7.8, 3.8)	4.22, dd (7.3, 3.9)
3′	2.97, dd (13.9, 4.0)	2.96, dd (13.9, 3.8)	2.64, dd (13.9, 3.7)	2.85, dd (13.9, 3.8)	2.96, dd (13.9, 3.9)
	2.78, dd (13.9, 7.1)	2.73, dd (13.9, 7.4)	2.24, dd (13.9, 8.1)	2.56, dd (13.9, 7.8)	2.76, dd (13.9, 7.3)
5′, 9′	7.20, d (7.0)	7.19, t (7.1)	7.05, d (7.1)	7.11, d (7.2)	7.20, d (7.2)
6′, 8′	7.24, t (7.0)	7.22, d (7.1)	7.15, t (7.1)	7.16, t (7.2)	7.23, t (7.2)
7′	7.17, t (7.0)	7.17, t (7.1)	7.12, t (7.1)	7.12, t (7.2)	7.17, t (7.2)
OMe	3.62, s		3.49, s	3.60, s	3.63, s

Compound **7** possessed the molecular formula $C_{27}H_{32}O_4N_2$ as deduced from the HRESIMS data. The ^1H and ^{13}C NMR spectra of **7** were similar to those of **4**, revealing the presence of one monosubstituted benzene ring, an indole moiety and a 3-methyl-but-2-en-1-yl side chain. However, the appearance of an aromatic proton signal at δ_H 6.82 (H-7), which was split to a doublet, suggested that the 3-methyl-but-2-en1-yl group was substituted on the benzene ring of the tryptophan moiety. The HMBC correlation from H_2-14 (δ_H 3.73) to C-5 (δ_C 126.8), C-6 (δ_C 135.4) and C-7 (δ_C 120.7), and from H-7 to C-5, C-9 (δ_C 108.5) and C-14 (δ_C 33.3) indicated the 3-methyl-but-2-enyl group to be located at C-6. The structure of **7** was determined by analysis of the 2D NMR spectra as shown in Figure 4.

Compound **8** possessed the molecular formula $C_{26}H_{30}O_4N_2$ as established by HRESIMS, thus lacking a methyl group compared to **7**. The ^1H and ^{13}C NMR spectra were almost identical to those of **7** except for the absence of signals of the methoxy group at C-1, which was further confirmed by detailed analysis of the 2D NMR data of **8**.

Compound **9** had the molecular formula $C_{26}H_{32}O_5N_2$ as determined by HRESIMS, corresponding to 12 degrees of unsaturation. The ^1H NMR spectra of **9** (Table 4) revealed the presence of a 1,2,4-trisubstituted benzene ring and a monosubstituted benzene ring, suggesting a substituent at C-7 or C-8 of the indole moiety. A 3-hydroxy-3-methylbutyl moiety was established based on the correlation between H_2-14 (δ_H 2.77) and H_2-15 (δ_H 1.80) together with the HMBC correlations from Me-17 (δ_H 1.24) and Me-18 (δ_H 1.25) to C-16 (δ_C 71.4) and C-15 (δ_C 47.8). In addition, the HMBC

correlation from H_2-14 to C-6 (δ_C 118.9), C-7 (δ_C 134.4) and C-8 (δ_C 123.5), from H-6 (δ_H 7.36) to C-4 (δ_C 109.4), C-8, C-10 (δ_C 137.1) and C-14 (δ_C 32.0), and from H-8 (δ_H 7.02) to C-6, C-10 and C-14 indicated the 3-hydroxy-3-methylbutyl moiety to be attached at C-7 (Figure 4).

Table 3. ^{13}C NMR data of compounds **6–10** (CD_3OD, 150 MHz).

No.	**6**[a]	**7**	**8**	**9**	**10**
1	176.4, C	173.7, C	175.0, C	175.8, C	175.6, C
2	54.3, CH	54.7, CH	54.4, CH	54.3, CH	54.1, CH
3	28.5, CH_2	30.3, CH_2	30.4, CH_2	28.3, CH_2	28.4, CH_2
4	110.0, C	110.1, C	110.4, C	109.4, C	109.7, C
5	129.6, C	126.8, C	127.0, C	129.8, C	127.7, C
6	119.8, CH	135.4 C	135.5 C	118.9 CH	119.8 CH
7	119.5, CH	120.7, CH	120.7, CH	134.4, C	121.0, CH
8	122.0, CH	122.7, CH	122.6, CH	123.5, CH	137.7, C
9	110.1, CH	108.5, CH	108.4, CH	110.0, CH	109.4, CH
10	137.4, C	139.3, C	139.3, C	137.1, C	138.8, C
12	127.3, CH	129.4, CH	129.3, CH	129.1, CH	128.5, CH
13		32.9, CH_3	32.9, CH_3	32.7, CH_3	32.7, CH_3
14	44.5, CH_2	33.3, CH_2	33.4, CH_2	32.0, CH_2	32.2, CH_2
15	121.4, CH	125.5, CH	125.5, CH	47.8, CH_2	47.8, CH_2
16	136.5, C	132.9, C	132.9, C	71.4, C	71.4, C
17	25.5, CH_3	25.9, CH_3	25.9, CH_3	29.3, CH_3	29.3, CH_3
18	17.8, CH_3	18.2, CH_3	18.3, CH_3	29.2, CH_3	29.2, CH_3
1′	175.4, C	176.1, C	176.1, C	175.9, C	175.8, C
2′	73.6, CH	73.8, CH	73.8, CH	73.8, CH	73.6, CH
3′	41.3, CH_2	41.7, CH_2	41.7, CH_2	41.6, CH_2	41.4, CH_2
4′	138.9, C	138.9, C	139.0, C	139.1, C	139.1, C
5′, 9′	130.5, CH	130.6 CH	130.6 CH	130.8 CH	130.8 CH
6′, 8′	128.8, CH	129.1, CH	129.1, CH	129.1, CH	129.1, CH
7′	127.1, CH	127.4 CH	127.4, CH	127.4, CH	127.4, CH
OCH_3		52.7, CH_3			

[a] Measured at 175 MHz.

Table 4. ^{1}H NMR data of compounds **6–10** (CD_3OD, 600 MHz).

No.	**6** [a]	**7**	**8**	**9**	**10**
2	4.66, m	4.71, dd (8.7, 5.6)	4.70, dd (8.9, 4.8)	4.67, m	4.67, m
3	3.23, dd (14.5, 6.1)	3.38, dd (15.0, 5.6)	3.45, dd (15.1, 4.8)	3.21, dd (14.8, 5.8)	3.20, dd (14.8, 5.9)
	3.17, dd (14.5, 4.7)	3.18, dd (15.0, 8.7)	3.20, dd (15.1, 8.9)	3.16, dd (14.8, 4.7)	3.13, dd (14.8, 4.7)
6	7.53, d (7.8)			7.36, s	7.40, d (8.0)
7	7.01, dd (7.8, 7.1)	6.82, d (7.2)	6.82, d (7.0)		6.91, d (8.0)
8	7.11, dd (8.3, 7.1)	7.06, dd (8.6, 7.2)	7.06, dd (8.3, 7.0)	7.02, d (8.3)	
9	7.27, d (8.3)	7.16, d (8.6)	7.15, d (8.3)	7.20, d (8.3)	7.11, s
12	6.80, s	6.82, s	6.84, s	6.68, s	6.63, s
13		3.70, s	3.69, s	3.68, s	3.68, s
14	4.65, m	3.73, m	3.77, dd (16.3, 6.8)	2.77, m	2.78, m
			3.73, dd (16.3, 6.8)		
15	5.32, br t (6.8)	5.31, br t (6.6)	5.32, br t (6.8)	1.80, m	1.79, m
17	1.72, s	1.76, s	1.76, s	1.24, s	1.26, s
18	1.83, s	1.77, s	1.77, s	1.25, s	1.26, s
2′	4.16, dd (8.0, 3.5)	4.19, dd (7.8, 3.9)	4.18, dd (8.0, 3.8)	4.19, dd (7.8, 3.6)	4.19, dd (7.6, 3.7)
3′	2.93, dd (13.9, 3.5)	2.88, dd (13.9, 3.9)	2.87, dd (13.9, 3.8)	2.95, dd (13.9, 3.6)	2.93, dd (13.9, 3.7)
	2.63, dd (13.9, 8.0)	2.62, dd (13.9, 7.8)	2.58, dd (13.9, 8.0)	2.65, dd (13.9, 7.8)	2.66, dd (13.9, 7.6)
5′, 9′	7.16, d (7.2)	7.11, d (6.9)	7.11, d (6.9)	7.17, d (7.2)	7.17, d (7.2)
6′, 8′	7.20, t (7.2)	7.14, t (6.9)	7.12, t (6.9)	7.20, t (7.2)	7.22, t (7.2)
7′	7.15, t (7.2)	7.10, t (6.9)	7.10, t (6.9)	7.15, t (7.2)	7.16, t (7.2)
OCH_3		3.66, s			

[a] Measured at 700 MHz.

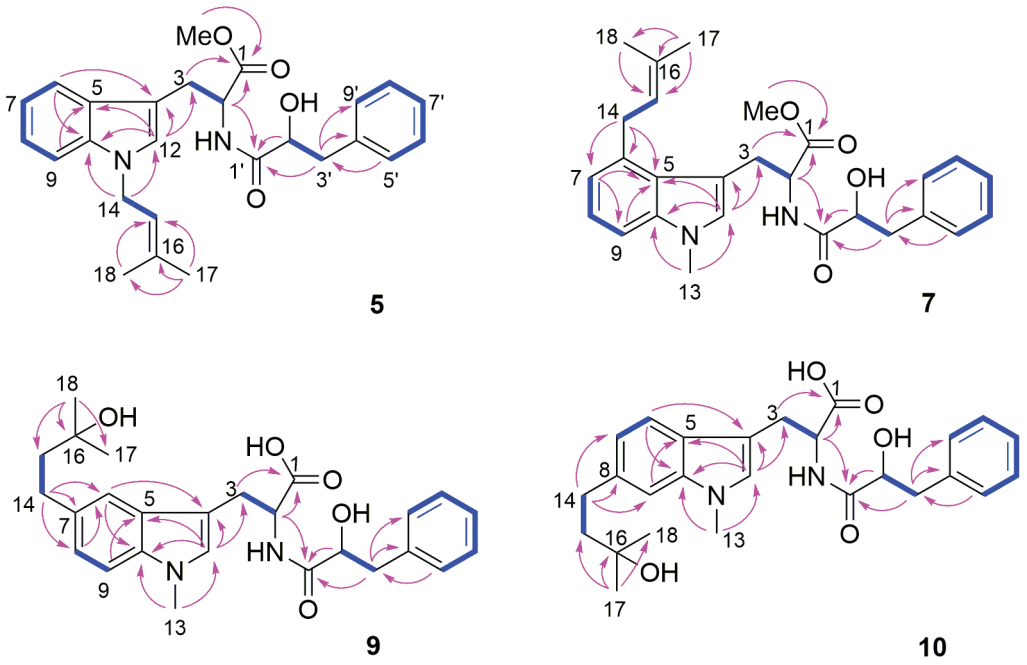

Figure 4. COSY and key HMBC correlations of compounds **5**, **7**, **9** and **10**.

Compound **10** shared the same molecular formula as **9**. The ^{1}H NMR data of **10** resembled those of compound **9** except for the chemical shifts of the aromatic protons of the indole moiety. The HMBC correlation from H_2-14 (δ_H 2.78) to C-7 (δ_C 121.0), C-8 (δ_C 137.7) and C-9 (δ_C 109.4), from H-7 (δ_H 6.91) to C-5 (δ_C 127.7), C-9 and C-14 (δ_C 32.3), and from H-9 (δ_H 7.11) to C-5, C-7 and C-14 confirmed that the 3-hydroxy-3-methylbutyl moiety was located at the C-8 position. The remaining substructure of **10** was the same as that of **9** as confirmed by detailed analysis of 2D NMR spectra of **10** (Figure 4).

Compounds **3**–**10** share the same core structure with compounds **1** and **2**, for which the absolute configuration had been assigned through X-ray analysis. Hence it is concluded on biogenetic terms that the absolute configuration of the former compounds is also 2*S*, 2′*S*. Compounds **11** and **12** were determined to have 2*S* absolute configuration by Marfey's reaction. Based on the close biogenetic similarity, the

absolute configuration at C-2′ of the latter two compounds is assumed to be *S*.

A plausible biosynthetic pathway of the indole alkaloids obtained from *A. aculeatus* is proposed to start from L-tryptophan and phenylpyruvate. The important intermediate **12** is suggested to be formed by a condensation reaction between L-tryptophan and L-phenyllactic acid. The indole metabolites isolated in this study could be produced by further methylation of **12** and prenylation of the indole nucleus of tryptophan as shown in figure 5.

All isolated compounds (**1**–**25**) were evaluated for their cytotoxicity against the L5178Y mouse lymphoma cell line. Secalonic acids D and F (**19** and **20**), asperdichrome (**21**) and RF 3192C (**22**) showed cytotoxicity with IC_{50} values of 3.4, 1.4, 7.3 and 23.7 μM, respectively, whereas the remaining compounds proved to be inactive when assayed at a dose of 10 μg/mL.

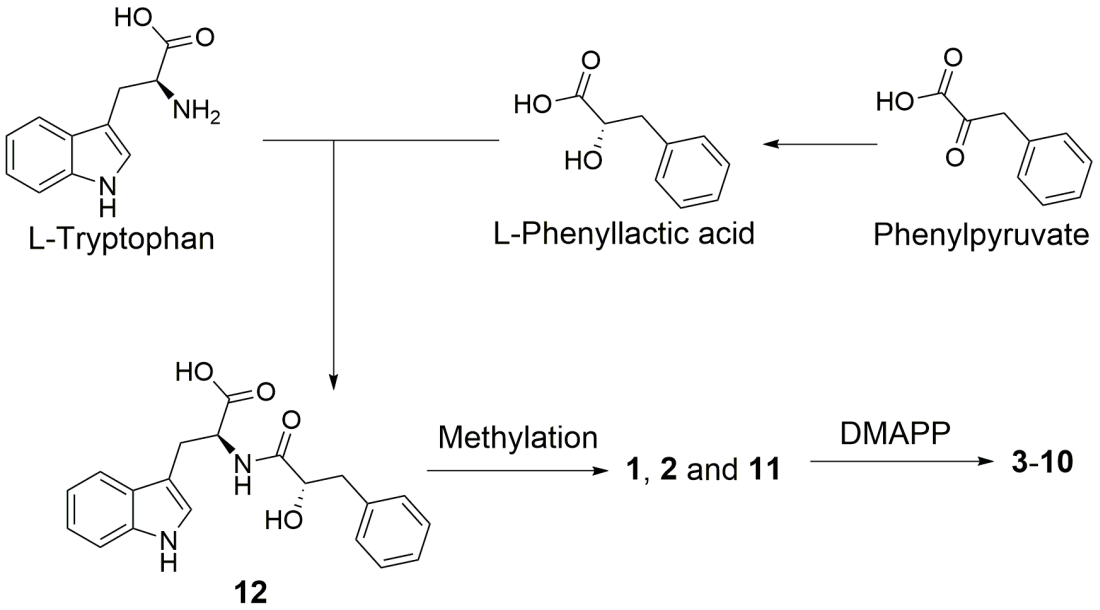

Figure 5. Plausible biosynthesis of indole alkaloids from *A. aculeatus.*

The results of the OSMAC experiments indicated that indole alkaloids were induced by nitrate but not by sodium in the medium. In the absence of nitrogen sources

favoured by the fungus including ammonium and glutamine, fungi are able to use secondary nitrogen sources such as nitrate, purines, urea, amines and amides etc., which is commonly known as nitrogen metabolite repression (NMR).[28] In fungi, the activity of nitrogen regulators for derepression of NMR genes, which also affect secondary metabolites formation, is regulated by the intracellular nitrogen status and extracellular nitrogen availability.[29,30] For example, the main GATA transcriptional regulator of nitrogen metabolism AreA accumulates in the nucleus in *Fusarium graminearum* with nitrate as sole nitrogen source, which is required for activation of the nitrate assimilation system including the nitrate reductase genes.[31] Thus, the biosynthesis of fungal secondary metabolites can be affected by the quality and quantity of the nitrogen sources. For example, 67% of secondary metabolites silent gene clusters of *Fusarium fujikuroi* were expressed based on the modification of nitrogen sources.[32] Furthermore, the natural product beauvericin was accumulated by *Fusarium oxysporum* by utilizing nitrate as sole nitrogen source.[33] In this study, the production of indole alkaloids was stimulated by the activation of the nitrate assimilation system in *A. aculeatus* due to the presenc of sodium nitrate in medium.

The indole alkaloids identified in this study showed no cytotoxic or antibacterial activity. However, the two known indole alkaloids (**11** and **12**) were claimed as plant growth regulators in a patent and showed pronounced rooting promoting effect.[34] It may hence be hypothesized that a high concentration of nitrate in host plants, as simulated in this study by addition of sodium nitrate to solid rice medium, may induce the production of plant growth stimulating indole alkaloids of the endophytic fungus *A.*

aculeatus.[35] This could lead to an increased growth and production of biomass by the host plant. In return, the fungus could receive nutrients, water, minerals and nitrogen from its host. Further studies will be necessary to evaluate this hypothesis.

Experimental Section

General Procedures. A Jasco P-2000 polarimeter was used to measure the optical rotation. 1D and 2D NMR spectra were recorded on Bruker Avance DMX 600 or 700 NMR spectrometers. Chemical shifts were referenced to the solvent residual peaks. Mass spectra were recorded with a LC-MS HP1100 Agilent Finnigan LCQ Deca XP Thermoquest and HRESIMS were measured with a UHR-QTOF maXis 4G (Bruker Daltonics) mass spectrometer. HPLC analysis was performed on a Dionex 3000 RS system coupled with an Ultimate 3000 pump and a photodiode array detector (DAD 300RS). The analytical column (125 × 4 mm) was prefilled with Eurosphere-10 C_{18} (Knauer, Germany), and the following gradient solvent system was used: 0 min (10% MeOH), 5 min (10% MeOH), 35 min (100% MeOH), and 45 min (100% MeOH). Semi-preparative HPLC was performed using a Merck Hitachi HPLC System (UV detector L-7400; pump L-7100; Eurosphere-100 C_{18}, 300 × 8 mm, Knauer) with MeOH-H_2O as mobile phase and a flow rate of 5.0 mL/min. Column chromatography was carried out using Merck MN silica gel 60 M (0.04–0.063 mm). TLC plates with silica gel F_{254} (Merck) were used to monitor and collect fractions under detection at 254 and 366 nm. Distilled and spectral-grade solvents were used for column chromatography and spectroscopic measurements, respectively.

Fungal Material and Cultivation. *A. aculeatus* was isolated from leaves of

Carica papaya collected in Awka in Nigeria and was identified by DNA amplification, sequencing of ITS region and by comparing with GenBank data (GeneBank accession No. KX137846) following standard procedures.[36]

The fungal strain was grown on solid rice medium (100 g rice and 100 mL distilled water autoclaved) in ten Erlenmeyer flasks (1 L each) at 22 ^{o}C under static conditions for 14 days. The OSMAC experiments were performed on rice medium containing either 3.5% NaCl, 3.5% NaBr, 3.5% NaI, 1% NaF, 3.5% $NaNO_3$, 3.5% NH_4Cl, 3.5% $(NH_4)_2SO_4$ or 3.5% CH_3COONH_4 under static conditions until they reached their stationary phase of growth (16 days except for rice media spiked with 1% NaF or 3.5% NH_4COOH where the fungus failed to grow).

Extraction and Isolation. Fungal cultures were extracted with EtOAc followed by evaporation under reduced pressure. Initial purification of the EtOAc extract (12.5 g) of the fungal culture fermented on rice was performed by partitioning between *n*-hexane and 90% aqueous MeOH. The 90% aqueous MeOH phase (9.2 g) was centrifuged and then fractionated by vacuum liquid chromatography on reversed-phase silica gel using a gradient elution of H_2O-MeOH (10:90 – 0:100) to give 10 fractions (Fr.1 to Fr.10).

Fr.2 (152 mg) was chromatographed on a Sephadex LH-20 column with MeOH followed by further purification using semi-preparative HPLC to give **17** (1.5 mg), **18** (7.0 mg) and **24** (0.5 mg). Compound **19** (30.2 mg) was obtained from Fr.3 (835 mg) by recrystallization. Part of Fr.3 was purified by semi-preparative HPLC to give **20** (20.0 mg). Fr.4 (208 mg) was subjected to a Sephadex LH-20 column with MeOH to

give two subfractions (Fr.4-1 and Fr.4-2). Fr.4-1 was further purified by a silica gel column with DCM/MeOH as mobile phase to give **15** (3.8 mg). Compound **1** (13.1 mg) was obtained by recrystallization from Fr.4-2. Fr.5 (160 mg) was separated by a Sephadex LH-20 column followed by purification using semi-preparative HPLC to yield **14** (0.7 mg) and **21** (8.2 mg). Compound **11** (3.2 mg), **22** (1.2 mg) and **25** (2.4 mg) were obtained from Fr.6 (54 mg) by semi-preparative HPLC. Fr.7 (101 mg) was subjected to a Sephadex LH-20 column with MeOH as mobile phase and then purified by semi-preparative HPLC to give **23** (2.0 mg) and **16** (0.8 mg).

The fungal cultures from the OSMAC experiments that were grown on rice medium containing different salts were extracted with EtOAc (2 × 500 mL) followed by solvent evaporation under reduced pressure. The obtained crude extracts were analyzed by HPLC. The EtOAc extracts (28.6 g) of fungal cultures that had been grown on rice medium (30 flasks) after adding 3.5% $NaNO_3$ were dissolved in MeOH and then subjected to vacuum filtering. The obtained MeOH solution was evaporated under reduced pressure and fractionated by vacuum liquid chromatography on silica gel using a gradient elution of *n*-hexane-EtOAc to give 24 fractions (Fr.N1 to Fr.N24). Fr.N19 (221 mg) was separated by a Sephadex LH-20 column with MeOH as mobile phase followed by semi-preparative HPLC to give **3** (3.5 mg) and **4** (15.0 mg). Fr.N22 (465 mg) was separated by a Sephadex LH-20 column with MeOH as mobile phase to give 3 fractions. Fr.N22-2 (54 mg) was further purified by semi-preparative HPLC to give **1** (10.1 mg), **2** (10.4 mg), **11** (3.5 mg), **12** (3.4 mg) and **13** (2.5 mg). Fr.N22-3 (380 mg) was further purified by a silica gel column with DCM-MeOH as mobile phase followed

by semi-preparative HPLC to give **5** (2.4 mg), **6** (0.9 mg), **7** (4.8 mg), **8** (4.7 mg), **9** (1.2 mg) and **10** (1.2 mg).

*Aculeatine A (**1**)*, white needle crystals; $[\alpha]_D^{20}$ +23 (*c* 0.25, MeOH); UV (MeOH): λ_{max} 221, 288 nm; HRESIMS *m/z* 381.1810 $[M+H]^+$ (calcd 381.1809 for $C_{22}H_{25}O_4N_2$); ^1H and ^{13}C NMR data see Tables 1 and 2.

*Aculeatine B (**2**)*, colorless needle crystals; $[\alpha]_D^{20}$ +3 (*c* 0.40, MeOH); UV (MeOH): λ_{max} 227, 288 nm; HRESIMS *m/z* 367.1653 $[M+H]^+$ (calcd 367.1652 for $C_{21}H_{23}O_4N_2$); ^1H and ^{13}C NMR data see Tables 1 and 2.

*Aculeatine C (**3**)*, white amorphous powder; $[\alpha]_D^{20}$ –54 (*c* 0.70, MeOH); UV (MeOH): λ_{max} 227, 288 nm; HRESIMS *m/z* 449.2439 $[M+H]^+$ (calcd 449.2435 for $C_{27}H_{33}O_4N_2$); ^1H and ^{13}C NMR data see Tables 1 and 2.

*Aculeatine D (**4**)*, white amorphous solid; $[\alpha]_D^{20}$ –47 (*c* 1.7, MeOH); UV (MeOH): λ_{max} 233, 286 nm; HRESIMS *m/z* 449.2435 $[M+H]^+$ (calcd 449.2435 for $C_{27}H_{33}O_4N_2$); ^1H and ^{13}C NMR data see Tables 1 and 2.

*Aculeatine E (**5**)*, white amorphous powder; $[\alpha]_D^{20}$ –2 (*c* 0.48, MeOH); UV (MeOH): λ_{max} 228, 287 nm; HRESIMS *m/z* 435.2281 $[M+H]^+$ (calcd 435.2278 for $C_{26}H_{31}O_4N_2$); ^1H and ^{13}C NMR data see Tables 1 and 2.

*Aculeatine F (**6**)*, white amorphous solid; $[\alpha]_D^{20}$ –11 (*c* 0.20, MeOH); UV (MeOH): λ_{max} 228, 288 nm; HRESIMS *m/z* 421.2122 $[M+H]^+$ (calcd 421.2122 for $C_{25}H_{29}O_4N_2$); ^1H and ^{13}C NMR data see Tables 3 and 4.

*Aculeatine G (**7**)*, white amorphous powder; $[\alpha]_D^{20}$ –24 (*c* 0.20, MeOH); UV (MeOH): λ_{max} 225, 291 nm; HRESIMS *m/z* 449.2435 $[M+H]^+$ (calcd 435.2435 for

$C_{27}H_{33}O_4N_2$) and *m/z* 471.2252 $[M+Na]^+$ (calcd. 471.2254 for $C_{27}H_{32}O_4N_2Na$); ^1H and ^{13}C NMR data see Tables 3 and 4.

*Aculeatine H (**8**)*, white amorphous powder; $[\alpha]_D^{20}$ –41 (*c* 0.94, MeOH); UV (MeOH): λ_{max} 226, 291 nm; HRESIMS *m/z* 435.2282 $[M+H]^+$ (calcd 435.2278 for $C_{26}H_{31}O_4N_2$) and *m/z* 457.2099 $[M+Na]^+$ (calcd. 457.2098 for $C_{26}H_{30}O_4N_2Na$); ^1H and ^{13}C NMR data see Tables 3 and 4.

*Aculeatine I (**9**)*, white amorphous solid; $[\alpha]_D^{20}$ –35 (*c* 0.24, MeOH); UV (MeOH): λ_{max} 225, 292 nm; HRESIMS *m/z* 453.2383 $[M+H]^+$ (calcd 453.2384 for $C_{26}H_{33}O_5N_2$); ^1H and ^{13}C NMR data see Tables 3 and 4.

*Aculeatine J (**10**)*, light yellow amorphous solid; $[\alpha]_D^{20}$ –19 (*c* 0.24, MeOH); UV (MeOH): λ_{max} 226, 287 nm; HRESIMS *m/z* 453.2380 $[M+H]^+$ (calcd 453.2384 for $C_{26}H_{33}O_5N_2$) and *m/z* 475.2201 $[M+Na]^+$ (calcd. 475.2203 for $C_{26}H_{32}O_5N_2Na$); ^1H and ^{13}C NMR data see Tables 3 and 4.

X-ray Crystallographic Analysis of 1 and 2. *Crystallization conditions*: Suitable single crystals of **1** and **2** were obtained by slow evaporation from methanol solution and selected under a polarized light microscope. *Data collection:* Compounds **1** and **2** were measured on a Bruker Kappa APEX2 CCD diffractometer with micro focus tube using Cu–Kα radiation (λ= 1.54178 Å). APEX2 was used for data collection,[37] SAINT for cell refinement and data reduction,[37] and SADABS for experimental absorption correction.[38] SHELXT was used for the structure solution by instrinsic phasing,[39] SHELXL-2017 was used for refinement by full-matrix least-squares on F^2.[40] The hydrogen atoms were positioned geometrically (with C-H = 0.95 Å for aromatic CH,

1.00 Å for tertiary CH, 0.99 Å for CH_2 and 0.98 Å for CH_3). The refinement was carried out using riding models (AFIX 43, 13, 23, 137, respectively), with Uiso(H) = 1.2 U_{eq} (CH, CH_2) and 1.5 U_{eq} (CH3). The hydrogen atoms in the hydroxy and amine groups were refined with U_{iso}(H) = 1.5 U_{eq}(O/N). The hydrogen atoms in the solvent methanol molecule in **2** were refined with U_{iso}(H) = 1.5 U_{eq}(O).

The absolute structures of compound **1** and **2** were determined using anomalous dispersion from Cu-Kα radiation, resulting in Flack parameters of -0.14(10) (**1**) and 0.00(3) (**2**) using Parsons quotient method.[41] Due to a rather high Flack parameter for **1**, its absolute structure was determined using likelihood methods.[42] DIAMOND was used for the drawing of all graphics.[43] PLATON for Windows was used for the analyses of hydrogen bonds and CH-π interactions.[44] The structural data for **2** has been deposited in the Cambridge Crystallographic Data Center (CCDC No. 1589955). Crystals of **1** did not diffract beyond θ = 44.9° (cf. desired 67.7°) for Cu-Kα radiation, resulting in only 1538 total (1484 observed with $I > 2\sigma(I)$) reflection versus 263 parameters for anisotropic refinement. Therefore the cif did not meet the requirements for publication and refinement data of compound **1** is only given in the Supporting Information.

*Crystal Data of **1**:* $C_{22}H_{24}N_2O_4$, M = 380.43, orthorhombic system, space group $P2_12_12_1$, a = 11.8099(7) Å, b = 11.8099(7) Å, c = 27.4081(17) Å, V = 1936.7(2) Å^3, Z = 4, D_{calc} = 1.305 g/cm^3, crystal size 0.12 × 0.03 × 0.03 mm^3, μ(Cu-Kα) = 0.73 mm^{-1}, 3.2° < θ < 44.9°, N_t = 16751, N = 1538 (R_{int} = 0.051), R_1 = 0.022, wR_2 = 0.053, S = 1.12, Flack parameter = –0.14(10), Hooft parameter = –0.09(8), probability for correct absolute structure $P2$ = 1.000.

Crystal Data of ***2****:* $C_{21}H_{22}N_2O_4 \cdot CH_4O$, M = 398.45, monoclinic system, space group *C*2, *a* = 23.52(2) Å, *b* = 5.994(5) Å, *c* = 15.843(13) Å, *V* = 2063(3) Å^3, *Z* = 4, D_{calc} = 1.283 g/cm^3, crystal size 0.20 × 0.10 × 0.05 mm^3, μ(Cu-Kα) = 0.75 mm^{-1}, 5.9° < θ < 67.5°, N_t = 11796, *N* = 3416 (R_{int} = 0.027), R_1 = 0.025, wR_2 = 0.067, *S* = 1.09, Flack parameter = 0.00(3), Hooft parameter = 0.00(3), probability for correct absolute structure *P*2 = 1.000.

Marfey's Reaction. Compounds **11** and **12** (0.5 mg) were hydrolyzed with 2 mL 6M HCl containing 0.4% β-mercaptoethanol at 110 °C for 24 h. The hydrolysate was evaporated to dryness and treated separately with 4M NaOH at room temperature for 4 h. 4M HCl was used to adjust the pH to 4. The above resulting solutions were evaporated until complete elimination of HCl and then resuspended in 50 μL H_2O. To 25 μL of each resulting solutions was added 50 μL FDAA (1% 1-fluoro-2-4-dinitrophenyl-5-L-alanine amide in acetone) and 10 μL $NaHCO_3$. The reaction tubes were covered with an aluminum paper and heated over a hot plate at 40 °C for 1 h. After cooling to room temperature, 5 μL of 2 M HCl was added and then evaporated to dryness. The residue was dissolved in 500 μL MeOH. L-tryptophan and D-tryptophan were treated separately with FDAA in the same manner. The analysis of FDAA derivatives were carried out using HPLC and LC-MS by comparison of the retention time and molecular weight.

Cytotoxicity Assay

Cytotoxicity was tested against the L5178Y mouse lymphoma cell line using the MTT method as described before.[9] Kahalalide F was used as positive control with a

IC_{50} value as 4.3 μM.

Acknowledgements

H.W. wishes to thank the China Scholarship Council, the Ministry of Education of China, for a doctoral scholarship. Financial support by the DFG (GRK 2158) and by the Manchot Foundation to P.P. is gratefully acknowledged. P.P. and R.S.O. acknowledge support by the International Scientific Partnership Program of King Saud University (ISPP# 0065).

Supplementary data

UV, HRESIMS, 1D and 2D NMR data of the new compounds **1**–**10**; Results of X-ray analysis of compound **1** and **2**.

References

1. Jia, M.; Chen, L.; Xin, H. L.; Zheng, C. J.; Rahman, K.; Han, T.; Qin, L. P. *Front. Microbiol*. **2016**, *7*, 906–919.
2. Kellogg, J. J.; Raja, H. A. *Phytochemi. Rev*. **2016**, *16*, 1–23.
3. Nisa, H.; Kamili, A. N.; Nawchoo, I. A.; Shafi, S.; Shameem, N.; Bandh, S. A. *Microb. Pathog*. **2015**, *82*, 50–59.
4. Liu, S.; Dai, H.; Makhloufi, G.; Heering, C.; Janiak, C.; Hartmann, R.; Mándi, A.; Kurtán, T.; Müller, W. E. G.; Lin, W. H.; Liu, Z.; Proksch, P. *J. Nat. Prod.* **2016**, *79*, 2332–2340.
5. Liu, S.; Dai, H.; Orfali, R. S.; Lin, W.; Liu, Z.; Proksch, P. *J. Agric. Food Chem.* **2016**, *64*, 3127–3132.
6. Kurita, K. L.; Glassey, E.; Linington, R. G. *Proc. Natl. Acad. Sci. U. S. A.* **2015**, *112*,

11999–12004.

7. Bode, H. B.; Bethe, B.; Höfs, R.; Zeeck, A. *ChemBioChem*. **2002**, *3*, 619–627.
8. Hammerschmidt, L.; Aly, A. H.; Abdel-Aziz, M.; Müller, W. E. G.; Lin, W.; Daletos, G.; Proksch, P. *Bioorg. Med. Chem.* **2015**, *23*, 712–719.
9. Wang, H.; Dai, H.; Heering, C.; Janiak, C.; Lin, W.; Orfali, R. S.; Müller, W. E. G.; Liu, Z.; Proksch, P. *RSC Advances*, **2016**, *6*, 81685–81693.
10. Hemphill, C. F.; Sureechatchaiyan, P.; Kassack, M. U.; Orfali, R. S.; Lin, W.; Deletos, G.; Proksch, P. *J. Antibiot.* **2017**, *70*, 726–732.
11. Andersen, R.; Büchi, G.; Kobbe, B.; Demain, A. L. *J. Org. Chem.* **1977**, *42*, 352–353.
12. Mizuno, K.; Yagi, A.; Satoi, S.; Takada, M.; Hayashi, M. *J. Antibiot.* **1977**, *30*, 297–302.
13. Miyata, M.; Kitamura, J.; Miyata, H. *Arch. Microbiol*. **1980**, *127*, 11–16.
14. Satoi, S.; Yagi, A.; Asano, K.; Mizuno, K.; Watanabe, T. *J. Antibiot.* **1977**, *30*, 303–307.
15. Ingavat, N.; Dobereiner, J.; Wiyakrutta, S.; Mahidol, C.; Ruchirawat, S.; Kittakoo P. *J. Nat. Prod.* **2009**, *72*, 2049–2052.
16. Khalil, Z. G.; Huang, X.; Raju, R.; Piggott, A. M.; Capon, R. J. *J. Org. Chem.* **2014**, *79*, 8700–8705.
17. Hayashi, H.; Furutsuka, K.; Shiono, Y. *J. Nat. Prod.* **1999**, *62*, 315–317
18. Nagel, D. W.; Pachler, K. G. R.; Steyn, P. S.; Vleggaar, R.; Wessels, P. L. *Tetrahedron* **1976**, *32*, 2625–2631.

19. Nozawa, K.; Nakajima, S.; Kawai, K.; Udagawa, S. *J. Chem. Soc. Perkin Trans. 1* **1988**, *9*, 2607−2610.

20. Banks, R. M.; Blanchflower, S. E.; Everett, J. R.; Manger, B. R.; Reading, C. *J. Antibiot.* **1997**, *50*, 840–846.

21. Takagi, M.; Motohashi, K.; Shin-Ya, K. *J. Antibiot.* **2010**, *63*, 393–395.

22. Yamazaki, H.; Ukai, K.; Namikoshi, M. *Tetrahedron Lett.* **2016**, *57*, 732–735.

23. Jain, S. V.; Bhadoriya, K. S.; Bari, S. B. *Med. Chem. Res.* **2012**, *21*, 1665–1676.

24. Ogawa, H.; Hasumi, K.; Sakai, K.; Murakawa, S.; Endo, A. *J. Antibiot.* **1991**, *44*, 762–767.

25. Königs, P.; Rinker, B.; Maus, L.; Nieger, M.; Rheinheimer, J.; Waldvogel, S. R. *J. Nat. Prod.* **2010**, *73*, 2064–2066.

26. Takahashi, H.; Hosoe, T.; Nozawa, K.; Kawai, K. *J. Nat. Prod.* **1999**, *62*, 1712–1713.

27. Wang, H.; Umeokoli, B. O.; Eze, P.; Heering, C.; Janiak, C.; Müller, W. E. G.; Orfali, R. S.; Hartmann, R.; Dai, H.; Lin, W.; Liu, Z.; Proksch, P. *Tetrahedron Lett.* **2017**, *58*, 1702–1705.

28. Marzluf, G. A. *Microbiol. Mol. Biol. Rev*. **1997**, *61*, 17–32.

29. Caddick, M. X.; Jones, M. G.; Van Tonder, J. M.; Le Cordier, H.; Narendja, F.; Strauss, J.; Morozov, I. Y. *Mol. Microbiol.* **2006**, *62*, 509–519.

30. Tudzynski, B. *Front. Microbiol.* **2014**, *5*, 656.

31. Min, K.; Shin, Y.; Son, H.; Lee, J.; Kim, J. C.; Choi, G. J.; Lee, Y. W. *FEMS Microbiol. Lett.* **2012**, *334*, 66–73.

32. Wiemann, P.; Tudzynski, B. *Fusarium: Genomics, Molecular and Cellular Biology*, **2013**, 111–142

33. López-Berges, M. S.; Schäfer, K.; Hera, C.; Di Pietro, A. *Fungal Genet. Biol.* **2014**, *62*, 78–84.

34. Maki, Y.; Soejima, H.; Sugiyama, T. *JP2014080406A*. **2014**.

35. Siebrecht, S.; Herdel, K.; Schurr, U.; Tischner, R. *Planta* **2003**, *217*, 783–793.

36. Kjer, J.; Debbab, A.; Aly, A. H.; Proksch, P. *Nat. Protoc.*, **2010**, *5*, 479–490.

37. Apex2, Data Collection Program for the CCD Area-Detector System; SAINT, Data Reduction and Frame Integration Program for the CCD Area-Detector System; Bruker Analytical X-ray Systems: Madison, WI, USA **1997−2012**.

38. Sheldrick, G. M. SADABS: Area-detector absorption correction; University of Goettingen: Germany **1996**.

39. Sheldrick, G. M. *Acta Crystallogr., Sect. A* **2008**, *64*, 112–122.

40. Sheldrick, G. M. *Acta Crystallogr., Sect. C* **2015**, *71*, 3–8.

41. (a) Flack, H. D.; Bernardinelli, G. *Acta Crystallogr., Sect. A* **1999**, *55*, 908–915. (b) Flack, H. *Acta Crystallogr., Sect. A* **1983**, *39*, 876–881.

42. Hooft, R. W. W.; Straver, L. H.; Spek, A. L. *J. Appl. Crystallogr.* **2008**, *41*, 96–103.

43. Brandenburg, K. Diamond (Version 4.4), Crystal and Molecular Structure Visualization, Bonn, Germany **2009-2017**.

44. (a) Spek, A. L. *Acta Crystallogr., Sect. D* **2009**, *65*, 148–155. (b) Spek, A. L. *J. Appl. Crystallogr.* **2003**, *36*, 7–13. (c) Spek, A. L. PLATON - A Multipurpose Crystallographic Tool; Utrecht University: Utrecht, The Netherlands **2008**.

(d) Farrugia, L. J. Windows implementation, Version 40608; University of Glasgow: Scotland, **2008**.

Supplementary Data

Indole Alkaloids Produced by an Endophytic Fungus *Aspergillus aculeatus* using an OSMAC Approach

Hao Wang [a], Peter M. Eze [b], Simon-Patrick Höfert [c], Christoph Janiak [c], Rudolf Hartmann [d], Festus B.C. Okoye [e], Charles O. Esimone [b], Raha S. Orfali [f], Haofu Dai [g], Zhen Liu [a,*], Peter Proksch [a,*]

[a]*Institute of Pharmaceutical Biology and Biotechnology, Heinrich-Heine-University Düsseldorf, Universitätsstrasse 1, 40225 Düsseldorf, Germany*

[b]*Department of Pharmaceutical Microbiology and Biotechnology, Faculty of Pharmaceutical Sciences, Nnamdi Azikiwe University, Awka, Nigeria*

[c]*Institute of Inorganic and Structural Chemistry, Heinrich-Heine-University Düsseldorf, Universitätsstrasse 1, 40225 Düsseldorf, Germany*

[d]*Institute of Complex Systems: Structural Biochemistry, Forschungszentrum Juelich, Wilhelm-Johnen-Straße, 52428 Juelich, Germany*

[e]*Department of Pharmaceutical and Medicinal Chemistry, Faculty of Pharmaceutical Sciences, Nnamdi Azikiwe University, Awka, Nigeria*

[f]*Department of Pharmacognosy, Faculty of Pharmacy, King Saud University, Riyadh, Saudi Arabia*

[g]*Key Laboratory of Biology and Genetic Resources of Tropical Crops, Ministry of Agriculture, Institute of Tropical Bioscience and Biotechnology, Chinese Academy of Tropical Agricultural Sciences, Haikou 571101, China*

Table of Contents

Figure S1. UV spectrum of **1**....102
Figure S2. HRESIMS of **1**....102
Figure S3. ^{1}H NMR (600 MHz, methanol-d_4) spectrum of **1**....103
Figure S4. ^{13}C NMR (150 MHz, methanol-d_4) spectrum of **1**....103
Figure S5. ^{1}H-^{1}H COSY (600 MHz, methanol-d_4) spectrum of **1**....104
Figure S6. HSQC (600 and 150 MHz, methanol-d_4) spectrum of **1**....104
Figure S7. HMBC (600 and 150 MHz, methanol-d_4) spectrum of **1**....105
Figure S8. UV spectrum of **2**....105
Figure S9. HRESIMS of **2**....106
Figure S10.^{1}H NMR (600 MHz, methanol-d_4) spectrum of **2**....106
Figure S11. ^{13}C NMR (150 MHz, methanol-d_4) spectrum of **2**....107
Figure S12. ^{1}H-^{1}H COSY (600 MHz, methanol-d_4) spectrum of **2**....107
Figure S13. HSQC (600 and 150 MHz, methanol-d_4) spectrum of **2**....108
Figure S14. HMBC (600 and 150 MHz, methanol-d_4) spectrum of **2**....108
Figure S15. UV spectrum of **3**....109
Figure S16. HRESIMS of **3**....109
Figure S17. ^{1}H NMR (600 MHz, methanol-d_4) spectrum of **3**....110
Figure S18. ^{13}C NMR (150 MHz, methanol-d_4) spectrum of **3**....110
Figure S19. ^{1}H-^{1}H COSY (600 MHz, methanol-d_4) spectrum of **3**....111
Figure S20. HSQC (600 and 150 MHz, methanol-d_4) spectrum of **3**....111
Figure S21. HMBC (600 and 150 MHz, methanol-d_4) spectrum of **3**....112
Figure S22. UV spectrum of **4**....112
Figure S23. HRESIMS of **4**....113
Figure S24. ^{1}H NMR (600 MHz, methanol-d_4) spectrum of **4**....113
Figure S25. ^{13}C NMR (150 MHz, methanol-d_4) spectrum of **4**....114
Figure S26. ^{1}H-^{1}H COSY (600 MHz, methanol-d_4) spectrum of **4**....114
Figure S27. HSQC (600 and 150 MHz, methanol-d_4) spectrum of **4**....115
Figure S28. HMBC (600 and 150 MHz, methanol-d_4) spectrum of **4**....115
Figure S29. UV spectrum of **5**....116
Figure S30. HRESIMS of **5**....116
Figure S31. ^{1}H NMR (600 MHz, methanol-d_4) spectrum of **5**....117
Figure S32. ^{13}C NMR (150 MHz, methanol-d_4) spectrum of **5**....117
Figure S33. ^{1}H-^{1}H COSY (600 MHz, methanol-d_4) spectrum of **5**....118
Figure S34. HSQC (600 and 150 MHz, methanol-d_4) spectrum of **5**....118
Figure S35. HMBC (600 and 150 MHz, methanol-d_4) spectrum of **5**....119
Figure S36. UV spectrum of **6**....119
Figure S37. HRESIMS of **6**....120
Figure S38. ^{1}H NMR (700 MHz, methanol-d_4) spectrum of **6**....120
Figure S39. ^{1}H-^{1}H COSY (700 MHz, methanol-d_4) spectrum of **6**....121
Figure S40. HSQC (700 and 175 MHz, methanol-d_4) spectrum of **6**....121
Figure S41. HMBC (700 and 175 MHz, methanol-d_4) spectrum of **6**....122
Figure S42. UV spectrum of **7**....122

Figure S43. HRESIMS of **7**....123
Figure S44. ^{1}H NMR (600 MHz, methanol-d_4) spectrum of **7**....123
Figure S45. ^{13}C NMR (150 MHz, methanol-d_4) spectrum of **7**....124
Figure S46. ^{1}H-^{1}H COSY (600 MHz, methanol-d_4) spectrum of **7**....124
Figure S47. HSQC (600 and 150 MHz, methanol-d_4) spectrum of **7**....125
Figure S48. HMBC (600 and 150 MHz, methanol-d_4) spectrum of **7**....125
Figure S49. UV spectrum of **8**....126
Figure S50. HRESIMS of **8**....126
Figure S51. ^{1}H NMR (600 MHz, methanol-d_4) spectrum of **8**....127
Figure S52. ^{13}C NMR (150 MHz, methanol-d_4) spectrum of **8**....127
Figure S53. ^{1}H-^{1}H COSY (600 MHz, methanol-d_4) spectrum of **8**....128
Figure S54. HSQC (600 and 150 MHz, methanol-d_4) spectrum of **8**....128
Figure S55. HMBC (600 and 150 MHz, methanol-d_4) spectrum of **8**....129
Figure S56. UV spectrum of **9**....129
Figure S57. HRESIMS of **9**....130
Figure S58. ^{1}H NMR (700 MHz, methanol-d_4) spectrum of **9**....130
Figure S59. ^{1}H-^{1}H COSY (600 MHz, methanol-d_4) spectrum of **9**....131
Figure S60. HSQC (700 and 175 MHz, methanol-d_4) spectrum of **9**....131
Figure S61. HMBC (700 and 175 MHz, methanol-d_4) spectrum of **9**....132
Figure S62. UV spectrum of **10**....132
Figure S63. HRESIMS of **10**....133
Figure S64. ^{1}H NMR (700 MHz, methanol-d_4) spectrum of **10**....133
Figure S65. ^{1}H-^{1}H COSY (600 MHz, methanol-d_4) spectrum of **10**....134
Figure S66. HSQC (700 and 175 MHz, methanol-d_4) spectrum of **10**....134
Figure S67. HMBC (700 and 175 MHz, methanol-d_4) spectrum of **10**....135
Results of X-ray analysis of compound 1....135
Results of X-ray analysis of compound 2....143

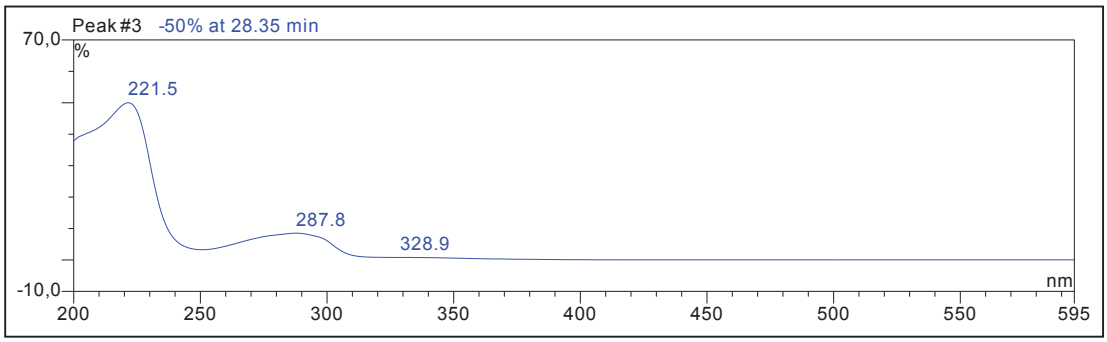

Figure S1. UV spectrum of **1**

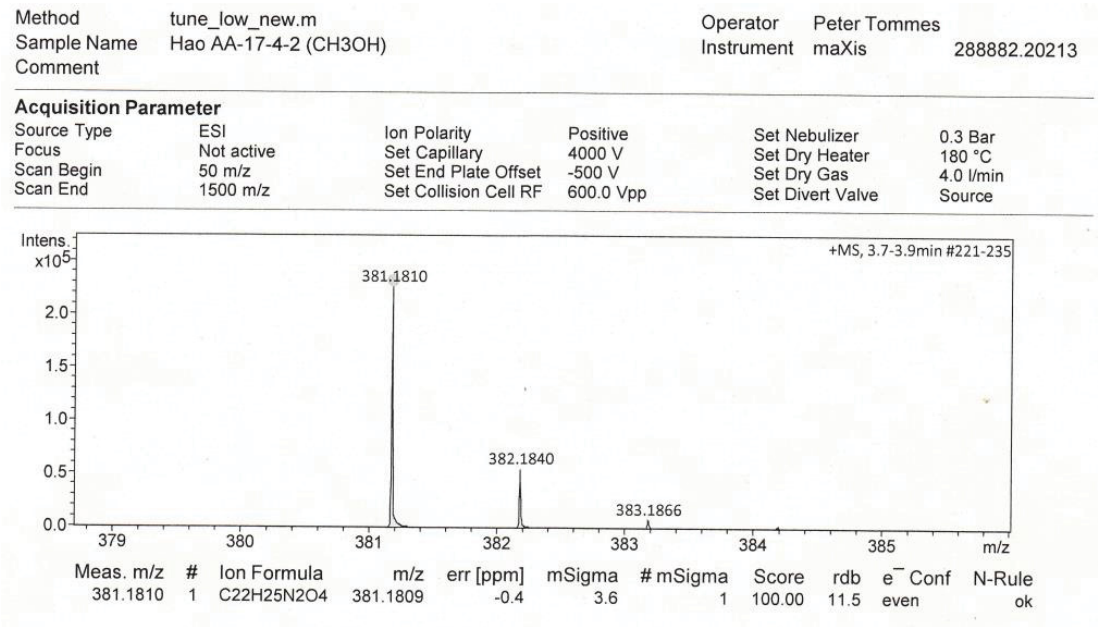

Figure S2. HRESIMS of **1**

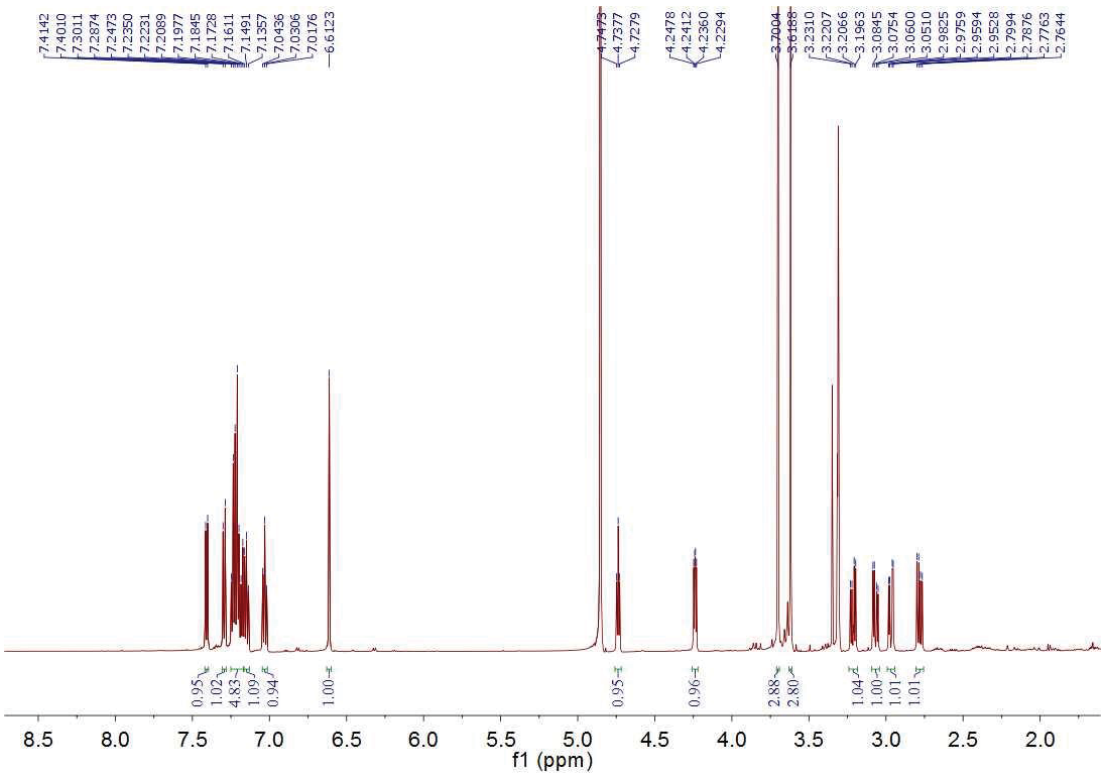

Figure S3. ^{1}H NMR (600 MHz, methanol-d_4) spectrum of **1**

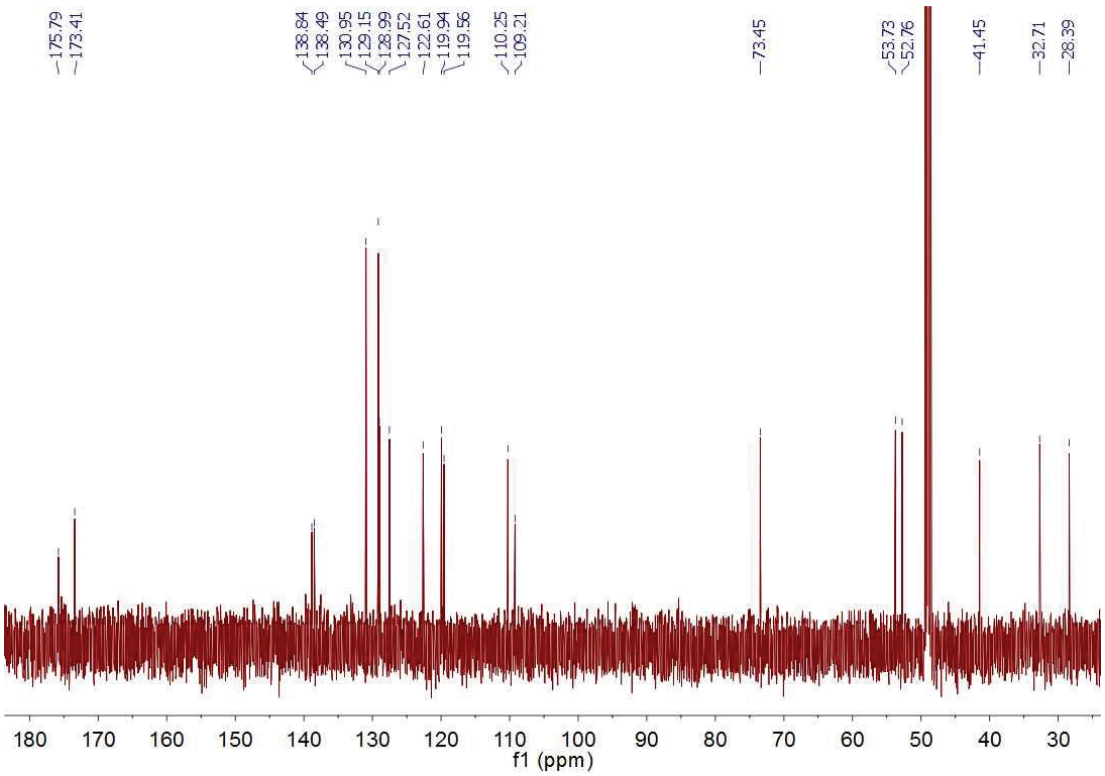

Figure S4. ^{13}C NMR (150 MHz, methanol-d_4) spectrum of **1**

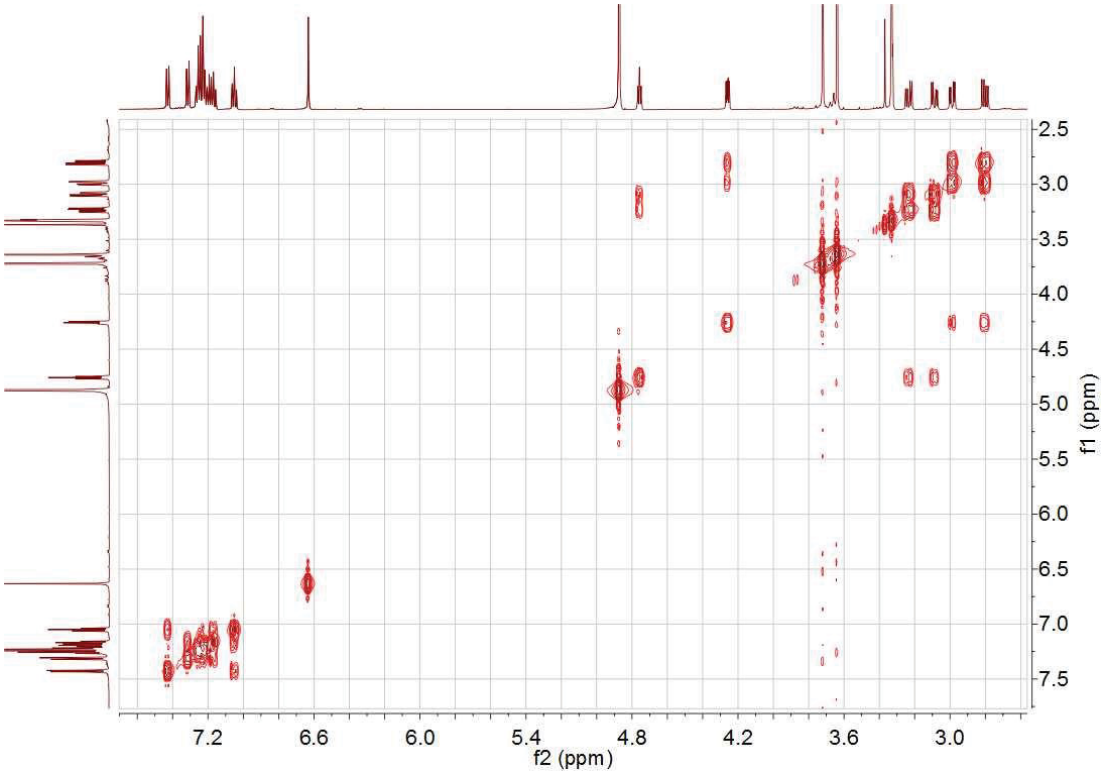

Figure S5. ^{1}H-^{1}H COSY (600 MHz, methanol-d_4) spectrum of **1**

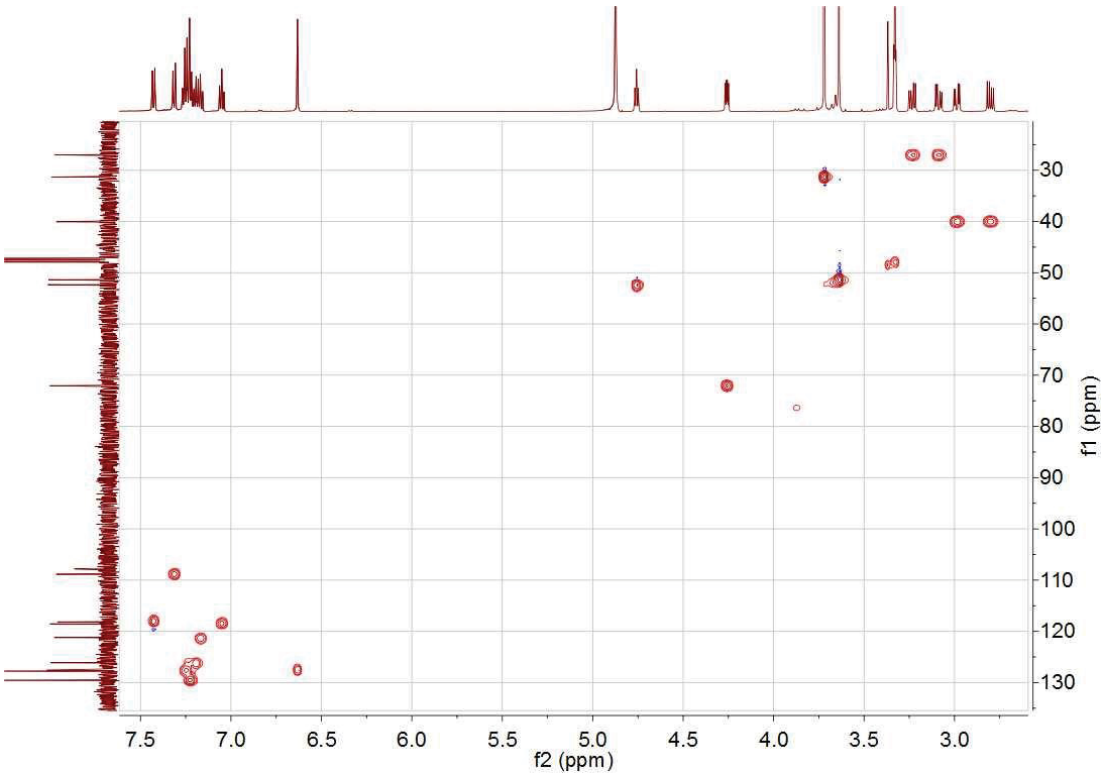

Figure S6. HSQC (600 and 150 MHz, methanol-d_4) spectrum of **1**

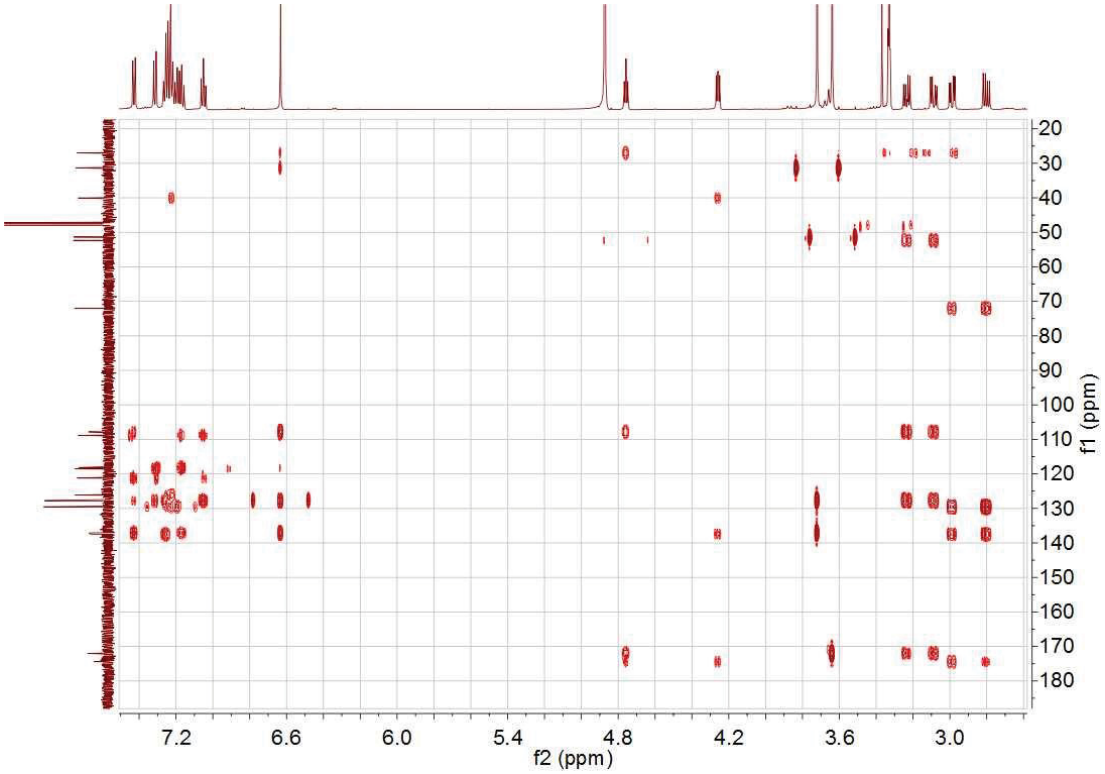

Figure S7. HMBC (600 and 150 MHz, methanol-d_4) spectrum of **1**

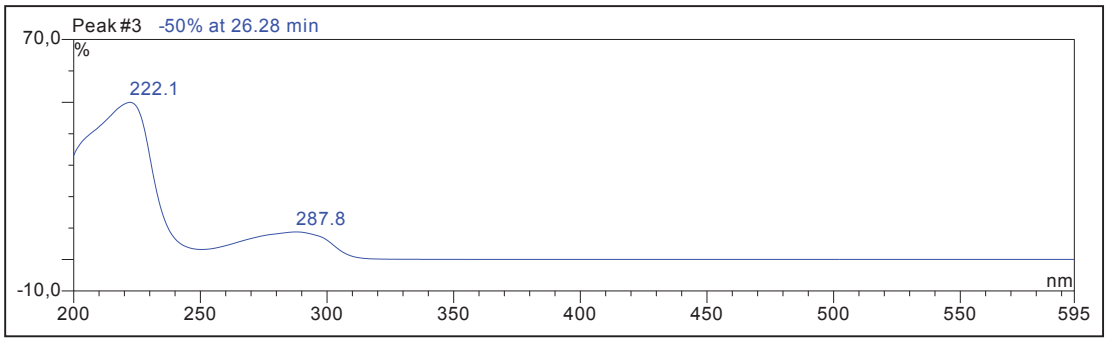

Figure S8. UV spectrum of **2**

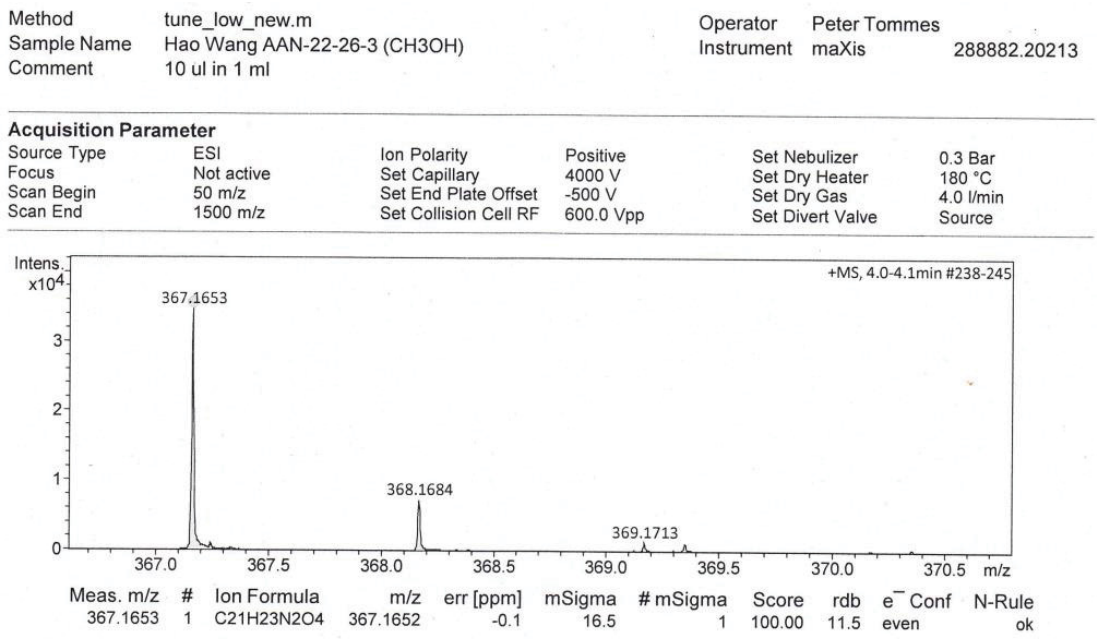

Figure S9. HRESIMS of **2**

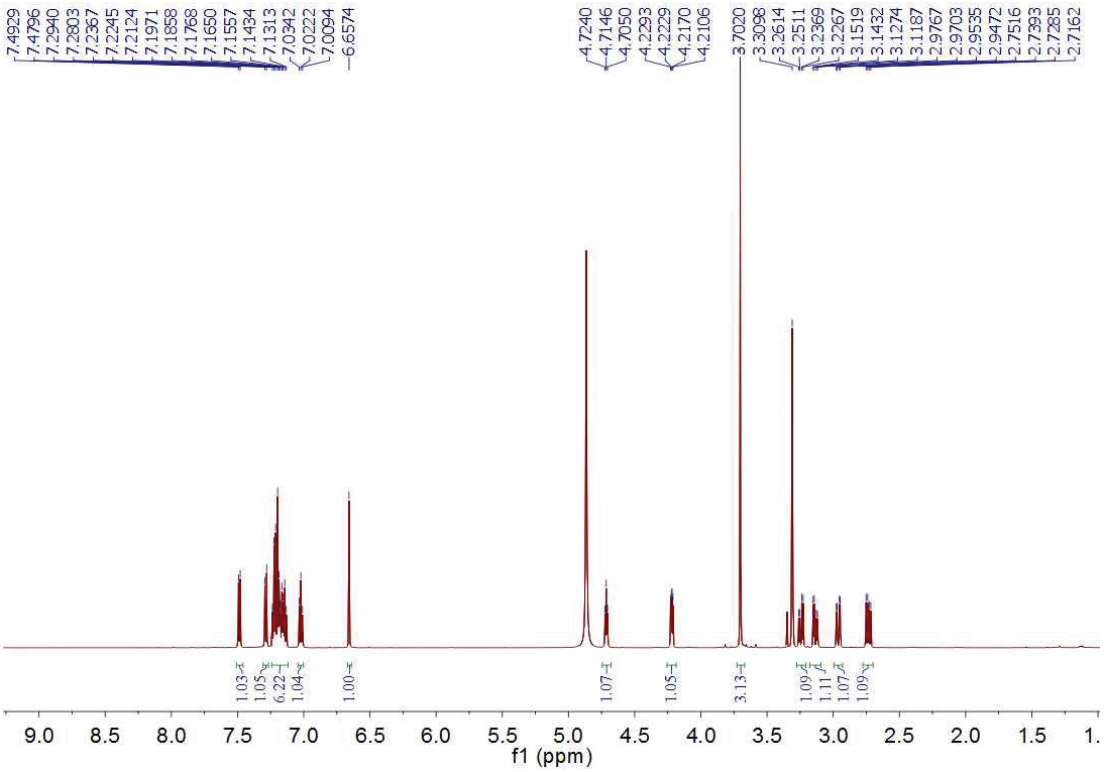

Figure S10. ^{1}H NMR (600 MHz, methanol-d_4) spectrum of **2**

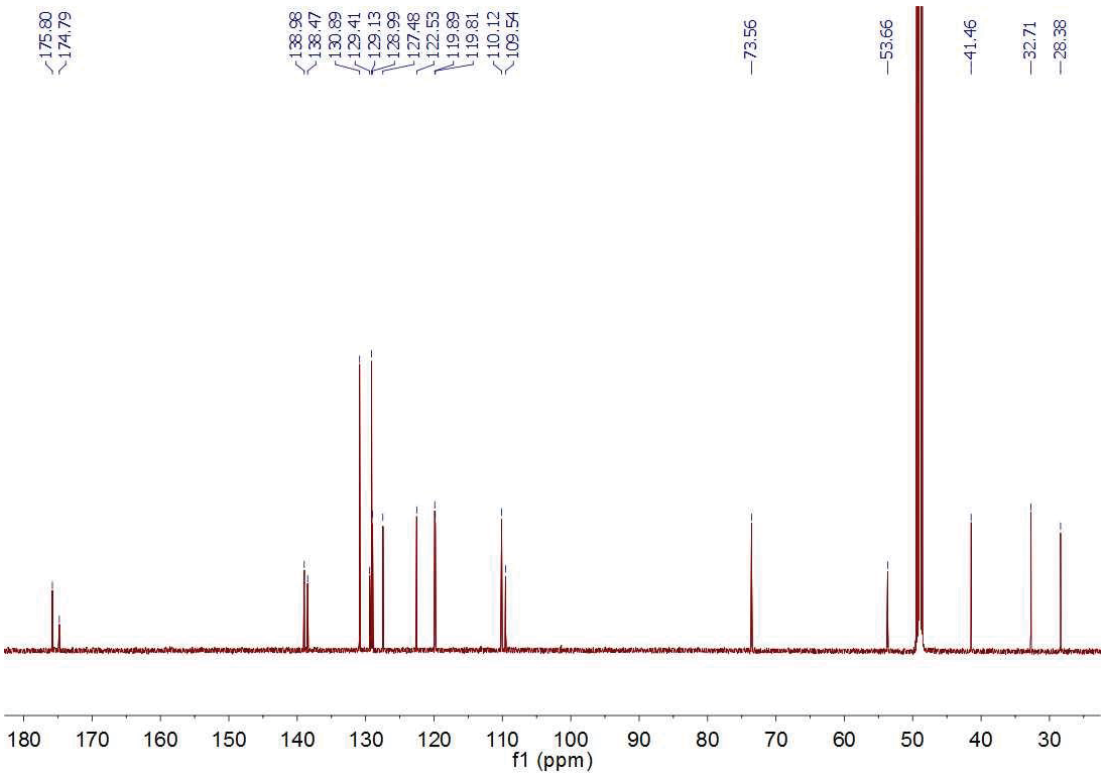

Figure S11. ^{13}C NMR (150 MHz, methanol-d_4) spectrum of **2**

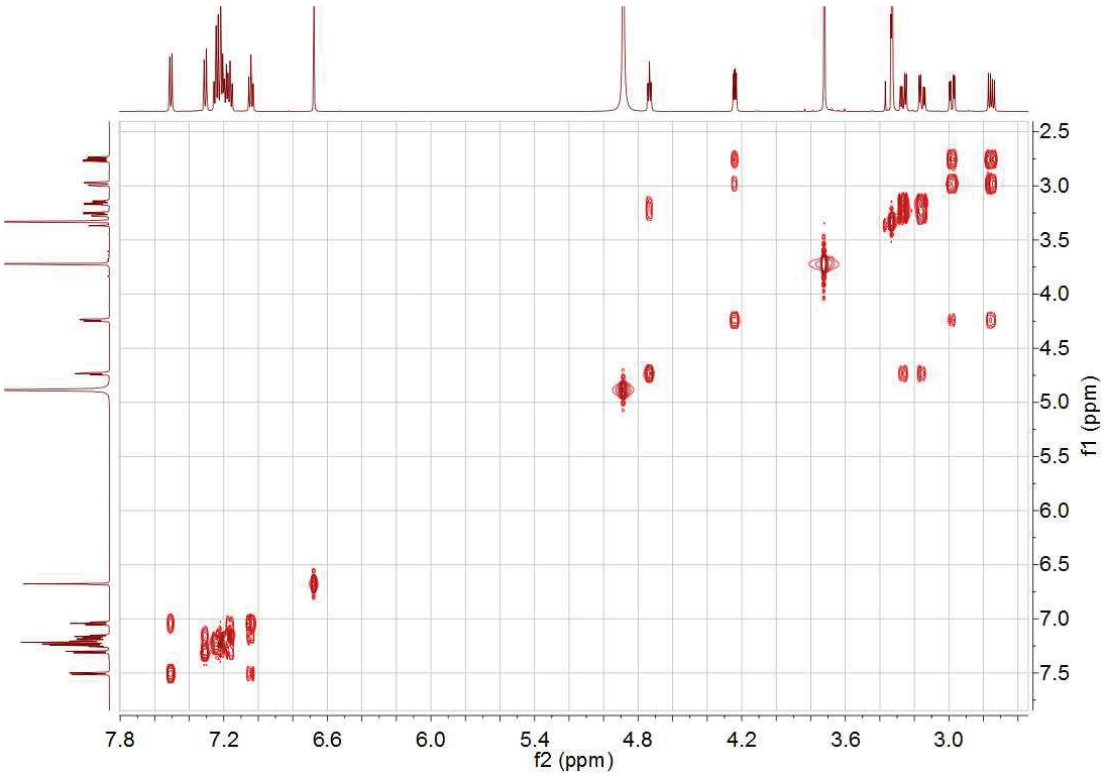

Figure S12. ^{1}H-^{1}H COSY (600 MHz, methanol-d_4) spectrum of **2**

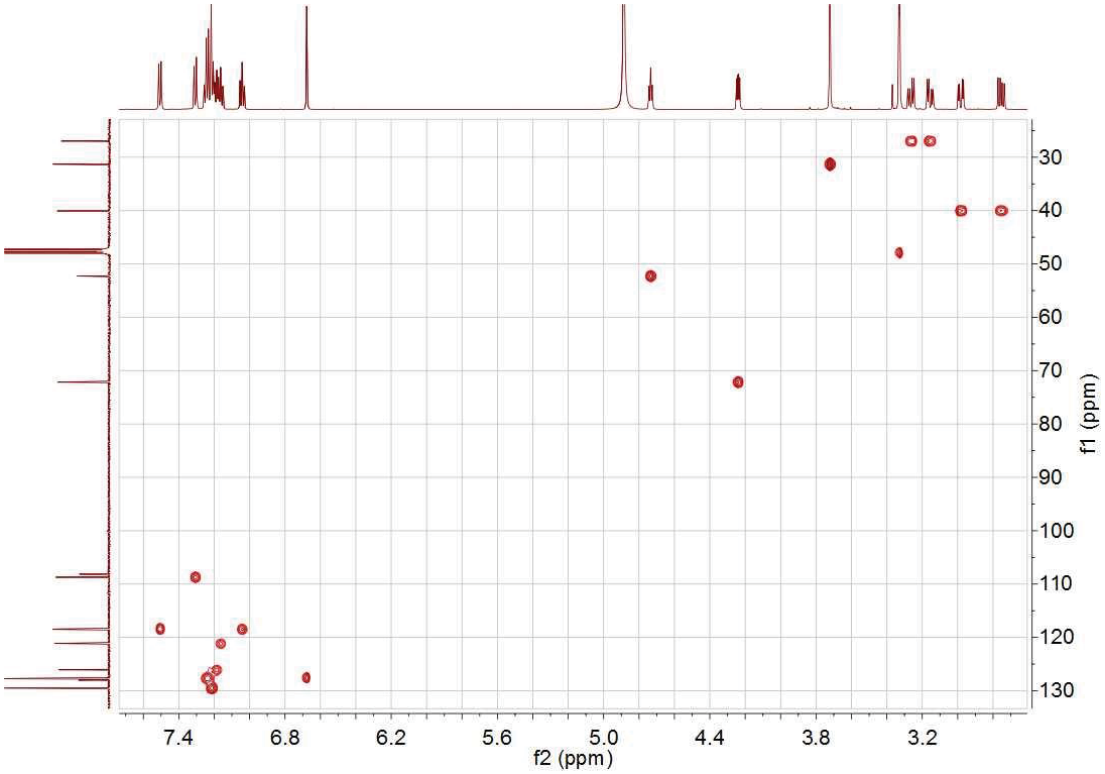

Figure S13. HSQC (600 and 150 MHz, methanol-d_4) spectrum of **2**

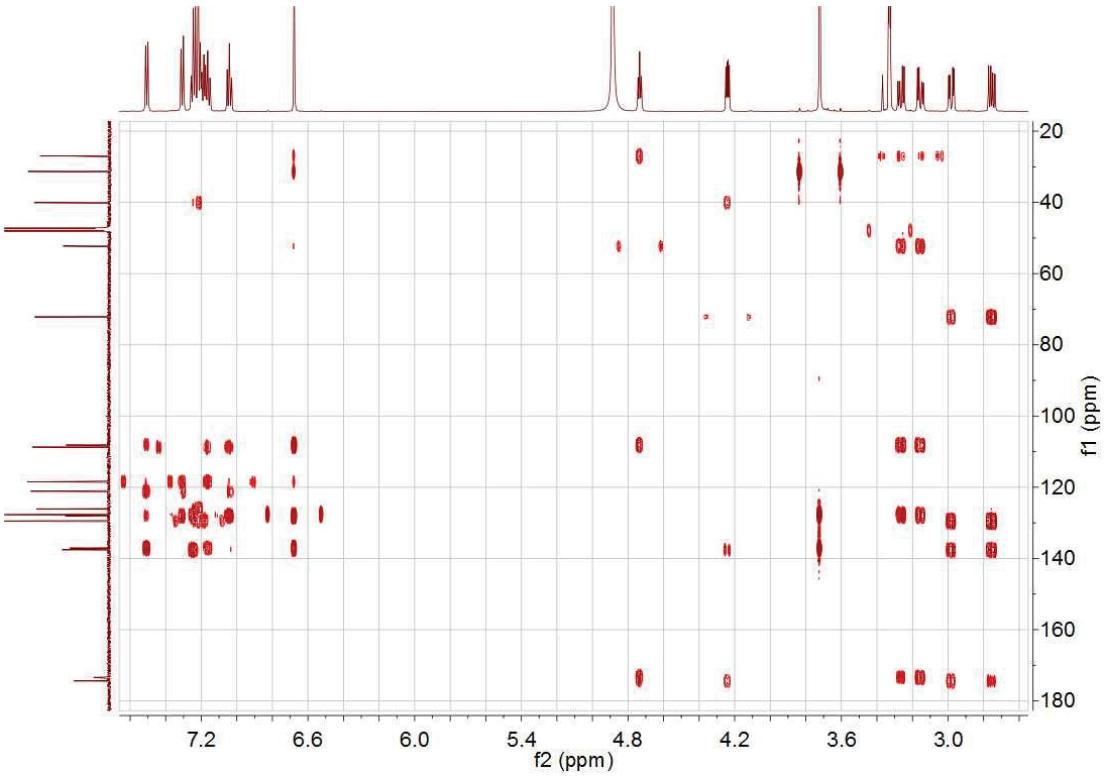

Figure S14. HMBC (600 and 150 MHz, methanol-d_4) spectrum of **2**

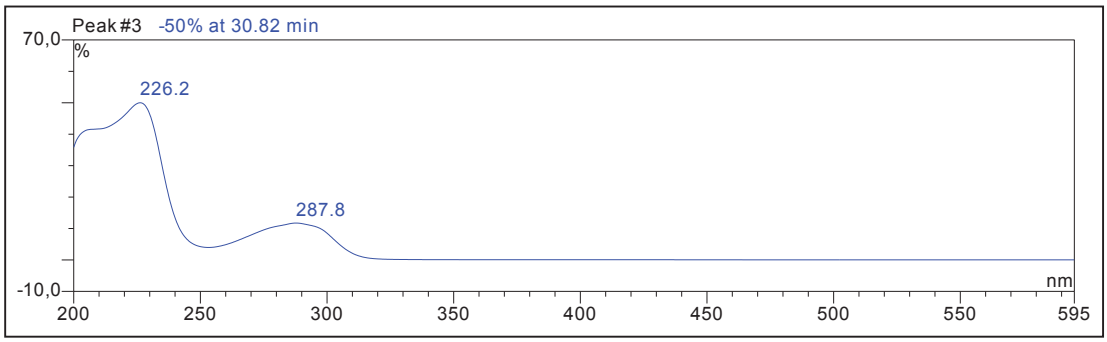

Figure S15. UV spectrum of **3**

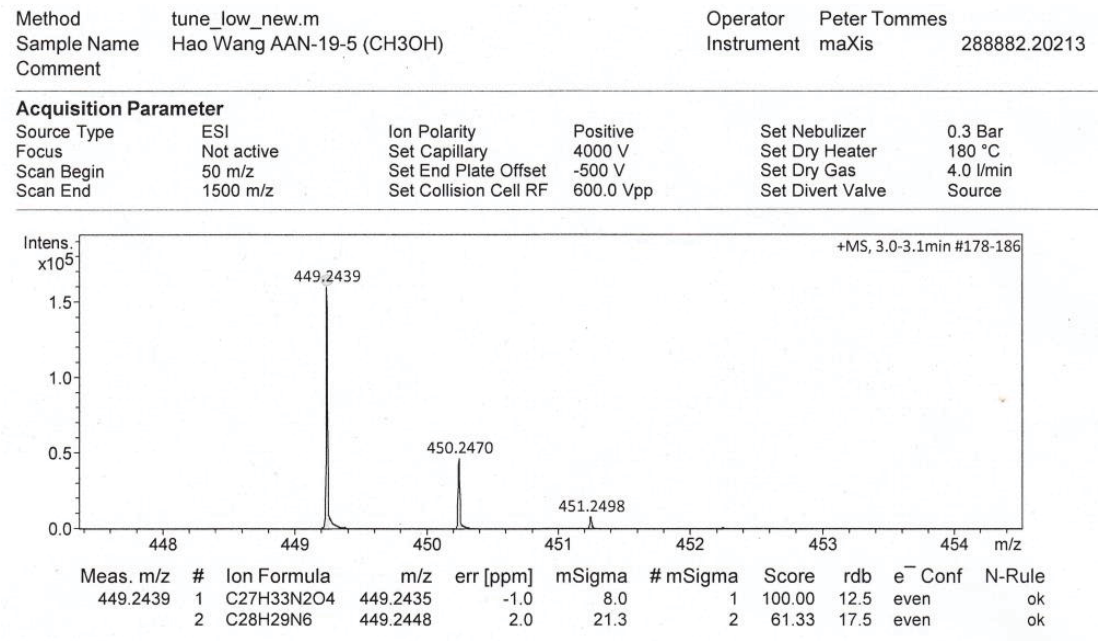

Figure S16. HRESIMS of **3**

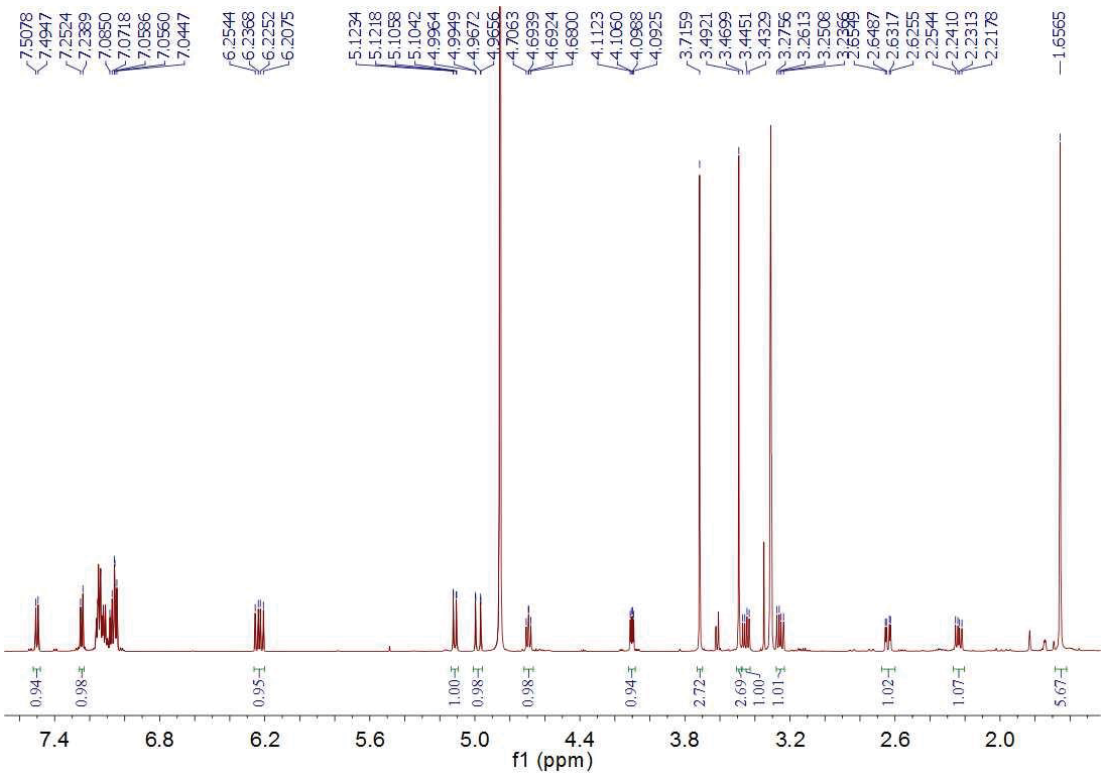

Figure S17. ^{1}H NMR (600 MHz, methanol-d_4) spectrum of **3**

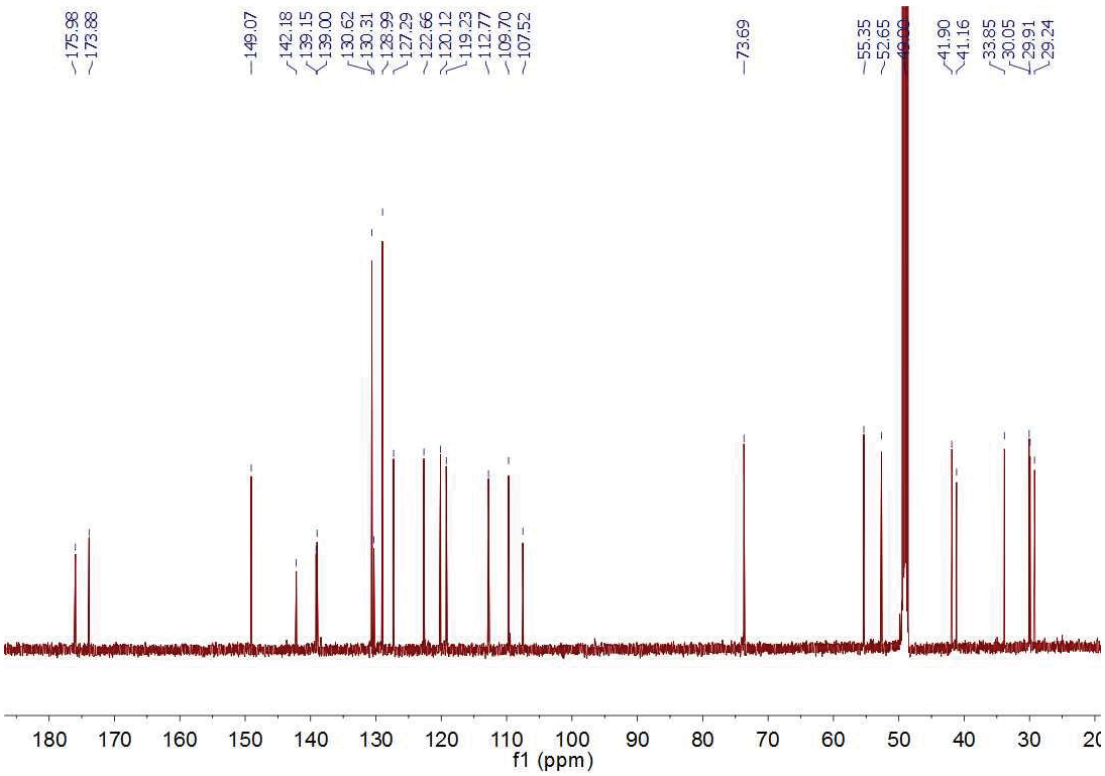

Figure S18. ^{13}C NMR (150 MHz, methanol-d_4) spectrum of **3**

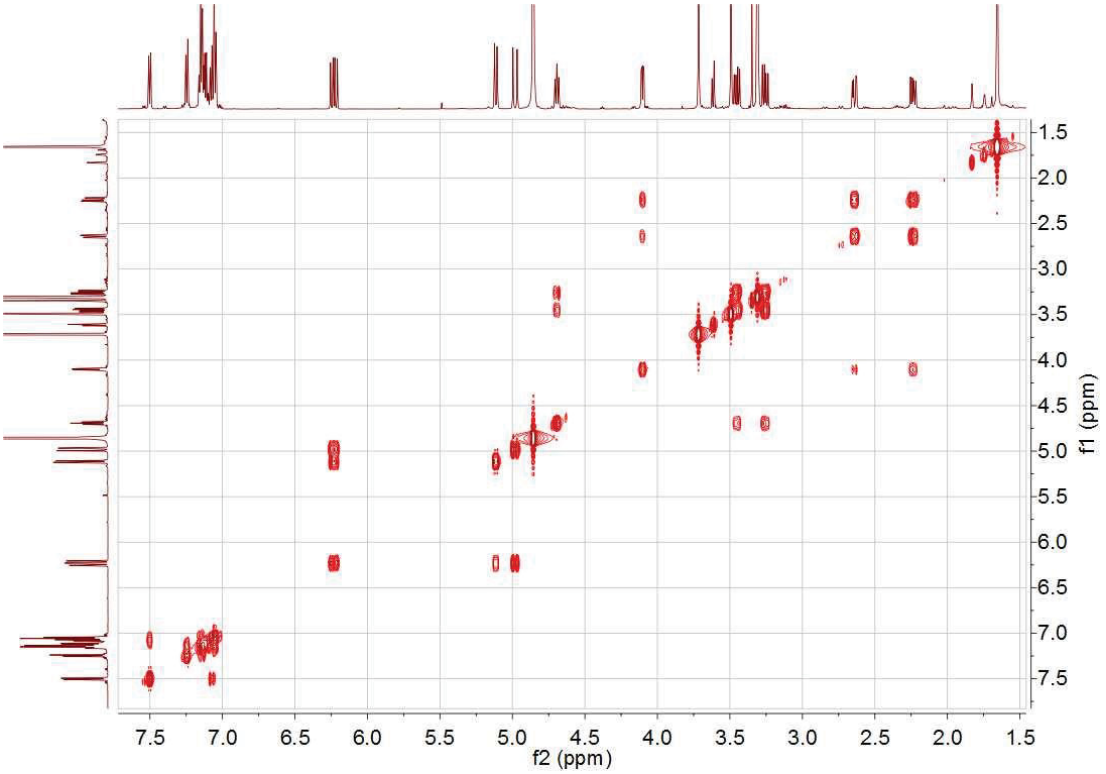

Figure S19. ^{1}H-^{1}H COSY (600 MHz, methanol-d_4) spectrum of **3**

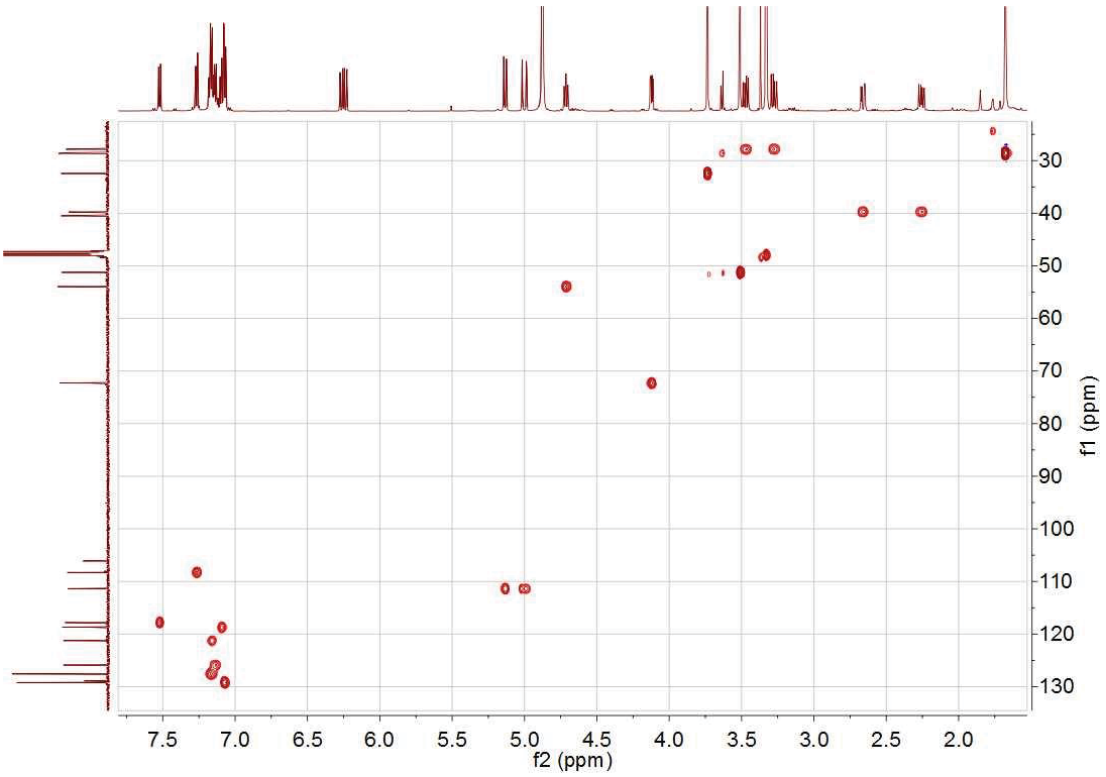

Figure S20. HSQC (600 and 150 MHz, methanol-d_4) spectrum of **3**

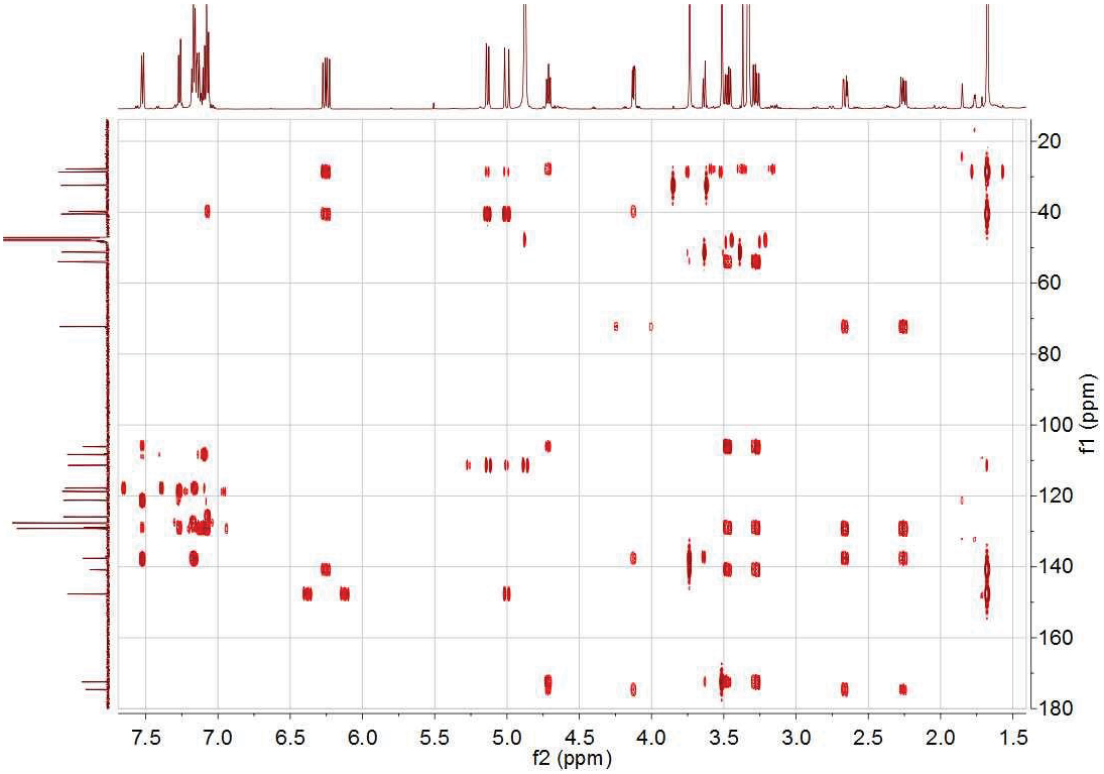

Figure S21. HMBC (600 and 150 MHz, methanol-d_4) spectrum of **3**

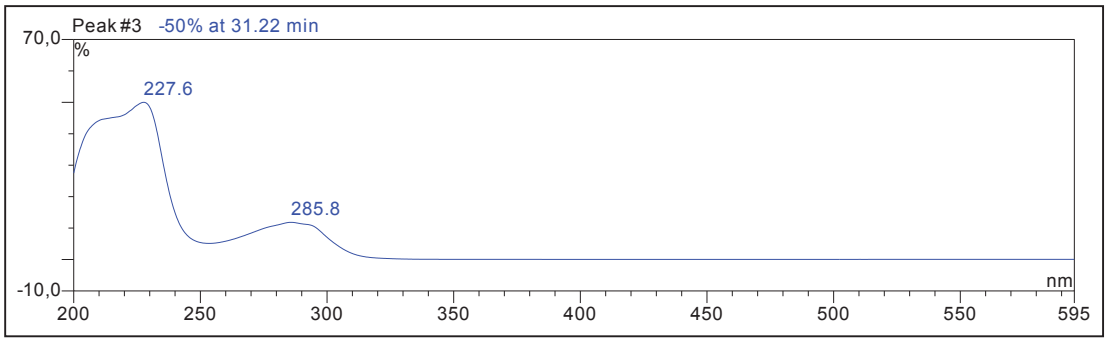

Figure S22. UV spectrum of **4**

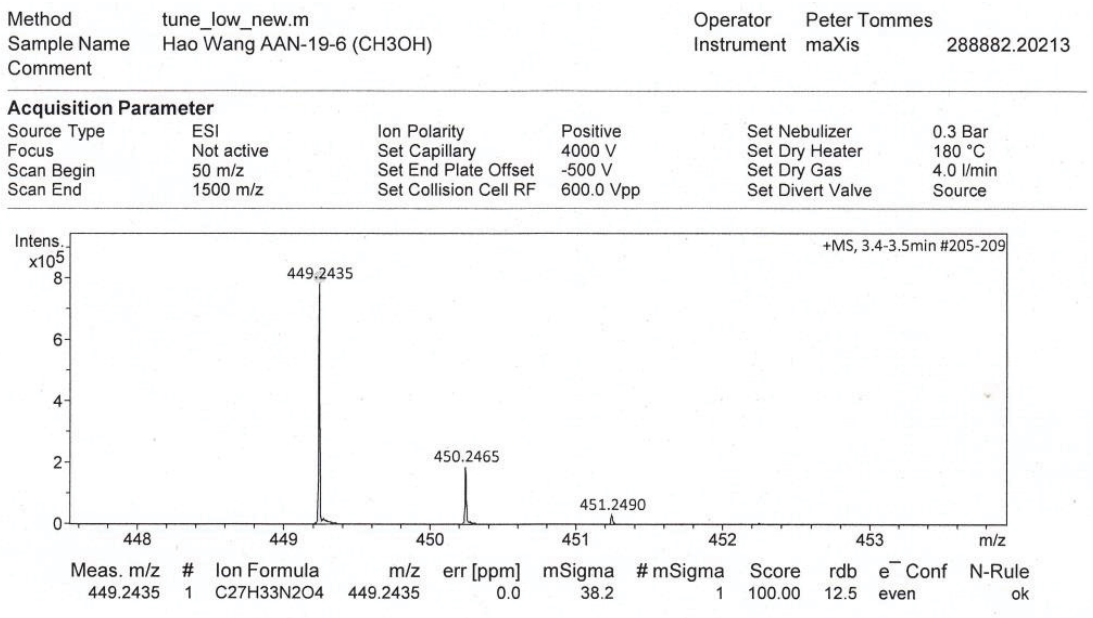

Figure S23. HRESIMS of **4**

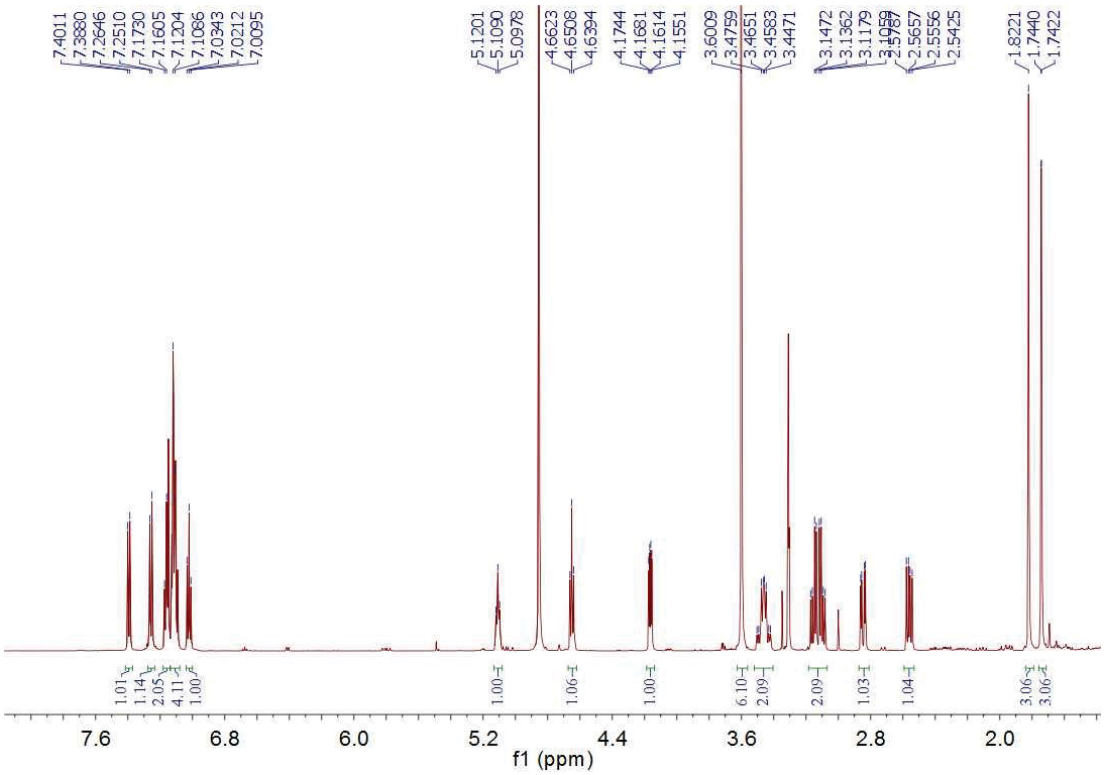

Figure S24. ^{1}H NMR (600 MHz, methanol-d_4) spectrum of **4**

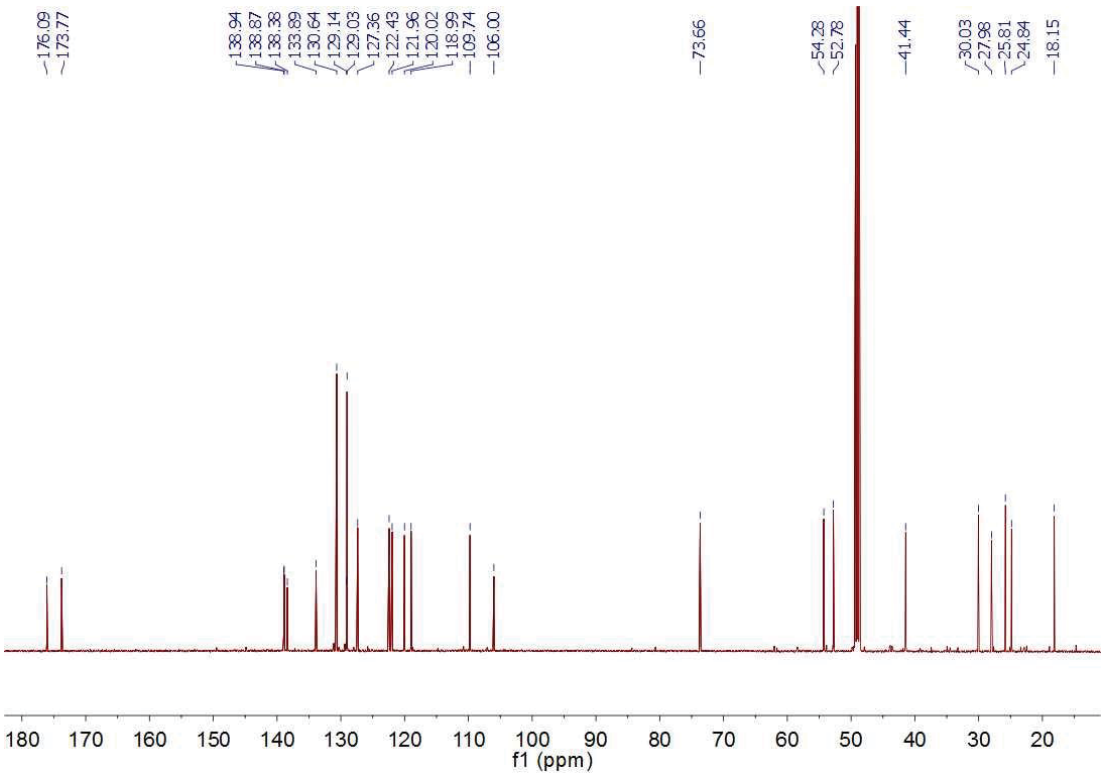

Figure S25. ^{13}C NMR (150 MHz, methanol-d_4) spectrum of **4**

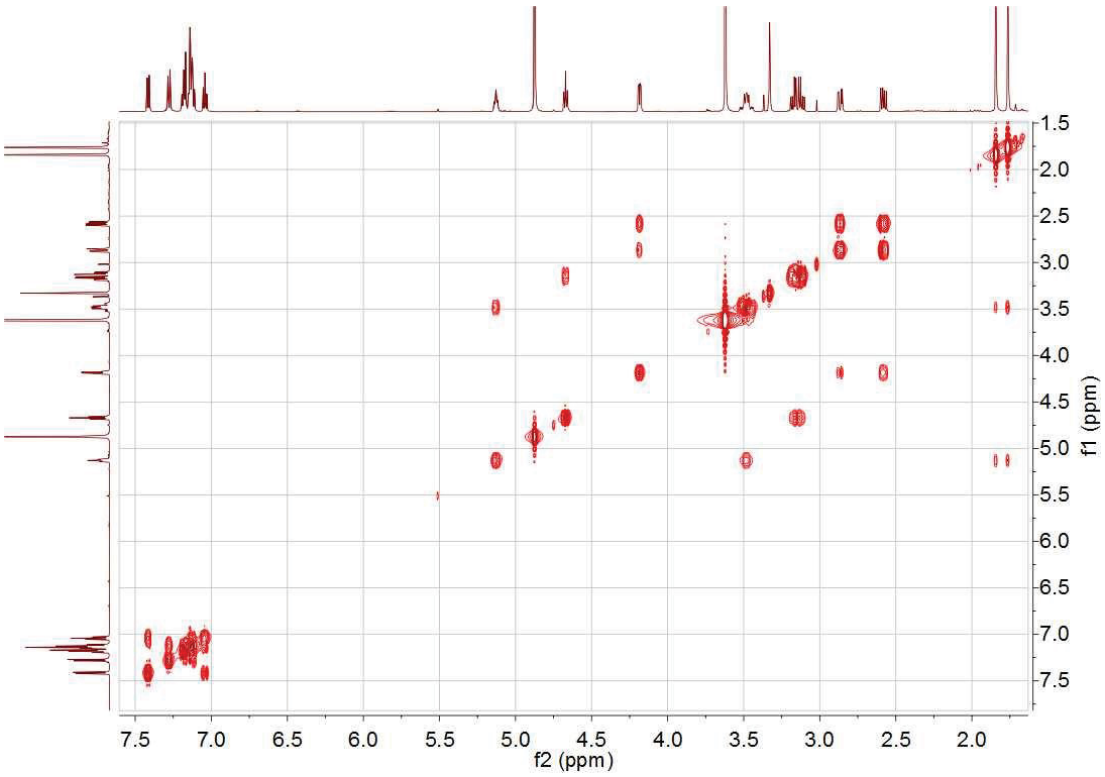

Figure S26. ^{1}H-^{1}H COSY (600 MHz, methanol-d_4) spectrum of **4**

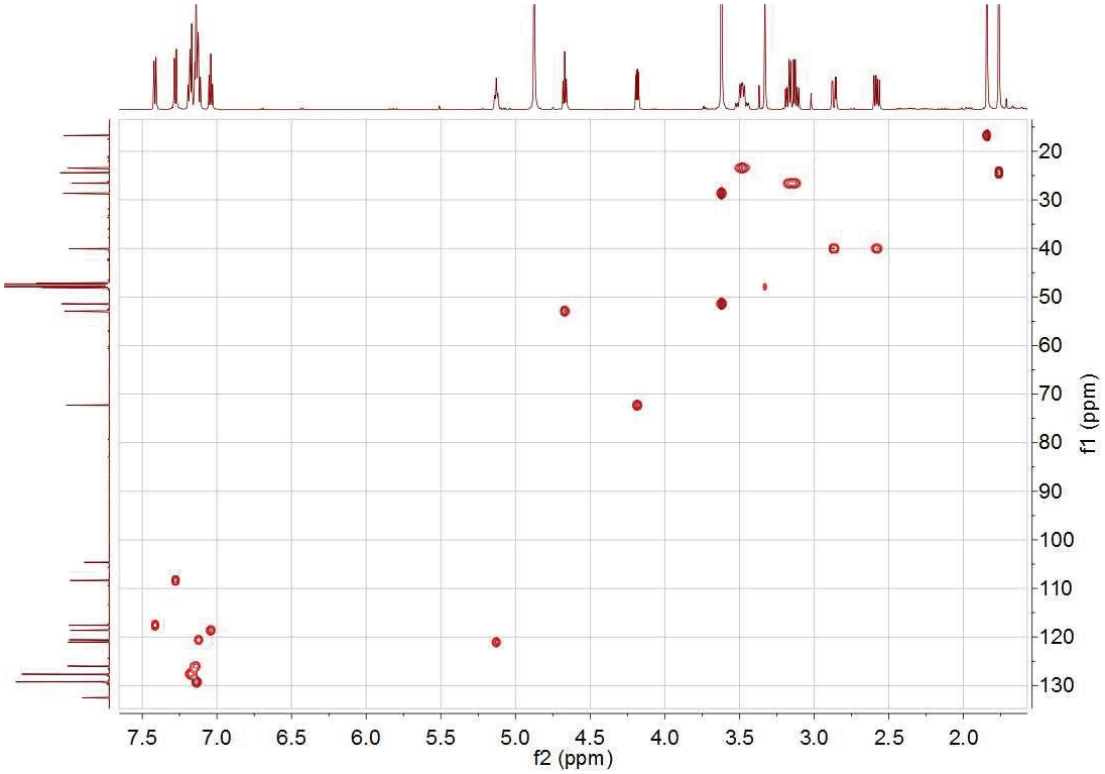

Figure S27. HSQC (600 and 150 MHz, methanol-d_4) spectrum of **4**

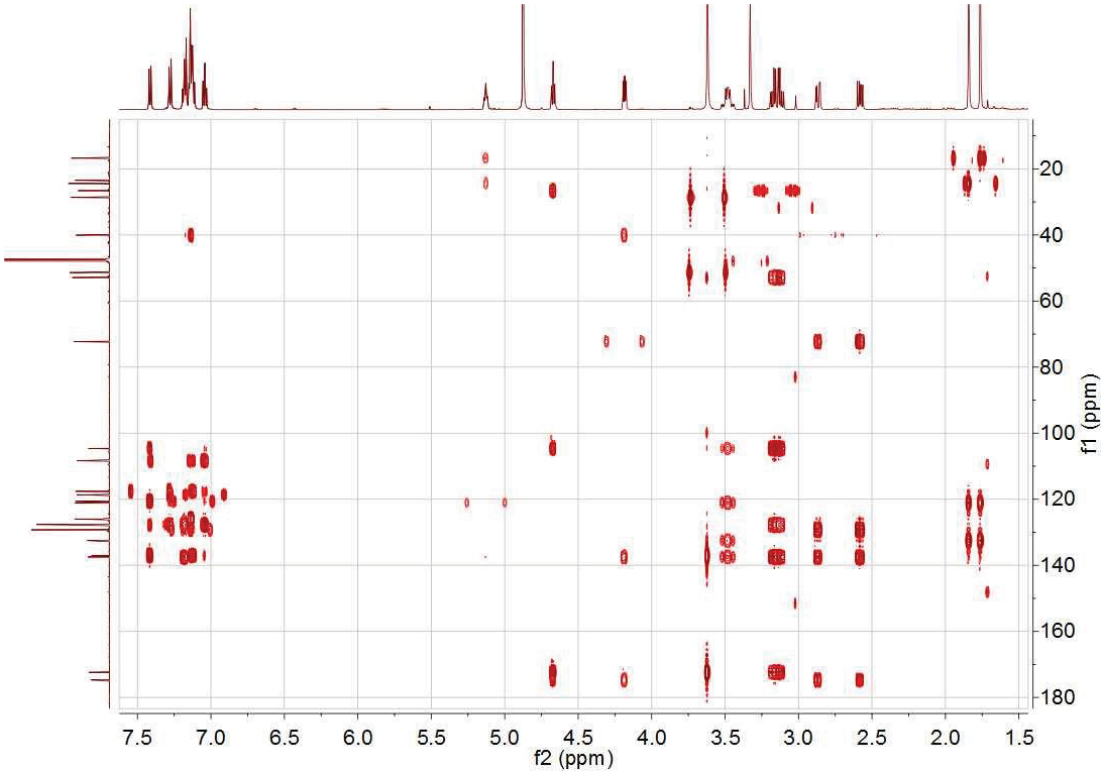

Figure S28. HMBC (600 and 150 MHz, methanol-d_4) spectrum of **4**

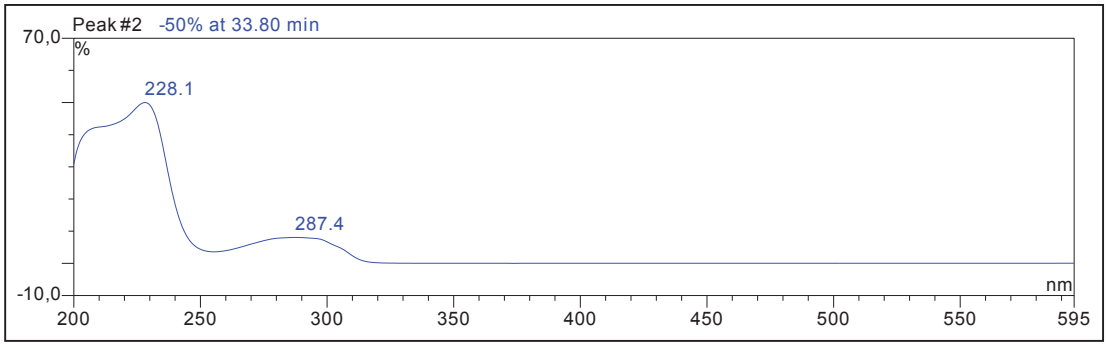

Figure S29. UV spectrum of **5**

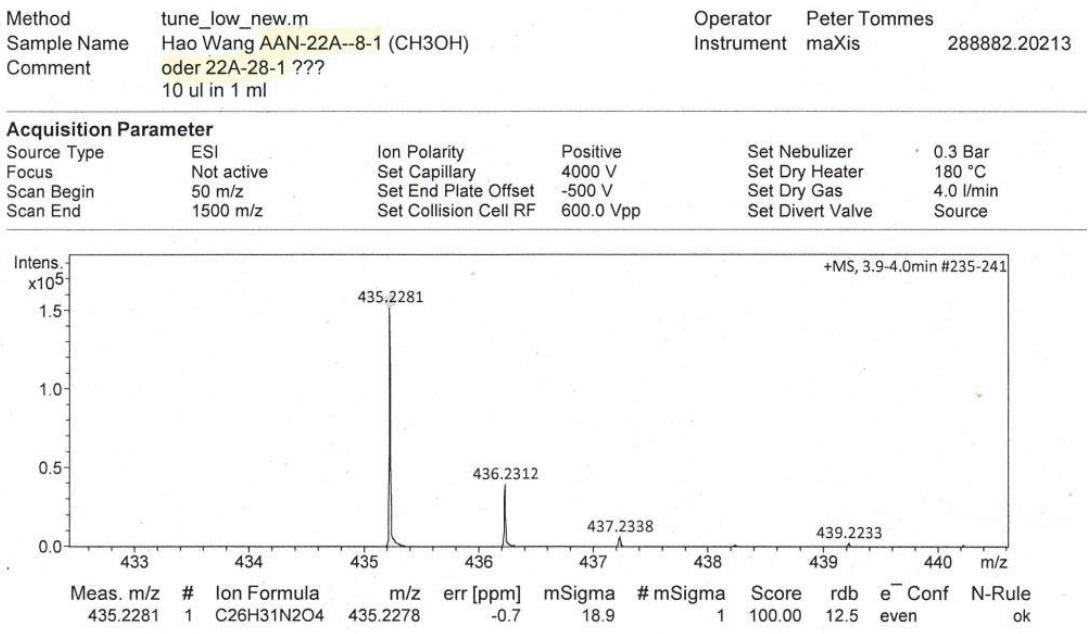

Figure S30. HRESIMS of **5**

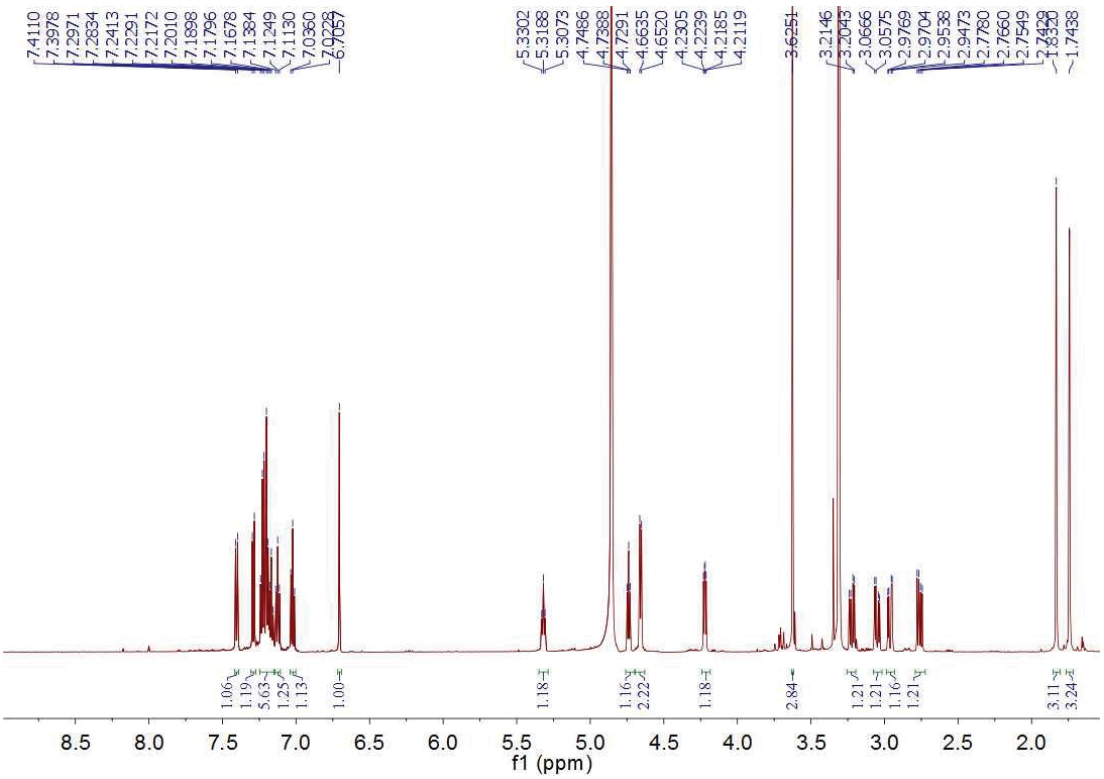

Figure S31. ^{1}H NMR (600 MHz, methanol-d_4) spectrum of **5**

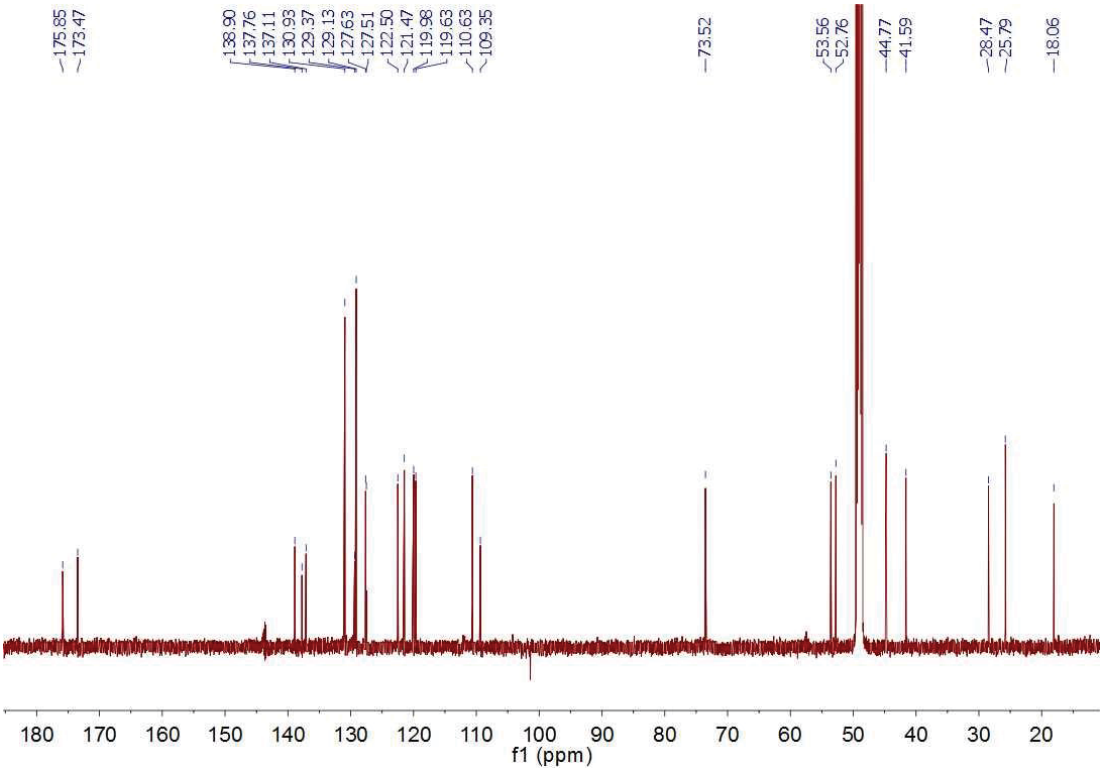

Figure S32. ^{13}C NMR (150 MHz, methanol-d_4) spectrum of **5**

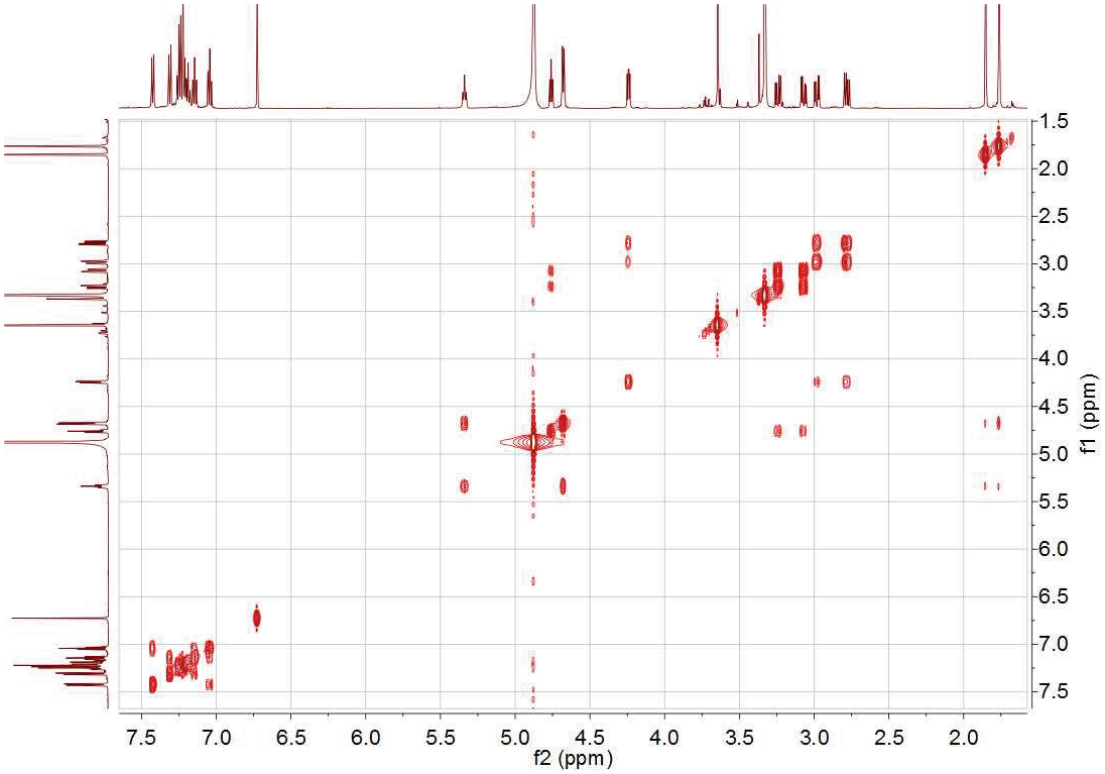

Figure S33. ^{1}H-^{1}H COSY (600 MHz, methanol-d_4) spectrum of **5**

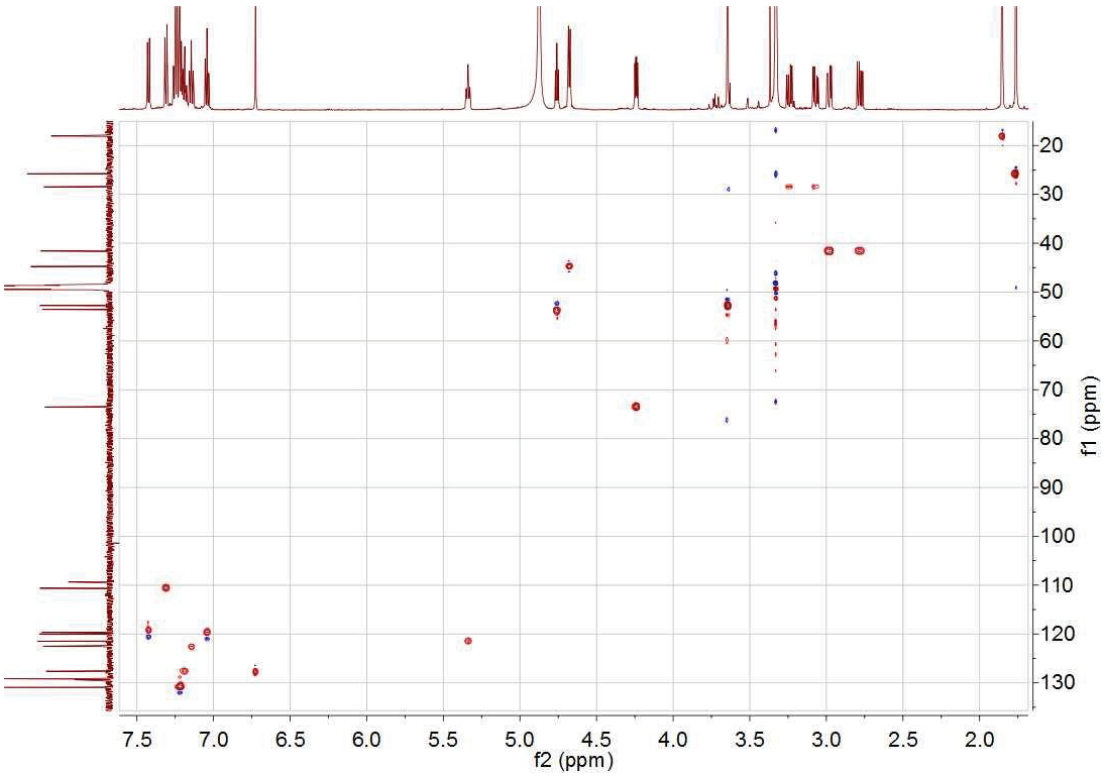

Figure S34. HSQC (600 and 150 MHz, methanol-d_4) spectrum of **5**

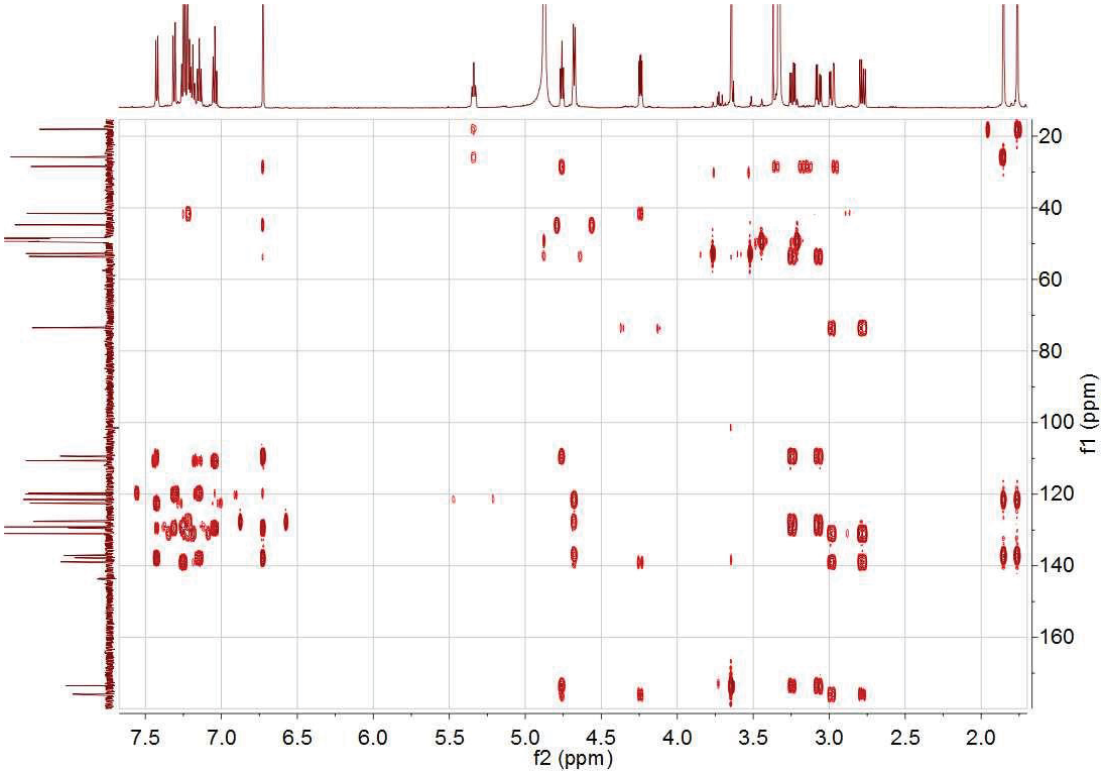

Figure S35. HMBC (600 and 150 MHz, methanol-d_4) spectrum of **5**

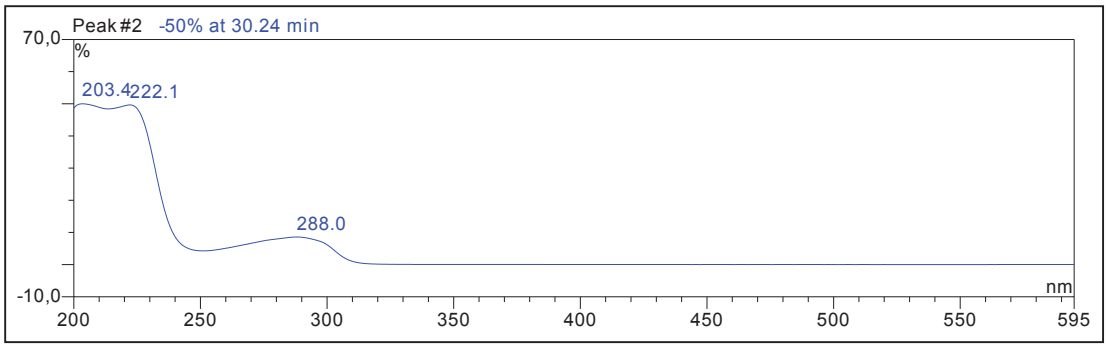

Figure S36. UV spectrum of **6**

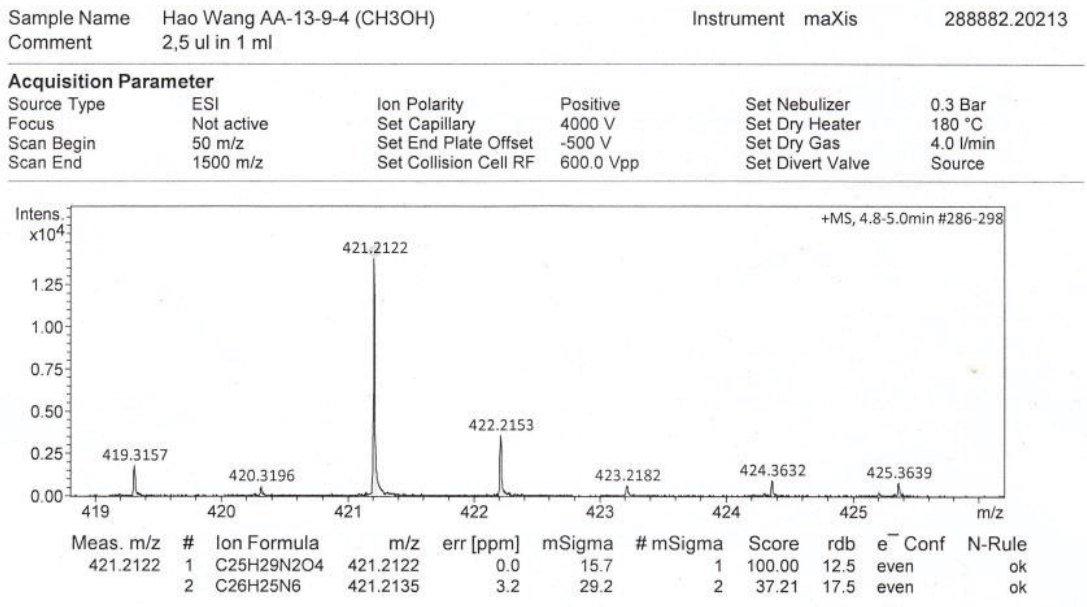

Figure S37. HRESIMS of **6**

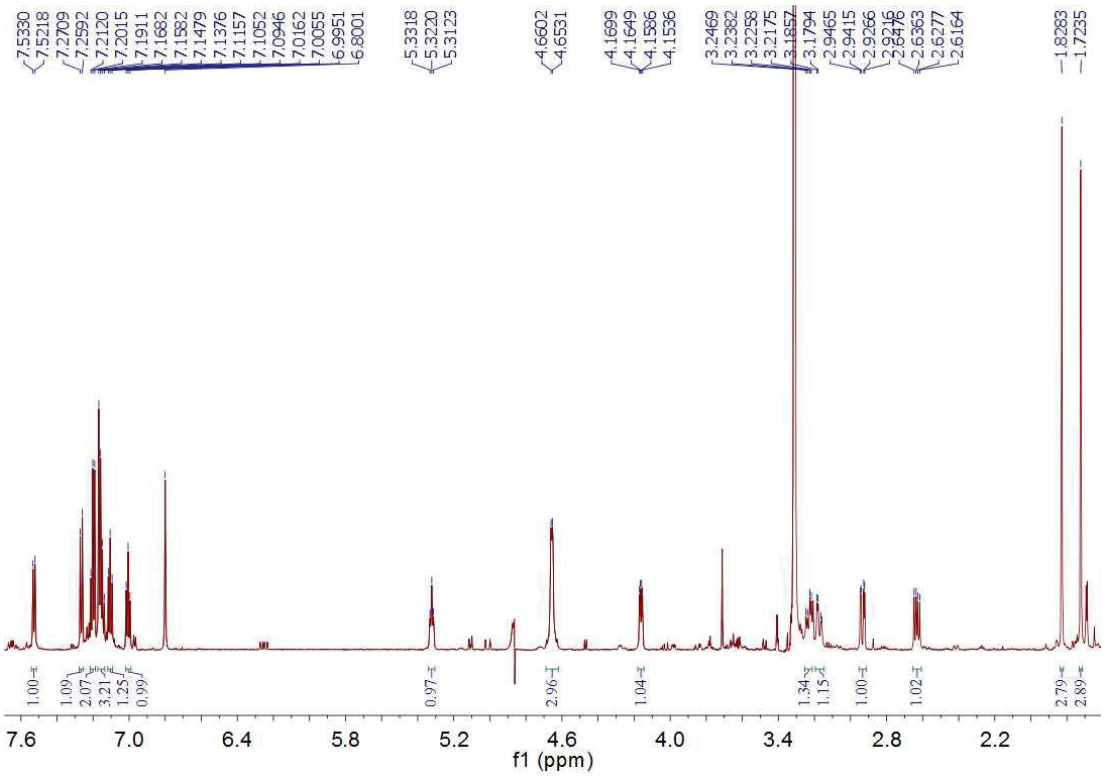

Figure S38. ^{1}H NMR (700 MHz, methanol-d_4) spectrum of **6**

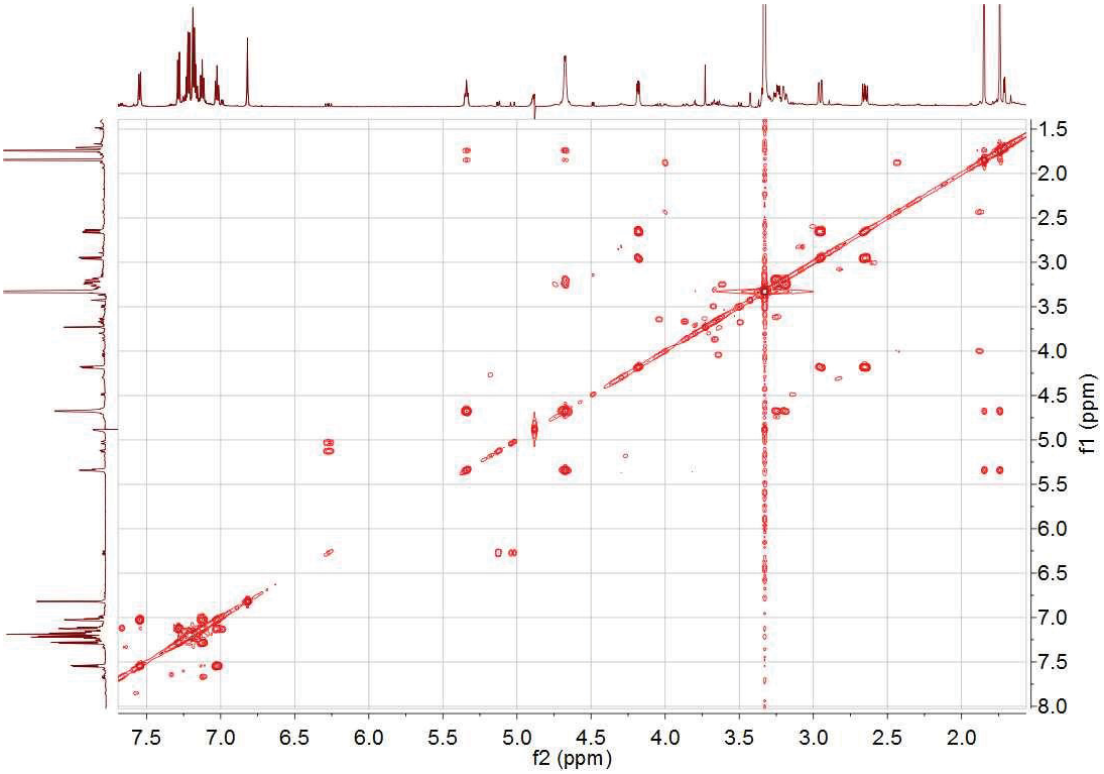

Figure S39. ^{1}H-^{1}H COSY (700 MHz, methanol-d_4) spectrum of **6**

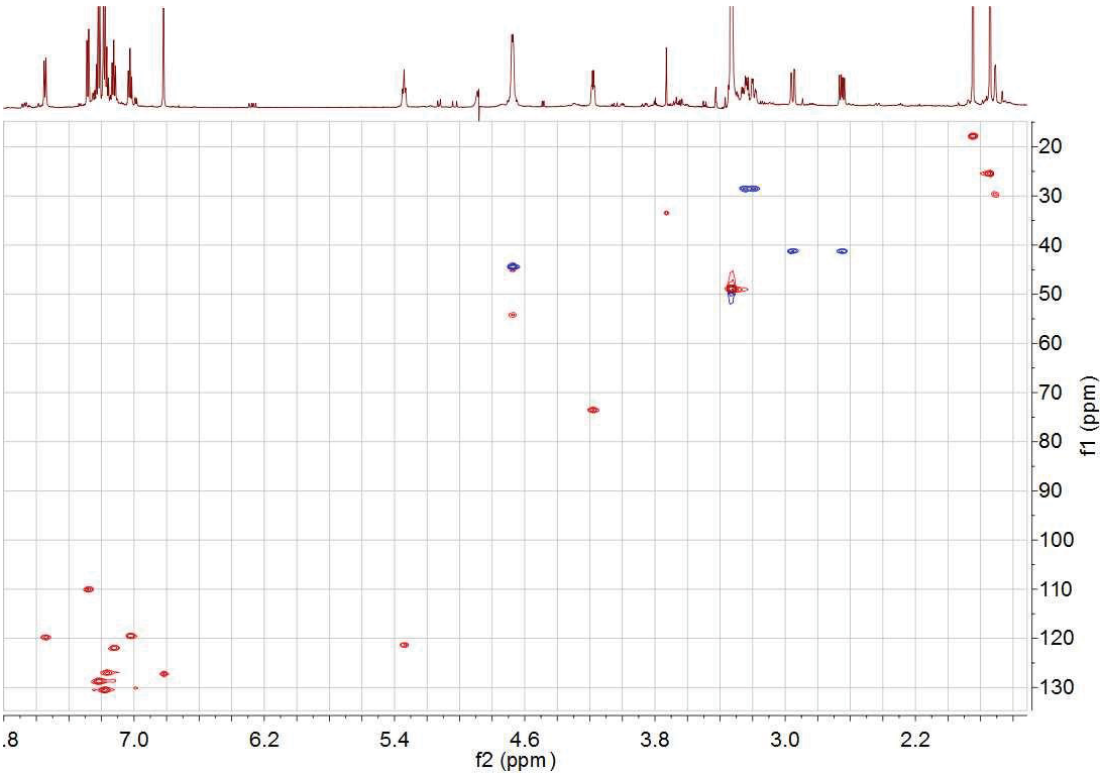

Figure S40. HSQC (700 and 175 MHz, methanol-d_4) spectrum of **6**

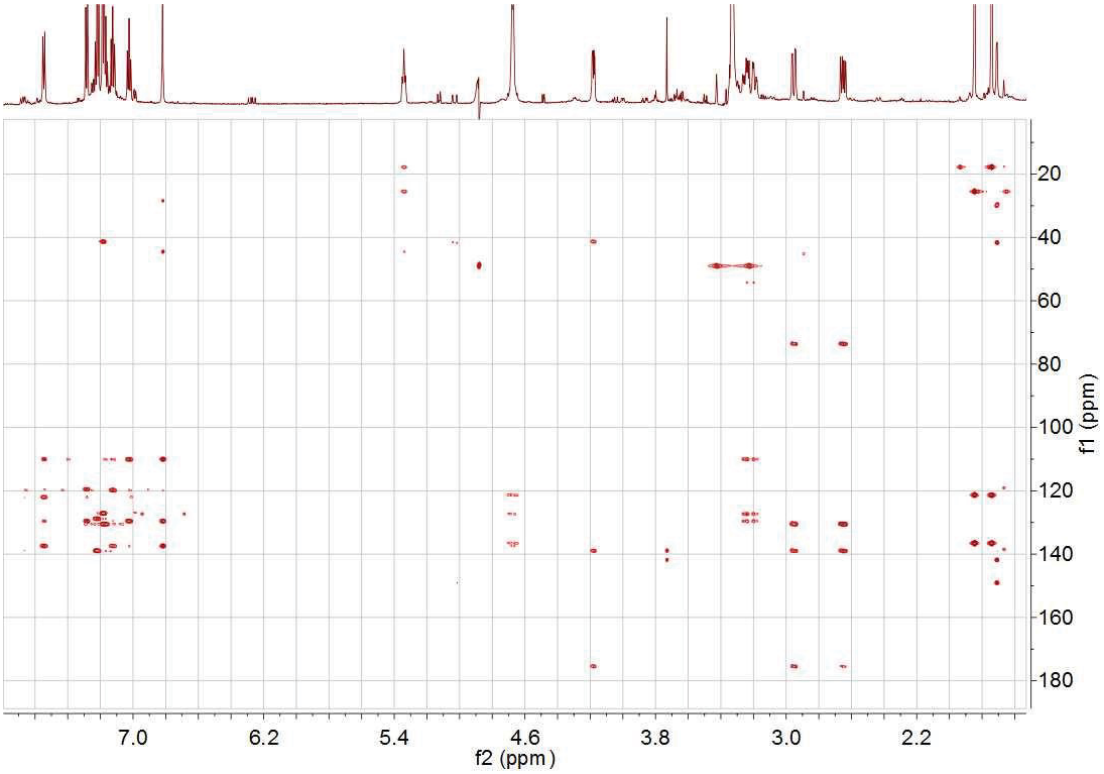

Figure S41. HMBC (700 and 175 MHz, methanol-d_4) spectrum of **6**

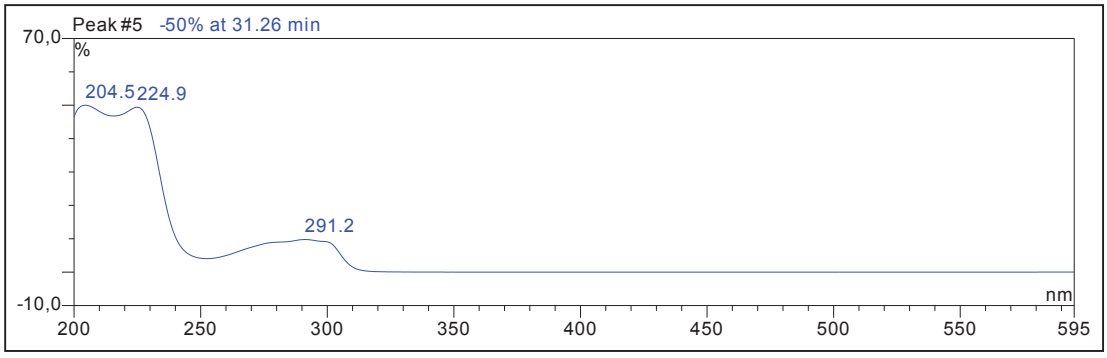

Figure S42. UV spectrum of **7**

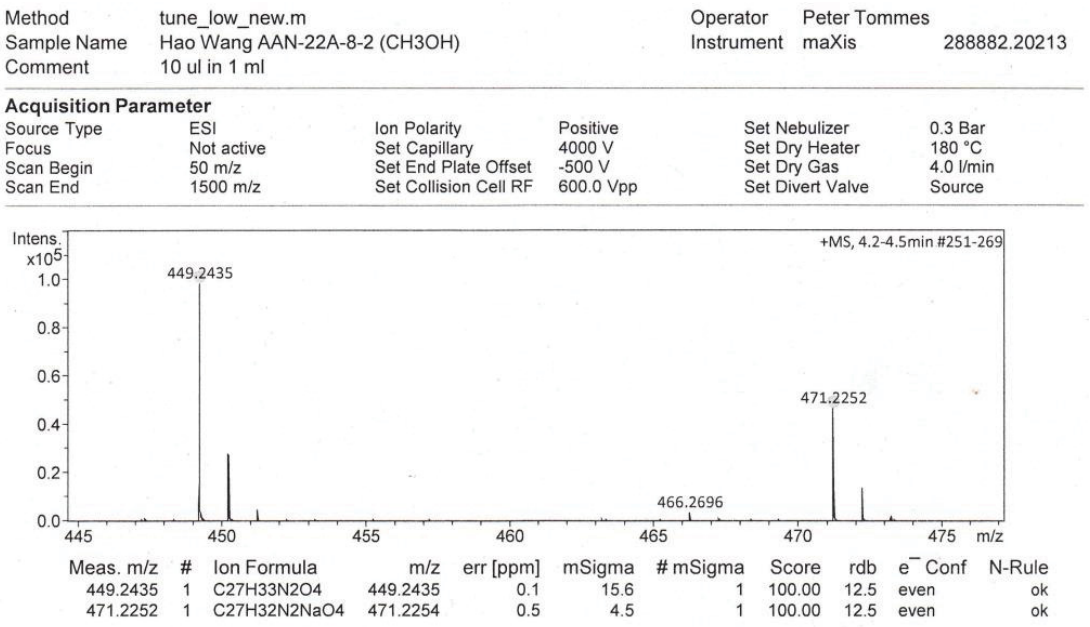

Figure S43. HRESIMS of **7**

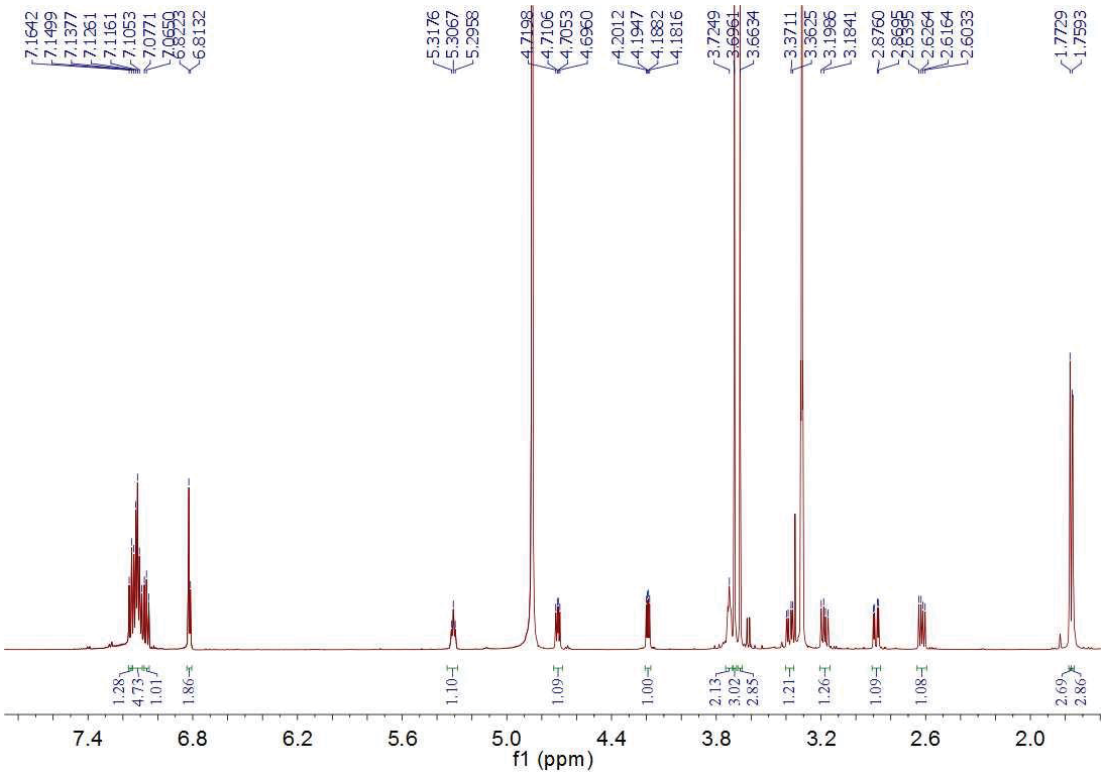

Figure S44. ^{1}H NMR (600 MHz, methanol-d_4) spectrum of **7**

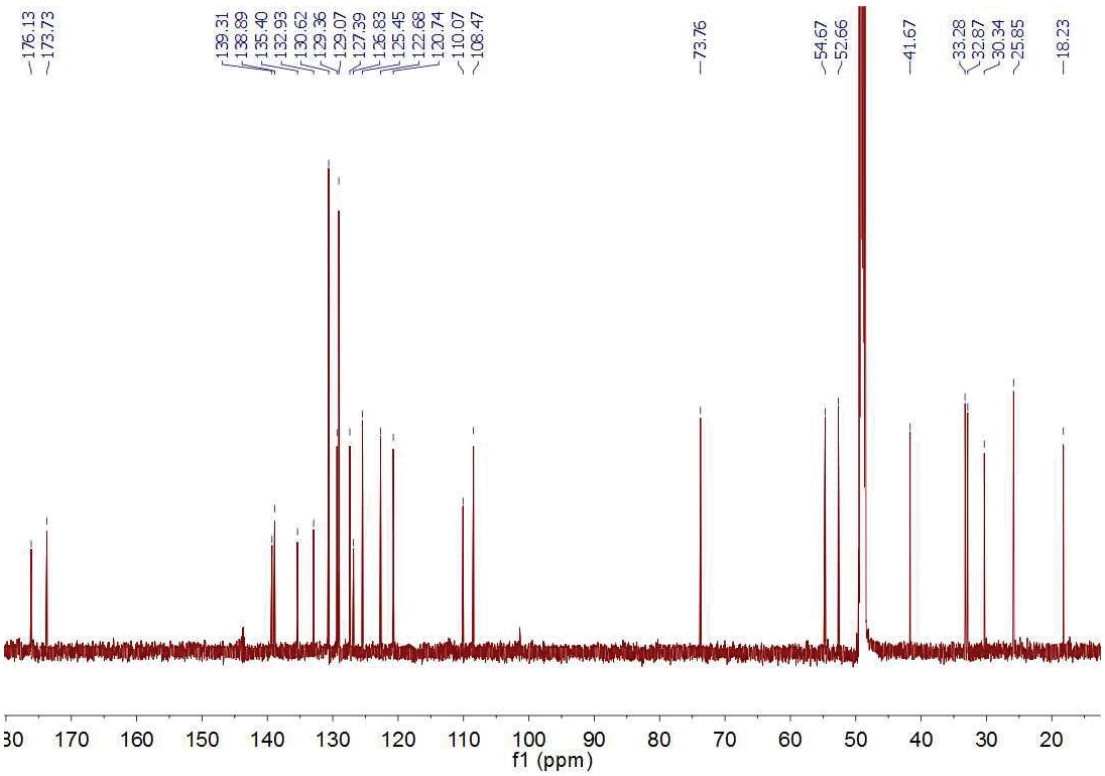

Figure S45. ^{13}C NMR (150 MHz, methanol-d_4) spectrum of **7**

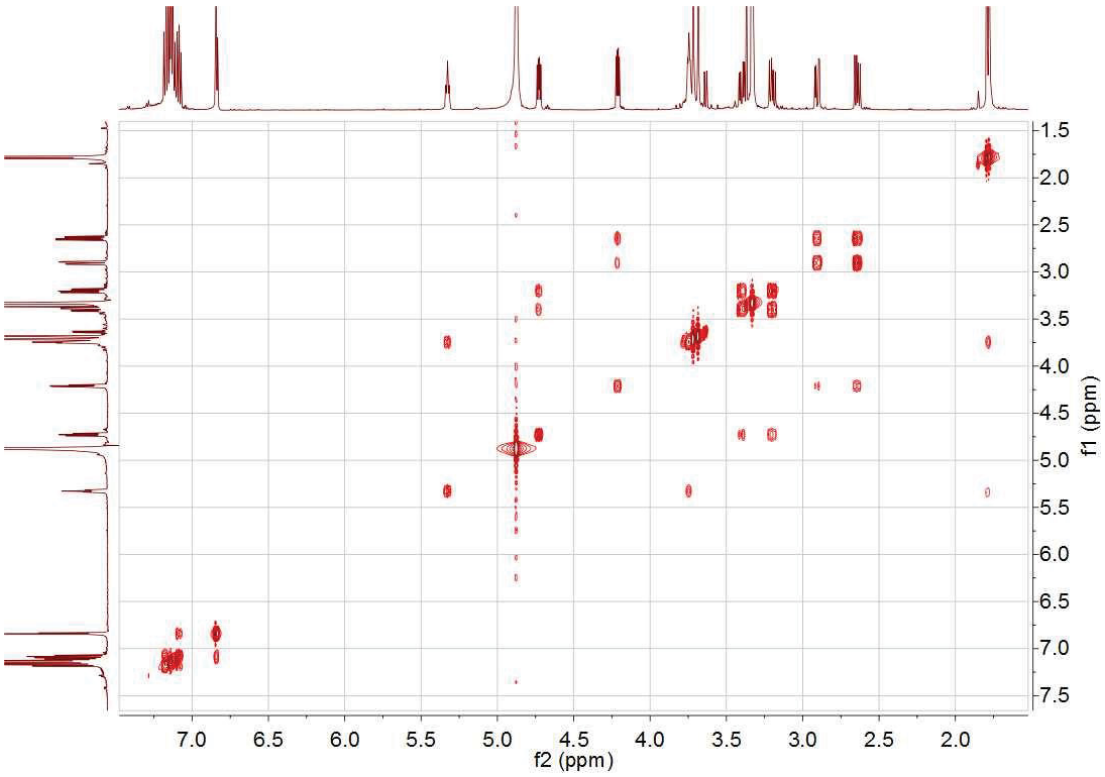

Figure S46. ^{1}H-^{1}H COSY (600 MHz, methanol-d_4) spectrum of **7**

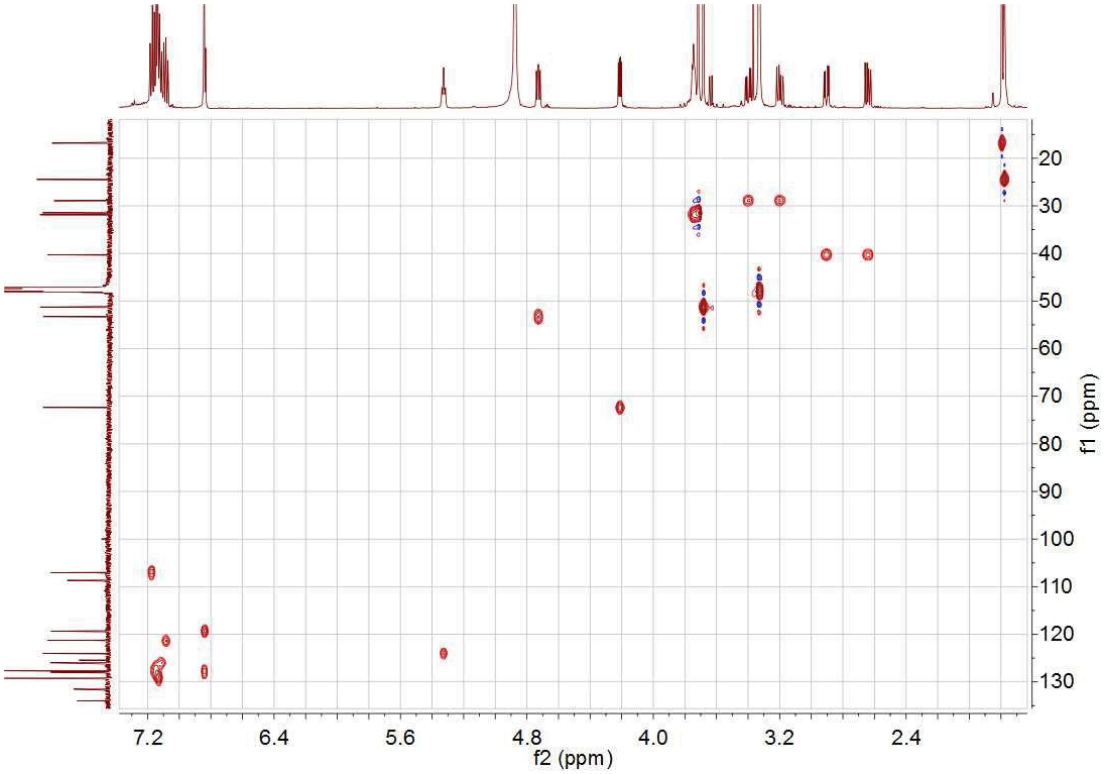

Figure S47. HSQC (600 and 150 MHz, methanol-d_4) spectrum of **7**

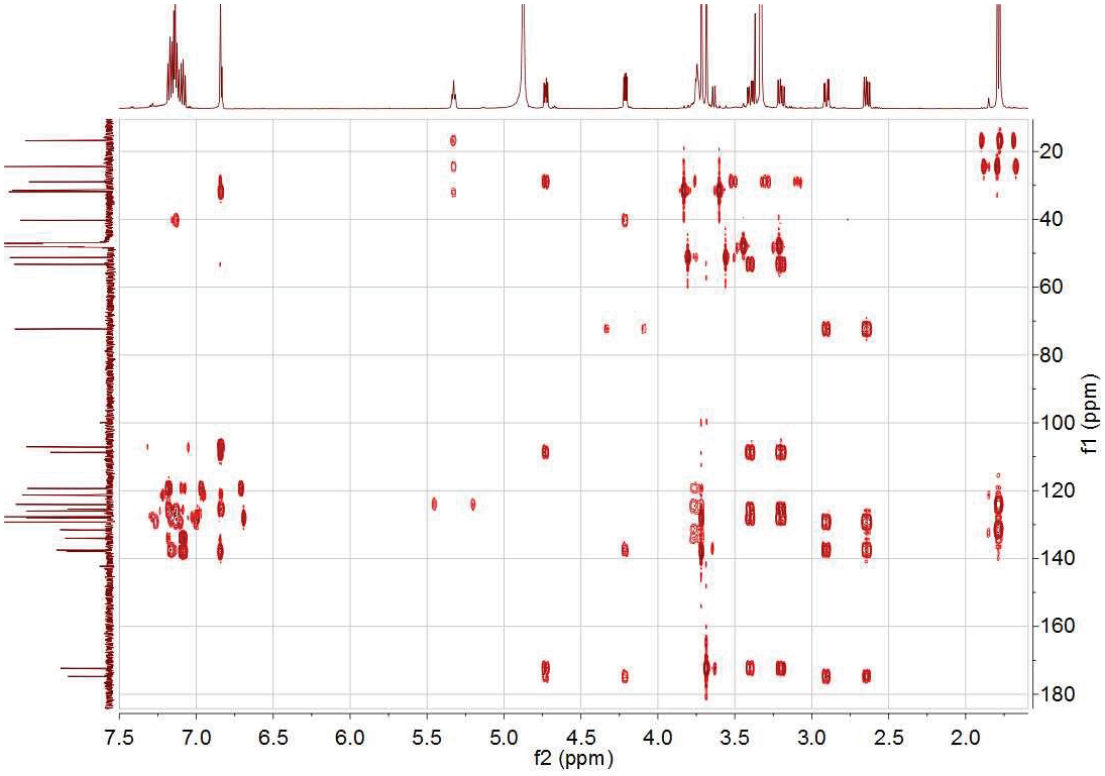

Figure S48. HMBC (600 and 150 MHz, methanol-d_4) spectrum of **7**

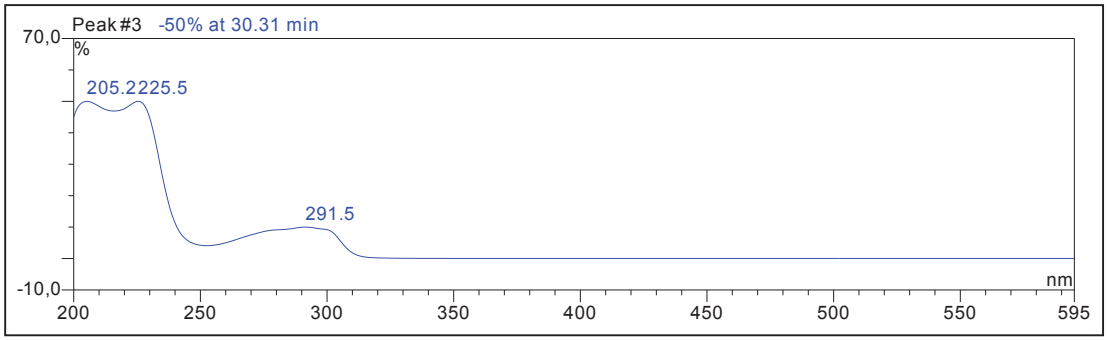

Figure S49. UV spectrum of **8**

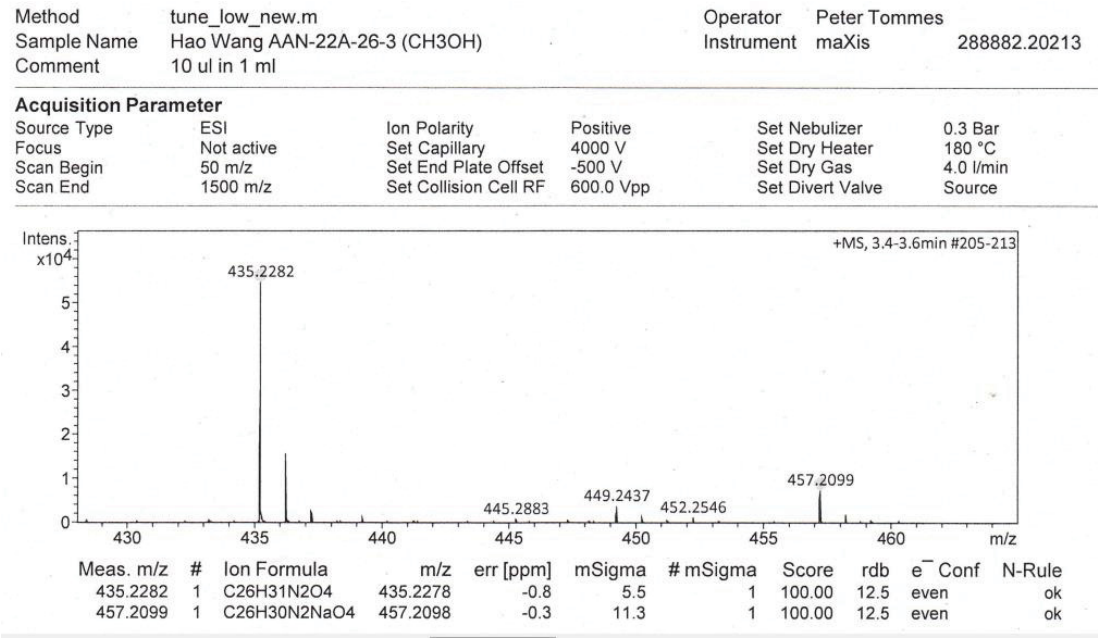

Figure S50. HRESIMS of **8**

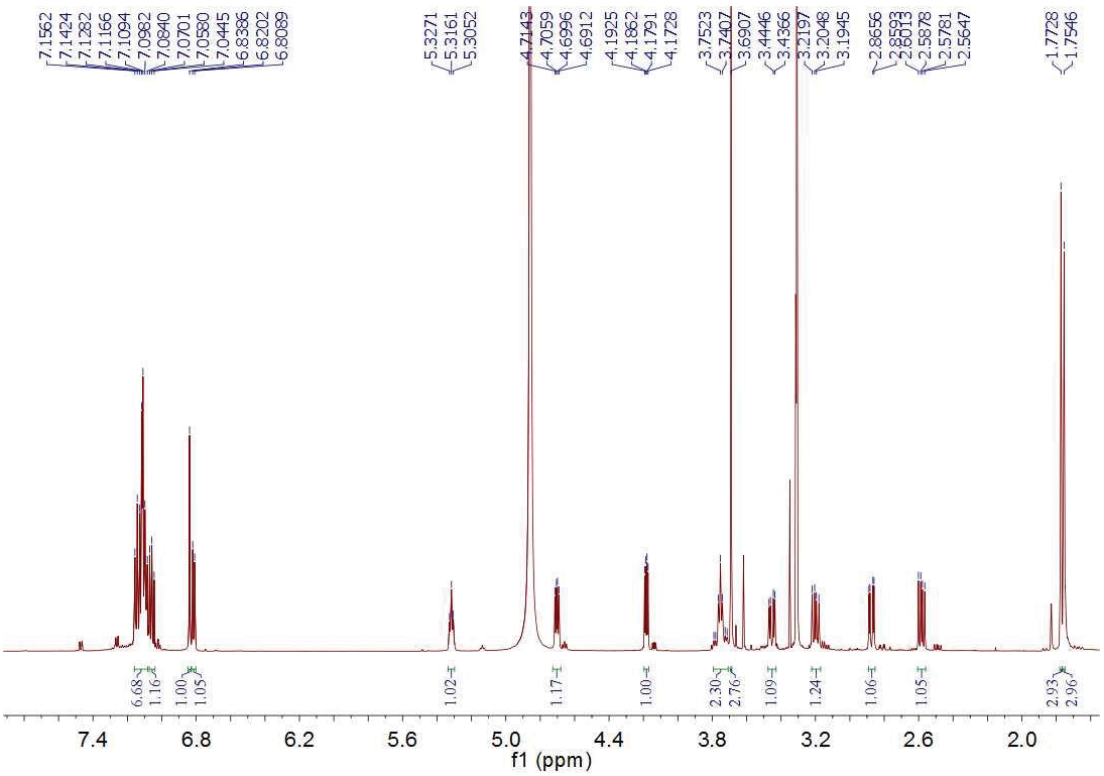

Figure S51. ^{1}H NMR (600 MHz, methanol-d_4) spectrum of **8**

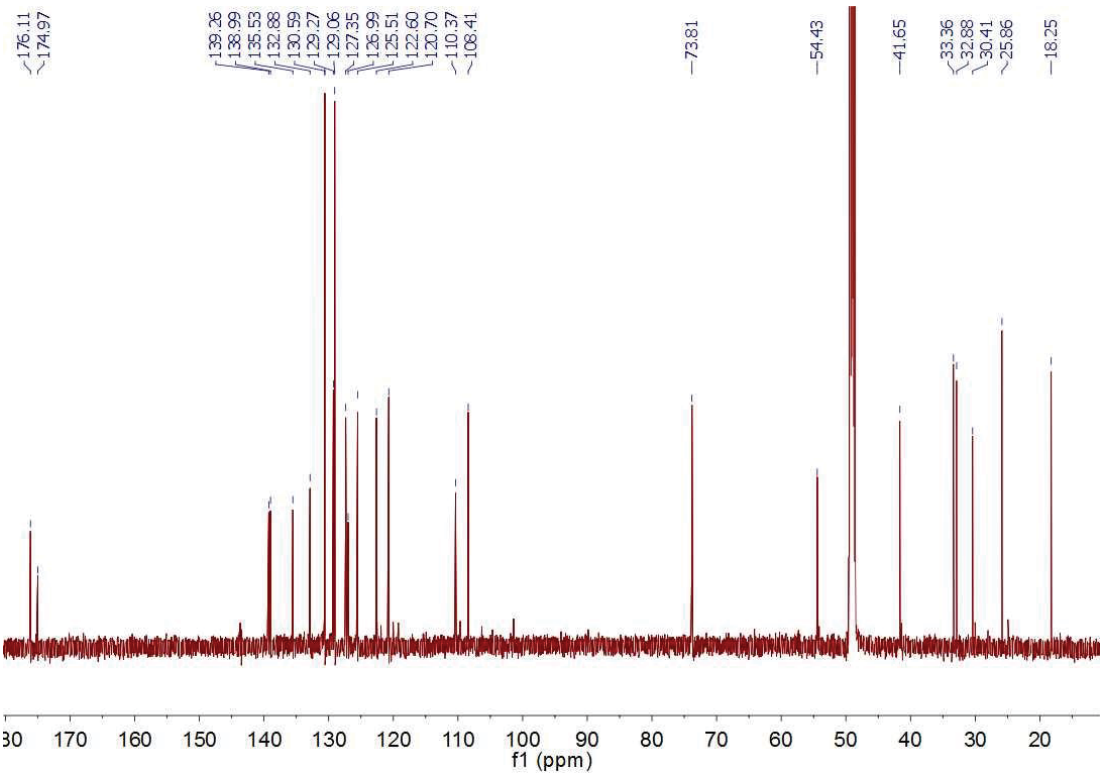

Figure S52. ^{13}C NMR (150 MHz, methanol-d_4) spectrum of **8**

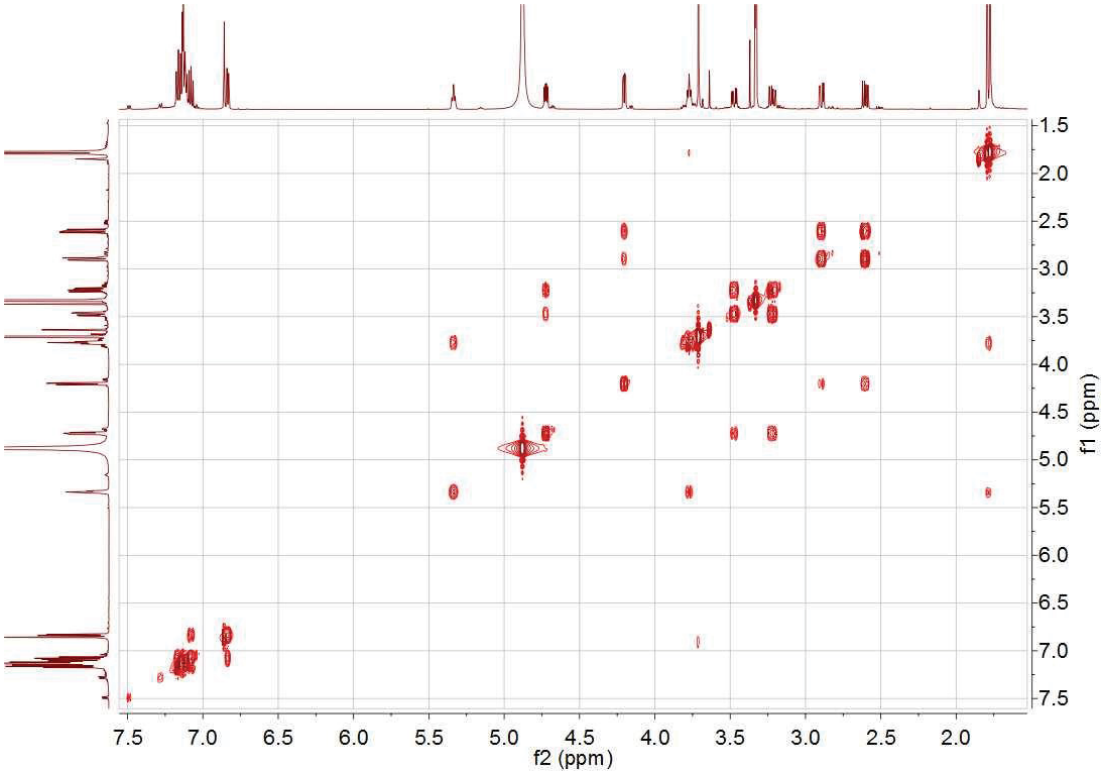

Figure S53. ^{1}H-^{1}H COSY (600 MHz, methanol-d_4) spectrum of **8**

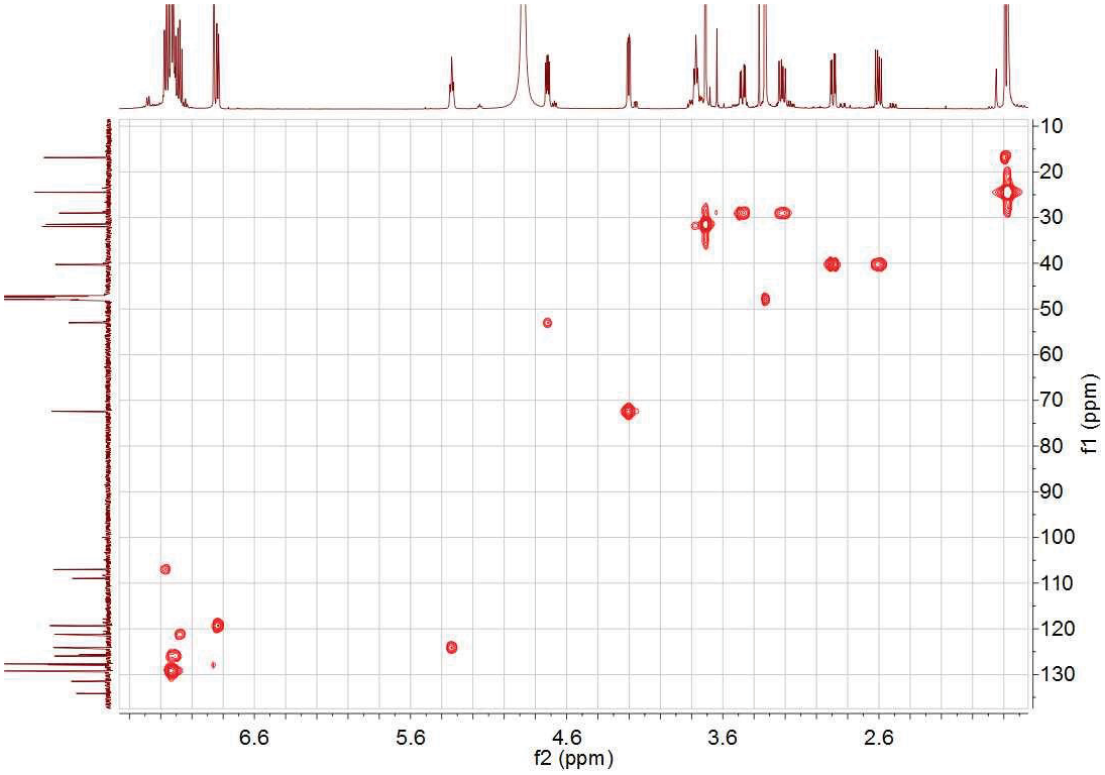

Figure S54. HSQC (600 and 150 MHz, methanol-d_4) spectrum of **8**

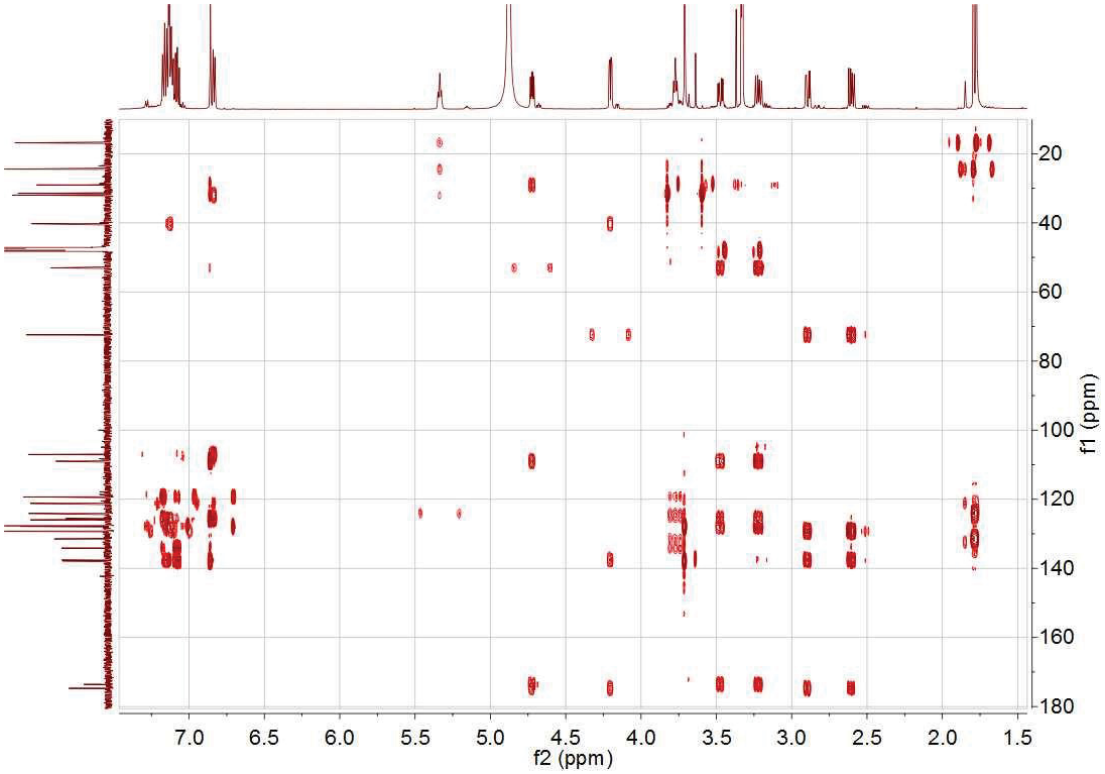

Figure S55. HMBC (600 and 150 MHz, methanol-d_4) spectrum of **8**

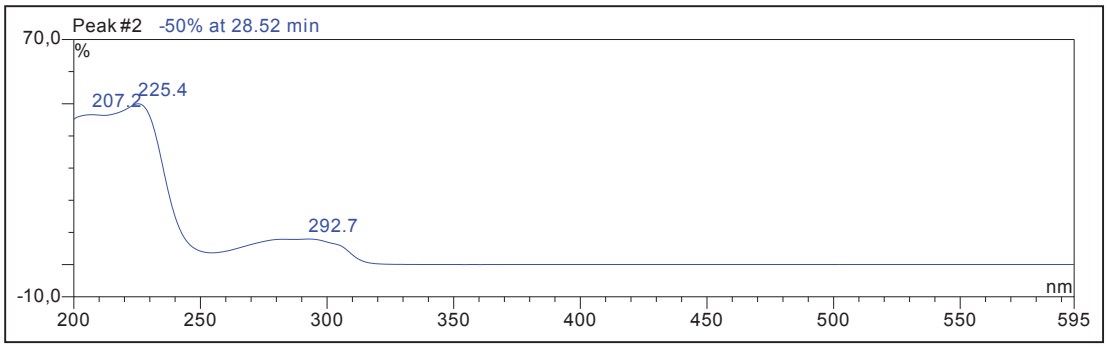

Figure S56. UV spectrum of **9**

Sample Name	Hao Wang AAN-22A-37-2 (CH3OH)	Instrument	maXis 288882.20213
Comment	10 ul in 1 ml		

Acquisition Parameter

Source Type	ESI	Ion Polarity	Positive	Set Nebulizer	0.3 Bar
Focus	Not active	Set Capillary	4000 V	Set Dry Heater	180 °C
Scan Begin	50 m/z	Set End Plate Offset	-500 V	Set Dry Gas	4.0 l/min
Scan End	1500 m/z	Set Collision Cell RF	600.0 Vpp	Set Divert Valve	Source

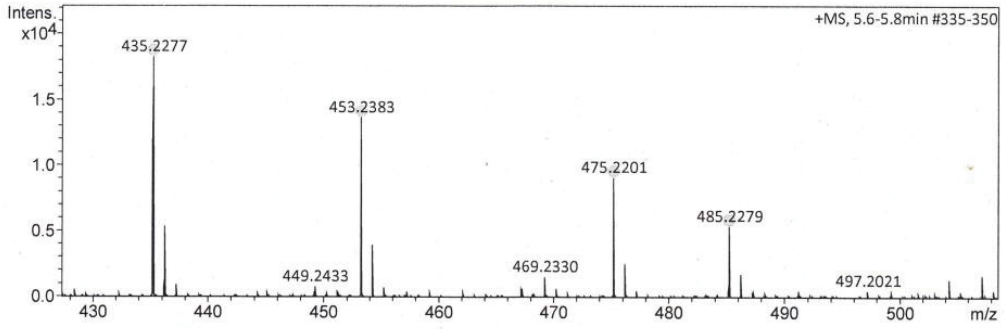

Meas. m/z	#	Ion Formula	m/z	err [ppm]	mSigma	# mSigma	Score	rdb	e¯ Conf	N-Rule
435.2277	1	C26H31N2O4	435.2278	0.3	1.9	1	100.00	12.5	even	ok
453.2383	1	C26H33N2O5	453.2384	0.2	3.5	1	100.00	11.5	even	ok
475.2201	1	C26H32N2NaO5	475.2203	0.5	8.3	1	100.00	11.5	even	ok
485.2279	1	C26H33N2O7	485.2282	0.7	11.9	1	100.00	11.5	even	ok
	2	C25H30N6NaO3	485.2272	-1.5	13.2	2	59.73	13.5	even	ok

Figure S57. HRESIMS of **9**

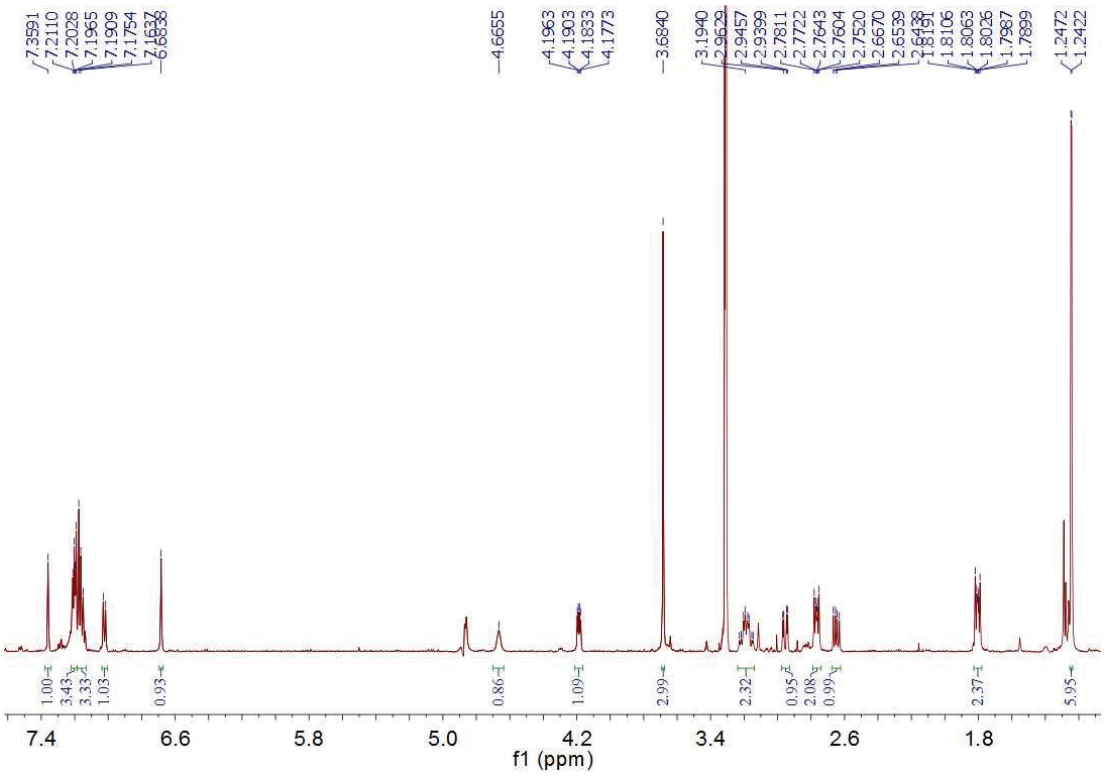

Figure S58. ^{1}H NMR (700 MHz, methanol-d_4) spectrum of **9**

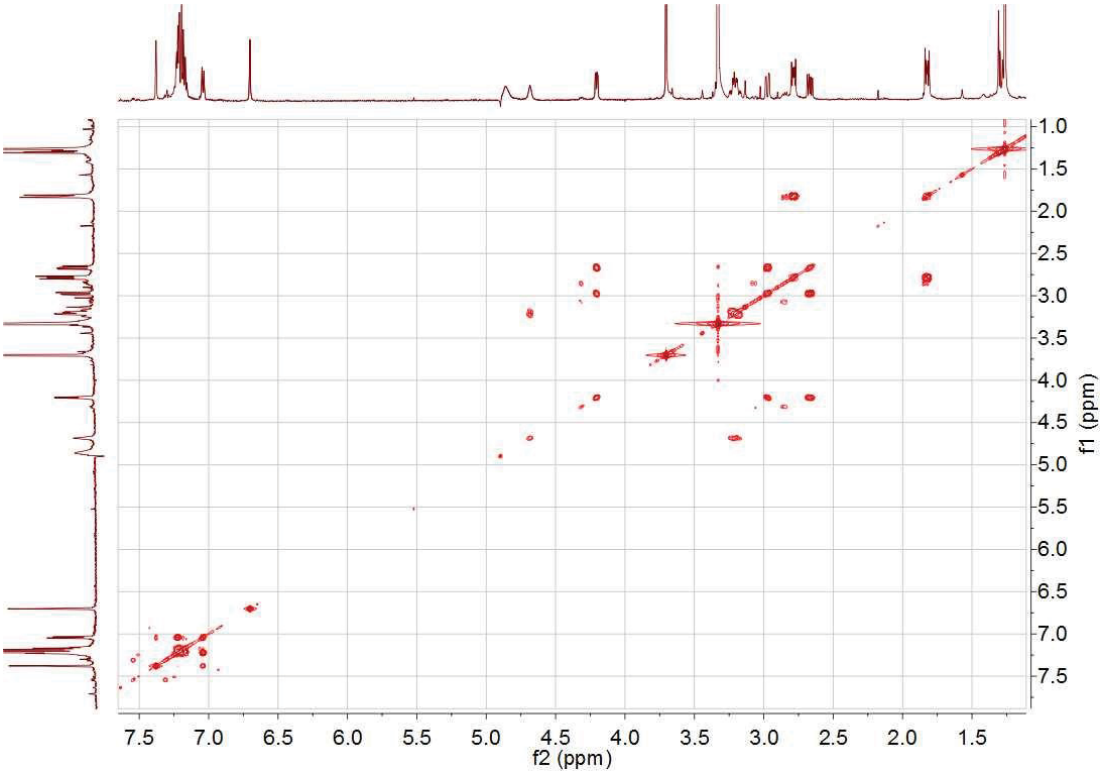

Figure S59. ^{1}H-^{1}H COSY (600 MHz, methanol-d_4) spectrum of **9**

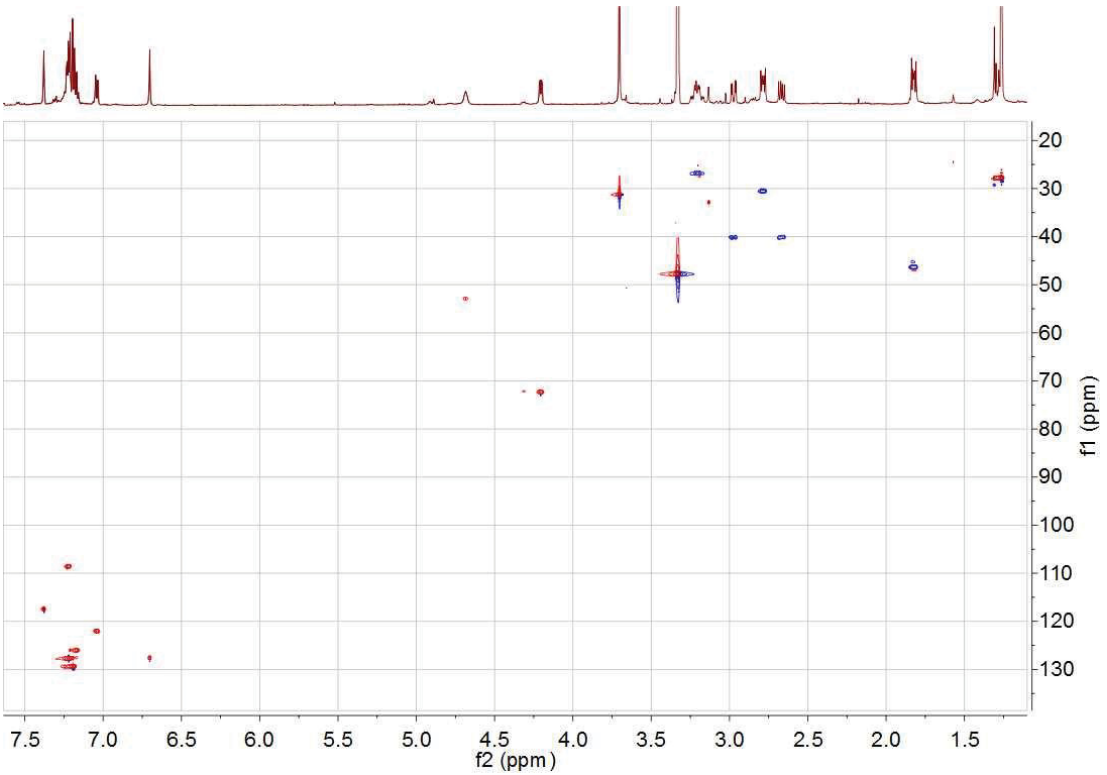

Figure S60. HSQC (700 and 175 MHz, methanol-d_4) spectrum of **9**

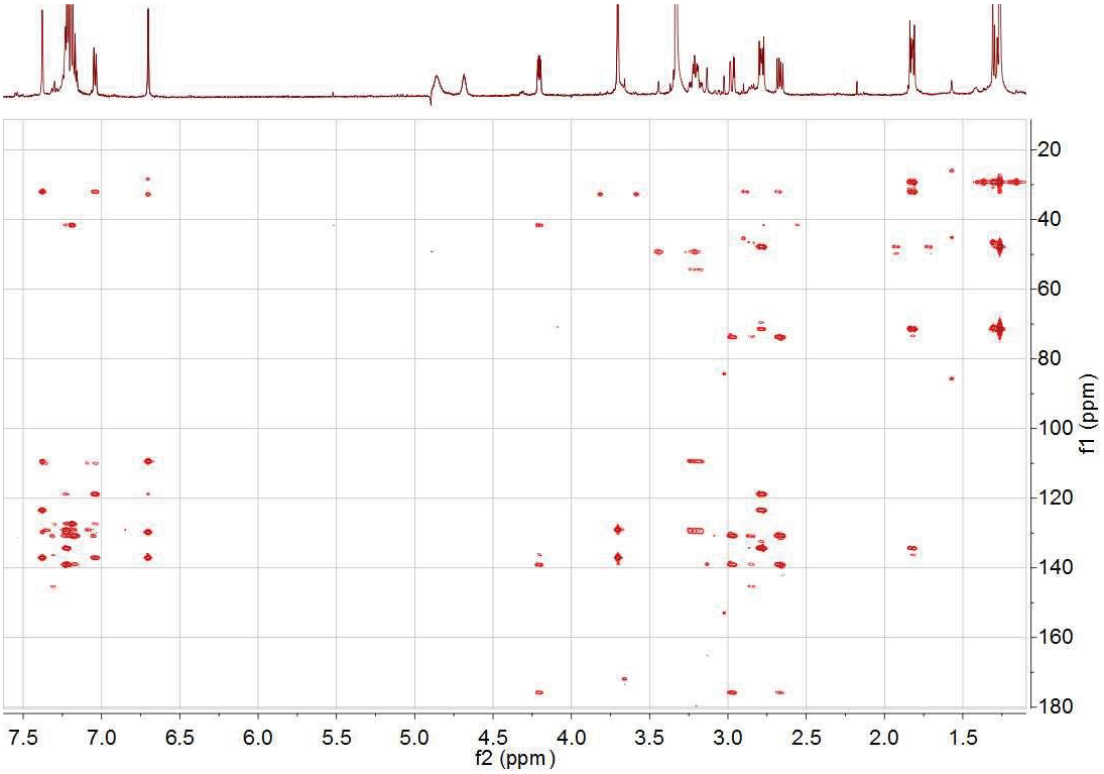

Figure S61. HMBC (700 and 175 MHz, methanol-d_4) spectrum of **9**

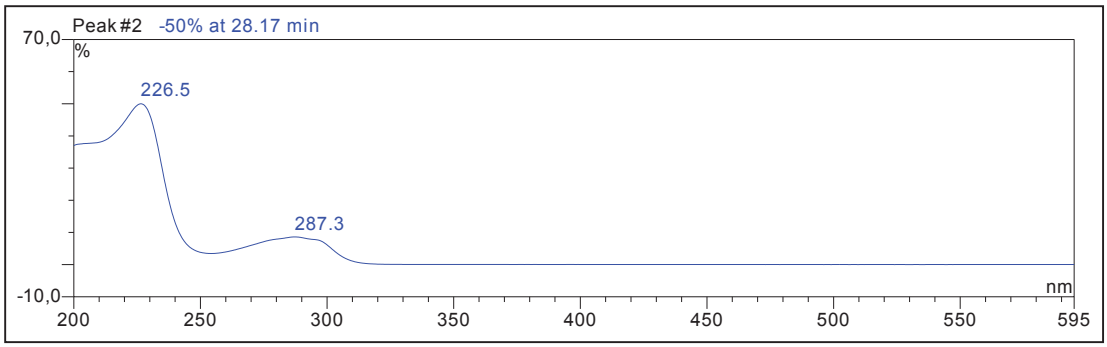

Figure S62. UV spectrum of **10**

Sample Name	Hao Wang AAN-22A-37-1 (CH3OH)	Instrument maXis	288882.20213
Comment	10 ul in 1 ml		

Acquisition Parameter

Source Type	ESI	Ion Polarity	Positive	Set Nebulizer	0.3 Bar
Focus	Not active	Set Capillary	4000 V	Set Dry Heater	180 °C
Scan Begin	50 m/z	Set End Plate Offset	-500 V	Set Dry Gas	4.0 l/min
Scan End	1500 m/z	Set Collision Cell RF	600.0 Vpp	Set Divert Valve	Source

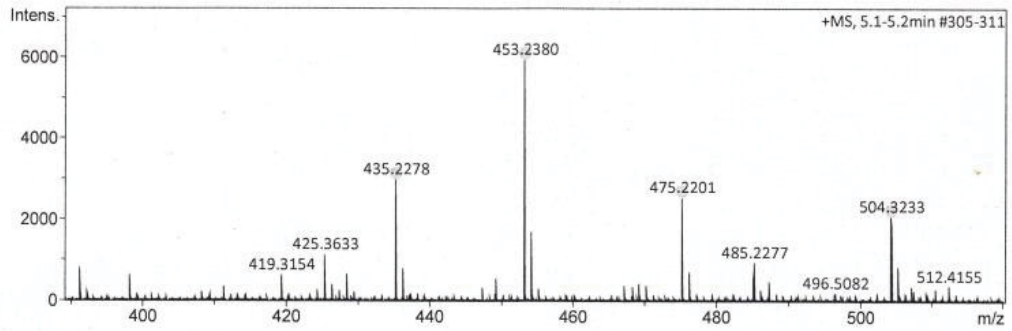

Meas. m/z	#	Ion Formula	m/z	err [ppm]	mSigma	# mSigma	Score	rdb	e¯ Conf	N-Rule
435.2278	1	C26H31N2O4	435.2278	0.2	13.9	1	100.00	12.5	even	ok
453.2380	1	C26H33N2O5	453.2384	0.8	4.7	1	100.00	11.5	even	ok
	2	C25H30N6NaO	453.2373	-1.5	7.2	2	61.27	13.5	even	ok
475.2201	1	C26H32N2NaO5	475.2203	0.6	9.3	1	100.00	11.5	even	ok
	2	C24H27N8O3	475.2201	0.0	12.0	2	80.38	15.5	even	ok
504.3233	1	C34H43NNaO	504.3237	0.8	17.3	1	100.00	13.5	even	ok

Figure S63. HRESIMS of **10**

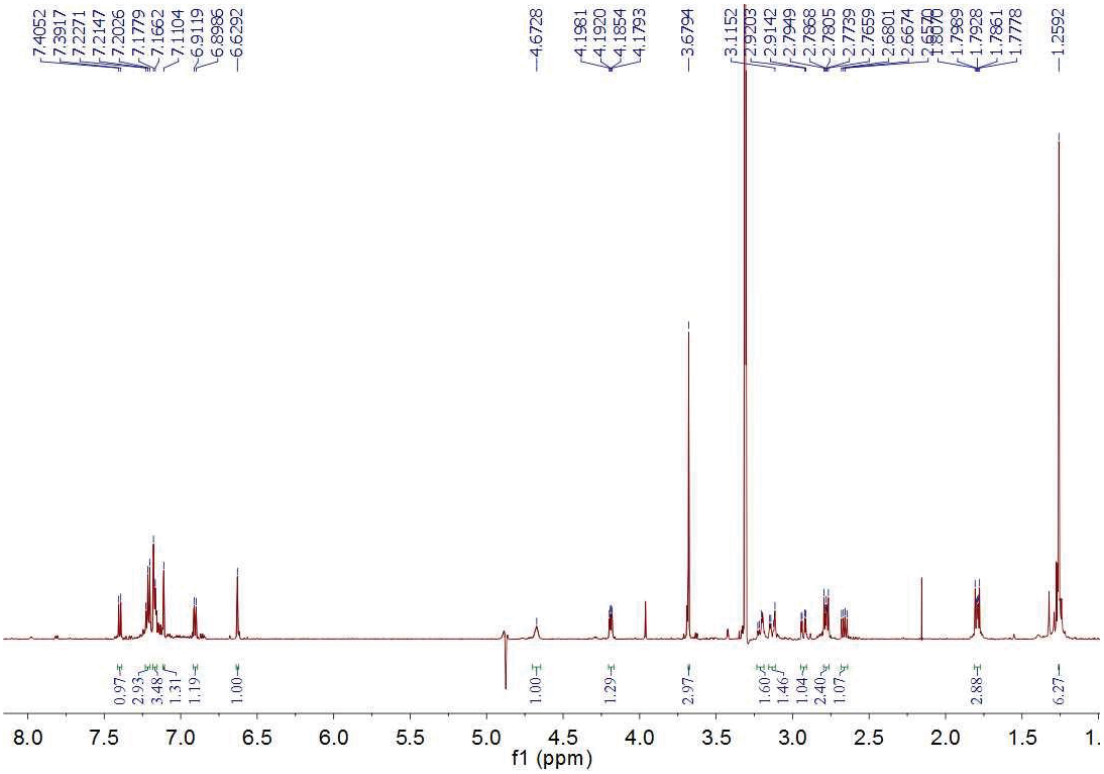

Figure S64. ^{1}H NMR (700 MHz, methanol-d_4) spectrum of **10**

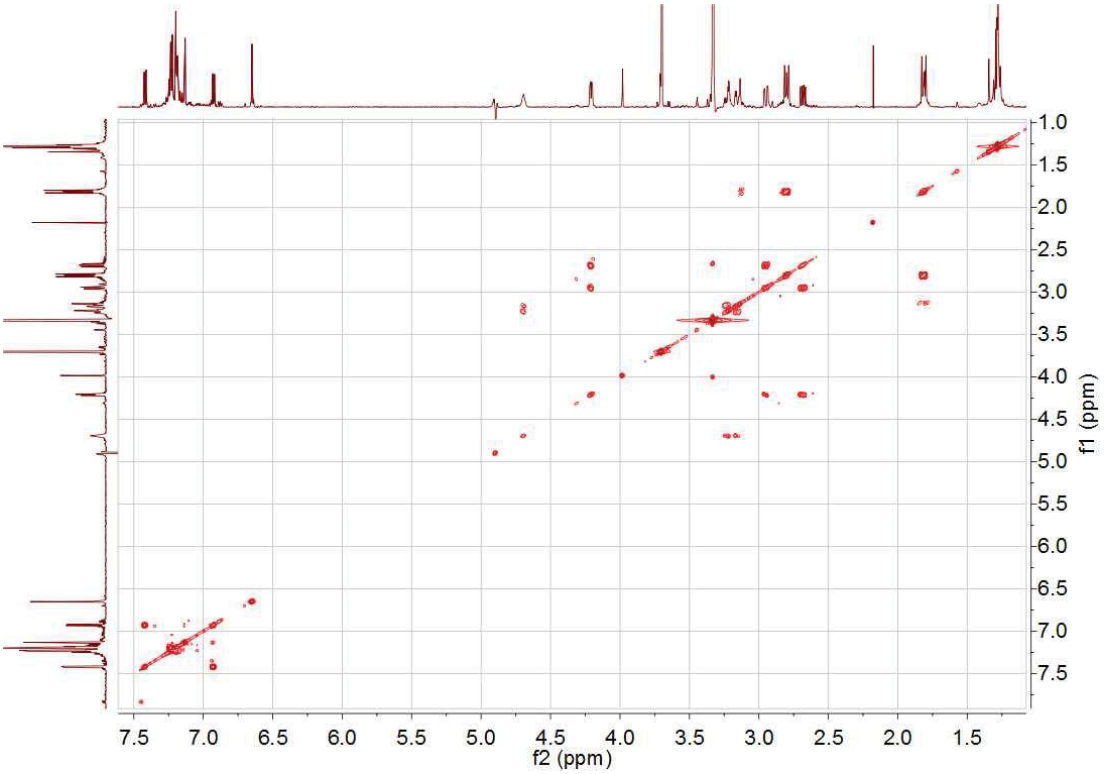

Figure S65. ^{1}H-^{1}H COSY (600 MHz, methanol-d_4) spectrum of **10**

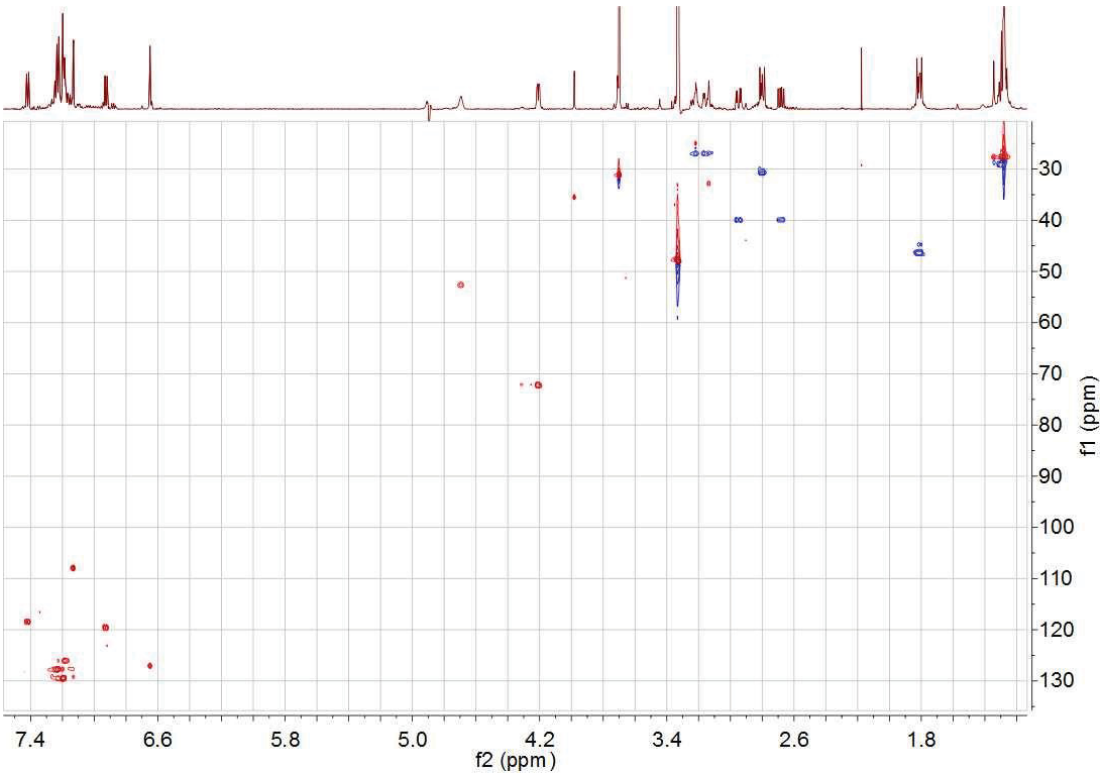

Figure S66. HSQC (700 and 175 MHz, methanol-d_4) spectrum of **10**

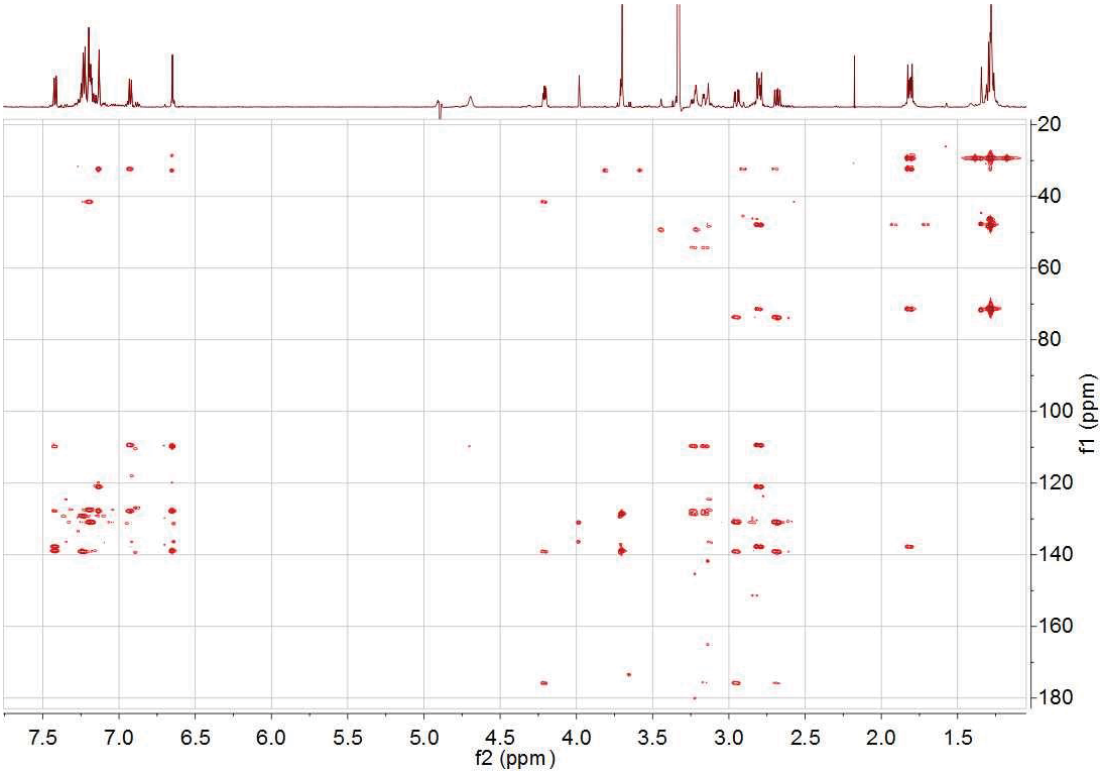

Figure S67. HMBC (700 and 175 MHz, methanol-d_4) spectrum of **10**

Results of X-ray analysis of compound 1

Due to very small crystal sizes and poor crystal quality of **1**, only a very low resolution was obtainable. Crystals of **1** did not diffract beyond q = 44.9° (cf. desired 67.7°) for Cu-Kα radiation, resulting in only 1538 total (1484 observed with $I > 2s(I)$) reflection versus 263 parameters for anisotropic refinement. Therefore the cif does not meet the requirements for publication. The relevance of the following reported analysis of **1** should not be overestimated and interpreted carefully.

Crystal data

$C_{22}H_{24}N_2O_4$	$Z = 4$
$M_r = 380.43$	$F(000) = 808$
Orthorhombic, $P2_12_12_1$	$D_x = 1.305$ Mg m^{-3}
$a = 5.9832$ (4) Å	Cu $K\alpha$ radiation, $\lambda = 1.54178$ Å
$b = 11.8099$ (7) Å	$\mu = 0.73$ mm^{-1}
$c = 27.4081$ (17) Å	$T = 140$ K
$V = 1936.7$ (2) Å^3	0.12 × 0.03 × 0.03 mm^3

Data collection

16751 measured reflections	$\theta_{max} = 44.9°$, $\theta_{min} = 3.2°$

1538 independent reflections	h = -5→5
1484 reflections with $I > 2\sigma(I)$	k = -10→10
R_{int} = 0.051	l = -25→24

Refinement

Refinement on F^2	Hydrogen site location: mixed
Least-squares matrix: full	H atoms treated by a mixture of independent and constrained refinement
$R[F^2 > 2\sigma(F^2)]$ = 0.022	$w = 1/[\sigma^2(F_o^2) + (0.0353P)^2]$ where $P = (F_o^2 + 2F_c^2)/3$
$wR(F^2)$ = 0.053	$(\Delta/\sigma)_{max}$ = 0.109
S = 1.12	$\Delta\rangle_{max}$ = 0.002 e Å^{-3}
1538 reflections	$\Delta\rangle_{min}$ = -0.001 e Å^{-3}
263 parameters	Absolute structure: Flack x determined using 561 quotients [(I+)-(I-)]/[(I+)+(I-)] (Parsons, Flack and Wagner, ActaCryst. B69 (2013) 249-259).
0 restraints	Absolute structure parameter: -0.14 (10)

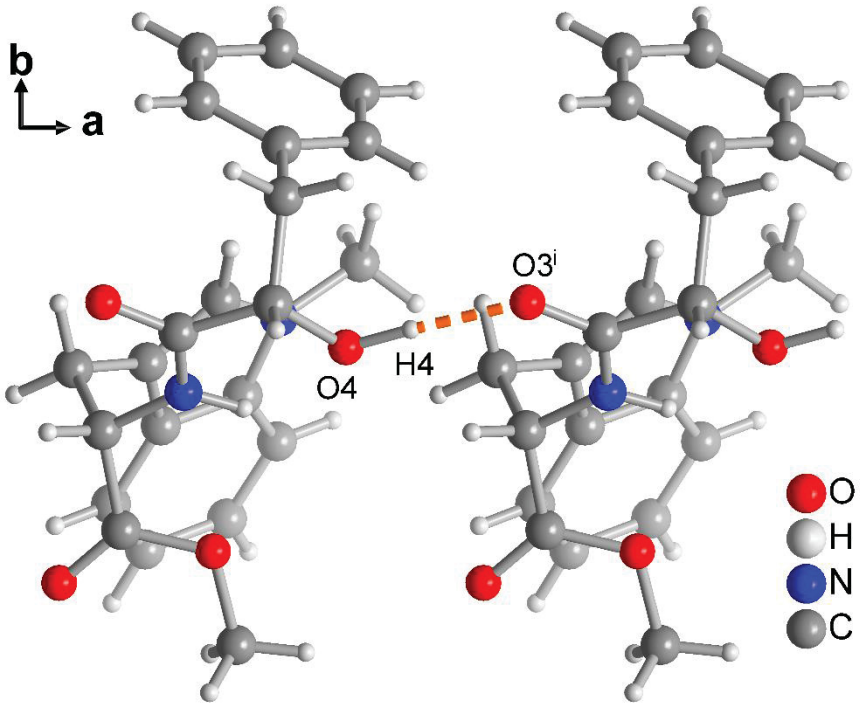

Figure S68. Section of the packing diagram of **1** showing the intermolecular H-bond (orange dashed line), which connects two symmetry equivalent molecules. Details for intermolecular H-bond:O4-H41.00 Å, H4···O3^{i}1.72 Å, O4···O3^{i}2.71 Å, O4-H4···O3^{i} 171 °, Symmetry code: (i) 1+x, y, z.

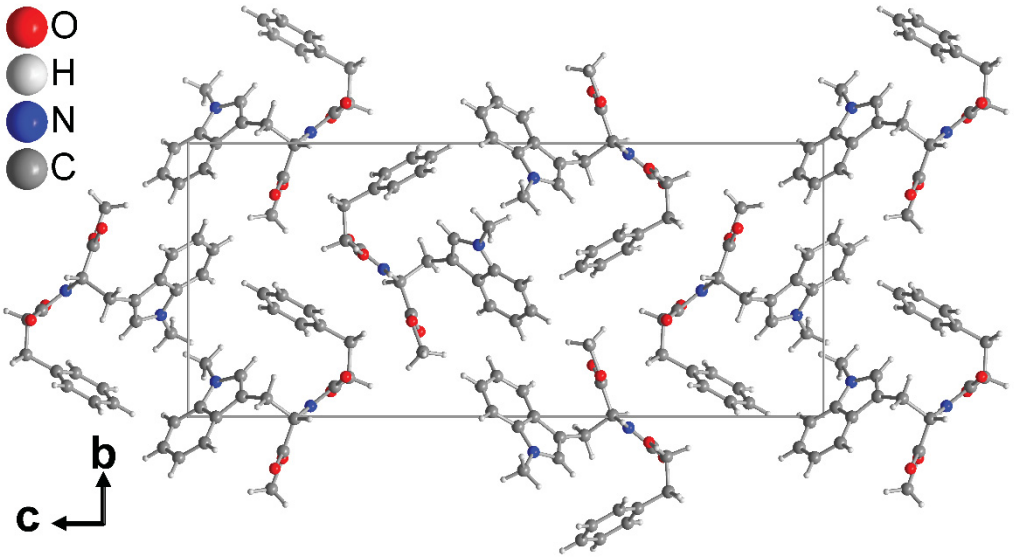

Figure S69. Section of the packing diagram of **1** along the *a*-plane.

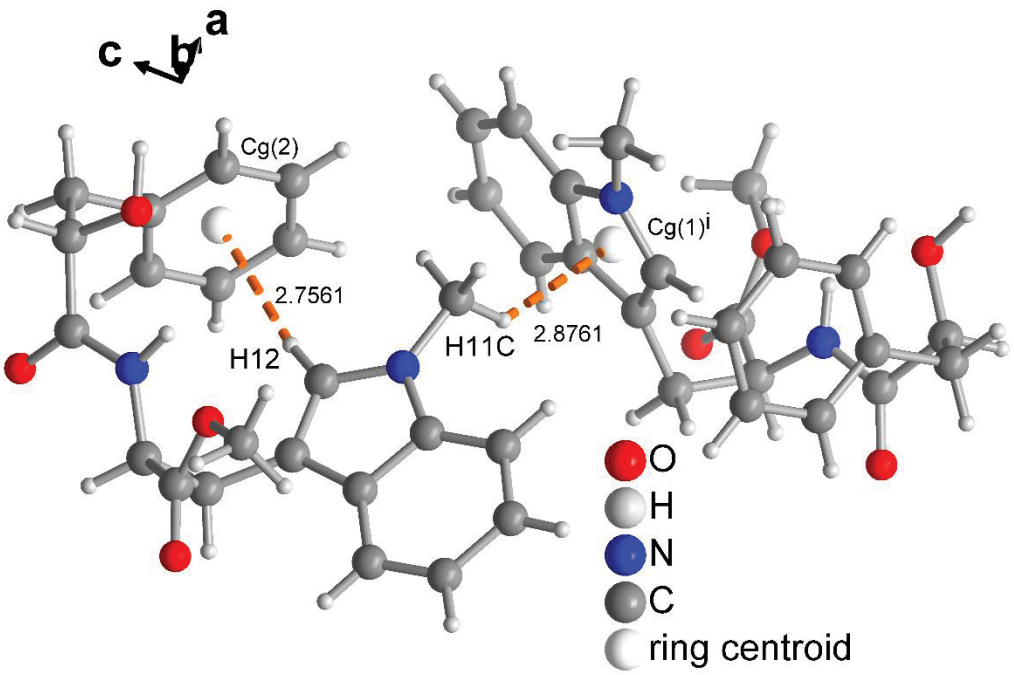

Figure S70. Section of the packing diagram of **1** showing short C-H···π distances (orange dashed lines), Symmetry code: (i) 1/2+x, 3/2–y, 1–z.

Fractional atomic coordinates and isotropic or equivalent isotropic displacement parameters (Å^2) for **1**

	x	*y*	*z*	U_{iso}*/U_{eq}
O1	0.7399 (4)	0.34906 (17)	0.64836 (7)	0.0909 (11)
O2	0.3774 (4)	0.31137 (19)	0.63605 (7)	0.0945 (11)
O3	0.4813 (4)	0.64653 (17)	0.74768 (8)	0.0954 (11)
O4	1.0531 (4)	0.59272 (17)	0.72463 (7)	0.0919 (11)
H4	1.206 (7)	0.614 (3)	0.7363 (12)	0.138*
N1	0.8953 (4)	0.6281 (2)	0.54317 (10)	0.0904 (11)
N2	0.6705 (4)	0.5395 (2)	0.69261 (10)	0.0829 (12)
C1	0.5235 (7)	0.3746 (3)	0.64940 (10)	0.0836 (12)
C1'	0.6583 (6)	0.6107 (3)	0.73038 (12)	0.0816 (12)
C2	0.4785 (5)	0.4938 (2)	0.66719 (10)	0.0836 (12)
H2A	0.349909	0.491273	0.690481	0.100*
C2'	0.8812 (5)	0.6445 (2)	0.75231 (11)	0.0868 (12)
H2'	0.888295	0.613592	0.786246	0.104*
C3	0.4106 (5)	0.5676 (2)	0.62314 (10)	0.0872 (12)
H3A	0.272345	0.536166	0.608656	0.105*
H3B	0.376498	0.644986	0.634843	0.105*
C3'	0.9070 (6)	0.7730 (2)	0.75521 (11)	0.0902 (12)
H3'A	0.785967	0.803460	0.776048	0.108*
H3'B	1.050747	0.790365	0.771485	0.108*
C4	0.5855 (5)	0.5748 (3)	0.58442 (11)	0.0835 (12)
C4'	0.9013 (6)	0.8338 (2)	0.70702 (11)	0.0875 (12)
C5	0.6170 (6)	0.4994 (3)	0.54359 (11)	0.0840 (12)
C5'	0.7087 (6)	0.8873 (3)	0.69095 (15)	0.0965 (13)
H5'	0.577497	0.884189	0.710434	0.116*
C6	0.4996 (6)	0.4054 (3)	0.52583 (12)	0.0917 (12)
H6	0.367778	0.379614	0.541631	0.110*
C6'	0.7037 (7)	0.9451 (3)	0.64715 (17)	0.1066 (14)
H6'	0.570499	0.981659	0.636781	0.128*
C7	0.5797 (7)	0.3513 (3)	0.48497 (13)	0.0979 (13)
H7	0.501918	0.287306	0.472672	0.118*

C7'	0.8941 (9)	0.9495 (3)	0.61842 (13)	0.1069 (13)
H7'	0.891743	0.988855	0.588197	0.128*
C8	0.7730 (7)	0.3883 (3)	0.46108 (12)	0.1003 (13)
H8	0.823619	0.348991	0.432935	0.120*
C8'	1.0863 (7)	0.8967 (3)	0.63383 (14)	0.0998 (13)
H8'	1.217081	0.899732	0.614213	0.120*
C9	0.8907 (6)	0.4804 (3)	0.47759 (13)	0.0952 (12)
H9	1.021989	0.505636	0.461436	0.114*
C9'	1.0901 (6)	0.8393 (3)	0.67758 (14)	0.0928 (12)
H9'	1.223776	0.802880	0.687774	0.111*
C10	0.8101 (6)	0.5353 (3)	0.51892 (12)	0.0859 (12)
C11	1.0860 (5)	0.6943 (3)	0.52737 (12)	0.1017 (13)
H11A	1.217021	0.645014	0.524475	0.153*
H11B	1.116301	0.753975	0.551336	0.153*
H11C	1.053512	0.728786	0.495626	0.153*
C12	0.7584 (6)	0.6502 (3)	0.58223 (12)	0.0876 (12)
H12	0.781007	0.710081	0.604827	0.105*
C13	0.7951 (5)	0.2372 (3)	0.63082 (12)	0.1049 (13)
H13A	0.733066	0.226758	0.598035	0.157*
H13B	0.731790	0.180286	0.652883	0.157*
H13C	0.957931	0.228532	0.629644	0.157*
H2	0.811 (6)	0.520 (3)	0.6831 (12)	0.126*

Atomic displacement parameters (Å^2) for **1.**

	U^{11}	U^{22}	U^{33}	U^{12}	U^{13}	U^{23}
O1	0.0855 (19)	0.0889 (17)	0.0982 (17)	0.0025 (11)	-0.0020 (11)	-0.0061 (12)
O2	0.0917 (19)	0.0958 (17)	0.0960 (16)	-0.0110 (12)	-0.0008 (12)	-0.0061 (11)
O3	0.0770 (18)	0.1059 (17)	0.1031 (16)	-0.0009 (12)	0.0050 (11)	-0.0147 (12)
O4	0.0755 (16)	0.0964 (16)	0.1039 (16)	0.0030 (11)	-0.0009 (12)	-0.0090 (10)
N1	0.085 (2)	0.095 (2)	0.091 (2)	-0.0040 (18)	0.0018 (17)	0.0051 (16)
N2	0.074 (2)	0.0886 (18)	0.0865 (19)	-0.0033 (14)	-0.0033 (16)	-0.0085 (16)
C1	0.081 (3)	0.092 (3)	0.079 (2)	-0.005 (2)	0.0023 (17)	0.0034 (18)
C1'	0.078 (3)	0.083 (2)	0.085 (2)	-0.0017 (19)	0.002 (2)	0.0008 (19)

C2	0.081 (2)	0.087 (2)	0.083 (2)	-0.0026 (17)	0.0012 (17)	-0.0048 (18)
C2'	0.077 (3)	0.097 (2)	0.087 (2)	0.0001 (19)	0.0000 (19)	-0.0057 (17)
C3	0.084 (2)	0.088 (2)	0.090 (2)	-0.0010 (17)	0.0008 (19)	-0.0023 (17)
C3'	0.086 (2)	0.090 (2)	0.095 (2)	-0.0037 (17)	-0.0017 (18)	-0.0123 (18)
C4	0.081 (3)	0.084 (2)	0.086 (2)	0.000 (2)	-0.002 (2)	0.0040 (18)
C4'	0.087 (3)	0.080 (2)	0.095 (2)	-0.002 (2)	-0.003 (2)	-0.0084 (17)
C5	0.084 (3)	0.086 (2)	0.082 (2)	0.006 (2)	-0.003 (2)	0.004 (2)
C5'	0.088 (3)	0.087 (2)	0.115 (3)	0.000 (2)	-0.004 (2)	-0.009 (2)
C6	0.096 (3)	0.092 (2)	0.087 (2)	-0.002 (2)	-0.0053 (18)	-0.0007 (19)
C6'	0.100 (3)	0.089 (3)	0.131 (3)	-0.0008 (19)	-0.016 (3)	0.003 (2)
C7	0.114 (3)	0.093 (2)	0.087 (2)	0.001 (2)	-0.005 (2)	-0.002 (2)
C7'	0.115 (4)	0.092 (2)	0.114 (3)	-0.013 (2)	-0.013 (3)	0.0082 (19)
C8	0.111 (3)	0.104 (3)	0.086 (2)	0.016 (2)	0.005 (2)	0.002 (2)
C8'	0.100 (3)	0.097 (2)	0.103 (3)	-0.011 (2)	0.001 (2)	0.002 (2)
C9	0.091 (3)	0.103 (3)	0.092 (3)	0.006 (2)	0.002 (2)	0.006 (2)
C9'	0.087 (3)	0.092 (2)	0.100 (2)	-0.0044 (18)	-0.001 (2)	-0.007 (2)
C10	0.086 (3)	0.088 (3)	0.084 (2)	0.0054 (19)	0.000 (2)	0.003 (2)
C11	0.086 (3)	0.109 (3)	0.111 (2)	-0.011 (2)	0.0017 (18)	0.0147 (19)
C12	0.090 (3)	0.087 (2)	0.085 (2)	0.004 (2)	0.000 (2)	-0.0001 (18)
C13	0.108 (3)	0.089 (3)	0.117 (2)	0.016 (2)	-0.0051 (19)	-0.0199 (19)

Geometric parameters (Å, º) for **1**

O1—C1	1.330 (4)	C4'—C9'	1.390 (4)
O1—C13	1.444 (3)	C5—C6	1.402 (4)
O2—C1	1.207 (3)	C5—C10	1.404 (4)
O3—C1'	1.235 (4)	C5'—C6'	1.381 (4)
O4—C2'	1.417 (3)	C5'—H5'	0.9500
O4—H4	1.00 (4)	C6—C7	1.375 (4)
N1—C12	1.373 (4)	C6—H6	0.9500
N1—C10	1.380 (4)	C6'—C7'	1.386 (5)
N1—C11	1.449 (4)	C6'—H6'	0.9500
N2—C1'	1.336 (4)	C7—C8	1.398 (4)
N2—C2	1.448 (4)	C7—H7	0.9500

N2—H2	0.91 (4)	C7'—C8'	1.375 (5)
C1—C2	1.514 (4)	C7'—H7'	0.9500
C1'—C2'	1.516 (4)	C8—C9	1.372 (4)
C2—C3	1.543 (4)	C8—H8	0.9500
C2—H2A	1.0000	C8'—C9'	1.378 (4)
C2'—C3'	1.528 (4)	C8'—H8'	0.9500
C2'—H2'	1.0000	C9—C10	1.391 (4)
C3—C4	1.493 (4)	C9—H9	0.9500
C3—H3A	0.9900	C9'—H9'	0.9500
C3—H3B	0.9900	C11—H11A	0.9800
C3'—C4'	1.504 (4)	C11—H11B	0.9800
C3'—H3'A	0.9900	C11—H11C	0.9800
C3'—H3'B	0.9900	C12—H12	0.9500
C4—C12	1.366 (4)	C13—H13A	0.9800
C4—C5	1.442 (4)	C13—H13B	0.9800
C4'—C5'	1.387 (4)	C13—H13C	0.9800
C1—O1—C13	115.9 (2)	C10—C5—C4	107.2 (3)
C2'—O4—H4	112 (2)	C6'—C5'—C4'	121.3 (3)
C12—N1—C10	107.8 (3)	C6'—C5'—H5'	119.4
C12—N1—C11	126.9 (3)	C4'—C5'—H5'	119.4
C10—N1—C11	125.1 (3)	C7—C6—C5	118.4 (3)
C1'—N2—C2	124.3 (3)	C7—C6—H6	120.8
C1'—N2—H2	116 (2)	C5—C6—H6	120.8
C2—N2—H2	120 (2)	C5'—C6'—C7'	119.7 (3)
O2—C1—O1	123.9 (3)	C5'—C6'—H6'	120.2
O2—C1—C2	123.0 (3)	C7'—C6'—H6'	120.2
O1—C1—C2	113.1 (3)	C6—C7—C8	121.6 (3)
O3—C1'—N2	124.0 (3)	C6—C7—H7	119.2
O3—C1'—C2'	120.8 (3)	C8—C7—H7	119.2
N2—C1'—C2'	115.1 (3)	C8'—C7'—C6'	119.7 (3)
N2—C2—C1	111.1 (3)	C8'—C7'—H7'	120.1

N2—C2—C3	112.0 (2)	C6'—C7'—H7'	120.1
C1—C2—C3	108.6 (2)	C9—C8—C7	121.1 (3)
N2—C2—H2A	108.3	C9—C8—H8	119.4
C1—C2—H2A	108.3	C7—C8—H8	119.4
C3—C2—H2A	108.3	C7'—C8'—C9'	120.3 (3)
O4—C2'—C1'	108.2 (2)	C7'—C8'—H8'	119.9
O4—C2'—C3'	112.5 (3)	C9'—C8'—H8'	119.9
C1'—C2'—C3'	111.8 (3)	C8—C9—C10	117.4 (3)
O4—C2'—H2'	108.1	C8—C9—H9	121.3
C1'—C2'—H2'	108.1	C10—C9—H9	121.3
C3'—C2'—H2'	108.1	C8'—C9'—C4'	121.0 (3)
C4—C3—C2	113.9 (2)	C8'—C9'—H9'	119.5
C4—C3—H3A	108.8	C4'—C9'—H9'	119.5
C2—C3—H3A	108.8	N1—C10—C9	129.4 (4)
C4—C3—H3B	108.8	N1—C10—C5	108.1 (3)
C2—C3—H3B	108.8	C9—C10—C5	122.5 (3)
H3A—C3—H3B	107.7	N1—C11—H11A	109.5
C4'—C3'—C2'	115.2 (2)	N1—C11—H11B	109.5
C4'—C3'—H3'A	108.5	H11A—C11—H11B	109.5
C2'—C3'—H3'A	108.5	N1—C11—H11C	109.5
C4'—C3'—H3'B	108.5	H11A—C11—H11C	109.5
C2'—C3'—H3'B	108.5	H11B—C11—H11C	109.5
H3'A—C3'—H3'B	107.5	C4—C12—N1	111.3 (3)
C12—C4—C5	105.6 (3)	C4—C12—H12	124.4
C12—C4—C3	126.8 (3)	N1—C12—H12	124.4
C5—C4—C3	127.4 (3)	O1—C13—H13A	109.5
C5'—C4'—C9'	118.0 (3)	O1—C13—H13B	109.5
C5'—C4'—C3'	121.0 (3)	H13A—C13—H13B	109.5
C9'—C4'—C3'	120.9 (3)	O1—C13—H13C	109.5
C6—C5—C10	118.9 (3)	H13A—C13—H13C	109.5
C6—C5—C4	133.9 (3)	H13B—C13—H13C	109.5

Hydrogen-bond geometry (Å, º) for **1**

D—H···*A*	*D*—H	H···*A*	*D*···*A*	*D*—H···*A*
O4—H4···O3^{i}	1.00 (4)	1.72 (4)	2.714 (3)	171 (3)
C2—H2*A*···O4^{ii}	1.00	2.34	3.212 (4)	146
C3′—H3′*A*···O2^{iii}	0.99	2.60	3.462 (4)	145
C3′—H3′*B*···O1^{iv}	0.99	2.62	3.500 (4)	148
N2—H2···O4	0.91 (4)	2.03 (3)	2.531 (3)	113 (3)

Symmetry codes: (i) *x*+1, *y*, *z*; (ii) *x*-1, *y*, *z*; (iii) -*x*+1, *y*+1/2, -*z*+3/2; (iv) -*x*+2, *y*+1/2, -*z*+3/2.

Results of X-ray analysis of compound 2

Crystal data

$C_{21}H_{22}N_2O_4 \cdot CH_4O$	$F(000) = 848$
$M_r = 398.45$	$D_x = 1.283$ Mg m^{-3}
Monoclinic, *C*2	Cu *K*α radiation, λ = 1.54178 Å
a = 23.52 (2) Å	Cell parameters from 9974 reflections
b = 5.994 (5) Å	θ = 5.9–67.5°
c = 15.843 (13) Å	μ = 0.75 mm^{-1}
β = 112.574 (17)°	*T* = 140 K
V = 2063 (3) Å^3	Needle, clear colourless
Z = 4	0.20 × 0.10 × 0.05 mm^3

Data collection

Bruker Kappa APEX-II CCD area detector diffractometer	3416 independent reflections
Radiation source: microfocus sealed tube	3283 reflections with $I > 2\sigma(I)$
Multilayer mirror monochromator	$R_{int} = 0.027$
ω scans, ϕ scans	$\theta_{max} = 65.6°$, $\theta_{min} = 5.9°$
Absorption correction: multi-scan (*SADABS*; Sheldrick, 1996)	*h* = -27→27
$T_{min} = 0.917$, $T_{max} = 1.000$	*k* = -7→7
11796 measured reflections	*l* = -15→18

Refinement

Refinement on F^2	Secondary atom site location: difference Fourier map
Least-squares matrix: full	Hydrogen site location: mixed
$R[F^2 > 2\sigma(F^2)] = 0.025$	H atoms treated by a mixture of independent and constrained refinement
$wR(F^2) = 0.067$	$w = 1/[\sigma^2(F_o^2) + (0.0393P)^2 + 0.5585P]$ where $P = (F_o^2 + 2F_c^2)/3$
$S = 1.09$	$(\Delta/\sigma)_{max} = 0.001$
3416 reflections	$\Delta\rangle_{max} = 0.19$ e Å^{-3}
276 parameters	$\Delta\rangle_{min} = -0.20$ e Å^{-3}
1 restraint	Absolute structure: Flack x determined using 1433 quotients [(I+)-(I-)]/[(I+)+(I-)] (Parsons, Flack and Wagner, ActaCryst. B69 (2013) 249-259).
Primary atom site location: structure-invariant direct methods	Absolute structure parameter: 0.00 (3)

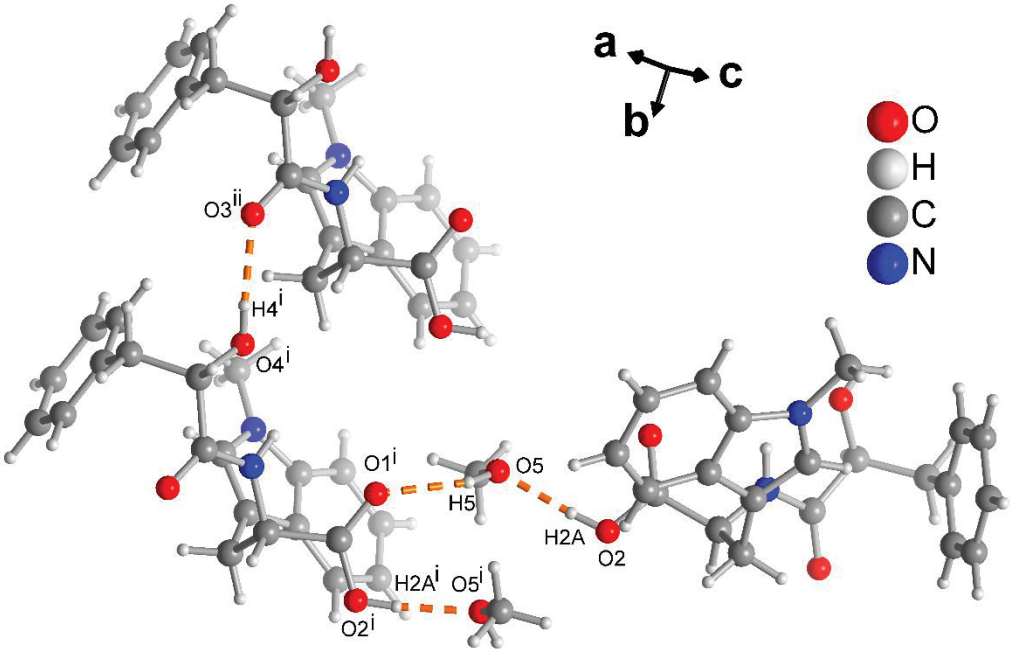

Figure S71. Section of the packing diagram of **2** showing the intermolecular H-bonds (orange dashed line) with methanole, which connect three symmetry equivalent molecules. Details for intermolecular H-bonds:
O2-H2A0.85 Å, H2A···O5 1.76 Å, O2···O52.61 Å, O4-H4···O5 172 °
O5-H5 0.81 Å, H5···O1^{i}2.03 Å, O5···O1^{i}2.80 Å, O5-H5···O1^{i} 158 °
O4^{i}-H4^{i} 0.84 Å, H4^{i}···O3^{ii}1.92 Å, O4^{i}···O3^{ii}2.74 Å, O4^{i}-H4^{i}···O3^{ii} 169 °
Symmetry codes: (i) 3/2–x, 1/2+y, 1–z, (ii) 3/2–x, –1/2+y, 1–z.

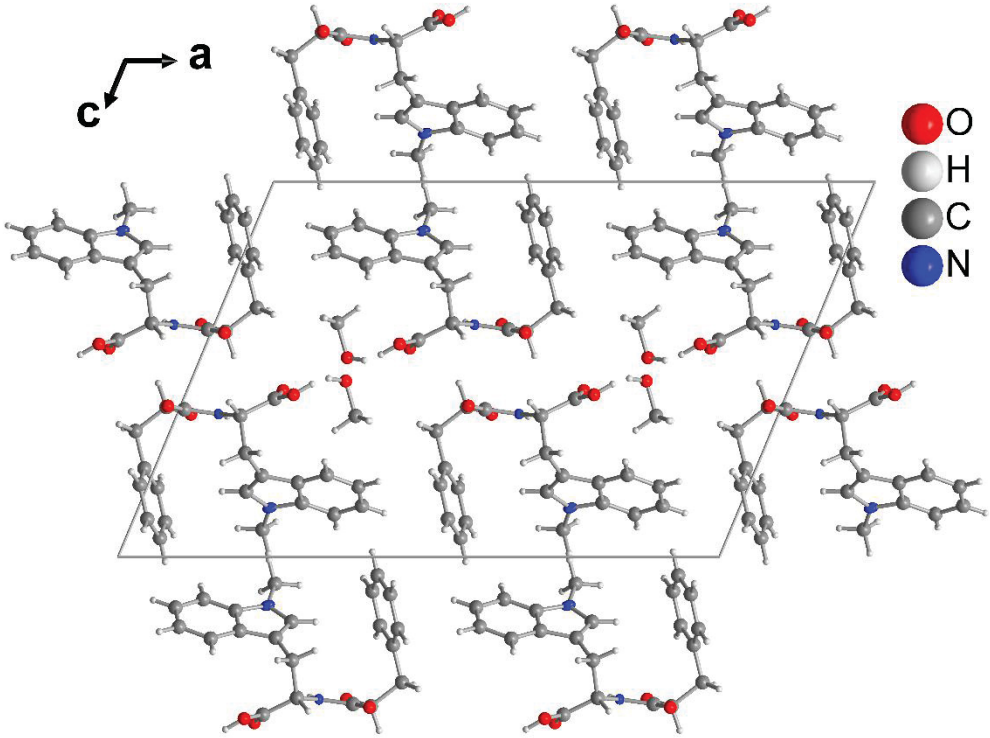

Figure S72. Sections of the packing diagram of **2** along the *b*-plane.

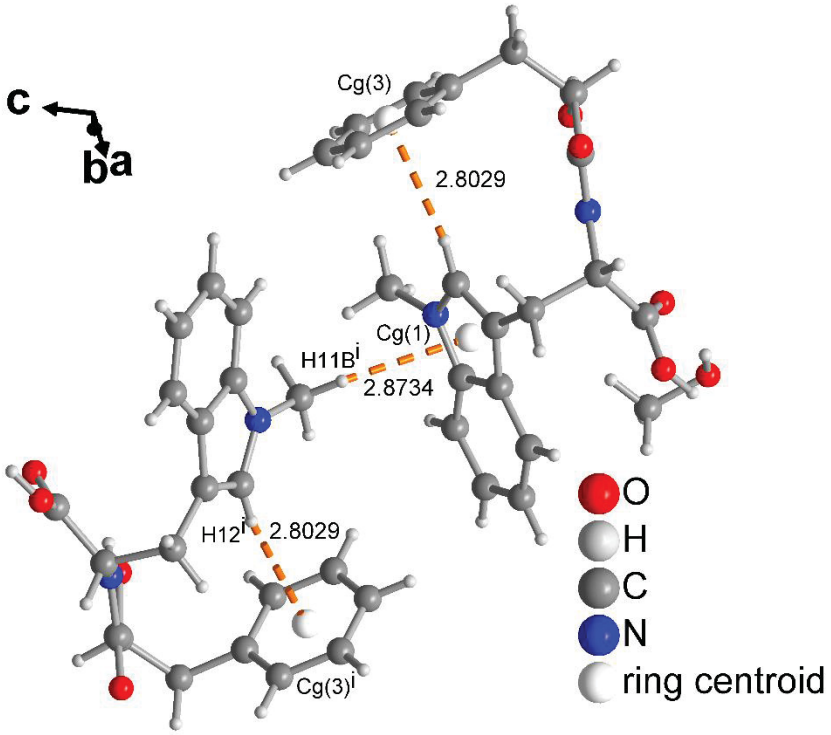

Figure S73. Section of the packing diagram of **2** showing short inter- and intramolecular C-H···π distances (orange dashed lines). Symmetry code: (i) 3/2–x, 1/2+y, 2–z.

Fractional atomic coordinates and isotropic or equivalent isotropic displacement parameters (Å^2) for **2**(Note that the atomic numbering in the deposited cif file is different to avoid the prime notation, that is C1' is C13, C2' is C14 etc.)

	x	*y*	*z*	U_{iso}*/U_{eq}
O1	0.65940 (5)	0.4911 (2)	0.55654 (9)	0.0217 (3)
H1	0.5844 (11)	0.409 (5)	0.6253 (16)	0.033*
C1'	0.50817 (8)	0.5468 (3)	0.60666 (12)	0.0152 (4)
C1	0.65075 (8)	0.6794 (3)	0.57838 (12)	0.0178 (4)
N1	0.71816 (7)	0.3323 (3)	0.86983 (11)	0.0250 (4)
C2'	0.47682 (7)	0.3204 (3)	0.60061 (12)	0.0169 (4)
H2'	0.446506	0.299653	0.536476	0.020*
H4	0.5045 (10)	0.027 (5)	0.6078 (15)	0.025*
C2	0.60559 (8)	0.7325 (3)	0.62335 (13)	0.0165 (4)
H2	0.577918	0.855216	0.587885	0.020*
O2	0.67925 (6)	0.8600 (2)	0.56768 (10)	0.0265 (3)
H2A	0.7028 (12)	0.838 (5)	0.5390 (19)	0.040*
N2	0.56793 (6)	0.5381 (2)	0.61929 (10)	0.0160 (3)
O3	0.47819 (5)	0.7223 (2)	0.59769 (9)	0.0200 (3)
C3'	0.44174 (7)	0.3112 (3)	0.66470 (13)	0.0199 (4)
H3'A	0.409841	0.429202	0.646610	0.024*
H3'B	0.420496	0.165526	0.656917	0.024*
C3	0.63959 (7)	0.8138 (3)	0.72350 (12)	0.0178 (4)
H3A	0.663461	0.949722	0.723412	0.021*
H3B	0.608736	0.854038	0.749306	0.021*
C4'	0.48241 (8)	0.3414 (3)	0.76430 (13)	0.0209 (4)
C4	0.68242 (8)	0.6407 (3)	0.78355 (13)	0.0168 (4)
O4	0.52225 (6)	0.1513 (2)	0.61967 (9)	0.0208 (3)
O5	0.74323 (6)	0.7709 (2)	0.46887 (10)	0.0268 (3)
H5	0.7733 (12)	0.847 (5)	0.4756 (18)	0.040*
C5'	0.48570 (9)	0.5465 (3)	0.80747 (15)	0.0278 (4)
H5'	0.462765	0.669628	0.773458	0.033*
C5	0.74738 (8)	0.6176 (3)	0.80238 (13)	0.0202 (4)
C6'	0.52212 (11)	0.5730 (4)	0.89961 (16)	0.0377 (5)

H6'	0.523658	0.713658	0.928073	0.045*
C6	0.79002 (9)	0.7470 (4)	0.78148 (15)	0.0297 (5)
H6	0.777465	0.879753	0.746484	0.036*
C7'	0.55615 (10)	0.3964 (4)	0.95023 (15)	0.0375 (5)
H7'	0.580928	0.415035	1.013260	0.045*
C7	0.85081 (10)	0.6769 (5)	0.81295 (16)	0.0432 (6)
H7	0.880124	0.763811	0.799645	0.052*
C9	0.82937 (9)	0.3510 (4)	0.88650 (15)	0.0359 (5)
H9	0.842420	0.218217	0.921334	0.043*
C9'	0.51729 (9)	0.1636 (3)	0.81604 (14)	0.0249 (4)
H9'	0.515962	0.022713	0.787889	0.030*
C8	0.86993 (9)	0.4796 (5)	0.86422 (17)	0.0443 (7)
H8	0.911732	0.434395	0.883824	0.053*
C8'	0.55377 (10)	0.1914 (4)	0.90802 (15)	0.0324 (5)
H8'	0.577237	0.069541	0.942298	0.039*
C13	0.70283 (11)	0.7748 (5)	0.37583 (17)	0.0506 (7)
H13A	0.726817	0.769836	0.337146	0.076*
H13B	0.678308	0.911986	0.363240	0.076*
H13C	0.675366	0.645225	0.362641	0.076*
C11	0.72095 (11)	0.1406 (3)	0.92782 (15)	0.0360 (5)
H11A	0.679408	0.104344	0.924008	0.054*
H11B	0.747256	0.175992	0.991249	0.054*
H11C	0.738067	0.012336	0.907200	0.054*
C12	0.66742 (8)	0.4651 (3)	0.82618 (13)	0.0209 (4)
H12	0.627514	0.438347	0.825792	0.025*
C10	0.76795 (8)	0.4230 (3)	0.85592 (13)	0.0239 (4)

Atomic displacement parameters (Å^2) for **2**(Note that the atomic numbering in the deposited cif file is different to avoid the prime notation, that is C1' is C13, C2' is C14 etc.)

	U^{11}	U^{22}	U^{33}	U^{12}	U^{13}	U^{23}
O1	0.0213 (6)	0.0195 (7)	0.0275 (8)	-0.0002 (5)	0.0130 (5)	-0.0035 (5)
C1'	0.0184 (8)	0.0161 (9)	0.0117 (9)	0.0006 (7)	0.0062 (6)	-0.0004 (6)

C1	0.0174 (8)	0.0212 (9)	0.0140 (10)	-0.0016 (7)	0.0048 (7)	0.0003 (7)
N1	0.0295 (8)	0.0200 (8)	0.0196 (9)	0.0003 (6)	0.0027 (6)	0.0021 (6)
C2'	0.0173 (8)	0.0133 (8)	0.0194 (9)	0.0009 (6)	0.0063 (7)	0.0012 (7)
C2	0.0191 (8)	0.0132 (8)	0.0185 (10)	0.0002 (6)	0.0086 (7)	0.0010 (6)
O2	0.0315 (7)	0.0230 (7)	0.0346 (9)	-0.0073 (6)	0.0236 (6)	-0.0033 (6)
N2	0.0166 (7)	0.0130 (7)	0.0193 (8)	0.0012 (6)	0.0080 (6)	0.0006 (6)
O3	0.0188 (6)	0.0148 (6)	0.0278 (8)	0.0018 (5)	0.0105 (5)	0.0015 (5)
C3'	0.0175 (8)	0.0174 (8)	0.0261 (10)	-0.0014 (7)	0.0099 (7)	0.0018 (7)
C3	0.0200 (8)	0.0145 (8)	0.0203 (10)	-0.0002 (7)	0.0092 (7)	-0.0020 (7)
C4'	0.0201 (8)	0.0232 (9)	0.0248 (11)	-0.0044 (7)	0.0145 (7)	0.0022 (8)
C4	0.0170 (8)	0.0164 (8)	0.0167 (9)	-0.0019 (6)	0.0064 (7)	-0.0039 (7)
O4	0.0210 (6)	0.0105 (6)	0.0321 (8)	0.0013 (5)	0.0115 (6)	0.0000 (5)
O5	0.0298 (7)	0.0242 (7)	0.0339 (9)	-0.0046 (5)	0.0205 (6)	0.0015 (6)
C5'	0.0362 (10)	0.0241 (10)	0.0278 (12)	-0.0037 (8)	0.0174 (8)	0.0014 (8)
C5	0.0196 (9)	0.0251 (9)	0.0153 (10)	-0.0022 (7)	0.0061 (7)	-0.0070 (7)
C6'	0.0554 (14)	0.0295 (11)	0.0322 (14)	-0.0120 (10)	0.0213 (11)	-0.0052 (9)
C6	0.0243 (9)	0.0434 (12)	0.0234 (11)	-0.0091 (9)	0.0113 (8)	-0.0080 (9)
C7'	0.0433 (12)	0.0448 (13)	0.0222 (12)	-0.0189 (10)	0.0104 (9)	-0.0002 (10)
C7	0.0221 (10)	0.0788 (18)	0.0320 (13)	-0.0113 (11)	0.0139 (9)	-0.0155 (12)
C9	0.0299 (10)	0.0456 (13)	0.0239 (11)	0.0139 (10)	0.0010 (8)	-0.0102 (10)
C9'	0.0248 (9)	0.0238 (10)	0.0290 (12)	-0.0009 (7)	0.0136 (8)	0.0040 (8)
C8	0.0177 (9)	0.0797 (19)	0.0316 (13)	0.0090 (10)	0.0052 (8)	-0.0190 (13)
C8'	0.0305 (10)	0.0365 (11)	0.0280 (12)	-0.0044 (9)	0.0088 (9)	0.0120 (9)
C13	0.0437 (13)	0.0762 (19)	0.0324 (14)	-0.0214 (13)	0.0149 (11)	-0.0051 (13)
C11	0.0502 (13)	0.0218 (10)	0.0263 (12)	-0.0008 (9)	0.0039 (10)	0.0046 (9)
C12	0.0194 (8)	0.0208 (9)	0.0204 (10)	-0.0023 (7)	0.0053 (7)	-0.0007 (7)
C10	0.0239 (9)	0.0269 (10)	0.0170 (10)	0.0044 (7)	0.0035 (7)	-0.0071 (7)

Geometric parameters (Å, º) for **2**(Note that the atomic numbering in the deposited cif file is different to avoid the prime notation, that is C1' is C13, C2' is C14 etc.)

O1—C1	1.220 (2)	O5—C13	1.415 (3)
C1'—O3	1.244 (2)	O5—H5	0.81 (3)
C1'—N2	1.343 (3)	C5'—C6'	1.389 (3)

C1'—C2'	1.529 (3)	C5'—H5'	0.9500
C1—O2	1.318 (2)	C5—C6	1.404 (3)
C1—C2	1.523 (3)	C5—C10	1.414 (3)
N1—C12	1.379 (3)	C6'—C7'	1.383 (3)
N1—C10	1.383 (3)	C6'—H6'	0.9500
N1—C11	1.457 (3)	C6—C7	1.387 (3)
C2'—O4	1.419 (2)	C6—H6	0.9500
C2'—C3'	1.536 (3)	C7'—C8'	1.390 (4)
C2'—H2'	1.0000	C7'—H7'	0.9500
C2—N2	1.450 (2)	C7—C8	1.407 (4)
C2—C3	1.556 (3)	C7—H7	0.9500
C2—H2	1.0000	C9—C8	1.374 (4)
O2—H2A	0.85 (3)	C9—C10	1.404 (3)
N2—H1	0.85 (3)	C9—H9	0.9500
C3'—C4'	1.510 (3)	C9'—C8'	1.388 (3)
C3'—H3'A	0.9900	C9'—H9'	0.9500
C3'—H3'B	0.9900	C8—H8	0.9500
C3—C4	1.503 (2)	C8'—H8'	0.9500
C3—H3A	0.9900	C13—H13A	0.9800
C3—H3B	0.9900	C13—H13B	0.9800
C4'—C5'	1.395 (3)	C13—H13C	0.9800
C4'—C9'	1.401 (3)	C11—H11A	0.9800
C4—C12	1.368 (3)	C11—H11B	0.9800
C4—C5	1.447 (3)	C11—H11C	0.9800
O4—H4	0.84 (3)	C12—H12	0.9500
O3—C1'—N2	124.38 (16)	C4'—C5'—H5'	119.6
O3—C1'—C2'	120.32 (15)	C6—C5—C10	119.08 (18)
N2—C1'—C2'	115.28 (15)	C6—C5—C4	133.80 (18)
O1—C1—O2	125.08 (17)	C10—C5—C4	107.07 (17)
O1—C1—C2	123.25 (16)	C7'—C6'—C5'	120.5 (2)
O2—C1—C2	111.66 (15)	C7'—C6'—H6'	119.7

C12—N1—C10	108.42 (17)	C5'—C6'—H6'	119.7
C12—N1—C11	126.31 (18)	C7—C6—C5	118.7 (2)
C10—N1—C11	125.05 (18)	C7—C6—H6	120.7
O4—C2'—C1'	108.35 (14)	C5—C6—H6	120.7
O4—C2'—C3'	112.68 (14)	C6'—C7'—C8'	119.4 (2)
C1'—C2'—C3'	111.02 (15)	C6'—C7'—H7'	120.3
O4—C2'—H2'	108.2	C8'—C7'—H7'	120.3
C1'—C2'—H2'	108.2	C6—C7—C8	121.3 (2)
C3'—C2'—H2'	108.2	C6—C7—H7	119.4
N2—C2—C1	109.60 (15)	C8—C7—H7	119.4
N2—C2—C3	111.28 (15)	C8—C9—C10	117.6 (2)
C1—C2—C3	111.40 (15)	C8—C9—H9	121.2
N2—C2—H2	108.1	C10—C9—H9	121.2
C1—C2—H2	108.1	C8'—C9'—C4'	120.7 (2)
C3—C2—H2	108.1	C8'—C9'—H9'	119.7
C1—O2—H2A	114 (2)	C4'—C9'—H9'	119.7
C1'—N2—C2	124.22 (15)	C9—C8—C7	121.4 (2)
C1'—N2—H1	117.1 (16)	C9—C8—H8	119.3
C2—N2—H1	118.7 (16)	C7—C8—H8	119.3
C4'—C3'—C2'	113.64 (15)	C9'—C8'—C7'	120.4 (2)
C4'—C3'—H3'A	108.8	C9'—C8'—H8'	119.8
C2'—C3'—H3'A	108.8	C7'—C8'—H8'	119.8
C4'—C3'—H3'B	108.8	O5—C13—H13A	109.5
C2'—C3'—H3'B	108.8	O5—C13—H13B	109.5
H3'A—C3'—H3'B	107.7	H13A—C13—H13B	109.5
C4—C3—C2	112.74 (15)	O5—C13—H13C	109.5
C4—C3—H3A	109.0	H13A—C13—H13C	109.5
C2—C3—H3A	109.0	H13B—C13—H13C	109.5
C4—C3—H3B	109.0	N1—C11—H11A	109.5
C2—C3—H3B	109.0	N1—C11—H11B	109.5
H3A—C3—H3B	107.8	H11A—C11—H11B	109.5
C5'—C4'—C9'	118.27 (19)	N1—C11—H11C	109.5

C5'—C4'—C3'	120.78 (17)	H11A—C11—H11C	109.5
C9'—C4'—C3'	120.94 (18)	H11B—C11—H11C	109.5
C12—C4—C5	106.08 (16)	C4—C12—N1	110.73 (17)
C12—C4—C3	127.31 (16)	C4—C12—H12	124.6
C5—C4—C3	126.48 (17)	N1—C12—H12	124.6
C2'—O4—H4	108.4 (16)	N1—C10—C9	130.3 (2)
C13—O5—H5	109.2 (19)	N1—C10—C5	107.70 (16)
C6'—C5'—C4'	120.79 (19)	C9—C10—C5	122.0 (2)
C6'—C5'—H5'	119.6		

Hydrogen-bond geometry (Å, º) for **2**

D—H···*A*	*D*—H	H···*A*	*D*···*A*	*D*—H···*A*
O2—H2···O5	0.85 (3)	1.76 (3)	2.609 (2)	172 (3)
O4—H4···O3^{i}	0.85 (3)	1.91 (3)	2.744 (3)	169 (2)
N2—H2*A*···O4	0.84 (3)	2.11 (2)	2.557 (3)	112.6 (18)
C2—H2B···O4^{ii}	1.00	2.37	3.172 (3)	136
C2′—H2′···O1^{iii}	1.00	2.62	3.375 (3)	132
O5—H5···O1^{iv}	0.81 (3)	2.03 (3)	2.803 (3)	158 (3)

Symmetry codes: (i) *x*, *y*-1, *z*; (ii) *x*, *y*+1, *z*; (iii) -*x*+1, *y*, -*z*+1; (iv) -*x*+3/2, *y*+1/2, -*z*+1.

Publication 3

Secondary metabolites of the lichen-associated fungus *Apiospora montagnei*.

Published in "*Tetrahedron Letters*".

Publication 3
Tetrahedron Letters 58 (2017) 1702–1705

Contents lists available at ScienceDirect

Tetrahedron Letters

journal homepage: www.elsevier.com/locate/tetlet

Secondary metabolites of the lichen-associated fungus *Apiospora montagnei*

Hao Wang [a,1], Blessing O. Umeokoli [a,b,1], Peter Eze [a,c], Christian Heering [d], Christoph Janiak [d], Werner E.G. Müller [e], Raha S. Orfali [f], Rudolf Hartmann [g], Haofu Dai [h], Wenhan Lin [i], Zhen Liu [a,*], Peter Proksch [a,*]

[a] Institute of Pharmaceutical Biology and Biotechnology, Heinrich-Heine-University Düsseldorf, Universitätsstrasse 1, 40225 Düsseldorf, Germany
[b] Department of Pharmaceutical and Medicinal Chemistry, Nnamdi Azikiwe University, Awka, Nigeria
[c] Department of Pharmaceutical Microbiology and Biotechnology, Nnamdi Azikiwe University, Awka, Nigeria
[d] Institute of Inorganic and Structural Chemistry, Heinrich-Heine-University Düsseldorf, Universitätsstrasse 1, 40225 Düsseldorf, Germany
[e] Institut für Physiologische Chemie, Universitätsmedizin der Johannes Gutenberg-University Mainz, Duesbergweg 6, 55128 Mainz, Germany
[f] Department of Pharmacognosy, Faculty of Pharmacy, King Saud University, Riyadh, Saudi Arabia
[g] Institute of Complex Systems: Strukturbiochemie, Forschungszentrum Juelich, Wilhelm-Johnen-Straße, 52428 Juelich, Germany
[h] Key Laboratory of Biology and Genetic Resources of Tropical Crops, Ministry of Agriculture, Institute of Tropical Bioscience and Biotechnology, Chinese Academy of Tropical Agricultural Sciences, Haikou 571101, China
[i] State Key Laboratory of Natural and Biomimetic Drugs, Peking University, Beijing 100191, China

ARTICLE INFO

Article history:
Received 12 December 2016
Revised 16 March 2017
Accepted 17 March 2017
Available online 19 March 2017

Keywords:
Apiospora montagnei
Cytotoxicity
X-ray diffraction

ABSTRACT

The endolichenic fungus *Apiospora montagnei* isolated from the lichen *Cladonia* sp. was cultured on solid rice medium, yielding the new diterpenoid libertellenone L (**1**), the new pyridine alkaloid, 23-*O*-acetyl-*N*-hydroxyapiosporamide (**2**) and the new xanthone derivative 8-hydroxy-3-hydroxymethyl-9-oxo-9*H*-xanthene-1-carboxylic acid methyl ether (**3**) together with 19 known compounds (**4**–**22**). The structures of the new compounds were elucidated by 1D and 2D NMR spectra as well as by HRESIMS data. The absolute configuration of the new 6,7-*seco*-libertellenone derivative **1** was determined by single-crystal X-ray diffraction. Four additional known compounds **23**–**26** were isolated when NaCl or NH_4Cl were added to solid rice medium. Compounds **7**–**9**, **18** and **26** exhibited significant cytotoxicity against the L5178 murine lymphoma cell line with IC_{50} values of 2.6, 0.2, 2.1, 2.7 and 1.7 μM, respectively.

Introduction

Lichens are symbiotic associations between fungi (mycobionts) and photoautotrophic, algal partners (photobionts), producing numerous bioactive secondary metabolites such as usnic acid, diffractaic acid, and physodic acid.[1,2] In addition to the photobiont and the mycobiont, lichens harbour a wide array of associated microorganisms including endolichenic fungi that are likewise prolific sources of bioactive secondary metabolites.[3–6] Over 140 new natural products including alkaloids, quinones, sulfur-containing chromenones and terpenes were isolated from 30 endolichenic microorganisms during the past decade.[7] Considering that there are nearly 20,000 identified lichens, a further exploration of endolichenic fungi as sources for new compounds is promising.

During our ongoing search for bioactive secondary metabolites from fungi,[8–10] the fungus *Apiospora montagnei* was isolated from the lichen *Cladonia* sp. *A. montagnei*, which is also known as *Arthrinium arundinis*, has previously been obtained from various sources such as sponges, algae, soil and mouse dung.[11–14] This is the first report of this fungus from lichen thalli. Previous chemical investigations of *A. montagnei* revealed a series of diverse secondary metabolites, such as the cyclopeptides TMC-95A–D,[11] the diterpene myrocin A[12] and the pydidone alkaloids arthpyrones A–C, apiosporamide and *N*-hydroxyapiosporamide.[13,14] In this study, the EtOAc extract of the fungus when fermented on solid rice medium yielded the new diterpenoid libertellenone L (**1**), the new pyridine alkaloid 23-*O*-acetyl-*N*-hydroxyapiosporamide (**2**) and the likewise new xanthone derivative 8-hydroxy-3-hydroxymethyl-9-oxo-9*H*-xanthene-1-carboxylic acid methyl ether (**3**) as well as 19 known compounds (**4**–**22**). Furthermore, addition of NaCl to

* Corresponding authors.
E-mail addresses: zhenfeizi0@sina.com (Z. Liu), proksch@uni-duesseldorf.de (P. Proksch).
[1] H. Wang and B.O. Umeokoli contributed equally to this study.

http://dx.doi.org/10.1016/j.tetlet.2017.03.052
0040-4039/

solid rice medium led to isolation of compounds **23** and **24** that were both undetectable in controls. Addition of NH_4Cl induced accumulation of compounds **25** and **26** that were likewise not detected in fungal controls. All isolated compounds (**1**–**26**) were evaluated for their cytotoxicity against the L5178Y mouse lymphoma cell line. Compounds **7**–**9**, **18** and **26** exhibited strong cytotoxicity with IC_{50} values ranging from 0.2 to 2.6 μM.

Results and discussion

Compound **1** was isolated as colorless crystals. Its molecular formula was established as $C_{20}H_{26}O_5$ by HRESIMS, implying 8 degrees of unsaturation. The ^{13}C NMR spectrum of **1** (Table 1) showed 20 carbon signals that account for three methyl, six methylene, four methine and six quaternary carbons. The presence of a terminal double bond in **1** was proposed by the observation of the olefinic methine CH-15 (δ_C 146.9, δ_H 6.05) and the olefinic methylene CH_2-16 (δ_C 112.5, δ_H 5.06 and 5.04) as well as by the COSY correlations between them. On the basis of the COSY correlations between $H_{\alpha\beta}$-11 (δ_H 3.32 and 2.29) and $H_{\alpha\beta}$-12 (δ_H 1.94 and 1.45) and the HMBC correlations from Me-17 (δ_H 0.92) to C-12 (δ_C 26.4), C-13 (δ_C 39.8), C-14 (δ_C 70.7) and C-15, from $H_{\alpha\beta}$-11 and H-14 to C-8 (δ_C 124.1), and from $H_{\alpha\beta}$-11, H_{β}-12 and H-14 to C-9 (δ_C 168.6), the nature of the cyclohexene ring *C* was established (Fig. 2). The COSY correlations between H-1 (δ_H 4.20)/$H_{\alpha\beta}$-2 (δ_H 2.06 and 1.91) and $H_{\alpha\beta}$-2/$H_{\alpha\beta}$-3 (δ_H 1.77 and 1.69) along with the HMBC correlations from H-1 and H-14 to C-7 (δ_C 167.5), from Me-18 (δ_H 1.32) to C-3 (δ_C 31.3), C-4 (δ_C 45.1), C-5 (δ_C 52.3) and C-19 (δ_C 81.3), and from Me-20 (δ_H 1.31) to C-1 (δ_C 85.0), C-5, C-9 and C-10 (δ_C 42.0) indicated the presence of fused rings *A* and *B* in **1**. Furthermore, the cyclopentane lactone ring *D* was established from the HMBC correlations from H-5 (δ_H 2.81) and $H_{\alpha\beta}$-19 (δ_H 3.95 and 4.02) to C-6 (δ_C 175.6). Thus, the planar structure of **1** was elucidated as shown in Fig. 2.

The relative configuration of compound **1** was determined by investigation of the coupling constants and the ROESY correlations. The coupling constants ($^3J_{1,2\alpha}$ = 12.5 Hz, $^3J_{1,2\beta}$ = 4.4 Hz, $^3J_{2\alpha,3\alpha}$ = 3.5 Hz, $^3J_{2\alpha,3\beta}$ = 13.0 Hz, $^3J_{2\beta,3\alpha}$ = $^3J_{2\beta,3\beta}$ = 3.5 Hz) together with the NOE correlations between H-1/H-2β, H-1/H-3β, H-1/H-5, H-3β/H-5, H-3β/H-19β, H-5/19β and between H-2α/Me-18, H-2α/Me-20, H-3α/Me-18, H-19α/Me-18 suggested a chair conformation of the cyclohexane ring *A* with H-1 and H-5 being β-oriented while Me-18 and Me-20 are α-oriented (Fig. 3). The β-orientation of H-11β was deduced from its NOE relationship with H-5. Moreover, the NOE correlations from Me-17 to H-11β, H-12β and H-14 suggested that these protons were on the same face of ring *C*. The absolute configuration of **1** was determined as 1*R*, 4*R*, 5*S*, 10*S*, 13*R* and 14*S* by X-ray single crystal analyses (Fig. 4).

Table 1
^1H (600 MHz) and ^{13}C (150 MHz) NMR data for **1** in CD_3OD.

Position	δ_C	δ_H (*J* in Hz)
1	85.0, CH	4.20 (dd, 12.5, 4.4)
2	24.5, CH_2	2.06 (α-H, dddd, 13.0, 13.0, 12.5, 3.5)
		1.91 (β-H, dddd, 13.0, 4.4, 3.5, 3.5)
3	31.3, CH_2	1.77 (α-H, ddd, 13.0, 3.5, 3.5)
		1.69 (β-H, ddd, 13.0, 13.0, 3.5)
4	45.1, C	
5	52.3, CH	2.81 (s)
6	175.6, C	
7	167.5, C	
8	124.1, C	
9	168.6, C	
10	42.0, C	
11	25.2, CH_2	3.32 (α-H, br dd, 20.8, 6.5)
		2.29 (β-H, ddd, 20.8, 10.7, 7.0)
12	26.4, CH_2	1.94 (α-H, ddd, 13.4, 10.7, 6.5)
		1.45 (β-H, br dd, 13.4, 7.0)
13	39.8, C	
14	70.7, CH	3.92 (s)
15	146.9, CH	6.05 (dd, 17.6, 11.0)
16	112.5, CH_2	5.06 (dd, 17.6, 1.3)
		5.04 (dd, 11.0, 1.3)
17	20.9, CH_3	0.92 (s)
18	22.0, CH_3	1.32 (s)
19	81.3, CH_2	4.02 (β-H, d, 7.9)
		3.95 (α-H, d, 7.9)
20	14.6, CH_3	1.31 (s)

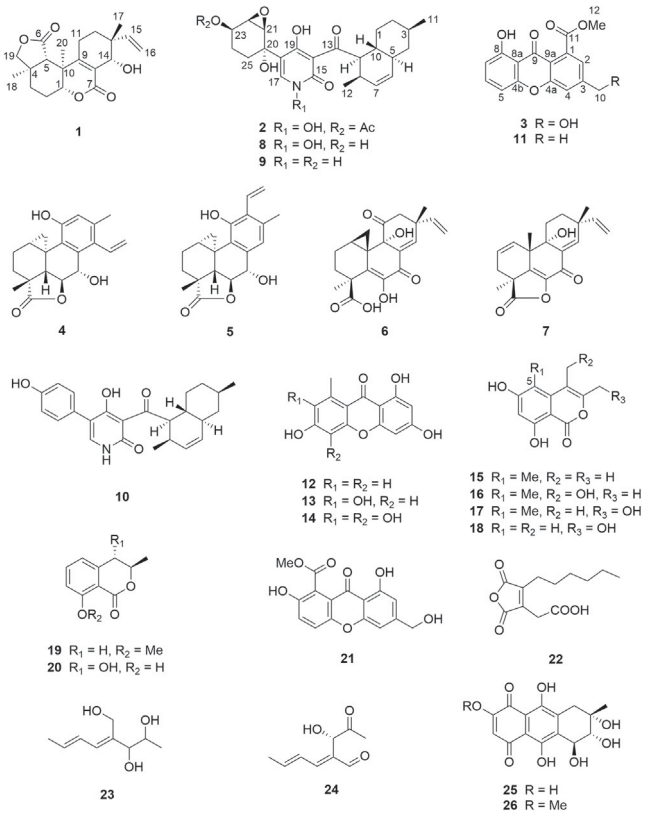

Fig. 1. Structures of compounds isolated from *A. montagnei*.

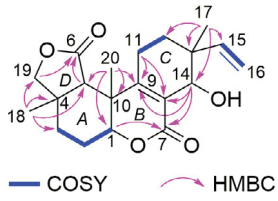

Fig. 2. COSY and key HMBC correlations of **1**.

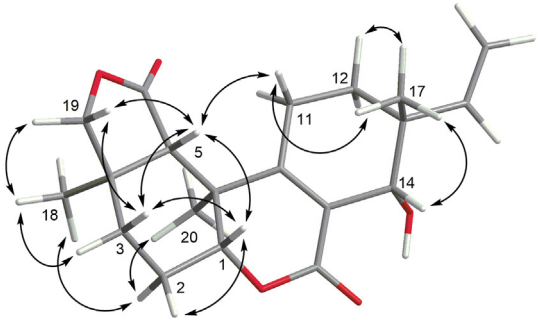

Fig. 3. Key NOE correlations of **1**.

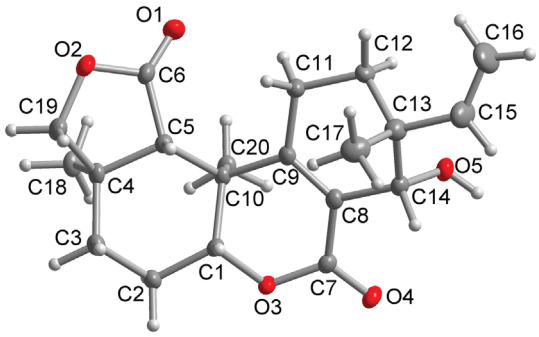

Fig. 4. Molecular structure of **1** from single-crystal X-ray diffractometry.

Comparison of the structure of **1** with that of co-isolated known pimarane diterpenoid libertellenone G (**7**)[15] revealed that compound **1** represents the first example of a 6,7-*seco*-libertellenone derivative,[15–19] for which the name libertellenone L is proposed. A biosynthetic pathway for **1** is proposed through 5,6-enol-keto-tautomerization, 6,7-oxidation-cleavage following by 1,7- and 6,19-esterification Fig. 5.

Compound **2** possessed the molecular formula $C_{26}H_{33}O_8N$ as determined by HRESIMS. Its NMR data (Table 2) were similar to those of *N*-hydroxyapiosporamide (**8**),[14,20] suggesting that **2** was an analogue of the latter compound. The presence of an additional acetyl group in **2** was deduced from its molecular weight being 42 amu higher than that of **8** and by NMR signals (δ_C 172.4 and 20.8, δ_H 2.07, s) which are indicative for an acetyl group. The HMBC correlation from H-23 (δ_H 5.18, ddd) to the acetyl carbonyl carbon indicated the additional *O*-acetyl group to be located at the C-23 position. Detailed analysis of the 2D NMR spectra of **2** revealed that its remaining substructures were identical to those of **8**. The relative configuration of **2** was determined by the similarity of the NOE relationships compared to **8**. Based on the similar specific rotation of **2** compared with **8** and biogenetic considerations, the absolute configuration of **2** was proposed to be identical to that of **8**. Thus, compound **2** was elucidated as 23-*O*-acethyl-*N*-hydroxyapiosporamide, representing a new pyridine alkaloid.

The molecular formula of **3** was determined to be $C_{16}H_{12}O_6$ by its HRESIMS data. Its UV spectrum showed absorption bands at λ_{max} 231, 257, 289 and 368 nm, similar to those of the co-isolated known xanthone derivative, 8-hydroxy-3-methyl-9-oxo-9*H*-xathene-1-carboxylic acid methyl ether (**11**).[21] The NMR data of **3** (Table 3) resembled those of **11** except for the aromatic methyl group which was replaced by a hydroxymethyl group (δ_C 63.5, δ_H 4.79, s, CH_2-10) in **3**. The extra hydroxymethyl group of **3** was attached at C-3, which was evident from the HMBC correlations from H_2-10 to C-2 (δ_C 121.6), C-3 (δ_C 152.6) and C-4 (δ_C 117.1), and in turn from H-2 (δ_H 7.36) and H-4 (δ_H 7.67) to C-10. Thus, the structure of **3** was elucidated as shown in Fig. 1.

The remaining known compounds (**4**–**22**) were identified as arthrinin A (**4**),[22] arthrinin B (**5**),[22] myrocin A (**6**),[12] libertellenone G (**7**),[15] *N*-hydroxyapiosporamide (**8**),[14,20] apiosporamide (**9**),[13,23] didymellamide B (**10**),[24] 8-hydroxy-3-methyl-9-oxo-9*H*-xanthene-1-carboxylic acid methyl ether (**11**),[21] norlichexanthone (**12**),[25] anomalin A (**13**),[25] anomalin B (**14**),[25] decarboxycitrinone (**15**),[26] 6,8-dihydroxy-4-hydroxymethyl-3,5-dimethyl-isochromen-1-one (**16**),[27] decarboxyhydroxycitrinone (**17**),[17] acremonone G (**18**),[28] *O*-methylmellein (**19**),[29] *trans*-4-hydroxymellein (**20**),[30] sydowinin B (**21**),[31] and 2-carboxymethyl-3-*n*-hexylmaleic acid anhydride (**22**).[32,33]

Table 2
^1H (600 MHz) and ^{13}C (150 MHz) NMR data for **2** in CD_3OD.

Position	δ_C	δ_H (*J* in Hz)
1	31.0, CH_2	1.92 (m)
		0.89 (m)
2	36.6, CH_2	1.74 (m)
		1.03 (m)
3	34.4, CH	1.50 (m)
4	43.2, CH_2	1.75 (m)
		0.79 (m)
5	43.2, CH	1.82 (m)
6	131.7, CH	5.40 (br d, 9.8)
7	132.6, CH	5.59 (ddd, 9.8, 4.5, 2.7)
8	32.4, CH	2.85 (m)
9	54.6, CH	4.44 (dd, 11.3, 5.8)
10	37.6, CH	1.57 (m)
11	22.9, CH_3	0.92 (d, 6.5)
12	18.4, CH_3	0.82 (d, 7.2)
13	211.8, C	
14	108.6, C	
15	159.7, C	
17	140.0, CH	8.03 (s)
18	115.4, C	
19	175.5, C	
20	70.6, C	
21	59.5, CH	3.61 (d, 3.8)
22	54.9, CH	3.54 (dd, 3.8, 3.3)
23	70.0, CH	5.18 (ddd, 5.7, 5.7, 3.3)
24	23.0, CH_2	1.97 (m)
		1.48 (m)
25	30.5, CH_2	2.19 (m)
		1.79 (m)
OAc	172.4, C	
	20.8, CH_3	2.07 (s)

Furthermore, addition of NaCl resulted in accumulation of compounds **23** and **24** that were both undetectable in control extracts. Compounds **23** and **24** were identified as the known (*E*,*E*)-4-hydroxymethyl-4,6-octadien-2,3-diol[34] and lachnellin B,[35] respectively. When NH_4Cl was added to rice medium, compounds **25** and **26** were detected as major components whereas both were missing in fungal controls. Compounds **25** and **26** were identified as the known 6-*O*-demethylbostrycin (**25**)[36] and bostrycin (**26**).[37]

All compounds (**1**–**26**) were tested for their cytotoxic activity against the mouse lymphoma cell line (L5178Y) utilizing the MTT assay (Table 4). Compounds **7**–**9**, **18** and **26** exhibited significant cytotoxicity against the L5178 murine lymphoma cell line with IC_{50} values of 2.6, 0.2, 2.1, 2.7 and 1.7 μM, respectively. Comparison of the cytotoxicity of pyridine alkaloids (**2**, **8**, **9** and **10**) revealed that acetylation of 23-OH (**2** vs. **8**) and aromatization from C-20 to C-25 (**10** vs. **9**) led to total loss of cytotoxicity while loss of the hydroxy group at the N-16 position (**9** vs. **8**) increased the activity around 10-fold. The significant cytotoxicity of compound **7** could be caused by the disappearance of the cyclopropane ring compared to **4**–**6**. Among the isolated isocoumarins (**15**–**18**), only compound **18** which lacks a methyl substituent at C-5 is active. Compared to bostrycin (**26**), 6-*O*-demethylbostrycin (**25**) shows no cytotoxicity.

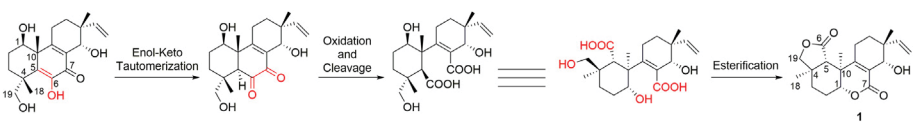

Fig. 5. Plausible biosynthesis of **1**.

Table 3
^{1}H (700 MHz) and ^{13}C (175 MHz) NMR data for **3** in CD_3OD.

Position	δ_C[a]	δ_H (*J* in Hz)
1	134.6, C	
2	121.6, CH	7.36 (br s)
3	152.6, C	
4	117.1, CH	7.67 (br s)
4a	157.5, C	
4b	157.1, C	
5	107.9, CH	7.04 (dd, 8.3, 0.9)
6	138.2, CH	7.69 (t, 8.3)
7	111.4, CH	6.81 (dd, 8.3, 0.9)
8	162.6, C	
8a	109.6, C	
9	181.9, C	
9a	116.8, C	
10	63.5, CH_2	4.79 (s)
11	171.1, C	
12	53.2, CH_3	3.98 (s)

[a] Data extracted from HSQC and HMBC spectra.

Table 4
Cytotoxicity against the L5178 murine lymphoma cell.

Compound[b]	IC_{50} (μM)
6	13.1
7	2.6
8	0.2
9	2.1
18	2.7
26	1.7
Kahalalide F[a]	4.3

[a] Positive control.
[b] The remaining compounds were not active at the dose of 20 μM.

Besides, all isolated compounds were further tested for their antimicrobial activities against *Mycobacterium tuberculosis*, *Staphylococcus aureus* (ATCC25923), *S. aureus* (ATCC700699), *Enterococcus faecalis* (ATCC29212), *E. faecalis* (ATCC51299), *E. faecium* (ATCC35667), *E. faecium* (ATCC700221) and *Acinetobacter baumannii* (ATCCBAA1605) but none of them was found to be active at the dose of 20 μg/mL.

In conclusion, cultivation of fungus *A. montagnei* as described in this study yielded five pimarane diterpenoids (**1**, **4**–**7**), four pyridine alkaloids (**2**, **8**–**10**), six xanthone derivatives (**3**, **11**–**14**, **21**), six isocoumarins (**15**–**20**) and five other metabolites (**22**–**26**), of which three (**1**–**3**) are new. Addition of either NaCl or NH_4Cl to solid rice medium diversified the natural product pattern of the fungus. Compound **1**, whose absolute configuration was determined by X-ray diffraction, represented the first example of 6,7-*seco*-libertellenone derivative and a plausible biosynthetic pathway for the formation of this compound was proposed. Several compounds (**7**–**9**, **18** and **26**) were found to exhibit significant cytotoxicity against the L5178Y mouse lymphoma cell line and preliminary structure-activity relationships were proposed.

Acknowledgements

H.W. wishes to thank the China Scholarship Council, the Ministry of Education of China, for a doctoral scholarship. We further wish to thank Dr. Huiqin Chen and Dr. Margareta Proksch (both Heinrich-Heine-University Duesseldorf, Germany) for help during lichen collection and isolation of the fungus. Financial support to P.P. by the Manchot-Foundation is gratefully acknowledged. P.P. and R.S.O. acknowledge support by the International Scientific Partnership Program ISPP# 0065 at King Saud University.

A. Supplementary data

Supplementary data (UV, MS and NMR spectra of **1**, **2** and **3** as well as X-ray data of **1**) associated with this article can be found, in the online version, at http://dx.doi.org/10.1016/j.tetlet.2017.03.052.

References

1. Ranković B, Kosanić M. *Lichen Secondary Metabolites*. Switzerland: Springer International Publishing; 2015. 1–26.
2. Shrestha G, Larry L, Clair St. *Phytochem Rev*. 2013;12:229–244.
3. Arnold AE, Miadlikowska J, Higgins KL, et al. *Syst Biol*. 2009;58:283–297.
4. Jiao Y, Li G, Wang HY, et al. *Chem Biodiversity*. 2015;12:1095–1104.
5. Dou Y, Wang X, Jiang D, et al. *Drug Discovery Ther*. 2014;8:84–88.
6. Zhang F, Li L, Niu S, et al. *J Nat Prod*. 2012;75:230–237.
7. Kellogg JJ, Raja HA. *Phytochem Rev*. 2016;1–23.
8. Uzor PF, Ebrahim W, Osadebe PO, et al. *Fitoterapia*. 2015;105:147–150.
9. Elnaggar MS, Ebada SS, Ashour ML, et al. *Tetrahedron*. 2016;72:2411–2419.
10. Liu S, Dai H, Makhloufi G, et al. *J Nat Prod*. 2016;79:2332–2340.
11. Koguchi Y, Kohno J, Nishio M, et al. *J Antibiot*. 2014;67:171–174.
12. Klemke C, Kehraus S, Wright AD, König GM. *J Nat Prod*. 2004;67:1058–1063.
13. Alfatafta AA, Gloer JB, Scott JA, Malloch D. *J Nat Prod*. 1994;57:1696–1702.
14. Wang J, Wei X, Qin X, et al. *Org Lett*. 2015;656–659.
15. Tan R, Wei W, Jiang R, Zhao G. Faming Zhuanli Shenqing 2013, CN 103073527 A 20130501.
16. Oh D-C, Jensen PR, Kauffman CA, Fenical W. *Bioorg Med Chem*. 2005;13:5267–5273.
17. Tsukada M, Fukai M, Miki K, et al. *J Nat Prod*. 2011;74:1645–1649.
18. Lu X-L, Liu J-T, Liu X-Y, et al. *J Antibiot*. 2014;67:171–174.
19. Wei W, Gao J, Shen Y, Chu YL, Xu Q, Tan RX. *Eur J Org Chem*. 2014;5728–5734.
20. Lee JC, Coval SJ, Clardy J. *J Antibiot*. 1996;49:693–696.
21. Li C, Zhang J, Shao C, Ding W, She Z, Lin Y. *Chem Nat Compd*. 2011;47:382–384.
22. Ebada SS, Schulz B, Wray V, et al. *Bioorg Med Chem*. 2011;19:4644–4651.
23. Williams DR, Kammler DG, Donnell AF, Goundry WRF. *Angew Chem Int Ed*. 2005;44:6715–6718.
24. Haga A, Tamoto H, Ishino M, et al. *J Nat Prod*. 2013;76:750–754.
25. Abdel-Lateff A, Klemke C, König GM, Wright AD. *J Nat Prod*. 2003;66:706–708.
26. Whyte AC, Gloer JB, Scott JA, Malloch D. *J Nat Prod*. 1996;59:765–769.
27. Krohn K, Sohrab MH, Aust HJ, Draeger S, Schulz B. *Nat Prod Res*. 2004;18:277–285.
28. Rukachaisirikul V, Rodglin A, Sukpondma Y, Phongpaichit S, Buatong J, Sakayaroj J. *J Nat Prod*. 2012;75:853–858.
29. Glauser G, Gindro K, Fringeli J, de Joffrey JP, Rudaz S, Wolfender JL. *J Agric Food Chem*. 2009;57:1127–1134.
30. Asha KN, Chowdhury R, Hasan CM, Rashid MA. *Acta Pharm*. 2004;54:57–63.
31. Hamasaki T, Sato Y, Hatsuda Y. *Agric Biol Chem*. 1975;39:2341–2345.
32. Weidenmüller HL, Cavagna F, Fehlhaber HW, Präve P. *Tetrahedron Lett*. 1972;33:3519–3522.
33. Haval KP, Argade NP. *J Org Chem*. 2008;73:6936–6938.
34. Fuchser J, Zeeck A. *Liebigs Ann*. 1997;87–95.
35. Semar M, Anke H, Arendholz WR, Veiten R, Steglich W. *Z Naturforsch C: J Biosci*. 1996;51:500–512.
36. Kelly TR, Saha JK. *J Org Chem*. 1985;50:3679–3685.
37. Chen H, Zhong L, Long Y, et al. *Mar Drugs*. 2012;10:932–952.

Supplementary Data

Secondary Metabolites of the Lichen-Associated Fungus *Apiospora montagnei*

Hao Wang,[a,§] Blessing O. Umeokoli,[a,b,§] Peter Eze,[a,c] Christian Heering,[d] Christoph Janiak,[d] Werner E. G. Müller,[e] Raha S. Orfali,[f] Rudolf Hartmann,[g] Haofu Dai,[h] Wenhan Lin,[i] Zhen Liu,[a,*] Peter Proksch[a,*]

[a]*Institute of Pharmaceutical Biology and Biotechnology, Heinrich-Heine-University Düsseldorf, Universitätsstrasse 1, 40225 Düsseldorf, Germany*

[b]*Department of Pharmaceutical and Medicinal Chemistry, Nnamdi Azikiwe University, Awka, Nigeria*

[c]*Department of Pharmaceutical Microbiology and Biotechnology, Nnamdi Azikiwe University, Awka, Nigeria*

[d]*Institute of Inorganic and Structural Chemistry, Heinrich-Heine-University Düsseldorf, Universitätsstrasse 1, 40225 Düsseldorf, Germany*

[e]*Institut für Physiologische Chemie, Universitätsmedizin der Johannes Gutenberg-University Mainz, Duesbergweg 6, 55128 Mainz, Germany*

[f]*Department of Pharmacognosy, Faculty of Pharmacy, King Saud University, Riyadh, Saudi Arabia*

[g]*Institute of Complex Systems: Strukturbiochemie, Forschungszentrum Juelich, Wilhelm-Johnen-Straße, 52428 Juelich, Germany*

[h]*Key Laboratory of Biology and Genetic Resources of Tropical Crops, Ministry of Agriculture, Institute of Tropical Bioscience and Biotechnology, Chinese Academy of Tropical Agricultural Sciences, Haikou 571101, China*

[i]*State Key Laboratory of Natural and Biomimetic Drugs, Peking University, Beijing 100191, China*

*Corresponding authors.
Tel.: +49 211 81 14163; fax: +49 211 81 11923;
e-mail: zhenfeizi0@sina.com (Z. Liu),
proksch@uni-duesseldorf.de (P. Proksch)

[§]H. Wang and B.O. Umeokoli contributed equally to this study

Table of Contents

Experimental Section……...……159

Figure S1. HRESIMS of **1**……165

Figure S2. ^{1}H NMR (600 MHz, methanol-d_4) spectrum of **1**……165

Figure S3. ^{13}C NMR (150 MHz, methanol-d_4) spectrum of **1**……166

Figure S4. ^{1}H-^{1}H COSY (600 MHz, methanol-d_4) spectrum of **1**……166

Figure S5. HSQC (600 and 150 MHz, methanol-d_4) spectrum of **1**……167

Figure S6. HMBC (600 and 150 MHz, methanol-d_4) spectrum of **1**……167

Figure S7. ROESY (600 MHz, methanol-d_4) spectrum of **1**……168

Figure S8. HRESIMS of **2**……168

Figure S9. ^{1}H NMR (600 MHz, methanol-d_4) spectrum of **2**……169

Figure S10. ^{13}C NMR (150 MHz, methanol-d_4) spectrum of **2**……169

Figure S11. ^{1}H-^{1}H COSY (600 MHz, methanol-d_4) spectrum of **2**……170

Figure S12. HSQC (600 and 150 MHz, methanol-d_4) spectrum of **2**……170

Figure S13. HMBC (600 and 150 MHz, methanol-d_4) spectrum of **2**……171

Figure S14. ROESY (600 MHz, methanol-d_4) spectrum of **2**……171

Figure S15. HRESIMS of **3**……172

Figure S16. ^{1}H NMR (700 MHz, methanol-d_4) spectrum of **3**……172

Figure S17. HSQC (700 and 175 MHz, methanol-d_4) spectrum of **3**……173

Figure S18. HMBC (700 and 175 MHz, methanol-d_4) spectrum of **3**……173

Figure S19. Packing diagram and hydrogen-bonding network in **1**……174

Experimental Section

General Procedures. Optical rotations were measured using a Jasco P-2000 polarimeter. NMR spectra were recorded on Bruker Avance DMX 600 or 700 NMR spectrometeror. Chemical shifts were referenced to the solvent residual peaks. Mass spectra were recorded with a LC-MS HP1100 Agilent Finnigan LCQ Deca XP Thermoquest and HRESIMS were recorded with a UHR-QTOF maXis 4G (Bruker Daltonics) mass spectrometer. HPLC analysis was performed on a Dionex UltiMate-3400SD system coupled with an LPG-3400SD pump and a photodiode array detector (DAD 300RS). The analytical column (125 × 4 mm) was prefilled with Eurosphere-10 C_{18} (Knauer), and the following gradient was used: 0 min (10% MeOH), 5 min (10% MeOH), 35 min (100% MeOH), 45 min (100% MeOH). Semi-preparative HPLC was performed using a Merck Hitachi HPLC System (UV detector L-7400; pump L-7100; Eurosphere-100 C_{18}, 300 × 8 mm, Knauer), with MeOH-H_2O as mobile phase. Column chromatography was carried out using Merck MN silica gel 60 M (0.04–0.063 mm). TLC plates with silica gel F_{254} (Merck) were used to monitor and collect fractions. Distilled and spectral grade solvents were used for column chromatography and spectroscopic measurements, respectively.

Fungal Material and Cultivation. The fungus was isolated from the lichen *Cladonia sp.* collected in Garding (province of Schleswig-Holstein) in Germany in March 2015. The fungus was identified as *A. montagnei* by DNA amplification, sequencing of the ITS region and by comparison with GenBank data (GeneBank accession No. KX137848) following standard procedures.[1]

The axenic fungal strain was grown on solid rice medium (100 g rice and 100 mL distilled water autoclaved) in ten Erlenmeyer flasks (1 L each) at 22 ºC under static conditions for 14 days. The halogen incorporation experiments were performed on rice medium after addition of 5% sodium chloride, 5% sodium bromide or 5% sodium iodide in each Erlenmeyer flask. The effects of different nitrogen sources on metabolite profiles were examined by adding 1% peptone, 1% yeast extract (YE) or 1% ammonium chloride to rice medium to Erlenmeyer flasks.

Extraction and Isolation. Each fungal culture was extracted with EtOAc (2 × 500 mL) followed by solvent evaporation under reduced pressure. Each fungal extract was analyzed by HPLC and LCMS. The EtOAc extract (13g) of the axenic fungal culture growing on rice medium was fractionated by vacuum liquid chromatography (VLC) on silica gel using a gradient elution of *n*-hexane/EtOAc (1:0 to 0:1) and then of dichloromethane (DCM)/MeOH (1:0 to 0:1) to give 23 fractions (Fr. A–W). Fr. D (115 mg) was further purified with semi-preparative HPLC to give **15** (0.5 mg), **11** (1.5 mg) and **22** (17.0 mg). Fr. E (252 mg) was subjected to a Sephadex LH-20 column with MeOH as mobile phase to give 8 subfractions (Fr. E1–E8), of which Fr. E3 was a pure compound **7** (21.0 mg). Fr. E5 was separated by semi-preparative HPLC to yield **12** (20.0 mg), **4** (20.0 mg), **5** (1.5 mg) and **20** (0.5 mg). Compounds **6** (5.0 mg) and **13** (60 mg) were obtained from Fr. F after separation by a Sephadex LH-20 column using MeOH as mobile phase. Fr. G (345.2 mg) was chromatographed on a Sephadex LH-20 column with MeOH as mobile phase to obtain 11 subfractions (Fr. G1–G11). After purification by semi-preparative HPLC, Fr. G3 yielded compound **19** (1.8 mg), **1** (5.0

mg) and **21** (1.8 mg), while Fr. G5 yielded **18** (0.5 mg), **16** (1.0 mg), **17** (1.0 mg), **3** (0.8 mg) and **10** (0.5 mg). Fr. H (460 mg) was subjected to a Sephadex LH-20 column using MeOH as mobile phase to give **14** (15.0 mg). Fr. K (100 mg) was purified by semi-preparative HPLC to afford **8** (10.0 mg), **9** (3.0 mg) and **2** (3.2mg).

The EtOAc extract (1.8 g) of fungal culture grown on solid rice medium containing 5% sodium chloride was fractionated by reversed-phase vacuum liquid chromatography (RP-VLC) using a gradient elution of H_2O/MeOH (90:10, 80:20, 70:30 and 0:100) to give 6 fractions (Fr. 1–6). Fr. 2 and 4 were purified by semi-preparative HPLC to yield **23** (1.5 mg) and **24** (2.0 mg), respectively.

The fungal extract (2.2 g) from the solid rice medium culture containing 1% ammonium chloride was fractionated by RP-VLC using a gradient elution of H_2O/ MeOH (85:15, 75:25, 65:35, 55:45, 45:55 and 0:100) and gave 9 fractions (Fr. 1–9). Fr. 3 was purified by semi-preparative HPLC to afford **25** (0.8 mg). **26** (2.0 mg) was obtained by recrystallization from Fr. 5.

*Libertellenone L (**1**)*, colorless needle crystals; $[\alpha]_D^{20}$ -3 (*c* 0.2, MeOH); UV (MeOH): λ_{max} 228 nm; HRESIMS *m/z* 347.1854 $[M + H]^+$ (calcd 347.1853 for $C_{20}H_{27}O_5$); ^1H and ^{13}C NMR data see Table 1.

*23-O-Acetyl-N-hydroxyapiosporamide (**2**)*, light yellow solid; $[\alpha]_D^{20}$ -77 (*c* 0.2, MeOH); UV (MeOH): λ_{max} 201, 283, 340 nm; HRESIMS *m/z* 488.2280 $[M + H]^+$ (calcd 488.2279 for $C_{26}H_{34}O_8N$); ^1H and ^{13}C NMR data see Table 2.

*8-Hydroxy-3-hydroxymethyl-9-oxo-9H-xanthene-1-carboxylic acid methyl ether (**3**)*, yellow needles; UV (MeOH): λ_{max}231, 257, 289 and 368 nm; HRESIMS *m/z*

301.0707 $[M + H]^+$ (calcd 301.0707 for $C_{16}H_{13}O_6$); ^1H and ^{13}C NMR data see Table 3.

Cytotoxicity Assay. Cytotoxicity was tested against the mouse lymphoma cell line L5178Y using the MTT assay as previously described.[2] Kahalalide F (IC_{50} 4.3 μM) and 0.1% DMSO were used as positive and negative controls, respectively.

X-ray Analysis and Crystal Data of 1. *Crystallization conditions*: X-ray quality crystals of **1** were obtained by slow evaporation from methanol solution. A suitable single crystal was carefully selected under a polarizing microscope. *Data collection*: Bruker Kappa APEX2 CCD diffractometer (with microfocus tube), Cu–Kα radiation (λ = 1.54178 Å), multilayer mirror, ω- and ϕ-scan; data collection with APEX2, cell refinement and data reduction with SAINT,[3] experimental absorption correction with SADABS.[4] *Structure Analysis and Refinement*: The structure was solved by direct methods using SHELXS-97; refinement was done by full-matrix least squares on F^2 using the SHELXL-97 program suite.[5] All non-hydrogen positions were refined with anisotropic displacement parameters. Hydrogen atoms were positioned geometrically (with ß-95 Å for olefinic CH, 1.00 Å for tertiary CH, 0.99 Å for CH_2 and 0.98 Å for CH_3) and refined using riding models (AFIX 43, 93, 13, 23 and 137, respectively), with $U_{iso}(H) = 1.2U_{eq}(CH, CH_2)$ and $1.5U_{eq}(CH_3)$. The hydrogen atom on the hydroxyl group was found and refined with $U_{iso}(H) = 1.5U_{eq}(O)$.

Crystal data and details on the structure refinement are given in Table S1. Graphics were drawn with DIAMOND.[6] The structural data has been deposited with the Cambridge Crystallographic Data Center (CCDC 1517632).

Table S1. Crystal data and structure refinement for **1**.

CCDC number	1517632
Empirical formula	$C_{20}H_{26}O_5$
M/g mol^{-1}	346.41
Crystal size/mm^3	0.5 x 0.1 x 0.01
Temperature/K	140(2)
θ range/° (completeness)	5.5-67.1 (96.5%)
h; k; l range	±8; -7, 8; -19, 18
Crystal system	Monoclinic
Space group	*P* 2_1 (no. 4)
a/Å	7.4991(4)
b/Å	7.2339(4)
c/Å	16.0494(9)
α/°	90
β/°	93.632(3)
γ/°	90
V/Å³	868.90(8)
Z	2
D_{calc}/g cm^{-3}	1.324
μ (Mo Kα)/mm^{-1}	0.768
F(000)	372
Max./min. transmission	0.7529/0.6438
Reflections collected	5413
Independent reflect. (R_{int})	2593 (0.0232)
Data/restraints/parameters	2593/1/232
Max./min. Δρ/e Å^{-3} [a]	0.155/-0.189
R_1/wR_2 [I>2σ(I)] [b]	0.0287/0.0748
R_1/wR_2 (all data) [b]	0.0289/0.0752
Goodness-of-fit on F^2 [c]	1.060
Flack parameter [d]	0.05(5)

[a] Largest difference peak and hole; [b] $R_1 = [\sum(||F_o| - |F_c||)/\sum|F_o|]$; $wR_2 = [\sum[w(F_o^2 - F_c^2)^2]/\sum[w(F_o^2)^2]]^{1/2}$; [c] Goodness-of-fit $= [\sum[w(F_o^2 - F_c^2)^2]/(n - p)]^{1/2}$; [d] Absolute structure parameter[7–8].

References

7. Kjer, J; Debbab, A; Aly, AH; Proksch, P. *Nat. Protoc.* **2010**, *5*, 479−490.
8. Ashour, M.; Edrada, R.; Ebel, R.; Wray, V.; Wätjen, W.; Padmakumar, K.; Müller, W. E. G.; Lin W. H.; Proksch, P. *J. Nat. Prod.* **2006**, *69,* 1547−1553.
9. Apex2, Data Collection Program for the CCD Area-Detector System; SAINT, Data Reduction and Frame Integration Program for the CCD Area-Detector System. Bruker Analytical X-ray Systems, Madison, Wisconsin, USA, 1997-2006.
10. Sheldrick, G. M. Program SADABS: Area-detector absorption correction, University of Göttingen, Germany, **1996**.
11. Sheldrick, G. M. *Acta Crystallogr. Sect. A* **2008**, *64*, 112−122.
12. Brandenburg, K. Diamond (Version 3.2), Crystal and Molecular Structure Visualization, Crystal Impact – K. Brandenburg & H. Putz Gbr, Bonn (Germany) **2009**.
13. Flack, H. D.; Sadki, M.; Thompson, A. L.; Watkin, D. J. *Acta Crystallogr. Sect. A* **2011**, *67*, 21−34.
14. Flack, H. D.; Bernardinelli, G. *Chirality* **2008**, *20*, 681−690.

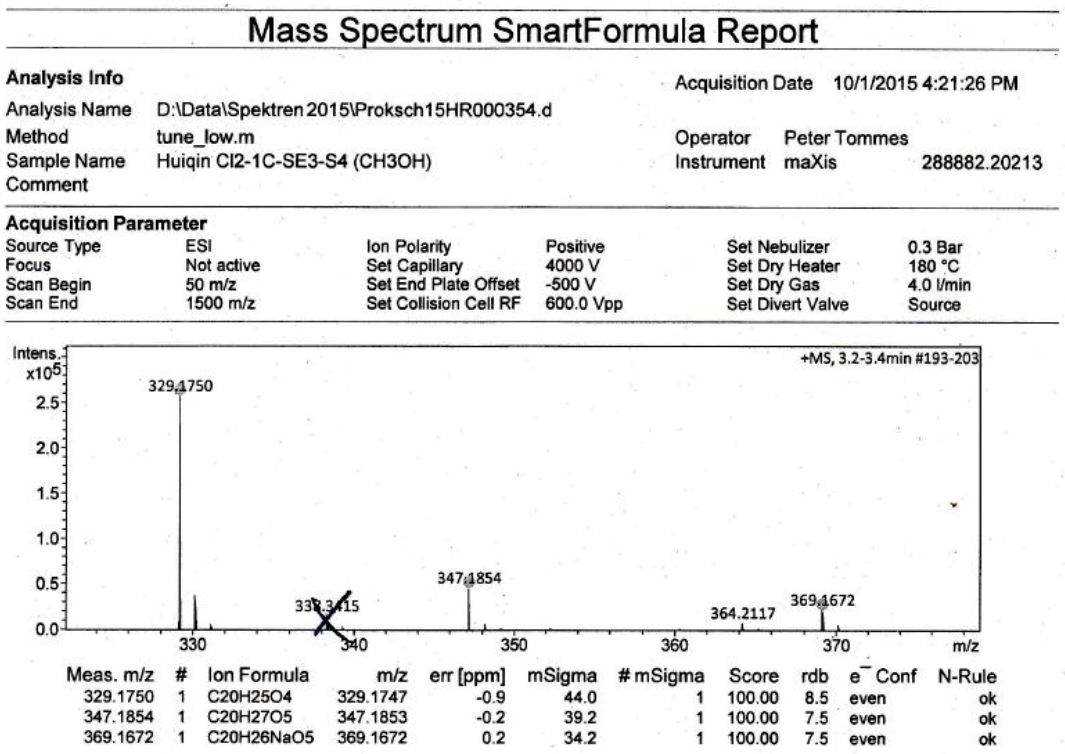

Mass Spectrum SmartFormula Report

Analysis Info

Analysis Name	D:\Data\Spektren 2015\Proksch15HR000354.d	Acquisition Date	10/1/2015 4:21:26 PM
Method	tune_low.m	Operator	Peter Tommes
Sample Name	Huiqin Cl2-1C-SE3-S4 (CH3OH)	Instrument	maXis 288882.20213
Comment			

Acquisition Parameter

Source Type	ESI	Ion Polarity	Positive	Set Nebulizer	0.3 Bar
Focus	Not active	Set Capillary	4000 V	Set Dry Heater	180 °C
Scan Begin	50 m/z	Set End Plate Offset	-500 V	Set Dry Gas	4.0 l/min
Scan End	1500 m/z	Set Collision Cell RF	600.0 Vpp	Set Divert Valve	Source

Meas. m/z	#	Ion Formula	m/z	err [ppm]	mSigma	# mSigma	Score	rdb	e⁻ Conf	N-Rule
329.1750	1	C20H25O4	329.1747	-0.9	44.0	1	100.00	8.5	even	ok
347.1854	1	C20H27O5	347.1853	-0.2	39.2	1	100.00	7.5	even	ok
369.1672	1	C20H26NaO5	369.1672	0.2	34.2	1	100.00	7.5	even	ok

Figure S1. HRESIMS of **1**

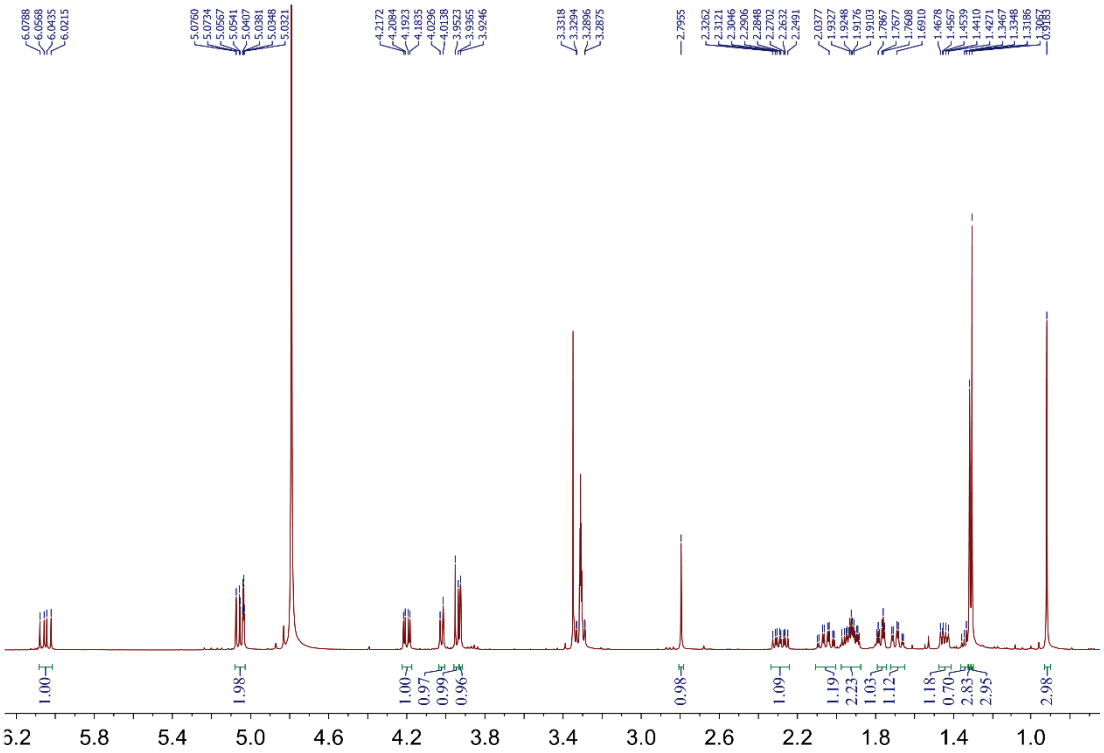

Figure S2. ^{1}H NMR (600 MHz, methanol-d_4) spectrum of **1**

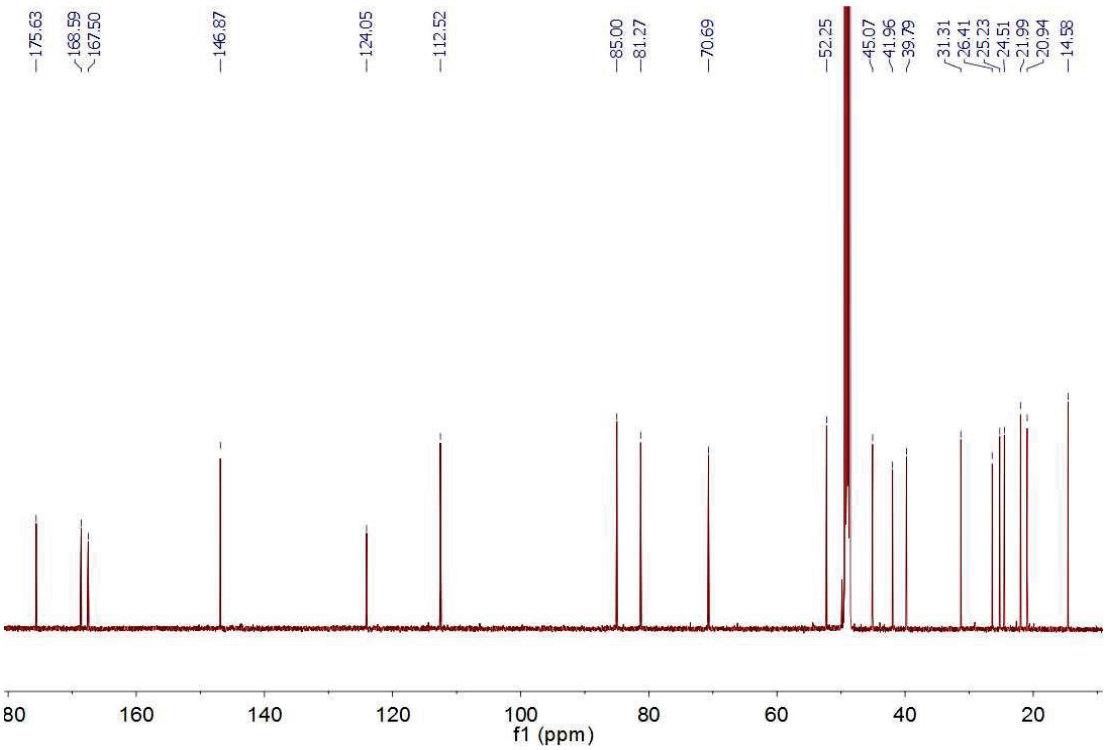

Figure S3. ^{13}C NMR (150 MHz, methanol-d_4) spectrum of **1**

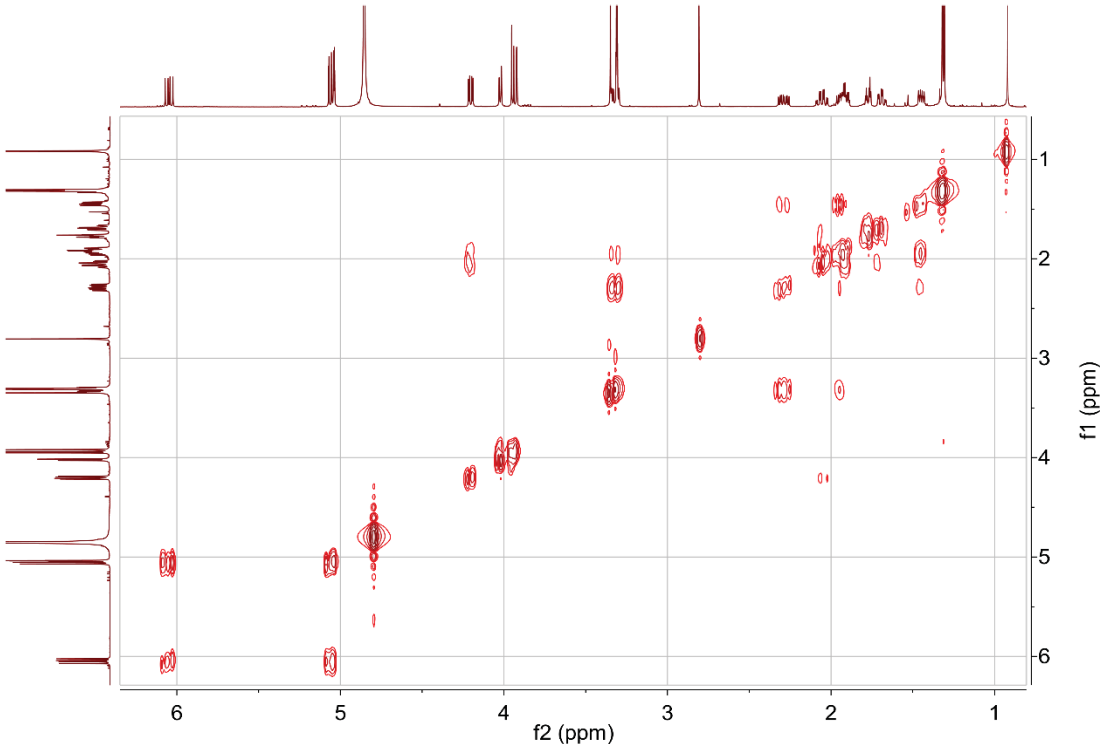

Figure S4. ^{1}H-^{1}H COSY (600 MHz, methanol-d_4) spectrum of **1**

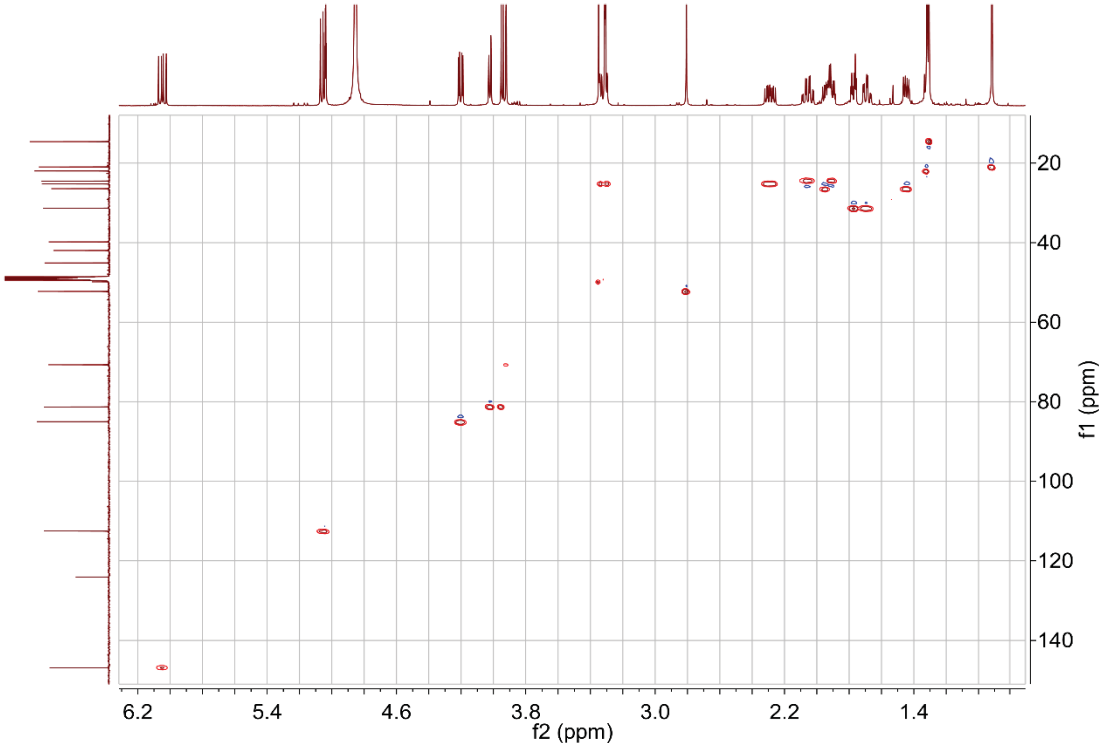

Figure S5. HSQC (600 and 150 MHz, methanol-d_4) spectrum of **1**

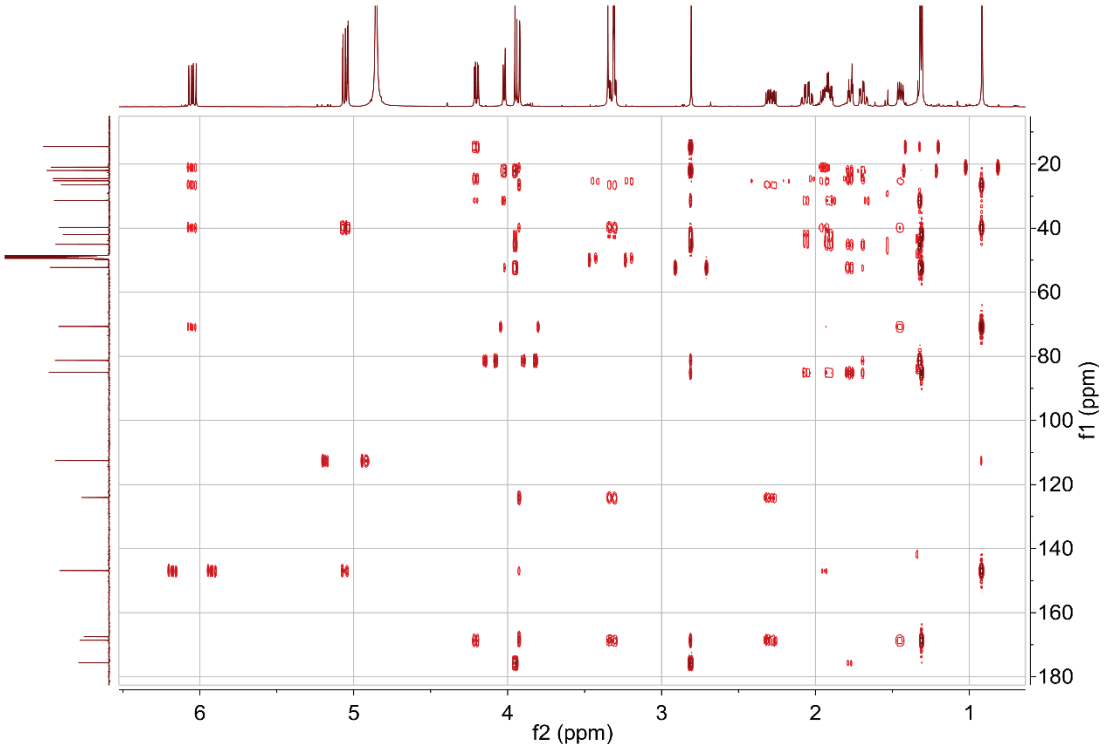

Figure S6. HMBC (600 and 150 MHz, methanol-d_4) spectrum of **1**

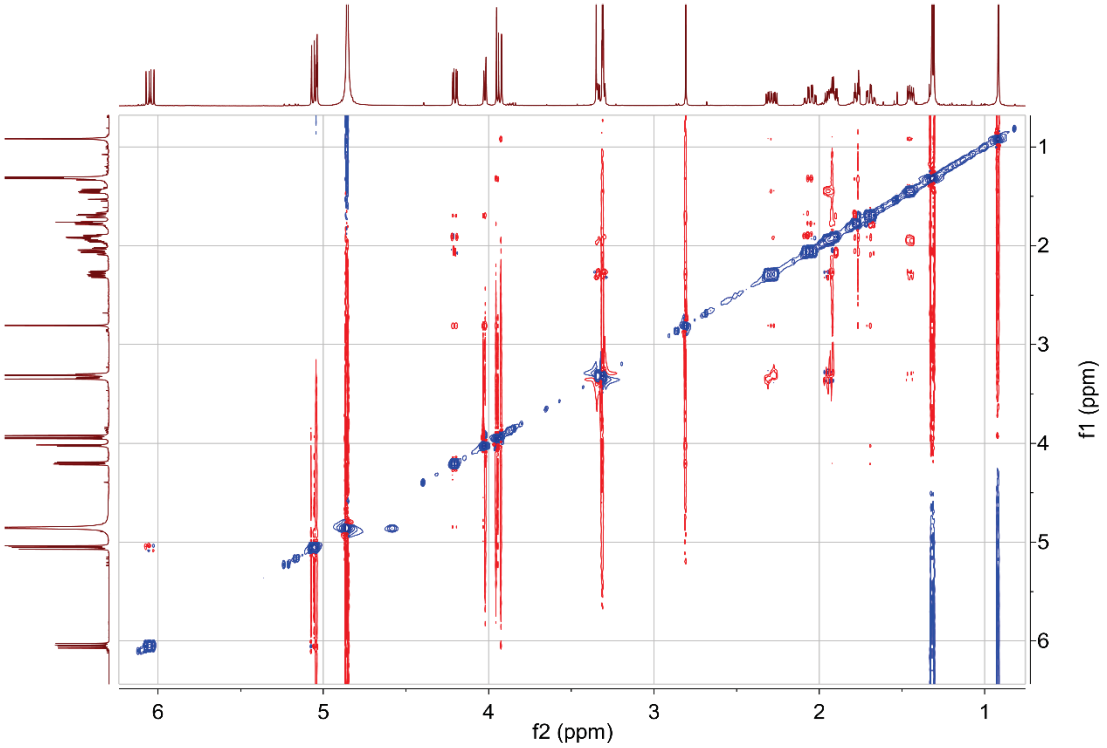

Figure S7. ROESY (600 MHz, methanol-d_4) spectrum of **1**

Mass Spectrum SmartFormula Report

Analysis Info

Analysis Name	D:\Data\Spektren 2015\Proksch15HR000349.d	Acquisition Date	9/29/2015 1:24:30 PM
Method	tune_low.m	Operator	Peter Tommes
Sample Name	U. Blessing CL2-IK-N-SE7-S3 (CH3OH)	Instrument	maXis 288882.20213
Comment			

Acquisition Parameter

Source Type	ESI	Ion Polarity	Positive	Set Nebulizer	0.3 Bar
Focus	Not active	Set Capillary	4000 V	Set Dry Heater	180 °C
Scan Begin	50 m/z	Set End Plate Offset	-500 V	Set Dry Gas	4.0 l/min
Scan End	1500 m/z	Set Collision Cell RF	600.0 Vpp	Set Divert Valve	Source

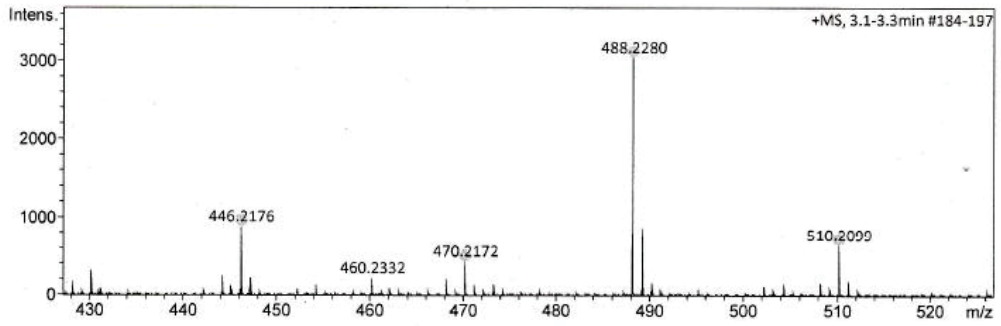

Meas. m/z	#	Ion Formula	m/z	err [ppm]	mSigma	# mSigma	Score	rdb	e⁻ Conf	N-Rule
446.2176	1	C24H32NO7	446.2173	-0.5	26.8	1	100.00	9.5	even	ok
470.2172	1	C26H32NO7	470.2173	0.3	28.6	1	100.00	11.5	even	ok
488.2280	1	C26H34NO8	488.2279	-0.3	5.9	1	100.00	10.5	even	ok
510.2099	1	C26H33NNaO8	510.2098	-0.2	29.1	1	100.00	10.5	even	ok

Figure S8. HRESIMS of **2**

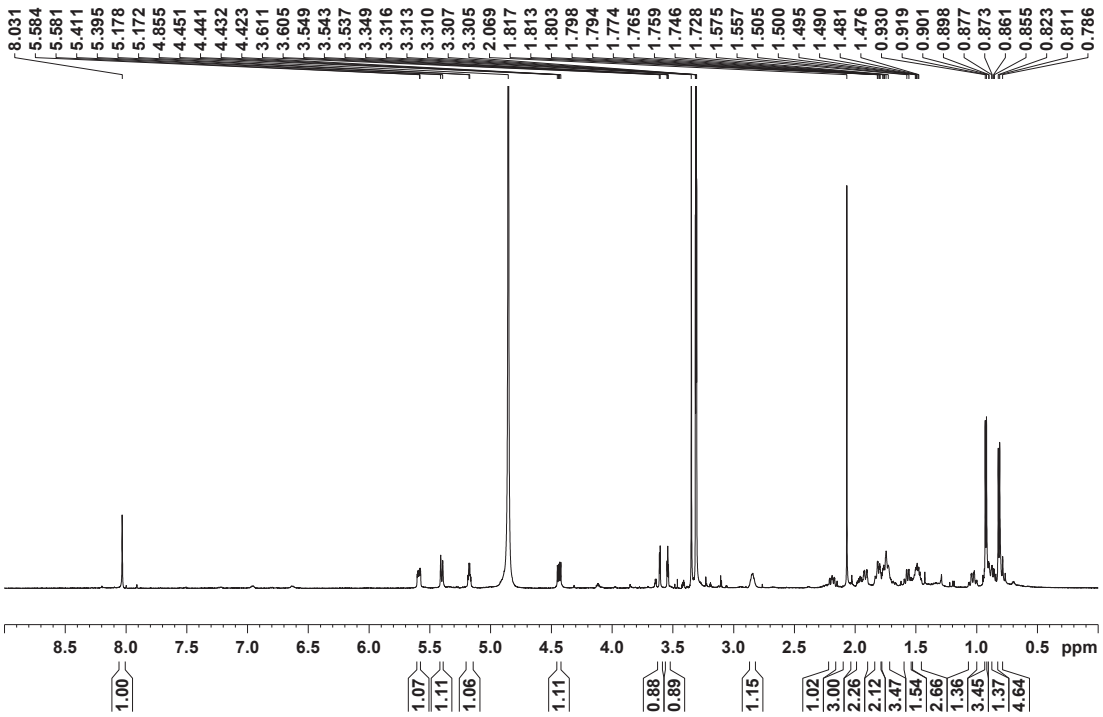

Figure S9. ^{1}H NMR (600 MHz, methanol-d_4) spectrum of **2**

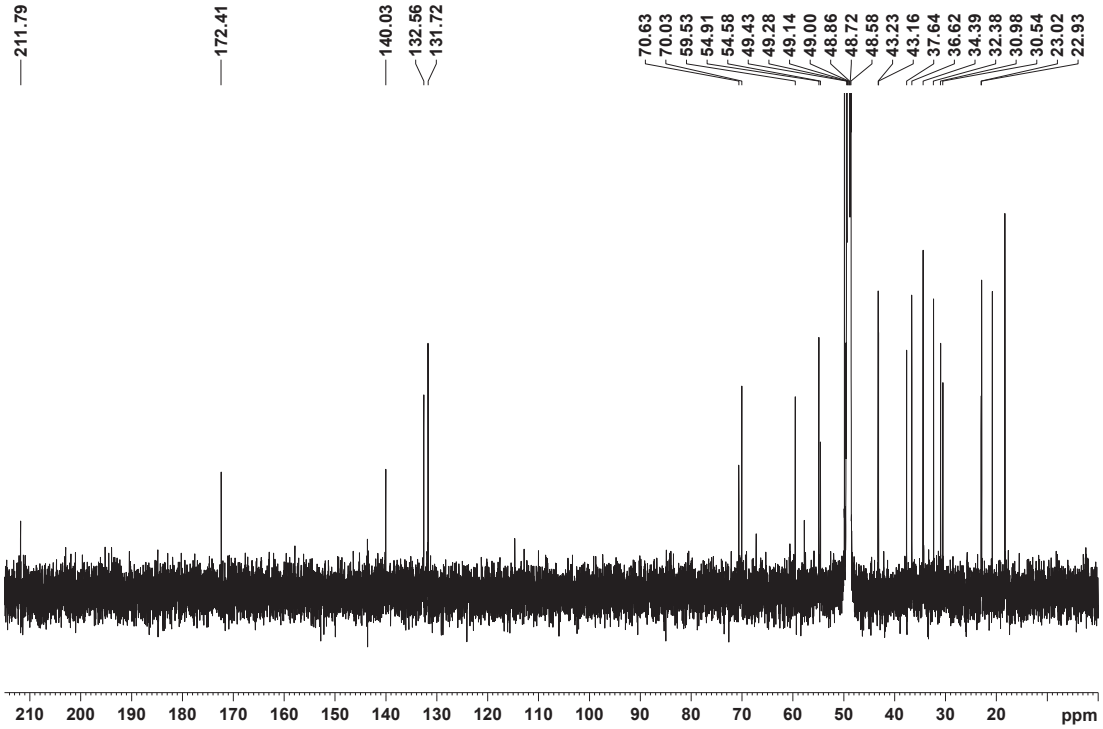

Figure S10. ^{13}C NMR (150 MHz, methanol-d_4) spectrum of **2**

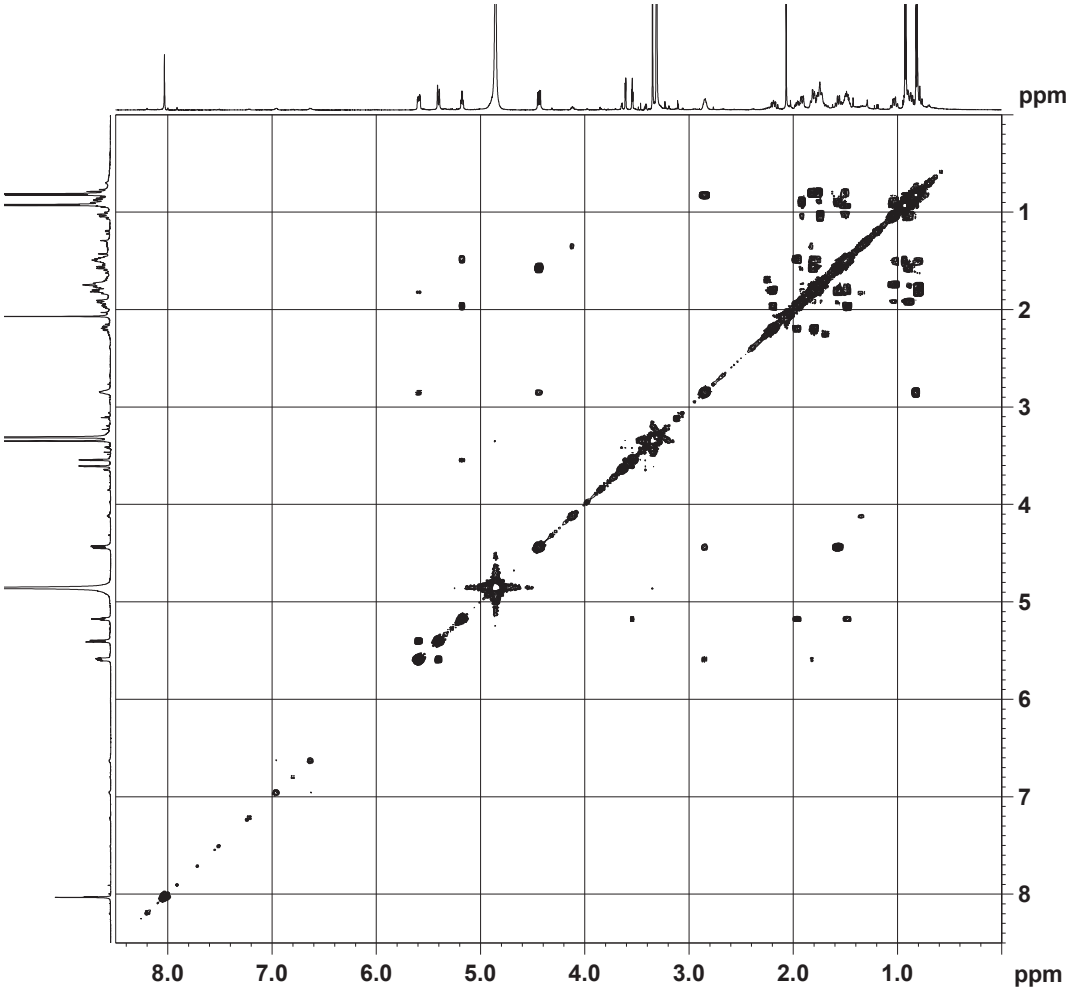

Figure S11. ^{1}H-^{1}H COSY (600 MHz, methanol-d_4) spectrum of **2**

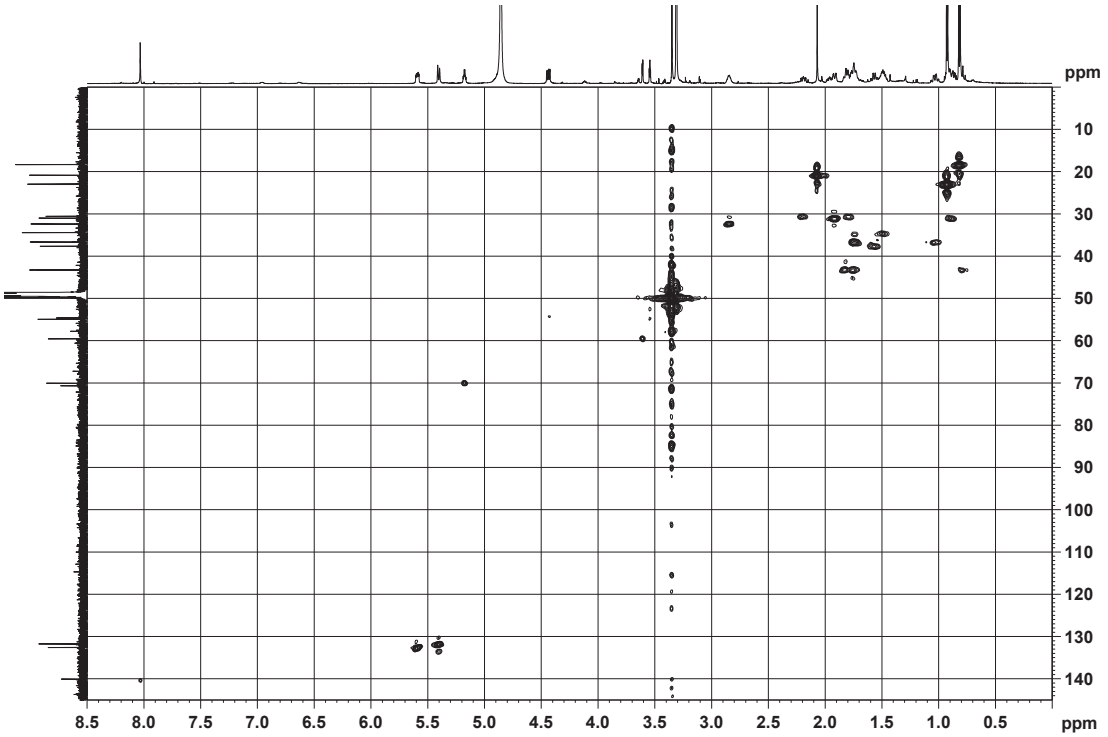

Figure S12. HSQC (600 and 150 MHz, methanol-d_4) spectrum of **2**

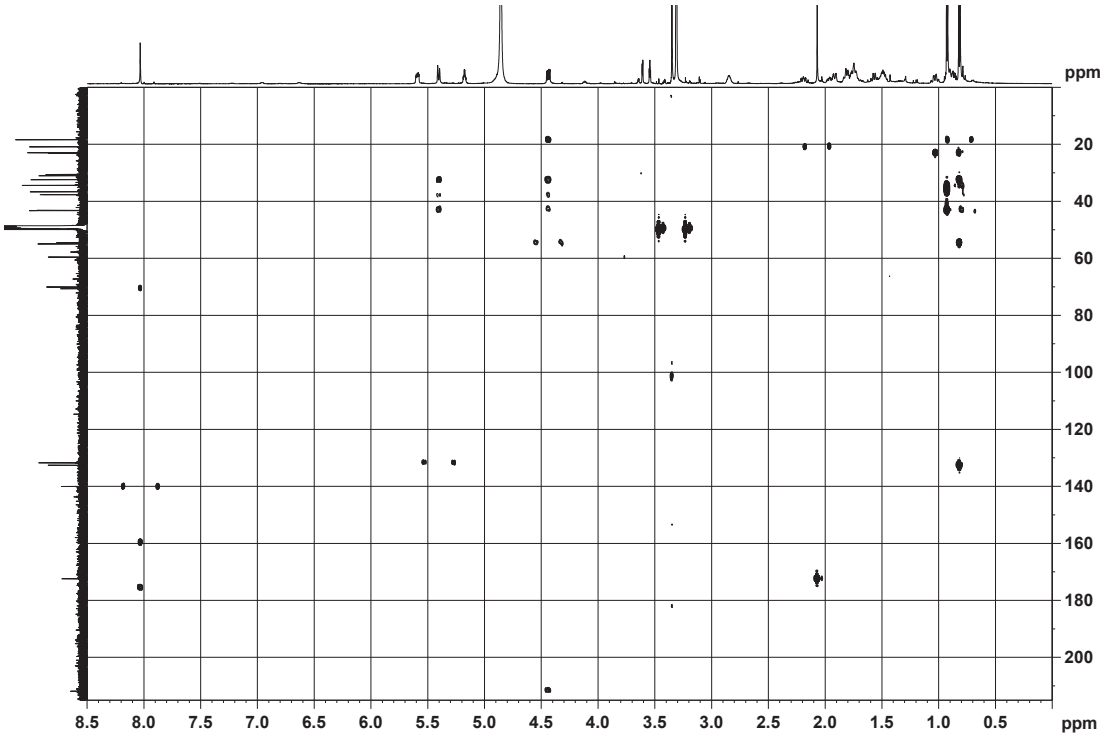

Figure S13. HMBC (600 and 150 MHz, methanol-d_4) spectrum of **2**

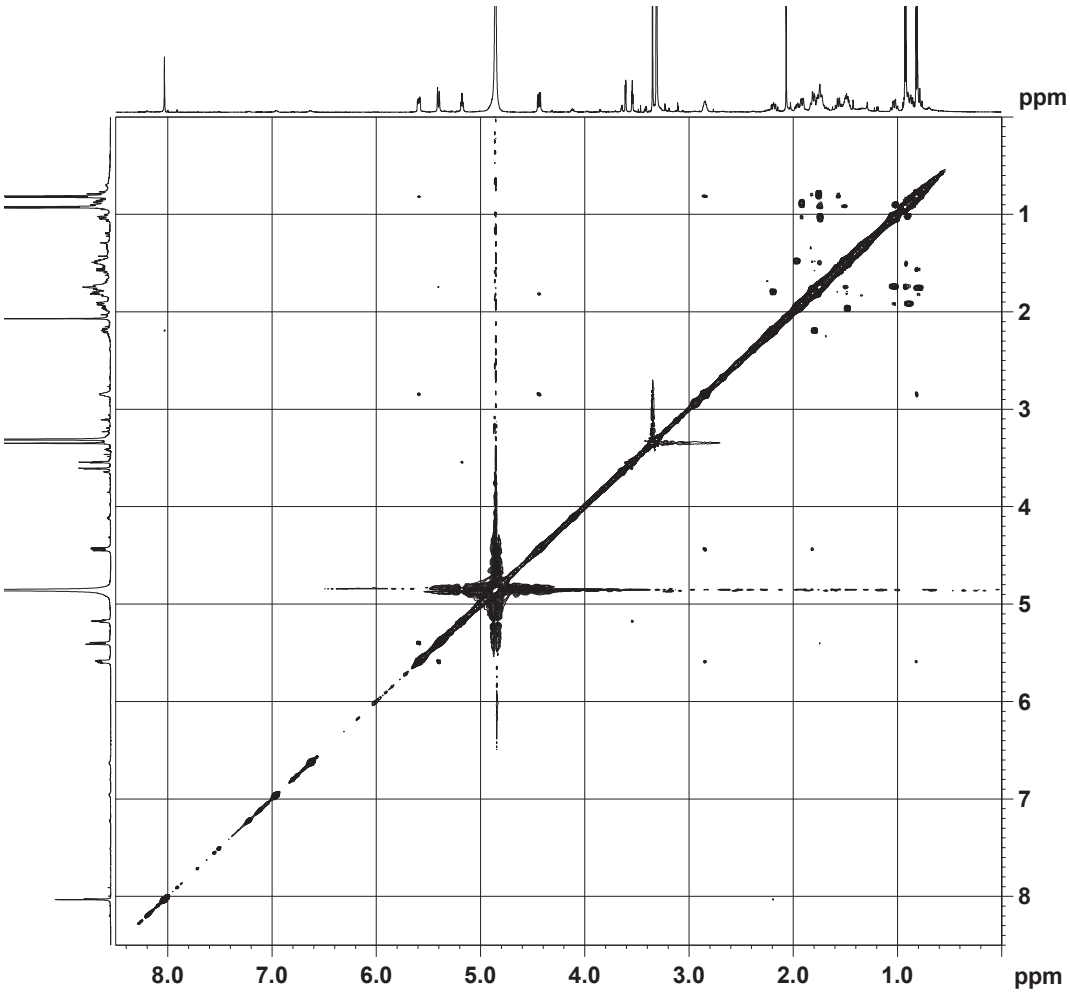

Figure S14. ROESY (600 MHz, methanol-d_4) spectrum of **2**

Mass Spectrum SmartFormula Report

Analysis Info

Analysis Name	D:\Data\Spektren 2015\Prokscb15HR000348.d	Acquisition Date	9/29/2015 12:20:43 PM
Method	tune_low.m	Operator	Peter Tommes
Sample Name	U. Blessing CL2-IG-SE5-S6 (CH3OH)	Instrument	maXis 288882.20213
Comment	5 ul in 1000 ul		

Acquisition Parameter

Source Type	ESI	Ion Polarity	Positive	Set Nebulizer	0.3 Bar
Focus	Not active	Set Capillary	4000 V	Set Dry Heater	180 °C
Scan Begin	50 m/z	Set End Plate Offset	-500 V	Set Dry Gas	4.0 l/min
Scan End	1500 m/z	Set Collision Cell RF	600.0 Vpp	Set Divert Valve	Source

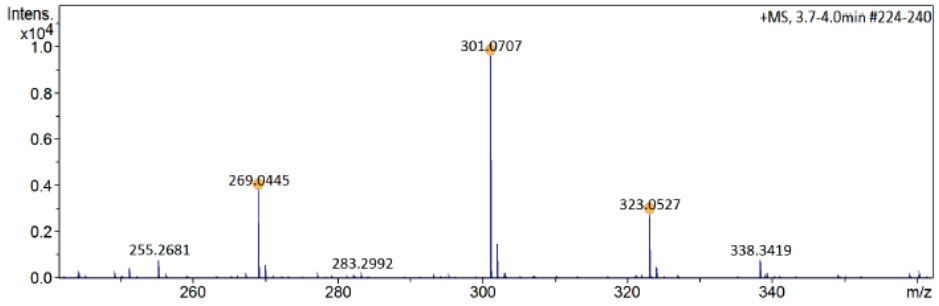

Meas. m/z	#	Ion Formula	m/z	err [ppm]	mSigma	# mSigma	Score	rdb	e⁻ Conf	N-Rule
269.0445	1	C15H9O5	269.0444	-0.3	16.4	1	100.00	11.5	even	ok
301.0707	1	C16H13O6	301.0707	-0.3	14.1	1	100.00	10.5	even	ok
323.0527	1	C16H12NaO6	323.0526	-0.4	16.5	1	100.00	10.5	even	ok

Figure S15. HRESIMS of **3**

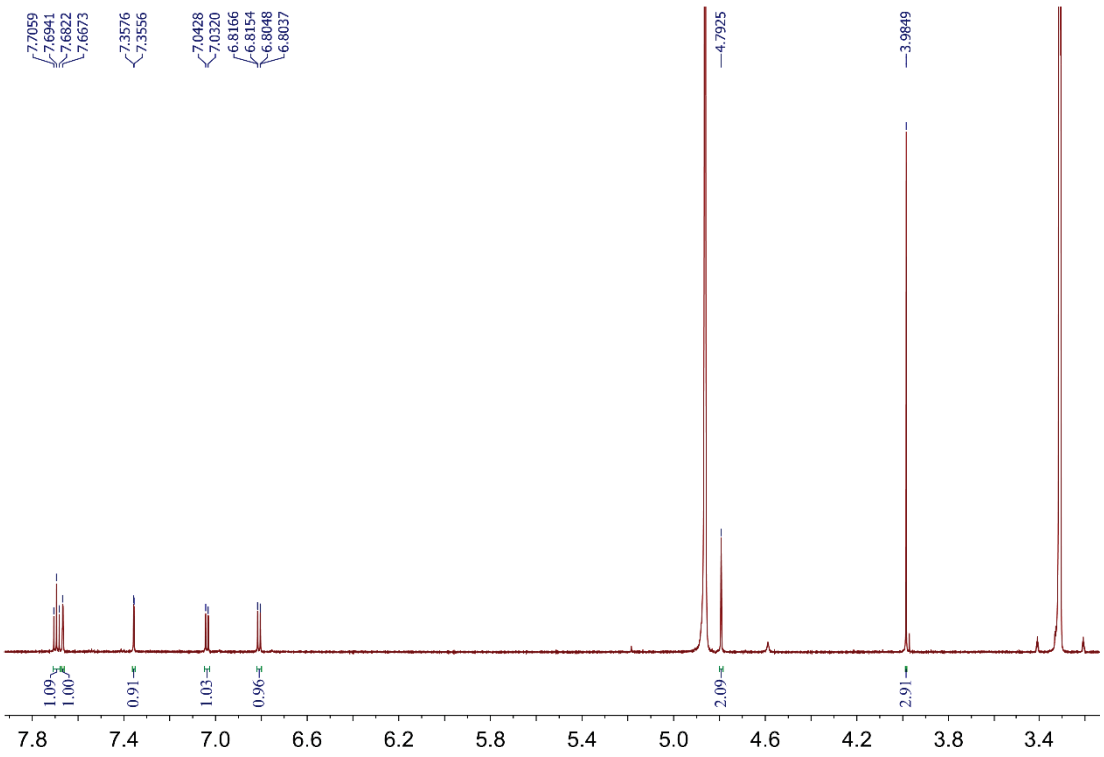

Figure S16. ^{1}H NMR (700 MHz, methanol-d_4) spectrum of **3**

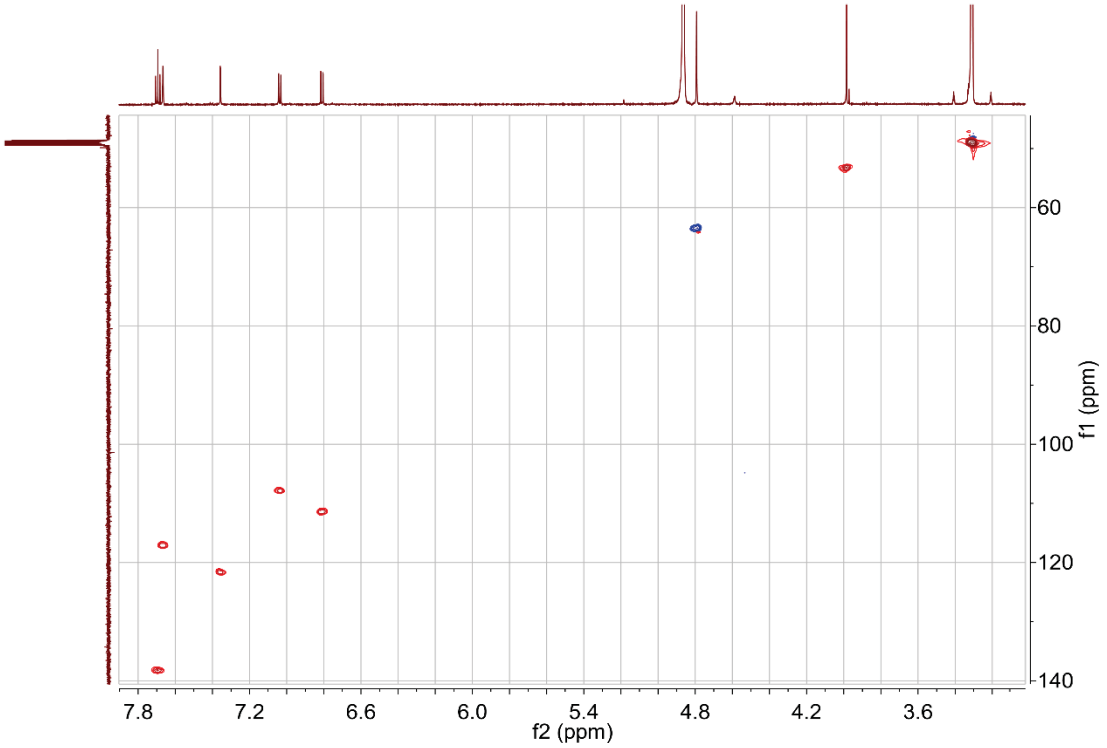

Figure S17. HSQC (700 and 175 MHz, methanol-d_4) spectrum of **3**

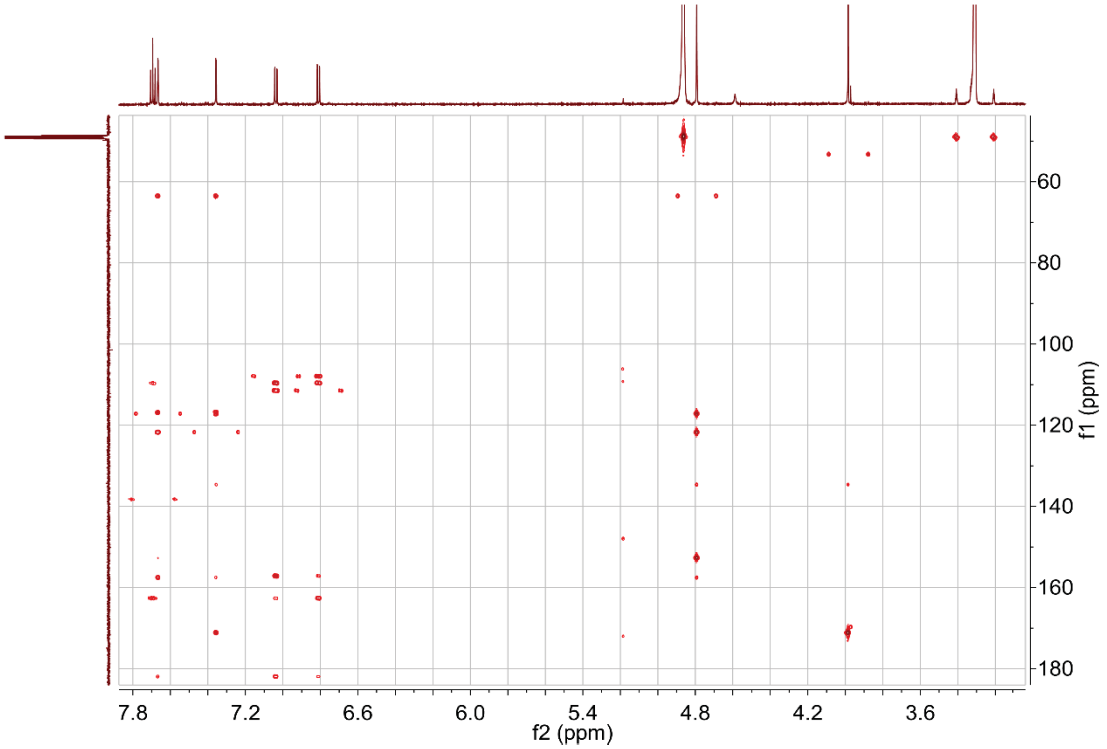

Figure S18. HMBC (700 and 175 MHz, methanol-d_4) spectrum of **3**

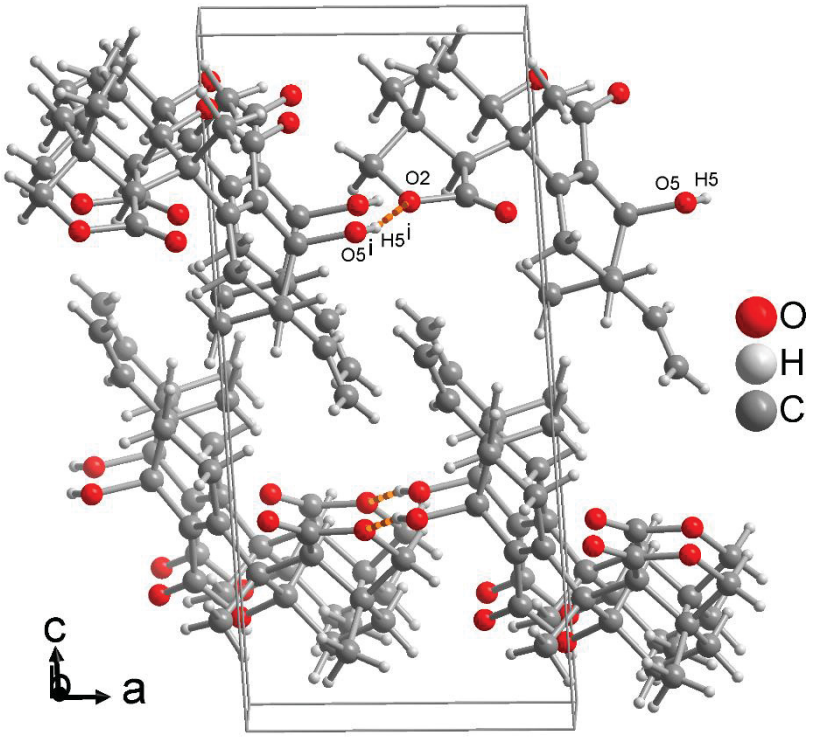

Figure S19. Packing diagram and hydrogen-bonding network in **1**. H-bond details $H5^{i}\cdots O2$ 2.12(3) Å, $O5^{i}\cdots O2$ 2.931(2) Å, $O5^{i}$-$H5^{i}\cdots O2$ 166(3)°, symm. transformation i = –1+x, –1+y, z.

5. Discussion

5.1 Induction of new secondary metabolites using the OSMAC approach

Fungi can produce a tremendous number of secondary metabolites, which possess a multitude of functions such as communication signals, virulence factors and medical applications (Aly and Proksch, 2011). Sequencing data of fungal genomes indicate that more than 70% of secondary metabolic gene clusters are silent under standard laboratory culture conditions (Galagan *et al*., 2003; Debbab and Proksch, 2012; Rutledge and Challis, 2015). OSMAC is an effective approach to activate silent secondary metabolic gene clusters thereby resulting in an accumulation of compounds of enhanced chemical diversity by modification of cultivation parameters including media type and composition, pH values, temperature, shape of culturing flask and aeration (Daletos *et al*., 2017). Hence, several OSMAC approaches were applied in this dissertation to explore the potential of fungal natural products from three promising fungi.

5.1.1 Inducing brominated tyrosine-derived alkaloids by halogen incorporation.

The halogen incorporation experiments of the soil-associated fungus *Gymanscella dankaliensis* were performed on rice medium with or without addition of 3.5% sodium chloride, 3.5% sodium bromide, 3.5% sodium iodide, or 2.0% sodium fluoride at 27 ^{o}C. The fungus grew slower on solid rice medium after adding halogen salts and did not grow on medium with addition of sodium fluoride due to the toxic effect of fluoride ion to fungi (Li *et al*., 2013). Interestingly, several chlorinated and brominated natural products were detected by LC-MS based on their isotope patterns. Iodine was not incorporated into the analyzed compounds, but led to the presence of some new peaks with retention times between 21 and 25 minute (Figure 5.1.1.1). Unfortunately, these peaks were not isolated due to their instability during the isolation process. Further OSMAC experiments were performed on rice medium by adding 3.5% sodium bromide or 10% sodium bromide. The two obtained ethyl acetate crude extracts from rice cultures with addition of sodium bromide showed identical peaks as indicated by HPLC

and LC-MS analysis (Figure 5.1.1.1). The amount of the crude extract (4.7 g per flask) obtained from the rice medium with addition of 3.5% sodium bromide was much bigger than that obtained from the rice medium (1.5 g per flask) with addition of 10% sodium bromide. The halogen incorporation experiments led to the targeted isolation of seven new brominated tyrosine-derived alkaloids, gymnastatins T–Y and dankastatin D, together with three known analogues gymnastatins I–K based on their characteristic UV absorption and typical isotope patterns. The absolute configuration of alkaloids was determined by X-ray single crystal analysis.

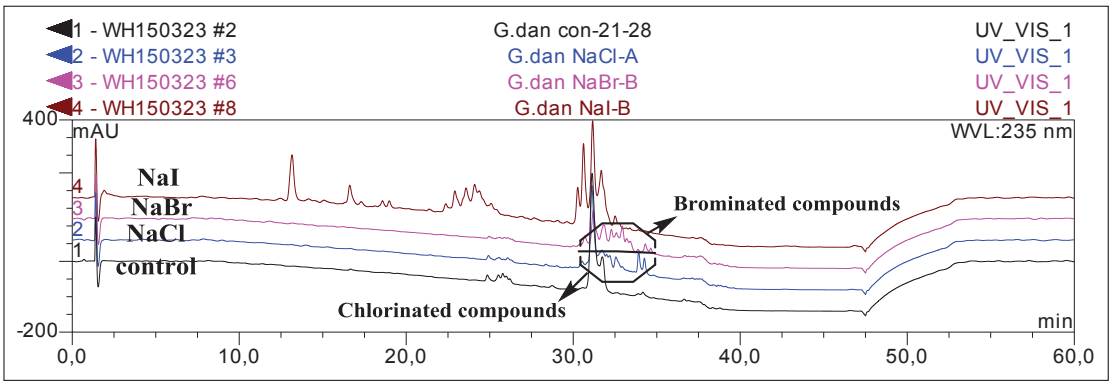

Figure 5.1.1.1 HPLC analysis of fungal extracts grown on rice medium with or without addition of 3.5% sodium halide.

A serious of chlorinated tyrosine-derived alkaloids were reported from the fungus *G. dankaliensis* derived from a marine sponge *Halichondria* sp. and exhibited similar molecular structures to the above brominated alkaloids in which the bromine atoms were replaced by chlorine atoms (Amagata *et al*., 1998; Amagata *et al*., 2006; Amagata *et al*., 2008; Amagata *et al*., 2013; Hammerschmidt *et al*., 2015). The biosynthesis of these halogenated compounds from *G. dankaliensis* was probably catalyzed by halogenases that incorporate chlorine and bromine atoms. Halogenases can be characterized into two groups: the haloperoxidases comprising heme iron peroxidases and vanadium peroxidases, which require hydrogen peroxide; and the highly substrate-specific halogenases comprising flavin-dependent halogenases and α-ketoglutarate-dependent (also called non-heme iron-dependent) halogenases, which utilize dioxygen (Latham *et al*., 2017). In this fungus, it is not known whether halogenases or

haloperoxidases catalyze the bromination, but the halogenation in the electron-rich *ortho* position of the tyrosine moiety was the first step before oxidation and cyclization. The non-halogenated end product gymnastatin N is formed when the fermentation was performed on solid rice medium, and this compound suggested to be key an intermediate for halogenation (Hammerschmidt *et al*., 2015). Further OSMAC approaches were performed by fermentation of *G. dankaliensis* on solid rice medium with addition of 3.5% sodium bromide and different amounts of L-tryptophan ranging from 0.033% to 1.32%. No brominated tryptophan derivatives were detected in the resulted crude extracts using HPLC and LC-MS analysis, suggesting that the enzyme was specific to tyrosine as a substrate. The fungus was further cultured on solid millet medium with addition of 3.5% sodium bromide, leading to the accumulation of a new natural product 7-dehydroxygymnastatin N which indicated that the 7-hydroxy group of the tyrosine moiety is necessary for bromination during the biosynthesis of brominated tyrosine-derived alkaloids. A modified plausible biosynthetic pathway of brominated alkaloids was proposed (Amagata *et al*., 2006; Hammerschmidt *et al*., 2015) (Figure 5.1.1.2).

So far, more than 5,000 halogenated bioactive natural products have been reported (Gribble, 2015). The introduction of halide atoms has a profound effect on the structure-activity relationship of natural products due to their steric effects, electronic effects, electrostatic similitude and hydrophobic effects. For example, the halogen substituents are necessary for antimicrobial activity of the antibiotic vancomycin (Harris *et al*., 1985). A large amount of pharmaceuticals on the market possess halogens, such as the anxiolytic drugs bromazepan and brimonidine, which are used to treat open-angle glaucoma, ocular hypertension and reddened skin (Wermuth, 2015). Compared to hundreds of chlorinated fungal metabolites, only a few brominated fungal metabolites have been reported so far. The halogen incorporation experiment is an effective approach to explore potential halogenated bioactive natural products from fungi. Addition of sodium bromide to rice medium led to an increase of structural diverse brominated tyrosine-derived alkaloids that showed cytotoxicity against the mouse

lymphoma cell line L5178Y with IC_{50} values ranging from 0.078 to 14.1 μM. Among them, gymnastatins I–J, T and W exhibited significant activity with IC_{50} values of 0.55, 0.078, 1.3 and 0.99 μM, respectively. Structure-activity relationship analysis of brominated alkaloids suggested that the conjugated ketone system, the potentially reactive substructure of brominated alkaloids, enhanced the cytotoxicity.

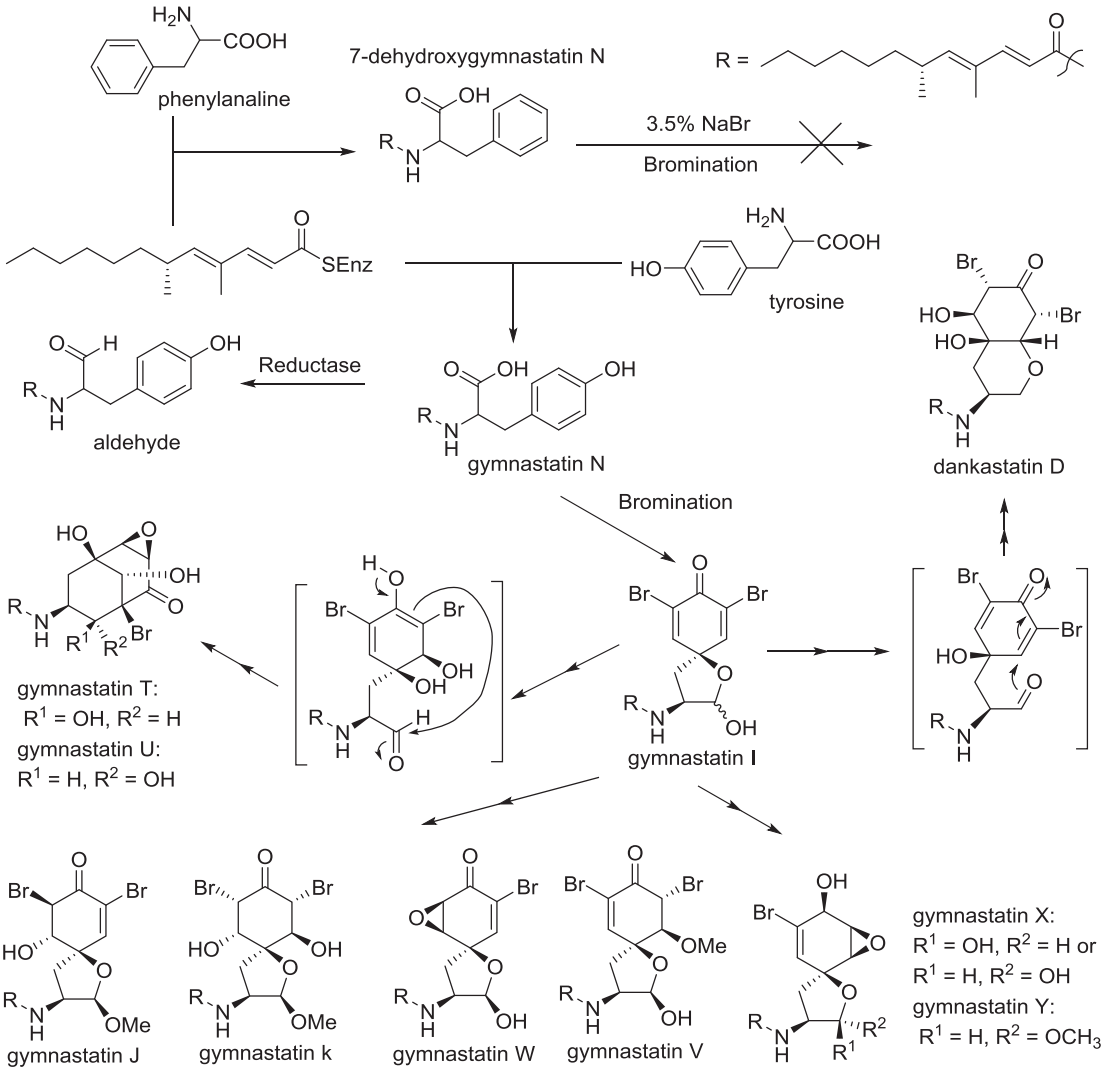

Figure 5.1.1.2 Plausible biosynthesis of brominated alkaloids from *G. dankaliensis*.

5.1.2 Inducing indole alkaloids from *A. aculeatus* by addition of nitrate

OSMAC experiments of the endophytic fungus *Aspergillus aculeatus* isolated from leaves of *Carica papaya* induced the production of indole alkaloids following addition of sodium nitrate to solid rice medium. Fermentation of *A. aculeatus* on solid rice medium without sodium nitrate led to the isolation of only one new indole alkaloid

aceleatine A together with secalonic acids and other known compounds. The OSMAC studies with this fungus were carried out in two parts: the halogen incorporation experiments, which were performed on rice medium with addition of 3.5% sodium chloride, 3.5% sodium bromide, 3.5% sodium iodide, or 1% sodium fluoride; and the effects of different nitrogen sources on metabolic profiles, which were examined by adding 3.5% sodium nitrate, 3.5% ammonium chloride, 3.5% ammonium sulfate, or 3.5% ammonium acetate to the rice medium. The fungus did not grow on rice medium with addition of 1% sodium fluoride or 3.5% ammonium acetate. This probably was caused by the higher concentration of toxic agent ammonia in the rice medium due to adding ammonium acetate, since the acetate anion would concomitantly supply the alkalinity which pushes the NH_4^+/NH_3 equilibrium to the toxic free ammonia form. A similar growth inhibition of fungi was reported for by ammonium bicarbonate (DePasquale and Montville, 1990). Furthermore, acetic acid also showed growth inhibition of the fungus with no growth at 50 mM, much weaker than ammonia, which completely killed the fungus at 300 ppm (17.6 nM) (Kang, Park and Go, 2003; Veverka, Stolcova and Ruzek, 2007).

The obtained ethyl acetate crude extracts from OSMAC experiments of *A. aculeatus* were analyzed by HPLC. Interestingly, two new peaks at retention time around 31 min were observed from the culture after adding 3.5% sodium nitrate, showing identical UV absorption to the new compound aculeatine A. Then a large scale fermentation of *A. aculeatus* was performed on rice medium by adding 3.5% sodium nitrate with or without 0.1% L-tryptophan in fifteen flasks. HPLC analysis of the obtained extracts revealed that adding L-tryptophan to rice medium did not enhance the production of indole alkaloids. Nine new additional indole alkaloids aculeates B–J were isolated. The absolute configuration of indole alkaloids was determined by X-ray single crystal analysis and Marfey's method together with comparison of NMR data with the literature.

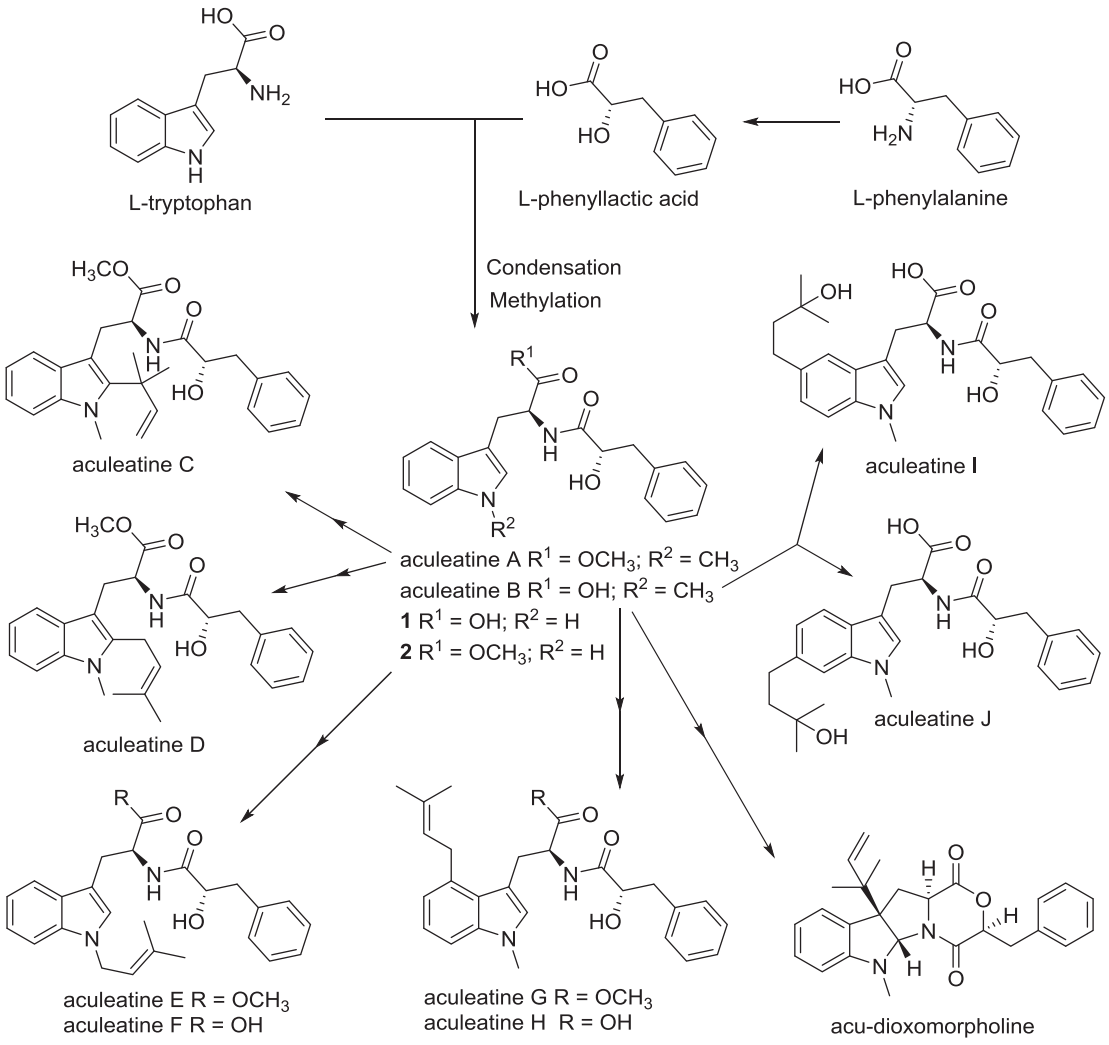

Figure 5.1.2 Plausible biosynthesis of indole alkaloids from *A. aculeatus*.

Among all isolated indole alkaloids, eight of them with an isopentyl substitutent were not detected in rice cultures by following addition of other salts. Many fungal metabolites are prenylated, such as ergot alkaloids, roquefortines, tryprostatins and notoamides (Tudzynski, Correia and Keller, 2001; Sumarah, Miller and Blackwell, 2005 Cui *et al*., 1995; Kato *et al*., 2007). The biosynthesis of prenylated indole alkaloids in fungi was studied by identification of biosynthetic gene clusters including fumigaclavine, fumitremorgin, acetylaszonalenin etc. (Li, 2010; Xu *et al*., 2014). The type of indole alkaloids isolated in this study was rarely reported as natural products so far (Khalil *et al*., 2014). A plausible biosynthetic pathway of aculeatines and their analogues modified after fumitremorgin is proposed starting from L-tryptophan and phenyllactic acid (Figure 5.1.2). The alkaloids were produced after condensation,

methylation, prenylation, oxidation and cyclization.

The above results suggested that indole alkaloids were induced by nitrate but not by sodium in the medium. In the absence of nitrogen sources favoured by the fungus including ammonium and glutamine, fungi are able to use secondary nitrogen sources such as nitrate, purines, urea, amines and amides etc., which is called nitrogen metabolite repression (NMR) (Marzluf, 1997). In fungi, the activity of nitrogen regulators for derepression of NMR genes, which also affect secondary metabolites formation, is regulated by the intracellular nitrogen status and extracellular nitrogen availability (Caddick *et al*., 2006; Tudzynski, 2014). For example, the main GATA transcriptional regulator of nitrogen metabolism AreA accumulates in the nucleus in *F. graminearum* with nitrate as sole nitrogen source, which is required for activation of the nitrate assimilation system including the nitrate reductase genes (Min *et al*., 2012). Thus, the biosynthesis of fungal secondary metabolites can be affected by the quality and quantity of the nitrogen sources. For example, 67% of secondary metabolites silent gene clusters with various types of genes in *Fusarium fujikuroi* were expressed based on the modification of nitrogen sources (Wiemann and Tudzynski, 2013). Furthermore, the natural product beauvericin was inducted from *F. oxysporum* by utilizing nitrate as the sole nitrogen source (López-Berges *et al*., 2014). In this study, the production of indole alkaloids was probably affected by the activation of the nitrate assimilation system in *A. aculeatus* due to the high concentration of sodium nitrate in rice medium.

Among the secondary metabolites isolated from *A. aculeatus*, secalonic acids D and F exhibited strong cytotoxicity against the mouse lymphoma cell line L5178Y and human ovarian cancer cell line A2780. Recently, it was found that secalonic acid D inhibited VEGF-mediated angiogenesis without apparent toxic effects (either orally or intraperitoneal), which has a potential utilization as a cancer-selective therapeutic agent (Guru *et al*., 2015). The indole alkaloids showed no cytotoxic or antibacterial activity. However, the two known indole alkaloids (**1** and **2**) were synthesized as plant growth regulators in a patent, which showed high rooting promoting effect (Maki, Soejima and Sugiyama, 2014). This led to the hypothetis that the function of indole alkaloids is

related to the symbiotic relationship with its host *Carica papaya*. A high concentration of nitrate in the plant, especially in leaves, may induce the production of plant growth regulator indole alkaloids of the endophytic fungus *A. aculeatus* (Siebrecht *et al*., 2003). The induced plant growth regulator from fungus may increase the growth and biomass of the host plant. In return, the fungus received nutrients, water, minerals and nitrogen from its host. This hypothesis was not verified due to the limited amount of isolated indole alkaloids.

5.1.3 Inducing new secondary metabolites from *A. montagnei* through the OSMAC approach

The OSMAC experiments with the endolichenic fungus *Apiospora montagnei* obtained from the lichen *Cladonia* sp. led to the isolation of four additional compounds compared to cultures of the fungus grown only on rice. Three new secondary metabolites incliding libertellenone L, 23-*O*-acetyl-*N*-hydroxyapiosporamide and 8-hydroxy-3-hydroxymethyl-9-oxo-9*H*-xanthene-1-carboxylic acid methyl ester, together with 19 known compounds were isolated from *A. montagnei* when cultured on solid rice medium. The absolute configuration of the new compound libertelenone L was determined by single crystal X-ray diffraction. To increase the diversity of secondary metabolites, halogen incorporation experiments were performed using rice medium with addition of 5% sodium chloride, 5% sodium bromide or 5% sodium iodide. The resulting crude extracts were analyzed by HPLC and LC-MS. Interestingly, unlike the fungal extracts obtained from the solid rice medium with addition of 5% NaBr or 5% NaI which showed similar HPLC chromatograms when compared to the controls, two new peaks (*E*,*E*)-4-hydroxymethyl-4,6-octadien-2,3-diol and lachnellin B were detected and isolated from rice fungal culture following addition of 5% NaCl. Moreover, a roughly 90-fold enhanced accumulation of *N*-hydroxyapiosporamide was found. However, halogenated metabolites were not detected based on their characteristic isotope patterns in LC-MS analysis. Furthermore, the effects of different nitrogen sources on metabolic profiles were examined by adding 1% peptone, 1% yeast extract (YE), 1% corn steep liquor (CSL) or 1% ammonium chloride to the rice medium.

The HPLC profiles of the extracts following addition of peptone, yeast extract or corn steep liquor were similar to those of controls in our experiments. However, cultivation on rice medium with 1% ammonium chloride led to the isolation of two additional compounds 6-*O*-demethylbostrycin and bostrycin. Bostrycin exhibited significant cytotoxic activity against the murine lymphoma cell line L5178Y with an IC_{50} value of 1.7 μM.

5.2 OSMAC approach: an easily executed, effective and potently method to express silent gene clusters of secondary metabolites

In our search for anticancer and antibacterial nature products from fungi, OSMAC approaches were applied to increase the diversity of secondary metabolites from three promising fungi by adding halide to the solid rice medium or by modification of the nitrogen sources, leading to isolation of various types of natural products. Among them, compounds gymnastatins I–J, T and W, secalonic acids D and F, libertellenone G, *N*-hydroxyapiosporamide, apiosporamide, acremonone G and bostrycin exhibited significant cytotoxic activity against the murine lymphoma cell line L5178Y. These results highlight that the OSMAC approach is an efficient way to induce the production of bioactive secondary metabolites. Additional OSMAC experiments can be applied to the aboved three fungi to express secondary metabolites gene clusters as well, such as modification of carbon sources, adjusting pH and temperature, adding metal ions, organic compounds or natural products to the medium etc.

Hundreds of secondary metabolites were induced by the OSMAC approach as reported in the literature, however, the mechanism of induction is not yet well understood. Usually, the formation of secondary metabolites is regulated by pathway-specific and global regulators that control half of the known secondary metabolic gene clusters, and by signal transduction pathways that adapt to environmental changes (Macheleidt *et al*., 2016). In the past two decades, a great progress in understanding these mechanism has been made. Several global regulators have been identified including pH regulation factor PacC (Tilburn *et al*., 1995; Trushina *et al*., 2013), nitrogen metabolism regulators AreA and AreB (Tudzynski, 2014), carbon metabolism

regulator CreA (Dowzer *et al*., 1991; Wang *et al*., 2017) and the velvet complex (Bayram and Braus, 2011). However, it is still a long way to fully understand the molecular mechanisms of induction of fungal secondary metabolites using an OSMAC approach to express silent gene clusters for anticancer and antibacterial drugs or drug candidates.

References

Alvin, A., Miller, K. I., and Neilan, B. A. (2014) Exploring the potential of endophytes from medicinal plants as sources of antimycobacterial compounds. *Microbiological Research*, **169** (7), 483–495

Aly, A. H., Debbab, A., and Proksch, P. (2011) Fungal endophytes: unique plant inhabitants with great promises. *Applied microbiology and biotechnology*, **90** (6), 1829–1845.

Amagata, T., Doi, M., Ohta, T., Minoura, K., and Numata, A. (1998) Absolute stereostructures of novel cytotoxic metabolites, gymnastatins A–E, from a *Gymnascella* species separated from a *Halichondria* sponge. *Journal of the chemical society, Perkin transactions 1*, **21**, 3585–3600.

Amagata, T., Minoura, K., and Numata, A. (2006) Gymnastatins F−H, cytostatic metabolites from the sponge-derived fungus *Gymnascella dankaliensis*. *Journal of natural products*, **69** (10), 1384–1388.

Amagata, T., Tanaka, M., Yamada, T., Chen, Y. P., Minoura, K., and Numata, A. (2013) Additional cytotoxic substances isolated from the sponge-derived *Gymnascella dankaliensis*. *Tetrahedron Letters*, **54** (45), 5960–5962.

Amagata, T., Tanaka, M., Yamada, T., Minoura, K., and Numata, A. (2008). Gymnastatins and dankastatins, growth inhibitory metabolites of a *Gymnascella* species from a *Halichondria* sponge. *Journal of natural products*, **71** (3), 340–345.

Anscher, M. S., Chang, M. G., Moghanaki, D., Rosu, M., Mikkelsen, R. B., Holdford, D., Skinner, V., Grob, B. M., Sanyal, A., Wang, A., Mukhopadhyay, N. D. (2016) A phase II study to prevent radiation-induced rectal injury with lovastatin. *American journal of clinical oncology*.

Appendino, G., Fontana, G., Pollastro F. (2010) Natural products drug discovery. *Comprehensive natural products chemistry II*, **3**, 205–235.

Arnold, A. E., Maynard, Z., Gilbert, G. S., Coley, P. D., and Kursar, T. A. (2000) Are tropical fungal endophytes hyperdiverse? *Ecology letters*, **3** (4), 267–274.

Avery, V. M., Camp, D., Carroll, A. R., Jenkins, I. D., Quinn, R. J. (2010) The identification of bioactive natural products by high throughput screening (HTS). *Comprehensive natural products chemistry II*, **3**, 177–203.

Ávila, N., Tarragó-Castellanos, M. R., and Barrios-González, J. (2017) Environmental cues that induce the physiology of solid medium: a study on lovastatin production by *Aspergillus terreus*. *Journal of applied microbiology*, **122** (4), 1029–1038.

Bayram, Ö., and Braus, G. H. (2011) Coordination of secondary metabolism and development in fungi: the velvet family of regulatory proteins. *FEMS microbiology reviews*, **36** (1), 1–24.

Bhushan, R., and Brückner, H. (2004) Marfey's reagent for chiral amino acid analysis: a review. *Amino acids*, **27** (3–4), 231–247.

Blackwell, M. (2011) The Fungi: 1, 2, 3… 5.1 million species? *American journal of botany*, **98** (3), 426–438.

Brown, S., and O'Connor, S. E. (2015) Halogenase engineering for the generation of new natural product analogues. *ChemBioChem*, **16** (15), 2129–2135.

Caddick, M. X., Jones, M. G., van Tonder, J. M., Le Cordier, H., Narendja, F., Strauss, J., and Morozov, I. Y. (2006) Opposing signals differentially regulate transcript stability in *Aspergillus nidulans*. *Molecular microbiology*, **62** (2), 509–519.

Cavalla, D. (2013) Predictive methods in drug repurposing: gold mine or just a bigger haystack? *Drug discovery today*, **18** (11), 523–532.

Chagas, F. O., Dias, L. G., and Pupo, M. T. (2013) A mixed culture of endophytic fungi increases production of antifungal polyketides. *Journal of chemical ecology*, **39** (10), 1335–1342.

Cole, P. A. (2008) Chemical probes for histone-modifying enzymes. *Nature chemical biology*, **4** (10), 590–597.

Colegate, S. M., and Molyneux, R. J. (Eds.). (2007) Bioactive natural products: detection, isolation, and structural determination. *CRC press*.

Cragg, G. M., Grothaus, P. G., and Newman, D. J. (2014) New horizons for old drugs and drug leads. *Journal of natural products*, **77** (3), 703–723.

Cui, C. B., Kakeya, H., Okada, G., Onose, R., Ubukata, M., Takahashi, I., Isono, K.,

and Osada, H. (1995) Tryprostatins A and B, novel mammalian cell cycle inhibitors produced by *Aspergillus fumigatus*. *The Journal of antibiotics*, **48** (11), 1382–1384.

Daletos, G., Ebrahim, W., Ancheeva, E., El-Neketi, M., and Proksch, P. (2017) Natural products from deep-sea-derived fungi–a new source of novel bioactive compounds? *Current medicinal chemistry*.

Daletos, G., Ebrahim, W., Ancheeva, E., El-Neketi, M., Lin, WH., Proksch, P. (2017) Microbial coculture and OSMAC approach as strategies to induce cryptic fungal biogenetic gene clusters. *Chemical biology of natural products*, **8**, 233–284.

de Medeiros, L. S., Abreu, L. M., Nielsen, A., Ingmer, H., Larsen, T. O., Nielsen, K. F., and Rodrigues-Filho, E. (2015) Dereplication-guided isolation of depsides thielavins S–T and lecanorins D–F from the endophytic fungus *Setophoma* sp. *Phytochemistry*, **111**, 154–162.

Debbab, A., Aly, A. H., and Proksch, P. (2013) Mangrove derived fungal endophytes–a chemical and biological perception. *Fungal diversity*, **61** (1), 1–27.

DePasquale, D. A., and Montville, T. J. (1990) Mechanism by which ammonium bicarbonate and ammonium sulfate inhibit mycotoxigenic fungi. *Applied and environmental microbiology*, **56** (12), 3711–3717.

Dewick, P. M. (2002) *Medicinal natural products: a biosynthetic approach*. John Wiley & Sons.

Elander, R. P. (2003) Industrial production of *β*-lactam antibiotics. *Applied microbiology and biotechnology*, **61**, 385–392.

Eyberger, A. L., Dondapati, R., and Porter, J. R. (2006) Endophyte fungal isolates from *Podophyllum peltatum* produce podophyllotoxin. *Journal of natural products*, **69** (8), 1121–1124.

Galagan, J. E., Calvo, S. E., Borkovich, K. A., Selker, E. U., Read, N. D., Jaffe, D., FitzHugh, W., Ma, L., Smirnov, S., Purcell, S., Rehman, B., Elkins, T., Engels, R., Wang, S., Nielsen, C. B., Butler, J., Endrizzi, M., Qui, D., Lanakiev, P., Bell-Pedersen, D., Nelson, M. A., Werner-Washburne, M., Selitrennikoff, C. P., Kinsey, J. A., Braun, E. L. Zelter, A., Schulte, U., Kothe, G. O., Jedd, G., Mewes, W.,

Staben, C., Marcotte, E., Greenberg, D., Roy, A., Foley, K., Naylor, J., Stange-Thomann, N., Barrett, R., Gnerre, S., Kamal, M., Kamvysselis, M., Mauceli, E., Bielke, C., Rudd, S., Frishman, D., Krystofova, S., Rasmussen, C., Metzenberg, R. L., Perkins, D. D., Kroken, S., Cogoni, C., Macino, G., Catcheside, D., Li, W., Pratt, R. J., Osmani, S. A., DeSouza, C. P. C., Glass, L., Orbach, M. J., Berglund, J. A., Voelker, R., Yarden, O., Plamann, M., Seiler, S., Dunlap, J., Radford, A., Aramayo, R., Natvig, D. O., Alex, L. A., Mannhaupt, G., Ebbole, D. J., Freitag, M., Paulsen, I., Sachs, S. S., Lander, E. S., Nusbaum, C., and Birren, B. (2003) The genome sequence of the filamentous fungus Neurospora crassa. *Nature*, **422** (6934), 859–868.

Gams, W. (2007) Biodiversity of soil-inhabiting fungi. *Biodiversity and conservation*, **16** (1), 69–72.

Gaudêncio, S. P., and Pereira, F. (2015) Dereplication: racing to speed up the natural products discovery process. *Natural product reports*, **32** (6), 779–810.

Goswami, S., Vidyarthi, A. S., Bhunia, B., and Mandal, T. (2013) A review on lovastatin and its production. *Journal of biochemical technology*, **4** (1), 581–587.

Gribble, G. W. (2015) Biological activity of recently discovered halogenated marine natural products. *Marine drugs*, **13** (7), 4044–4136.

Guru, S. K., Pathania, A. S., Kumar, S., Ramesh, D., Kumar, M., Rana, S., Kumar, A., Malik, F., Sharma, P. R., Chandan, B. K., Jaglan, S., Sharma, J. P., Shah, B. A., Tasduq, S. A., Lattoo, S. K., Faruk, A., Saxena, A. K., Vishwakarma, R. A., Bhushan, S. (2015) Secalonic acid-D represses HIF1α/VEGF-mediated angiogenesis by regulating the Akt/mTOR/p70S6K signaling cascade. *Cancer research*, **75** (14), 2886–2896.

Hammerschmidt, L., Aly, A. H., Abdel-Aziz, M., Müller, W. E., Lin, W., Daletos, G., and Proksch, P. (2015) Cytotoxic acyl amides from the soil fungus *Gymnascella dankaliensis*. *Bioorganic & medicinal chemistry*, **23** (4), 712–719.

Harris, C. M., Kannan, R., Kopecka, H., and Harris, T. M. (1985) The role of the chlorine substituents in the antibiotic vancomycin: preparation and characterization of mono-and didechlorovancomycin. *Journal of the american*

chemical society, **107** (23), 6652–6658.

Harvey, A. L., Edrada-Ebel, R., and Quinn, R. J. (2015) The re-emergence of natural products for drug discovery in the genomics era. *Nature reviews drug discovery*, **14** (2), 111–129.

Hasan, S., Ansari, M. I., Ahmad, A., and Mishra, M. (2015) Major bioactive metabolites from marine fungi: A Review. *Bioinformation*, **11** (4), 176–181.

Hawksworth, D. L. (2004) Fungal diversity and its implications for genetic resource collections. *Studies in mycology*, **50**, 9–18.

Henrikson, J. C., Hoover, A. R., Joyner, P. M., and Cichewicz, R. H. (2009) A chemical epigenetics approach for engineering the in situ biosynthesis of a cryptic natural product from *Aspergillus niger*. *Organic & biomolecular chemistry*, **7** (3), 435–438.

Huxtable, R. J., and Schwarz, S. K. (2001) The isolation of morphine—first principles in science and ethics. *Molecular interventions*, **1** (4), 189.

Hyde, K. D., Jones, E. G., Leaño, E., Pointing, S. B., Poonyth, A. D., and Vrijmoed, L. L. (1998) Role of fungi in marine ecosystems. *Biodiversity and conservation*, **7** (9), 1147–1161.

Imhoff, J. F. (2016) Natural products from marine fungi—still an underrepresented resource. *Marine drugs*, **14** (1), 19.

Jalgaonwala, R. E., Mohite, B. V., and Mahajan, R. T. (2017) A review: natural products from plant associated endophytic fungi. *Journal of microbiology and biotechnology research*, **1** (2), 21–32.

Kang, H. C., Park, Y. H., and Go, S. J. (2003) Growth inhibition of a phytopathogenic fungus, *Colletotrichum* species by acetic acid. *Microbiological research*, **158** (4), 321–326.

Kato, H., Yoshida, T., Tokue, T., Nojiri, Y., Hirota, H., Ohta, T., Williams R. M., and Tsukamoto, S. (2007) Notoamides A–D: prenylated indole alkaloids isolated from a marine-derived fungus, *Aspergillus* sp. *Angewandte Chemie International Edition*, **46** (13), 2254-2256.

Kavanagh, Kevin. (2017) *Fungi: biology and applications*. John Wiley & Sons.

Kellogg, J. J., and Raja, H. A. (2017) Endolichenic fungi: a new source of rich bioactive secondary metabolites on the horizon. *Phytochemistry reviews*, **16** (2), 271–293.

Khalil, Z. G., Huang, X. C., Raju, R., Piggott, A. M., and Capon, R. J. (2014) Shornephine A: structure, chemical stability, and P-glycoprotein inhibitory properties of a rare diketomorpholine from an Australian marine-derived *aspergillus* sp. *The Journal of organic chemistry*, **79** (18), 8700–8705.

Kingston, D. G. (2010) Modern natural products drug discovery and its relevance to biodiversity conservation. *Journal of natural products*, **74** (3), 496–511.

Kusari, S., and Spiteller, M. (2011) Are we ready for industrial production of bioactive plant secondary metabolites utilizing endophytes?. *Natural product reports*, **28** (7), 1203–1207.

Kusari, S., Lamshöft, M., and Spiteller, M. (2009) *Aspergillus fumigatus* Fresenius, an endophytic fungus from *Juniperus communis* L. Horstmann as a novel source of the anticancer pro-drug deoxypodophyllotoxin. *Journal of applied microbiology*, **107** (3), 1019–1030.

Kusari, S., Lamshöft, M., Zühlke, S., and Spiteller, M. (2008) An endophytic fungus from *Hypericum perforatum* that produces hypericin. *Journal of natural products*, **71** (2), 159–162.

Kusari, S., Pandey, S. P., and Spiteller, M. (2013) Untapped mutualistic paradigms linking host plant and endophytic fungal production of similar bioactive secondary metabolites. *Phytochemistry*, **91**, 81–87.

Lagarde, A., Millot, M., Jargeat, P., Ouk, T. S., Sol, V., and Mambu, L. (2016) Cytotoxic activity of endolichenic fungi isolated from the lichen *Nephroma laevigatum*. *Planta medica*, **81** (S01), S1–S381.

Latham, J., Brandenburger, E., Shepherd, S. A., Menon, B. R., and Micklefield, J. (2017) Development of halogenase enzymes for use in synthesis. *Chemical Reviews*.

Li, L., Jiang, W., and Lu, Y. (2017) New strategies and approaches for engineering biosynthetic gene clusters of microbial natural products. *Biotechnology advances*.

Li, S. M. (2010) Prenylated indole derivatives from fungi: structure diversity, biological activities, biosynthesis and chemoenzymatic synthesis. *Natural product*

reports, **27** (1), 57–78.

Li, S., Smith, K. D., Davis, J. H., Gordon, P. B., Breaker, R. R., and Strobel, S. A. (2013) Eukaryotic resistance to fluoride toxicity mediated by a widespread family of fluoride export proteins. *Proceedings of the National Academy of Sciences*, **110** (47), 19018–19023.

López-Berges, M. S., Schäfer, K., Hera, C., and Di Pietro, A. (2014) Combinatorial function of velvet and AreA in transcriptional regulation of nitrate utilization and secondary metabolism. *Fungal Genetics and Biology*, **62**, 78–84.

Lutzoni, F., and Miadlikowska, J. (2009) Lichens. *Current biology*, **19** (13), 502–503.

Macheleidt, J., Mattern, D. J., Fischer, J., Netzker, T., Weber, J., Schroeckh, V., Valiante, V., and Brakhage, A. A. (2016) Regulation and role of fungal secondary metabolites. *Annual review of genetics*, **50**, 371–392.

Maki Y, Soejima H, Sugiyama T. (2014) Plant growth regulator: JP, JP2014080406A [P].

Martín, J. F., Liras, P., and García-Estrada, C. (2014) Roquefortine C and related prenylated indole alkaloids. *Biosynthesis and molecular genetics of fungal secondary metabolites*. 111–128.

Marzluf, G. A. (1997) Genetic regulation of nitrogen metabolism in the fungi. *Microbiology and Molecular Biology Reviews*, **61** (1), 17–32.

McMurry, J. E. (2014) Organic Chemistry with Biological Applications. *Cengage learning*.

Min, K., Shin, Y., Son, H., Lee, J., Kim, J. C., Choi, G. J., and Lee, Y. W. (2012) Functional analyses of the nitrogen regulatory gene areA in *Gibberella zeae*. *FEMS microbiology letters*, **334** (1), 66–73.

Miranda, R. U., Gómez-Quiroz, L. E., Mejía, A., and Barrios-González, J. (2013) Oxidative state in idiophase links reactive oxygen species (ROS) and lovastatin biosynthesis: differences and similarities in submerged-and solid-state fermentations. *Fungal biology*, **117** (2), 85–93.

Muggia, L., Kopun, T., and Grube, M. (2017) Effects of growth media on the diversity of culturable fungi from lichens. *Molecules*, **22** (5), 824–845.

Newman, D. J., and Cragg, G. M. (2016) Natural products as sources of new drugs from 1981 to 2014. *Journal of natural products*, **79** (3), 629–661.

Ng, L. T., Pascaud, A., and Pascaud, M. (1987) Hydrochloric acid hydrolysis of proteins and determination of tryptophan by reversed-phase high-performance liquid chromatography. *Analytical biochemistry*, **167** (1), 47–52.

Nielsen, K. F., and Larsen, T. O. (2015) The importance of mass spectrometric dereplication in fungal secondary metabolite analysis. *Frontiers in microbiology*, **6**, 71.

Ola, A. R., Thomy, D., Lai, D., Brötz-Oesterhelt, H., and Proksch, P. (2013) Inducing secondary metabolite production by the endophytic fungus *Fusarium tricinctum* through coculture with *Bacillus subtilis*. *Journal of natural products*, **76** (11), 2094–2099.

Paguigan, N. D., Al-Huniti, M. H., Raja, H. A., Czarnecki, A., Burdette, J. E., González-Medina, M., Medina-Franco, J. L., Polyak, S. J., Pearce, C. J., Croatt, M. P., Oberlies, N. H. (2017) Chemoselective fluorination and chemoinformatic analysis of griseofulvin: Natural vs fluorinated fungal metabolites. *Bioorganic & medicinal chemistry*, **25** (20), 5238–5246.

Pahan, K. (2006) Lipid-lowering drugs. *Cellular and molecular life sciences CMLS*, **63** (10), 1165–1178.

Paranagama, P. A., Wijeratne, E. K., and Gunatilaka, A. L. (2007) Uncovering biosynthetic potential of plant-associated fungi: effect of culture conditions on metabolite production by *Paraphaeosphaeria quadriseptata* and *Chaetomium chiversii* (1). *Journal of natural products*, **70** (12), 1939–1945.

Petersen, A. B., Rønnest, M. H., Larsen, T. O., and Clausen, M. H. (2014) The chemistry of griseofulvin. *Chemical reviews*, **114** (24), 12088–12107.

Puri, S. C., Nazir, A., Chawla, R., Arora, R., Riyaz-ul-Hasan, S., Amna, T., Ahmed, B., Verma, V., Singh, S., Sagar, R., Sharma, A., Kumar, R., Sharma, R. K., Qazi, G. N. (2006) The endophytic fungus *Trametes hirsuta* as a novel alternative source of podophyllotoxin and related aryl tetralin lignans. *Journal of biotechnology*, **122** (4), 494–510.

Puri, S. C., Verma, V., Amna, T., Qazi, G. N., and Spiteller, M. (2005) An endophytic fungus from *Nothapodytes foetida* that produces camptothecin. *Journal of natural products*, **68** (12), 1717–1719.

Raghukumar, C. (2008) Marine fungal biotechnology: an ecological perspective. *Fungal diversity*, **31**, 19–35.

Raghukumar, S. (2017) The marine environment and the role of fungi. *Fungi in coastal and oceanic marine ecosystems*. 15–36

Rahim, M. H. A., Harith, H. H., Montoya, A., and Abbas, A. (2017) Growth and lovastatin production by *Aspergillus terreus* under different carbohyrates as carbon sources. *Biocatalysis and agricultural biotechnology*, **10**, 379–385.

Rebacz, B., Larsen, T. O., Clausen, M. H., Rønnest, M. H., Löffler, H., Ho, A. D., and Krämer, A. (2007) Identification of griseofulvin as an inhibitor of centrosomal clustering in a phenotype-based screen. *Cancer research*, **67** (13), 6342–6350.

Rodrigues, T., Reker, D., Schneider, P., and Schneider, G. (2016) Counting on natural products for drug design. *Nature chemistry*, **8** (6), 531–541.

Rønnest, M. H., Raab, M. S., Anderhub, S., Boesen, S., Krämer, A., Larsen, T. O., and Clausen, M. H. (2012) Disparate SAR data of griseofulvin analogues for the dermatophytes *Trichophyton mentagrophytes*, *T. rubrum*, and MDA-MB-231 cancer cells. *Journal of medicinal chemistry*, **55** (2), 652–660.

Rutledge, P. J., and Challis, G. L. (2015) Discovery of microbial natural products by activation of silent biosynthetic gene clusters. *Nature reviews microbiology*, **13** (8), 509–523.

Schaefer, B. (2015) Natural products in the chemical industry. *Springer*.

Scharf, D. H., and Brakhage, A. A. (2013) Engineering fungal secondary metabolism: a roadmap to novel compounds. *Journal of biotechnology*, **163** (2), 179–183.

Schulz, B., Haas, S., Junker, C., Andrée, N., and Schobert, M. (2015) Fungal endophytes are involved in multiple balanced antagonisms. *Current science*, **109**, 39–45.

Seephonkai, P., Kongsaeree, P., Prabpai, S., Isaka, M., and Thebtaranonth, Y. (2006) Transformation of an irregularly bridged epidithiodiketopiperazine to

trichodermamide A. *Organic letters*, **8** (14), 3073–3075.

Siebrecht, S., Herdel, K., Schurr, U., and Tischner, R. (2003) Nutrient translocation in the xylem of poplar–diurnal variations and spatial distribution along the shoot axis. *Planta*, **217** (5), 783–793.

Singh, B. N., Upreti, D. K., Gupta, V. K., Dai, X. F., and Jiang, Y. (2017) Endolichenic fungi: A hidden reservoir of next generation biopharmaceuticals. *Trends in biotechnology*, **35** (9), 808–813.

Soukup, A. A., and Keller, N. P. (2012) Epigenetic approaches to natural product synthesis in fungi. *Drug discovery from natural products*, 198–217.

Stierle, A., Strobel, G., and Stierle, D. (1993) Taxol and taxane production by *Taxomyces andreanae*, an endophytic fungus of *Pacific yew*. *Science–New York then Washington*, **260**, 214.

Sumarah, M. W., Miller, J. D., and Blackwell, B. A. (2005) Isolation and metabolite production by *Penicillium roqueforti*, *P. paneum* and *P. crustosum* isolated in Canada. *Mycopathologia*, **159** (4), 571–577.

Tedersoo, L., Bahram, M., Cajthaml, T., Põlme, S., Hiiesalu, I., Anslan, S., Harend, H., Buegger, F., Pritsch, K., Koricheva, J., and Abarenkov, K. (2016) Tree diversity and species identity effects on soil fungi, protists and animals are context dependent. *The ISME journal*, **10** (2), 346–362.

Tedersoo, L., Bahram, M., Põlme, S., Kõljalg, U., Yorou, N. S., Wijesundera, R., Ruiz, L. V., Vasco-Palacios, A. M., Thu, P. Q., Suija, A., Smith, M. E., Sharp, C., Saluveer, E., Saitta, A., Rosas, M., Riit, T., Ratkowsky, D., Pritsch, K., Põldmaa, K., Pipenbring, M., Phosri, C., Peterson, M., Parts, K., Pärtel, K., Otsing, E., Nouhra, E., Njouonkou, A. L., Nilsson, R. H., Morgado, L. N., Mayor, J., May, T. W., Majuakim, L., Lodge, D. J., Lee S. S., Larsson, K., Kohout, P., Hosaka, K., Hiiesalu, I., Henkel, T. W., Harend, H., Guo, L. D., Greslebin, A., Grelet, G., Geml, J., Gates, G., Dunstan, W., Dunk, C., Drenkhan, R., Dearnaley, J., Kesel, A. D., Dang, T., Chen, X., Buegger, F., Brearley, F. Q., Bonito, G., Anslan, S., Abell, S., and Abarenkov, K. (2014) Global diversity and geography of soil fungi. *Science*, **346** (6213), 1256688.

Tilburn, J., Sarkar, S., Widdick, D. A., Espeso, E. A., Orejas, M., Mungroo, J., Penalva, M. A., and Arst Jr, H. N. (1995) The *Aspergillus* PacC zinc finger transcription factor mediates regulation of both acid-and alkaline-expressed genes by ambient pH. *The EMBO Journal*, **14** (4), 779–790.

Tobert, J. A. (2003) Lovastatin and beyond: the history of the HMG-CoA reductase inhibitors. *Nature reviews drug discovery*, **2** (7), 517–526.

Trushina, N., Levin, M., Mukherjee, P. K., and Horwitz, B. A. (2013) PacC and pH–dependent transcriptome of the mycotrophic fungus *Trichoderma virens*. *BMC genomics*, **14** (1), 138.

Tudzynski, B. (2014) Nitrogen regulation of fungal secondary metabolism in fungi. *Frontiers in microbiology*, **5**, 656.

Tudzynski, P., Correia, T., and Keller, U. (2001) Biotechnology and genetics of ergot alkaloids. *Applied microbiology and biotechnology*, **57** (5–6), 593–605.

Veverka, K., Stolcova, J., and Ruzek, P. (2007) Sensitivity of fungi to urea, ammonium nitrate and their equimolar solution UAN. *Plant Protection Science-UZPI (Czech Republic)*, **43** (4), 157–164.

Wang, B., Park, E. M., King, J. B., Mattes, A. O., Nimmo, S. L., Clendinen, C., Edison, A. S., Anklin, C., Cichewicz, R. H. (2015) Transferring fungi to a deuterium-enriched medium results in assorted, conditional changes in secondary metabolite production. *Journal of natural products*, **78** (6), 1415–1421.

Wang, Q. Q., Lu, Y., Ren, Z. Y., Chi, Z., Liu, G. L., and Chi, Z. M. (2017) CreA is directly involved in pullulan biosynthesis and regulation of Aureobasidium melanogenum P16. *Current genetics*, **63** (3), 471–485.

Wang, X., Sena-Filho, J. G., Hoover, A. R., King, J. B., Ellis, T. K., Powell, D. R., and Cichewicz, R. H. (2010) Chemical epigenetics alters the secondary metabolite composition of guttate excreted by an atlantic-forest-soil-derived *Penicillium citreonigrum*. *Journal of natural products*, **73** (5), 942.

Wei, Y., Liu, L., Zhou, X., Lin, J., Sun, X., and Tang, K. (2012) Engineering taxol biosynthetic pathway for improving taxol yield in taxol-producing endophytic fungus EFY-21 (*Ozonium* sp.). *African journal of biotechnology*, **11** (37), 9094–

9101.

Wermuth, C. G. (Ed.). (2015) *The practice of medicinal chemistry*. Academic Press.

Wiemann, P., and Keller, N. P. (2014) Strategies for mining fungal natural products. *Journal of industrial microbiology & biotechnology*, **41** (2), 301–313.

Wiemann, P., and Tudzynski, B. (2013) The nitrogen regulation network and its impact on secondary metabolism and pathogenicity. *Fusarium: Genomics, Molecular and Cellular Biology*, 111–142.

Wu, G., Zhou, H., Zhang, P., Wang, X., Li, W., Zhang, W., Liu, X., Liu, H., Keller, N. P., An, Z., Yin, W. B. (2016) Polyketide production of pestaloficiols and macrodiolide ficiolides revealed by manipulations of epigenetic regulators in an endophytic fungus. *Organic letters*, **18** (8), 1832–1835.

Wu, M. Y., and Yu, J. H. (2015) Epigenetics of fungal secondary metabolism related genes. *Biosynthesis and molecular genetics of fungal secondary metabolites*, **2**, 29–42.

Xu, L., Meng, W., Cao, C., Wang, J., Shan, W., and Wang, Q. (2015) Antibacterial and antifungal compounds from marine fungi. *Marine drugs*, **13** (6), 3479–3513.

Xu, P., Hu, G., Luo, C., and Liang, Z. (2016) DNA methyltransferase inhibitors: an updated patent review (2012-2015). *Expert opinion on therapeutic patents*, **26** (9), 1017–1030.

Xu, W., Gavia, D. J., and Tang, Y. (2014) Biosynthesis of fungal indole alkaloids. *Natural product reports*, **31** (10), 1474–1487.

Yamazaki, H., Rotinsulu, H., Narita, R., Takahashi, R., and Namikoshi, M. (2015) Induced production of halogenated epidithiodiketopiperazines by a marine-derived *Trichodermacf brevicompactum* with sodium halides. *Journal of natural products*, **78** (10), 2319–2321.

Yan, J. F., Broughton, S. J., Yang, S. L., and Gange, A. C. (2015) Do endophytic fungi grow through their hosts systemically? *Fungal ecology*, **13**, 53–59.

Yang, Y., Zhao, H., Barrero, R. A., Zhang, B., Sun, G., Wilson, I. W., Xie, F., Walker, K. D., Parks, J. W., Bruce, R., Guo, G., Chen, L., Zhang, Y., Huang, X., Tang, Q., Liu, H., Bellgard, M. I., Qiu, D., Lai, J., and Hoffman, A. (2014) Genome

sequencing and analysis of the paclitaxel-producing endophytic fungus *Penicillium aurantiogriseum* NRRL 62431. *BMC genomics*, **15** (1), 69.

Zheng, Y. G., Wu, J., Chen, Z., and Goodman, M. (2008) Chemical regulation of epigenetic modifications: opportunities for new cancer therapy. *Medicinal research reviews*, **28** (5), 645–687.

List of abbreviations

$[\alpha]_D$	Specific rotation at the sodium D-line
5-AC	5-Azacytidine
Å	Ångström
amu	Atomic mass unit
BGCs	Biosynthetic gene clusters
br	Broad
CD_3OD	Deuterated methanol
$CDCl_3$	Deuterated chloroform
CH_2Cl_2, DCM	Dichloromethane
CH_3COONH_4	Ammonium acetate
COSY	Correlation spectroscopy
CSL	Corn steep liquor
d	Doublet
dd	Doublet of doublet signal
ddd	Doublet of doublet of doublet signal
DMAPP	Dimethylallyl pyrophosphate
DMSO	Dimethyl sulfoxide
DNA	Deoxyribonucleic acid
DNMT	DNA methyltransferase
e. g.	Exempli gratia (for the sake of example)
et al.	et altera (and others)
EtOAc	Ethyl acetate
FDAA	1-fluoro-2-4-dinitrophenyl-5-L-alanine amide
g	Gram
h	hour
HCl	Hydrochloric acid
HDAC	Histone deacetylase
HMBC	Heteronuclear multiple bond connectivity
HMG-CoA	3-Hydroxy-3-methyl-glutaryl-CoA
HPLC	High performance liquid chromatography
HRESIMS	High resolution electrospray ionisation mass
HSQC	Heteronuclear single quantum coherence spectroscopy
HSQC	Heteronuclear single quantum coherence
Hz	Hertz
IC_{50}	Half maximal inhibitory concentration
ITS	Iternal transcriber spacers
KBr	Sodium bromide
L	Liter
LC-MS	Liquid chromatography-mass spectrometry
m	Multiplet signal
M	Mole
m/z	Mass per charge

MeOH	Methanol
mg	Milligram
MHz	Mega Herz
MIC	Minimum inhibitory concentration
min	Minute
mL	Milliliter
mm	Millimeter
MS	Mass spectrometry
MTT	3-(4,5-Dimethylthiazol-2-yl)-2,5-diphenyltetrazolium bromide
MW	Molecular weight
NaBr	Sodium bromide
NaCl	Sodium chloride
NaF	Sodium fluoride
NaI	Sodium iodide
$NaNO_3$	Sodium nitrate
NaOH	Sodium hydroxide
NH_4Cl	Ammonium chloride
$(NH_4)_2SO_4$	Ammonium sulfate
nm	Nanometer
NMR	nuclear magnetic resonance spectrometry
NMR	nitrogen metabolite repression
NOE	Nuclear Overhauser effect
OSMAC	One Strain MAny Compounds
PDB	Potato dextrose broth
ppm	Parts per million
ROESY	Rotating frame overhauser effect spectroscopy
RP 18	Reversed phase C18
s	Singlet signal
SAHA	Suberoylanilide hydroxamic acid
SAR	Structure and activity relationship
sp.	Species
t	Triplet signal
TFA	Trifluoroacetic acid
TLC	Thin layer chromatography
Trp	Tryptophan
TSA	Trichostatin A
UV	Ultra-violet
VLC	Vacuum liquid chromatography
YE	Yeast extract
μM	Micromolar

Research contributions

Publications

(1) **Hao Wang**, Haofu Dai, Christian Heering, Christoph Janiak, Wenhan Lin, Raha S. Orfali, Werner E. G. Müller, Zhen Liu and Peter Proksch. (2016) Targeted solid phase fermentation of the soil dwelling fungus *Gymnascella dankaliensis* yields new brominated tyrosine-derived alkaloids. *Royal Society of Chemistry Advances*, **6**, 81685–81693.

The first author contributed 60% to this publication. The first author's work involved all laboratory work including compound isolation, structure elucidation, and manuscript preparation.

(2) **Hao Wang**, Blessing O. Umeokoli, Peter Eze, Christian Heering, Christoph Janiak, Werner E. G. Müller, Raha S. Orfali, Rudolf Hartmann, Haofu Dai, Wenhan Lin, Zhen Liu, Peter Proksch. (2017) Secondary metabolites of the lichen-associated fungus *Apiospora montagnei*. *Tetrahedron Letters*, **58**, 1702–1705.

The first author contributed 30% to this publication. The first author's work involved part of laboratory work including compound isolation, structure elucidation that derived from OSMAC approach, and manuscript preparation.

(3) **Hao Wang**, Peter M. Eze, Christoph Janiak, Rudolf Hartmann, Festus B.C. Okoye, Charles O. Esimone, Raha S. Orfali, Haofu Dai, Zhen Liu, Peter Proksch. Indole alkaloids produced by an endophytic fungus *Aspergillus aculeatus* using an OSMAC approach (submitted to *Tetrahedron*).

The first author contributed 60% to this publication. The first author's work involved isolation and structure elucidation of all compounds except variecolactone, and manuscript preparation.

Erklärung

Hiermit erkläre ich ehrenwörtlich, dass ich die vorliegende Dissertation mit dem Titel „Sekundärmetaboliten aus Pilzen – Erhöhung der Diversität, Strukturaufklärung und Bioaktivität“ selbst angefertigt habe. Außer den angegebenen Quellen und Hilfsmitteln wurden keine weiteren verwendet. Diese Dissertation wurde weder in gleicher noch in abgewandelter Form in einem anderen Prüfungsverfahren vorgelegt. Weiterhin erkläre ich, dass ich früher weder akademische Grade erworben habe, noch dies versucht habe.

Düsseldorf, den 12.12.2017

Hao Wang

Acknowledgements

First of all, I would like to express my deepest appreciation to Prof. Dr. Peter Proksch for giving me this precious opportunity to pursue my doctoral research in fungal secondary metabolites and for the excellent working conditions and facilities at the Institute of Pharmaceutical Biology and Biotechnology, Heinrich Heine University, Düsseldorf. I would like to express my deep thanks and heartfelt gratitude for his admirable supervision, patient guidance, helpful suggestion and fruitful discussions for my study in Düsseldorf.

My special thanks to Prof. Dr. Haofu Dai (Institute of Tropical Bioscience and Biotechnology, Chinese Academy of Tropical Agriculture Science) for introducing me to Prof. Proksch and help to study in Germany.

I am deeply indebted to Dr. Zhen Liu for his help on valuable suggestions on my experiments, structure elucidations of compounds and preparations of manuscripts for publications.

I would like to express my appreciation to Prof. Dr. Matthias U. Kassack (Institute for Pharmaceutical and Medicinal Chemistry, Heinrich Heine University) for estimating my PhD study as second referee and conducting cytotoxicity assays.

My deep thanks to Prof. Dr. Werner E. G. Müller (Institute of Physiological Chemistry and Pathobiochemistry, University of Mainz) for cytotoxicity tests, and to Prof. Dr. Rainer Kalscheuer (Institute of Pharmaceutical Biology and Biotechnology, Heinrich Heine University) for antibiotic assays.

I would like to express my sincerely appreciation to Dr. Rudolf Hartmann (Institute of Complex Systems: Structural Biochemistry, Forschungszentrum Jülich, Germany) and Ms. Breuer for their NMR measurements, to Dr. Peter. Tommes (Institute of Inorganic and Structure Chemistry, Heinrich Heine University, Düsseldorf) for carrying out MS experiments, and to Prof. Dr. Claus Passreiter for his safety introduction.

I would like to express my gratitude to Prof. Christoph Janiak, Dr. Christian

Heering and Dr. Simon-Patrick Höfert (Institute of Inorganic and Structure Chemistry, Heinrich Heine University, Düsseldorf) for their collaboration on single-crystal X-ray diffraction.

I am deeply indebted to Mrs. Claudia Eckelskemper for her generous help of administration, and the technicians Mrs. Simone Miljanovic, Mrs. Waltraud Schlag, Mrs. Katja Friedrich, Mrs. Simone Mönninghoff-Pützer, Mrs. Eva Müller, Ms. Linda Wiegand, Mr. Dieter Jansen and Mrs. Heike Goldbach-Gecke for their generous help and support.

My sincere thanks to postdoctors Dr. Yang Liu, Dr. Georgios Daletos, Dr. Ramsay Kamdem, Dr. Weaam Ebrahim, Dr. Elena Ancheeva and Dr. Sherif Elsayed for their guidance and discussions.

I would like to express my deep thanks to my colleagues and friends Dr. Amin Mokhlesi, Dr. Andreas Marmann, Ms. Arta Kuci, Ms. Blessing Umeokoli, Ms. Catalina Perez Hemphill, Ms. Catherine Bogner, Ms. Chenyin Wang, Ms. Dina Elkashef. Mr. Feng Pan, Mr. Ferhat Oezkaya, Dr. Festus Okoye, Mr. Haiqian Yu, Prof. Han Xiao, Mr. Harwoko, Dr. Hendrick Niemann, Dr. Herve Sergi Akone, Dr. Huiqin Chen, Ms. Imke Form, Ms. Julia Werner, Ms. Kim Thao Le, Dr. Lene Hammerschmidt, Mr. Lei Wang, Ms. Lisa Kuppers, Ms. Mariam Moussa, Mr. Marian Frank, Ms. Miada Sakr, Ms. Mi-Yong Chung, Dr. Mohamed Elnaggar, Dr. Mousa Al Tarabeen, Ms. Nada Mohamed, Mr. Nam Michael Tran-Cong, Ms. Nihal Aktas, Ms. Ni Putu Ariantari, Ms. Pamela Nangmo Kemda, Mr. Peter Eze, Dr. Rini Muharini, Dr. Rudiyansyah, Dr. Shuai Liu, Mr. Tino Seidemann, Ms. Xiaoqin Yu, Dr.Yanbo Zeng, Ms. Ying Gao for their help and assistance, as well as the nice time enjoyed together.

My sincere thanks to the China Scholarship Council, Ministry of Education of China for the financial support in Germany.

In the end, I would like to express my deepest gratitude to my parents for everything they did to support and encourage me to finish this study.

Curriculum Vitae

Name: Hao Wang

Nationality: Chinese

Address: Heinrich Heine University Duesseldorf
Universitätsstraße 1
40225 Duesseldorf

E-mail: Hao.Wang@uni-duesseldorf.de

Educational background:

11. 2014 – present: Ph.D student in Pharmacy, Institute of Pharmaceutical Biology and Biotechnology, Heinrich Heine University, Duesseldorf, Germany

09. 2011 – 06. 2014: Master of Organic Chemistry, College of Chemistry and Molecular Engineering, Qingdao University of Science & Technology, China

09. 2007 – 07. 2011: Bachelor of Chemistry, College of Chemistry and Molecular Engineering, Qingdao University of Science & Technology, China

Publications:

1. **Hao Wang**, Blessing O. Umeokoli, Peter Eze, Christian Heering, Christoph Janiak, Werner E.G. Müller, Raha S. Orfali, Rudolf Hartmann, Haofu Dai, Wenhan Lin, Zhen Liu, Peter Proksch. Secondary metabolites of the lichen-associated fungus *Apiospora montagnei*. *Tetrahedron Letters*, 2017, *58*(17), 1702–1705.
2. **Hao Wang**, Haofu Dai, Christian Heering, Christoph Janiak, Wenhan Lin, Raha S. Orfali, Werner E.G. Müller, Zhen Liu, Peter Proksch. Targeted solid phase fermentation of the soil dwelling fungus *Gymnascella dankaliensis* yields new brominated tyrosine-derived alkaloids. *RSC Advances*, 2016, *6*(85), 81685–81693.
3. **Hao Wang**, Wenhua Dong, Wenjian Zuo, Shuai Liu, Huimin Zhong, Wenli Mei,

Haofu Dai. Five new sesquiterpenoids from *Dalbergia odorifera*. 2014, *Fitoterapia*, *95*, 16–21.

4. **Hao Wang**, Wenli Mei, Yanbo Zeng, Wenjian Zuo, Zhikai Guo, Liangliang Chen, Huimin Zhong, Haofu Dai. Phenolic compounds from *Dalbergia odorifera*. 2014, *Phytochemistry Letters*, *9*, 168–173.
5. **Hao Wang**, Wenhua Dong, Wenjian Zuo, Hui Wang, Huimin Zhong, Wenli Mei, Haofu Dai. Three new phenolic compounds from *Dalbergia odorifera*. 2014, *Journal of Asian natural products research*, *16*(12), 1109–1118.
6. Yanbo Zeng, **Hao Wang**, Ramsay S. T. Kamdem, Raha S. Orfali, Haofu Dai, Gamall Makhloufi, Christoph Janiak, Zhen Liu, Peter Proksch. A new cyclohexapeptide, penitropeptide and a new polyketide, penitropone from the endophytic fungus *Penicillium tropicum*. *Tetrahedron Letters*, 2016, *57*(27), 2998–3001.
7. Ramsay S. T. Kamdem, **Hao Wang**, Pascal Wafo, Weaam Ebrahim, Ferhat Can Özkaya, Gamall Makhloufi, Christoph Janiak, Parichat Sureechatchaiyan, Matthias U. Kassack, Wenhan Lin, Zhen Liu, Peter Proksch. Induction of new metabolites from the endophytic fungus *Bionectria* sp. through bacterial co-culture. *Fitoterapia*, 2017.